

THE STRUCTURE AND FLUXIONALITY OF TETRAHEDRAL  
COBALT-BASED ORGANOMETALLIC CLUSTERS

By

© KAREN ANN SUTIN, B.Sc.

A Thesis

Submitted to the School of Graduate Studies

in Partial Fulfillment of the Requirements

for the Degree

Doctor of Philosophy

McMaster University

February, 1990

## COBALT-BASED TETRAHEDRAL ORGANOMETALLIC CLUSTERS

**To my Parents**

**DOCTOR OF PHILOSOPHY (1990)**  
**(Chemistry)**

**McMaster University**  
**Hamilton, Ontario**

**Title:       The Structure and Fluxionality of Cobalt-Based  
              Tetrahedral Organometallic Clusters**

**Author:     Karen Ann Sutin, B.Sc., (McMaster University)**

**SUPERVISOR:    Dr. M.J. McGlinchey**

**NUMBER OF PAGES:    xix, 167**

## Abstract

A series of trimetal tetrahedra were synthesized with the goal of studying their structures and the mechanistic processes which occur during fluxionality of their ligands. The basic skeleton utilized was a  $\text{Co}_3\text{C}$  tetrahedron, varied to include Mo or W on occasion, but always maintaining the four-vertex core.

The bidentate ligands DIPHOS (bis-diphenylphosphinoethane) and ARPHOS (1-diphenylphosphino-2-diphenylarsinoethane) coordinate to tricobalt and mixed-metal clusters, bonding only at the cobalt vertices. The DIPHOS chelate remains tightly bound to the cluster while the carbonyl ligands migrate about the vertices. The ARPHOS ligand cleaves at the As-Co linkage and can move between Co vertices. This process, as well as the concomitant CO migration, is slowed on the NMR timescale at reduced temperature.

In a system with a carbonyl ligand bridging two cobalt vertices of a tricobalt cluster,  $\text{Co}_3(\text{CO})_4(\text{C}_5\text{H}_5)_2\text{C}-\text{C}_6\text{H}_5$ , the  $^{13}\text{C}$  NMR spectrum was observed to determine if the EHMO-predicted favoured orientation of the phenyl ring could be frozen out in solution in the NMR experiment. A xylyl ring was incorporated into the system as a probe for loss of mirror symmetry. At a range of temperatures, the clusters did not show cessation of the rotation. The tetrahedral cluster  $\text{Co}_3(\text{CO})_4(\text{C}_5\text{H}_5)_2\text{C}-\text{C}_6\text{H}_5$  crystallizes in the monoclinic space group  $\text{P}2_12_12_1$ , and the phenyl ring was found to be oriented parallel to the bridging CO unit, corresponding to the proposed structure as predicted by EHMO theory.

The bulky dinaphthyl fragment  $\text{CH}(\text{4-ClC}_{10}\text{H}_6)_2$  was incorporated into a tricobalt nonacarbonyl cluster as the capping ligand to investigate possible hindrance

to exchange of the CO ligands. Cessation of carbonyl exchange was observed on the DDT derivative and other analogues, but the relatively unstable dinaphthyl cluster showed no evidence of this behaviour, attributed to the inability of the naphthyl rings to rotate because of steric restrictions. The crystal structure of  $\text{Co}_3(\text{CO})_9\text{C}-\text{CH}-(4\text{-ClC}_{10}\text{H}_6)_2$  was solved.

The molecules  $\text{M}(\text{CP})(\text{CO})_2\text{Co}_2(\text{CO})_6\text{C}-\text{CO}_2\text{CH}(\text{CH}_3)_2$ , ( $\text{M} = \text{Mo}, \text{W}$ ;  $\text{CP} = (\text{C}_5\text{H}_5), (\text{C}_5\text{H}_4\text{CH}_3), [\text{C}_5(\text{CH}_3)_5]$ ) adopt two conformations at reduced temperatures in the NMR experiment, dependent on the position of the cyclopentadienyl ring: one involves the ring in a conventional axial position (accompanying CO ligands equatorial), while in the second isomer, the ring centroid is above the trimetal plane, with the two carbonyl ligands semi-bridged. Isomer interchange occurs rapidly at room temperature. The favoured isomer in the  $\text{C}_5\text{H}_5$  and  $\text{C}_5\text{H}_4\text{CH}_3$  clusters has the ring below the basal plane, while the larger  $\text{C}_5(\text{CH}_3)_5$  rings prefer the "up" position, allowing distribution of excess electron density to the remaining vertices via the carbonyl ligands.  $[\text{C}_5(\text{CH}_3)_5]\text{Mo}(\text{CO})_2\text{Co}_2(\text{CO})_6\text{C}-\text{CO}_2\text{CH}(\text{CH}_3)_2$  crystallizes in the space group  $\text{P}2_1/n$ , and displays the large  $\text{C}_5(\text{CH}_3)_5$  ring in the area of least unfavourable interaction with the bulk of the cluster.

## ACKNOWLEDGEMENTS

I would like to thank my supervisor, Dr. Michael J. McGlinchey, for his years of guidance, during which time he was not only accessible, but friendly and welcoming as well. He was always willing to help with any problem, showing great patience. I also enjoyed how he could make the research so much more rewarding by placing bets on what the result would be. The payoff was wonderful -- I've always been partial to Chardonnay.

For all their help in my research, I thank Brian Sayer and Ian Thompson for NMR and FTIR instruction, Romolo Faggiani, Steve Zweep, Dr. C.J.L. Lock, and Dr. Chris Frampton for crystallography help, Mike Malott for setting up the computer so that I could write my thesis, Dr. Joe Kolis for teaching me vacuum line techniques, and Dr. M. Mahendran for sharing his knowledge of organic chemistry whenever I needed it. I thank my laboratory group through all the years -- Peter, who taught me the proper attitude towards organometallics; Mike, who helped me get started on my research; Richard, Bavani, Reg, Debbie, Mike, Kris, Jan and Andreas, because they were always there to make the time in the lab just that much more interesting, and to offer suggestions if the column wasn't eluting properly.

The financial assistance of McMaster University and NSERC was gratefully received.

To those friends who kept me happy and enjoying school, thanks to Cathy, Paul, Howard, Lesley, Brad and Carol. I appreciate the support of my brothers Doug, Dave, Paul and Mark, who didn't make fun of me for staying in school this long. I thank my parents who supported and encouraged me during my twenty-five years of education, always patting me on the back whenever I brought home some good work.

And of course, thanks go to my husband Nick, who is always happy to discuss my research and all my other interests, and who is an inspiration to me.



## TABLE OF CONTENTS

### CHAPTER ONE

(1.1)	Cobalt Cluster History	1
	(1.1.1) Synthesis	1
	(1.1.2) Reactivity	3
	(1.1.2.1) Carbonyl Substitution	3
	(1.1.2.2) Apical Group Manipulation	4
	(1.1.2.3) Vertex Substitution	7
(1.2)	Structural Studies	8
	(1.2.1) Static Structures	8
	(1.2.1.1) X-Ray Crystallography	8
	(1.2.1.2) Molecular Orbital Studies	10
	(1.2.1.3) Isolobality	20
	(1.2.2) Dynamic Structures	24
	(1.2.2.1) Fluxionality	25
	(1.2.2.2) Detection Methods	25
(1.3)	Catalysis	28
(1.4)	Development of Chirality	31

### CHAPTER TWO

(2.1)	Tetrahedral Clusters Bearing Chelating Ligands	35
	(2.1.1) Chelating Phosphines and Arsines	35
	(2.1.2) Methods of Analysis	37
(2.2)	A Simple System: $\text{Co}_3(\text{CO})_9\text{C-CO}_2\text{CH}(\text{CH}_3)_2$	39
	(2.2.1) NMR Study	39
	(2.2.2) DIPHOS Reactions	40
	(2.2.3) ARPHOS Incorporation	43
	(2.2.4) X-Ray Analysis of $\text{Co}_3(\text{CO})_7(\text{ARPHOS})\text{C-CO}_2\text{CH}(\text{CH}_3)_2$	48
(2.3)	Vertex Replacement	50
	(2.3.1) NMR Study of the Uncomplexed Clusters $(\text{CP})\text{M}(\text{CO})_2\text{Co}_2(\text{CO})_6\text{C-CO}_2\text{CH}(\text{CH}_3)_2$	51

(2.3.2)	Heterometallic Clusters with a Symmetric Chelating Ligand	52
(2.3.3)	Reaction of Heterometallic Systems with ARPHOS	54
(2.4)	Mass Spectrometric Analysis	57
(2.5)	Conclusion	59
<b>CHAPTER THREE</b>		
(3.1)	Clusters With the Focus on the Capping Group	60
(3.1.1)	Orientation of a Capping Phenyl Ring	60
(3.1.2)	Solution State: Dynamic or Static?	61
(3.1.3)	Solid State Geometries	64
(3.1.4)	A Second Explanation	66
(3.2)	A Model System: $\text{Co}_3(\text{C}_5\text{H}_5)_2(\text{CO})_4\text{C}-\text{C}_6\text{H}_5$	67
(3.2.1)	Synthesis	67
(3.2.2)	The Structure in the Solid State: X-Ray Diffraction Crystal Structure of $\text{Co}_3(\text{C}_5\text{H}_5)_2(\text{CO})_4\text{C}-\text{C}_6\text{H}_5$	67
(3.2.3)	Solution State NMR Study	69
(3.3)	A Labelled System: $\text{Co}_3(\text{CO})_4(\text{C}_5\text{H}_5)_2\text{C}-(3,4-(\text{CH}_3)_2\text{C}_6\text{H}_3)$	70
(3.3.1)	Synthesis	70
(3.3.2)	Nuclear Magnetic Resonance Study	71
(3.4)	Calculational Results	72
(3.4.1)	Van der Waals' Radii	72
(3.4.2)	Molecular Orbital Study	73
(3.5)	Conclusion	74
<b>CHAPTER FOUR</b>		
(4.1)	Extreme Bulk Capping the Cluster	75
(4.2)	Synthesis and NMR of the Starting Material $\text{Cl}_3\text{C}-\text{CH}(4-\text{ClC}_{10}\text{H}_6)_2$ , <u>25</u>	78
(4.3)	The New Cluster: $\text{Co}_3(\text{CO})_9\text{CCH}-(4-\text{ClC}_{10}\text{H}_6)_2$	78
(4.3.1)	Synthesis and NMR	78
(4.3.2)	Infrared Analysis	81

(4.3.3)	X-Ray Diffraction Crystal Structure of $\text{Co}_3(\text{CO})_9\text{CCH}-(4\text{-ClC}_{10}\text{H}_6)_2$	81
(4.4)	Conclusion	85
<b>CHAPTER FIVE</b>		
(5.1)	Introduction	86
(5.1.1)	Positions of Cyclopentadienyl Ligands in Tetrahedral Clusters	86
(5.1.2)	Possibilities For Preferential Ring Positioning	88
(5.1.3)	Statement of the Problem	89
(5.1.4)	Modes of Structure Elucidation	93
(5.2)	Study of Cyclopentadienyl Clusters	94
(5.2.1)	Synthesis of $(\text{CP})\text{M}(\text{CO})_2\text{Co}_2(\text{CO})_6\text{C}-\text{CO}_2\text{-}$ $\text{CH}(\text{CH}_3)_2$ , $\text{M} = \text{Mo, W}$ ; $\text{CP} = \text{C}_5\text{H}_5, \text{C}_5\text{H}_4\text{CH}_3$ and $\text{C}_5(\text{CH}_3)_5$ , <u>10-15</u>	94
(5.2.2)	NMR of the $(\text{C}_5\text{H}_5)\text{-}$ and $(\text{C}_5\text{H}_4\text{CH})_3\text{-}$ Ligated Clusters	94
(5.2.3)	Infrared Analysis	96
(5.3)	Comparison With a Known Compound	98
(5.3.1)	Synthesis of $(\text{C}_5\text{H}_5)\text{Mo}(\text{CO})_2\text{Co}_2(\text{CO})_6\text{C-}$ $\text{C}_6\text{H}_5$ , <u>28</u>	98
(5.3.2)	Solution State NMR Study	99
(5.3.3)	Solution State Infrared Analysis	100
(5.3.4)	The Solid State Structure	100
(5.3.5)	Solid State NMR Study	100
(5.3.6)	Solid State Infrared Analysis	101
(5.4)	A Second Look at the $(\text{C}_5\text{H}_5)$ and $(\text{C}_5\text{H}_4\text{CH}_3)$ Clusters: the Solid State	102
(5.5)	$\Delta\text{G}$ Values Between Isomers	104
(5.6)	Effect of Increased Bulk in the Ring	105
(5.6.1)	NMR of the $[\text{C}_5(\text{CH}_3)_5]$ Clusters	106
(5.6.2)	Infrared Investigation of the $[\text{C}_5(\text{CH}_3)_5]\text{-}$ $\text{Mo}(\text{CO})_2\text{Co}_2(\text{CO})_6\text{C}-\text{CO}_2\text{CH}(\text{CH}_3)$ Cluster	107

(5.6.3) X-Ray Diffraction Crystal Structure of [C <sub>5</sub> (CH <sub>3</sub> ) <sub>5</sub> ]Mo(CO) <sub>2</sub> Co <sub>2</sub> (CO) <sub>6</sub> C-CO <sub>2</sub> CH(CH <sub>3</sub> ) <sub>2</sub>	109
(5.7) Molecular Orbital Studies	111
(5.8) Cyclopentadienyl Ring Positions in Chiral Clusters	114
(5.8.1) Synthesis of (C <sub>5</sub> H <sub>5</sub> )Mo(CO) <sub>2</sub> Co <sub>2</sub> (CO) <sub>6</sub> C- CO <sub>2</sub> -C <sub>17</sub> O <sub>3</sub> H <sub>22</sub>	114
(5.8.2) NMR Study	115
(5.8.3) An Effectively Larger Ligand: The Menthyl Cluster	118
(5.8.4) Conclusion	120
 CHAPTER SIX	
Future Work	
(6.1) Further Work in Chelation	121
(6.2) Phenyl Rotation	122
(6.3) The Two-Isomer Cyclopentadienyl Clusters	123
(6.4) Conclusion	124
 CHAPTER SEVEN	
Experimental	
(7.1) Melting Point Technique	125
(7.2) Carbonyl Enrichments	126
(7.3) Syntheses and Spectral Data	126
Co <sub>3</sub> (CO) <sub>9</sub> C-CO <sub>2</sub> CH(CH <sub>3</sub> ) <sub>2</sub> , <u>7</u>	126
Co <sub>3</sub> (CO) <sub>7</sub> [(C <sub>6</sub> H <sub>5</sub> ) <sub>2</sub> P(CH <sub>2</sub> ) <sub>2</sub> P(C <sub>6</sub> H <sub>5</sub> ) <sub>2</sub> ]C-CO <sub>2</sub> CH(CH <sub>3</sub> ) <sub>2</sub> , <u>8</u>	126
Co <sub>3</sub> (CO) <sub>7</sub> [(C <sub>6</sub> H <sub>5</sub> ) <sub>2</sub> As(CH <sub>2</sub> ) <sub>2</sub> P(C <sub>6</sub> H <sub>5</sub> ) <sub>2</sub> ]C-CO <sub>2</sub> CH(CH <sub>3</sub> ) <sub>2</sub> , <u>9</u>	127
(C <sub>5</sub> H <sub>5</sub> )MoCo <sub>2</sub> (CO) <sub>8</sub> C-CO <sub>2</sub> CH(CH <sub>3</sub> ) <sub>2</sub> , <u>10</u>	128
(C <sub>5</sub> H <sub>4</sub> CH <sub>3</sub> )MoCo <sub>2</sub> (CO) <sub>8</sub> C-CO <sub>2</sub> CH(CH <sub>3</sub> ) <sub>2</sub> , <u>11</u>	128
[C <sub>5</sub> (CH <sub>3</sub> ) <sub>5</sub> ]MoCo <sub>2</sub> (CO) <sub>8</sub> C-CO <sub>2</sub> CH(CH <sub>3</sub> ) <sub>2</sub> , <u>12</u>	129
(C <sub>5</sub> H <sub>5</sub> )WCo <sub>2</sub> (CO) <sub>8</sub> C-CO <sub>2</sub> CH(CH <sub>3</sub> ) <sub>2</sub> , <u>13</u>	130
(C <sub>5</sub> H <sub>4</sub> CH <sub>3</sub> )WCo <sub>2</sub> (CO) <sub>8</sub> C-CO <sub>2</sub> CH(CH <sub>3</sub> ) <sub>2</sub> , <u>14</u>	131
[C <sub>5</sub> (CH <sub>3</sub> ) <sub>5</sub> ]WCo <sub>2</sub> (CO) <sub>8</sub> C-CO <sub>2</sub> CH(CH <sub>3</sub> ) <sub>2</sub> , <u>15</u>	132
[C <sub>5</sub> (CH <sub>3</sub> ) <sub>5</sub> ]MoCo <sub>2</sub> (CO) <sub>6</sub> [(C <sub>6</sub> H <sub>5</sub> ) <sub>2</sub> P(CH <sub>2</sub> ) <sub>2</sub> P(C <sub>6</sub> H <sub>5</sub> ) <sub>2</sub> ]C- CO <sub>2</sub> CH(CH <sub>3</sub> ) <sub>2</sub> , <u>16</u>	132

$[\text{C}_5(\text{CH}_3)_5]\text{WCo}_2(\text{CO})_6[(\text{C}_6\text{H}_5)_2\text{As}(\text{CH}_2)_2\text{P}(\text{C}_6\text{H}_5)_2]\text{C}-$ $\text{CO}_2\text{CH}(\text{CH}_3)_2$ , <u>17</u>	133
$\text{Co}_3(\text{C}_5\text{H}_5)_2(\text{CO})_4\text{C}-\text{C}_6\text{H}_5$ , <u>19</u>	134
$\text{Co}_3(\text{CO})_9\text{C}-(3,4-(\text{CH}_3)_2\text{C}_6\text{H}_3)$	135
$\text{Co}_3(\text{C}_5\text{H}_5)_2(\text{CO})_4\text{C}-(3,4-(\text{CH}_3)_2\text{C}_6\text{H}_3)$ , <u>20</u>	135
$\text{Co}_3(\text{CO})_9\text{C}-\text{CH}(4-\text{ClC}_{10}\text{H}_6)_2$ , <u>26</u>	136
$(\text{C}_5\text{H}_5)\text{Mo}(\text{CO})_2\text{Co}_2(\text{CO})_6\text{C}-\text{CO}_2\text{C}_{17}\text{O}_3\text{H}_{22}$ , <u>30</u>	137
$(\text{C}_5\text{H}_5)\text{Mo}(\text{CO})_2\text{Co}_2(\text{CO})_6\text{C}-\text{CO}_2-\text{C}_{10}\text{H}_{17}$ , <u>31</u>	138
 (7.4) Crystallography Tables	
$\text{Co}_3(\text{C}_5\text{H}_5)_2(\text{CO})_4\text{C}-\text{C}_6\text{H}_5$ , <u>19</u>	139
$\text{Co}_3(\text{CO})_9\text{C}-\text{CH}(4-\text{ClC}_{10}\text{H}_6)_2$ , <u>26</u>	145
$[\text{C}_5(\text{CH}_3)_5]\text{Mo}(\text{CO})_2\text{Co}_2(\text{CO})_6\text{C}-\text{CO}_2\text{CH}(\text{CH}_3)_2$ , <u>12</u>	153
References	162

## LIST OF TABLES

Table 1:	Groups Incorporated into the $\text{Co}_3(\text{CO})_9\text{C-R}$ Cluster Using the $\text{R-CCl}_3$ Reaction [5]	2
Table 2:	Clusters Prepared via the $[\text{PF}_6^-]$ Salts [13]	7
Table 3:	Polyhedra Shapes: <i>Closo</i> Clusters	13
Table 4:	Polyhedra Shapes: <i>Nido</i> and <i>Arachno</i> Clusters	14
Table 5:	Electronic Donations of Various Ligands	17
Table 6:	NMR Parameters of Several Nuclei [60]	38
Table 7:	Calculated Energies for Rotational Isomers of $\text{Co}_3(\text{C}_5\text{H}_5)_2(\text{CO})_4\text{C-C}_6\text{H}_5$	74
Table 8:	$^1\text{H}$ NMR Data of 1,1,1-trichloro-2,2-di-(4'-chloronaphthyl-1')-ethane, <u>25</u>	79
Table 9:	Calculated $\Delta\text{G}$ Values for the "Up" and "Down" Isomers of Molecules <u>10</u> , <u>11</u> , <u>13</u> , and <u>14</u>	105
Table 10A:	Crystal and Data Collection Parameters for $\text{Co}_3(\text{C}_5\text{H}_5)_2(\text{CO})_4\text{C-C}_6\text{H}_5$	139
Table 10B:	Atomic Positional Parameters and Temperature Factors ( $\text{\AA}^2$ ) for $(\text{C}_5\text{H}_5)_2\text{Co}_3(\text{CO})_4\text{C-C}_6\text{H}_5$	140
Table 10C:	Hydrogen Positional Parameters for $(\text{C}_5\text{H}_5)_2\text{Co}_3(\text{CO})_4\text{C-C}_6\text{H}_5$	141
Table 10D	Anisotropic Temperature Factors ( $\text{\AA}^2$ )( $\times 10^3$ ) for $(\text{C}_5\text{H}_5)_2\text{Co}_3(\text{CO})_4\text{C-C}_6\text{H}_5$	142
Table 10E:	Selected Bond Distances and Angles for $\text{Co}_3(\text{C}_5\text{H}_5)_2(\text{CO})_4\text{C-C}_6\text{H}_5$	143

Table 11A:	Crystal and Data Collection Parameters for $\text{Co}_3(\text{CO})_9\text{C-CH(4-ClC}_{10}\text{H}_6)_2$	145
Table 11B:	Atomic Positional Parameters and Temperature Factors ( $\text{\AA}^2$ ) for $\text{Co}_3(\text{CO})_9\text{C-CH(4-ClC}_{10}\text{H}_6)_2$	147
Table 11C:	Hydrogen Atom Positional Parameters and Temperature Factors ( $\text{\AA}^2$ ) for $\text{Co}_3(\text{CO})_9\text{C-CH(4-ClC}_{10}\text{H}_6)_2$	149
Table 11D:	Selected Bond Distances and Angles for $\text{Co}_3(\text{CO})_9\text{C-CH(4-ClC}_{10}\text{H}_6)_2$	150
Table 12A:	Crystal and Data Collection Parameters for $[\text{C}_5(\text{CH}_3)_5]\text{Mo}(\text{CO})_2\text{Co}_2(\text{CO})_6\text{C-CO}_2\text{CH}(\text{CH}_3)_2$	153
Table 12B:	Atomic Positional Parameters and Temperature Factors ( $\text{\AA}^2$ ) for $[\text{C}_5(\text{CH}_3)_5]\text{Mo}(\text{CO})_2\text{Co}_2(\text{CO})_6\text{C-CO}_2\text{CH}(\text{CH}_3)_2$	155
Table 12C:	Hydrogen Positional Parameters for $[\text{C}_5(\text{CH}_3)_5]\text{Mo}(\text{CO})_2\text{Co}_2(\text{CO})_6\text{C-CO}_2\text{CH}(\text{CH}_3)_2$	157
Table 12D:	Anisotropic temperature factors ( $\text{\AA}^2$ )( $\times 10^4$ ) for $[\text{C}_5(\text{CH}_3)_5]\text{Mo}(\text{CO})_2\text{Co}_2(\text{CO})_6\text{C-CO}_2\text{CH}(\text{CH}_3)_2$ with standard errors in parentheses.	158
Table 12E:	Selected Bond Distances and Angles for $[\text{C}_5(\text{CH}_3)_5]\text{Mo}(\text{CO})_2\text{Co}_2(\text{CO})_6\text{C-CO}_2\text{CH}(\text{CH}_3)_2$	160

## LIST OF SCHEMES

Scheme 1:	The Trichloroalkane Reaction in Cluster Preparation	2
Scheme 2:	The Aryl-Mercurial Reaction	4
Scheme 3:	Preparation of $\text{Co}_3(\text{CO})_9\text{C-arene}$	6
Scheme 4:	A Process Catalyzed by a $\text{Co}_3(\text{CO})_9\text{CR}$ Cluster	30
Scheme 5:	Preparation of $\text{Co}_3(\text{CO})_4(\text{C}_5\text{H}_5)_2\text{C-(3,4-(CH}_3)_2\text{C}_6\text{H}_3)$	71
Scheme 6:	Preparation of $(\text{C}_5\text{H}_5)\text{Mo}(\text{CO})_2\text{Co}_2(\text{CO})_6\text{C-CO}_2\text{-C}_{17}\text{O}_3\text{H}_{22}$ , <u>30</u>	115



## LIST OF FIGURES

Figure 1:	X-Ray Diffraction Crystal Structure of $\text{Co}_3(\text{CO})_9\text{CCH}_3$	8
Figure 2:	X-Ray Diffraction Crystal Structures of <u>4</u> , <u>5</u> and <u>6</u>	9
Figure 3:	Proposed Geometries of the Acylium Cation	10
Figure 4:	Electron Density in s, p, and d Orbitals	11
Figure 5:	$\text{B}_2\text{H}_6$ , Containing Three-Centre Two-Electron Bonds	12
Figure 6:	Bonding Molecular Orbitals of $\text{B}_6\text{H}_6^{-2}$	15
Figure 7:	d Electrons of the Transition Metals	16
Figure 8:	Molecular Orbital Diagram of $\text{Co}_3(\text{CO})_9\text{CH}$	18
Figure 9:	Hybridized Transition Metal Orbitals	21
Figure 10:	Frontier Orbitals Remaining on the Transition Metal After Coordination	22
Figure 11:	Hybridization of Remaining M.O.'s	22
Figure 12:	Frontier Orbitals of the $\text{Co}(\text{CO})_3$ Moiety	23
Figure 13:	Frontier Orbitals of the CH Fragment	23
Figure 14:	A Cyclo-Oligomerization Using a Catalyst	29
Figure 15:	Chirality by Virtue of the Skeleton	31
Figure 16:	Chirality Via Natural Products	32
Figure 17:	Chirality From a Bidentate Ligand	33
Figure 18:	Chirality Upon Cessation of Fluxionality	33
Figure 19:	Possible Intramolecular Carbonyl Motions	40
Figure 20:	$\text{Co}_3(\text{CO})_7(\text{DIPHOS})\text{C}-\text{CO}_2\text{CH}(\text{CH}_3)_2$ , Displaying <i>Cis</i> and <i>Trans</i> Nature of Chelate Protons	41

Figure 21:	Carbonyl Exchange in the Presence of a Bidentate Ligand	42
Figure 22:	$^{13}\text{C}$ NMR Spectrum of <u>9</u> , Carbonyl Region, S.F. = 62.9 MHz, T = 193 K	43
Figure 23:	Variable Temperature $^1\text{H}$ NMR Spectrum of $\text{Co}_3(\text{CO})_7(\text{ARPHOS})\text{C}-\text{CO}_2\text{CH}(\text{CH}_3)_2$ , <u>9</u> , S.F. = 250 MHz, Isopropyl Methyl Region	44
Figure 24:	Variable Temperature $^1\text{H}$ NMR Spectrum of <u>9</u> , Methylene Bridge Region, S.F. = 250 MHz, with Racemization Mechanisms	46
Figure 25:	Low Temperature $^{13}\text{C}$ NMR Spectrum of <u>9</u> , S.F. = 250 MHz, T = 183 K	47
Figure 26 A:	X-Ray Diffraction Crystal Structure of $\text{Co}_3(\text{CO})_7(\text{ARPHOS})\text{C}-\text{CO}_2\text{CH}(\text{CH}_3)_2$ , <u>9</u>	48
Figure 26 B:	X-Ray Diffraction Crystal Structure of $\text{Co}_3(\text{CO})_7(\text{ARPHOS})\text{C}-\text{CO}_2\text{CH}(\text{CH}_3)_2$ , showing half-chair conformation, (phenyl rings omitted for clarity)	48
Figure 27:	Variable Temperature $^{13}\text{C}$ NMR Spectrum of <u>12</u> , Carbonyl Region, S.F. = 69.2 MHz	50
Figure 28:	Variable Temperature $^{13}\text{C}$ NMR Spectra of <u>16</u> , Carbonyl Region, S.F. = 62.9 MHz	52
Figure 29 A:	Parent Peak Region of the FAB Mass Spectrum of $[\text{C}_5(\text{CH}_3)_5]\text{MoCo}_2(\text{CO})_6(\text{DIPHOS})\text{C}-\text{CO}_2\text{CH}(\text{CH}_3)_2$ , With Simulated Peak Envelope	56
Figure 29 B:	FAB Mass Spectrum of $[\text{C}_5(\text{CH}_3)_5]\text{MoCo}_2(\text{CO})_6(\text{DIPHOS})\text{C}-\text{CO}_2\text{CH}(\text{CH}_3)_2$	55
Figure 30:	Proposed Structure and $^{13}\text{C}$ NMR Assignments of <u>18</u>	61
Figure 31:	Molecular Orbital Diagram of the Fragments of $\text{Co}_3(\text{CO})_9\text{C}-\text{C}_6\text{H}_5$ , <u>4</u>	62

Figure 32:	Disordered Structures Observed in the X-Ray Diffraction Crystal Structure of $\text{Co}_3(\text{CO})_9\text{C}-\text{C}_6\text{H}_5$ , <u>4</u>	63
Figure 33:	Molecular Orbital Overlap in $\text{Fe}_2\text{Co}(\text{CO})_{10}\text{C}-(4-\text{CH}_3\text{C}_6\text{H}_4)$	63
Figure 34:	X-Ray Diffraction Crystal Structures of $(\text{C}_5\text{H}_5)\text{Mo}(\text{CO})_2\text{Co}_2(\text{CO})_6\text{C}-\text{C}_6\text{H}_5$ and $(\text{C}_5\text{H}_5)\text{W}(\text{CO})_2\text{Co}_2(\text{CO})_6\text{C}-(4-\text{CH}_3\text{C}_6\text{H}_4)$	64
Figure 35:	Structures of $\text{W}(\text{CO})_4\text{Re}(\text{CO})_5\text{Co}_2(\text{CO})_6\text{C}-(4-\text{CH}_3\text{C}_6\text{H}_4)$ and $\text{W}(\text{CO})_4\text{Re}(\text{CO})_5\text{Rh}_2(\text{C}_9\text{H}_7)_2-(\mu-\text{CO})\text{C}-(4-\text{CH}_3\text{C}_6\text{H}_4)$	65
Figure 36:	X-Ray Diffraction Crystal Structure of $\text{Fe}_2(\text{CO})_6(\mu-\text{CO})\text{W}(\text{C}_5\text{H}_5)(\text{CO})_2\text{C}-(4-\text{CH}_3\text{C}_6\text{H}_4)$	65
Figure 37:	A Second Explanation for the NMR Data -- Two Isomers Related to Carbonyl Distribution	66
Figure 38:	X-Ray Diffraction Crystal Structure of $\text{Co}_3(\text{C}_5\text{H}_5)_2(\text{CO})_4\text{C}-\text{C}_6\text{H}_5$ , <u>19</u>	68
Figure 39:	Two Possible Scenarios for Cessation of Fluxionality Upon Cooling of $\text{Co}_3(\text{C}_5\text{H}_5)_2(\text{CO})_4\text{C}-\text{C}_6\text{H}_5$ , <u>19</u>	70
Figure 40:	Possible Positions of the Xylyl Ring in <u>20</u> if Rotation Ceases on the NMR Timescale	71
Figure 41:	Space-Filling Diagrams of the Two Limiting Orientations of $\text{Co}_3(\text{CO})_4(\text{C}_5\text{H}_5)_2\text{C}-\text{C}_6\text{H}_5$	73
Figure 42:	Two Possible Orientations of the Capping Group With Respect to the Tetrahedron	77
Figure 43:	Two-Dimensional Proton-Proton Correlated NMR Spectrum of <u>25</u>	79
Figure 44:	X-Ray Diffraction Crystal Structure of $\text{Co}_3(\text{CO})_9\text{C}-(4-\text{ClC}_{10}\text{H}_6)_2$ , <u>26</u>	82

Figure 44 A:	X-Ray Diffraction Crystal Structure of $\text{Co}_3(\text{CO})_9\text{C}-(4\text{-ClC}_{10}\text{H}_6)_2$ , <u>26</u> , Showing Van Der Waals' Radii	82A
Figure 44 B:	X-Ray Diffraction Crystal Structure of $\text{Co}_3(\text{CO})_9\text{C}-(4\text{-ClC}_{10}\text{H}_6)_2$ , <u>26</u> , Space-filling Model	82B
Figure 45 A:	X-Ray Diffraction Crystal Structure of the Chlorophenyl Analogue to <u>26</u> , $\text{Co}_3(\text{CO})_9\text{C}-\text{CH}-(4\text{-ClC}_6\text{H}_4)_2$ , <u>21</u>	83
Figure 45 B:	Space-filling Models of $\text{Co}_3(\text{CO})_9\text{C}-\text{CH}-(4\text{-ClC}_6\text{H}_4)_2$ , <u>21</u> , and $\text{Co}_3(\text{CO})_9\text{C}-\text{CH}-(4\text{-ClC}_{10}\text{H}_6)_2$ , <u>26</u>	83
Figure 46:	Space-Filling Model of Cluster <u>21</u> : Two Conformations Generated by Rotation of the Phenyl Ring from its Crystallographic Position	84
Figure 47:	X-Ray Diffraction Crystal Structure of $(\text{C}_5\text{H}_5)\text{WCo}_2(\text{CO})_8\text{C}-(4\text{-CH}_3\text{C}_6\text{H}_4)$ , <u>27</u> , and $(\text{C}_5\text{H}_5)\text{MoCo}_2((\text{CO})_8\text{C}-\text{C}_6\text{H}_5)$ , <u>28</u>	87
Figure 48:	X-Ray Diffraction Crystal Structure of $\text{Fe}_3(\text{CO})_6(\mu\text{-CO})_2-(\eta^5\text{-C}_5\text{H}_5)\text{C}-\text{OCH}_3$	88
Figure 49:	Low Temperature $^{13}\text{C}$ NMR Spectrum of <u>10</u> , Carbonyl Region, T = 190 K, S.F. = 125 MHz	90
Figure 50:	Possible Distributions of Carbonyl Ligands about the Clusters	90
Figure 51:	Mechanism of Isomer Interconversion	92
Figure 52:	A Second Possible Mechanism of Isomer Interconversion	92
Figure 53:	Low Temperature $^{13}\text{C}$ NMR Spectra, Carbonyl Region, of Molecules <u>10</u> , <u>11</u> , <u>13</u> , and <u>14</u>	96

Figure 54:	Infrared Spectrum of $(C_5H_4CH_3)W(CO)_2Co_2-(CO)_6C-CO_2CH(CH_3)_2$ , <u>14</u> , Carbonyl Region, $(CH_2Cl_2)$	97
Figure 55:	Low Temperature $^{13}C$ NMR Spectrum of <u>29</u> , Carbonyl Region, $T = 190$ K	99
Figure 56:	Solution $(CH_2Cl_2)$ and Solid State (KBr) Infrared Spectra of <u>29</u> , Carbonyl Region	102
Figure 57:	Infrared Spectra of <u>14</u> , Solution $(CH_2Cl_2)$ and Solid State (KBr), Carbonyl Region	103
Figure 58:	Limiting Low Temperature $^{13}C$ NMR Spectrum of <u>12</u> and <u>15</u> , Carbonyl Region, $T = 190$ K, S.F. = 125 MHz	106
Figure 59:	X-Ray Diffraction Crystal Structure of $[(\eta^5-C_2B_9H_9(CH_3)_2)W(CO)_2Co_2(CO)_6C-C_6H_5] [P(C_6H_5)_4]^+$	107
Figure 60:	Solution $(CH_2Cl)_2$ and Solid State (KBr) Infrared Spectra of <u>12</u> , Carbonyl Region	108
Figure 61:	X-Ray Diffraction Crystal Structure of <u>12</u>	110
Figure 62:	Generation of Atomic Coordinates Through Rotation of the Vertex About an Axis	112
Figure 63:	Low Temperature $^{13}C$ NMR Spectrum of <u>30</u> , Carbonyl Region, S.F. = 125 MHz	116
Figure 64:	Carbonyl Group Exchange Under Varying Cyclopentadienyl Ring Positions	117
Figure 65:	Variable Temperature $^{13}C$ NMR Spectrum of <u>31</u> , Carbonyl Region, S.F. = 125 MHz	119

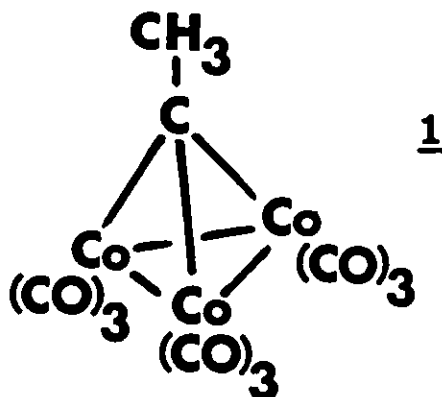
## CHAPTER ONE

The study of organometallic chemistry is one of the newest and most interesting areas of chemistry today. There is so much information yet to be discovered. The potential uses of these molecules are vast: already there has been application of organometallics in synthesis and catalysis, in the electronics industry, and in biomedicine. Clusters are particularly intriguing because of the possibility of designing them to fit our specifications. Daily, the journals are filled with new complexes, and each article has something new to teach us about the workings of organometallic molecules -- their structures, their interactions with other compounds, and the processes occurring within the molecules themselves.

### (1.1) COBALT CLUSTER HISTORY

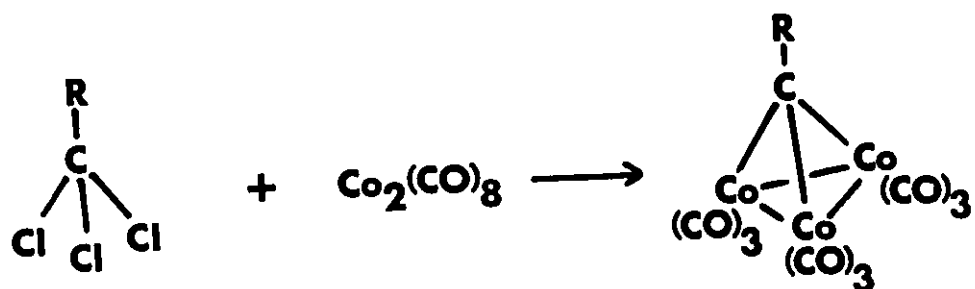
#### (1.1.1) SYNTHESIS

Tetrahedral tricobalt monocarbon clusters have been known since the late 1950's. The first reported molecule of this kind was discovered when the dicobalt cluster  $\text{Co}_2(\text{CO})_6\text{C}_2\text{H}_2$  was heated in methanol solution in the presence of aqueous sulfuric acid to give  $\text{Co}_3(\text{CO})_9\text{C-CH}_3$ , 1 [1].



It was not long before an improved synthesis of the tricobalt clusters was reported. Reaction of a trichlorinated organic compound with dicobalt octacarbonyl was found to lead to the replacement of the three chlorine atoms by  $\text{Co}(\text{CO})_3$  moieties [2,3,4].

Scheme 1: The Trichloroalkane Reaction in Cluster Preparation



This technique has been widely utilized since that time to synthesize tricobalt clusters with a variety of groups bound to the carbonyl carbon. A selection of these groups is presented in Table 1.

Table 1: Groups Incorporated into the  $\text{Co}_3(\text{CO})_9\text{C-R}$  Cluster Using the  $\text{R-CCl}_3$  Reaction [5]

Type of Group	R	Percent Yield
halogen	Cl	46
aliphatic	$\text{CH}_3$	43
aromatic	$\text{C}_6\text{H}_5$	29
silyl	$\text{Si}(\text{CH}_3)_3$	41
esters	$\text{C}(=\text{O})\text{OCH}_2\text{CH}_3$	53
alcohols	$\text{CH}_2\text{OH}$	0.8
alkenes	$\text{CH}=\text{CH}_2$	45

Though the synthesis of the clusters must be carried out in an anhydrous, oxygen-free environment because of the air-sensitivity of the  $\text{Co}_2(\text{CO})_8$  starting material, the finished products are mostly air-stable, with melting points generally above 373 K. The complexes are strongly coloured, commonly deep purples, greens, and browns, which aids in the purification process.

### (1.1.2) REACTIVITY

With a large number of compounds available, the reactivity of the tetrahedral clusters became of major interest. The bulk of the reactions fall into three categories: (i) carbonyl substitution; (ii) manipulation of the apical group; and (iii) vertex replacement.

#### (1.1.2.1) CARBONYL SUBSTITUTION

Many ligands other than the carbonyl group are readily reactive with tricobalt complexes. Arsines and phosphines, which are the focus of the study in Chapter Two, are two electron donors, and thus an arsine or phosphine can replace one carbonyl group on a complex [6,7]. Substitution of three carbonyl ligands on one cobalt vertex by a six-electron-donor arene ring can be accomplished by heating the cluster  $\text{Co}_3(\text{CO})_9\text{C-R}$  ( $\text{R} = \text{CH}_3, \text{C}_6\text{H}_5, \text{F}$ ) in an excess of arene [8], resulting in a very labile product -- when left in air, many of these products revert to the nonacarbonyl complex.

Replacement of the axial carbonyls on each cobalt moiety is achieved via heating of cyclooctatetraene (COT) under reflux with the  $\text{Co}_3(\text{CO})_9\text{C-R}$  cluster. This compound is fluxional and loses COT easily, regenerating the original molecule in air [9].

Donors of odd numbers of electrons can replace carbonyl groups also, as



seen with the cyclopentadienyl (Cp) ligand, a five e<sup>-</sup> donor: the resulting cluster bears two Cp ligands on adjacent Co vertices, with a carbonyl group bridging the two Co atoms of interest [10]. This system will be studied in further detail in Chapter Three.

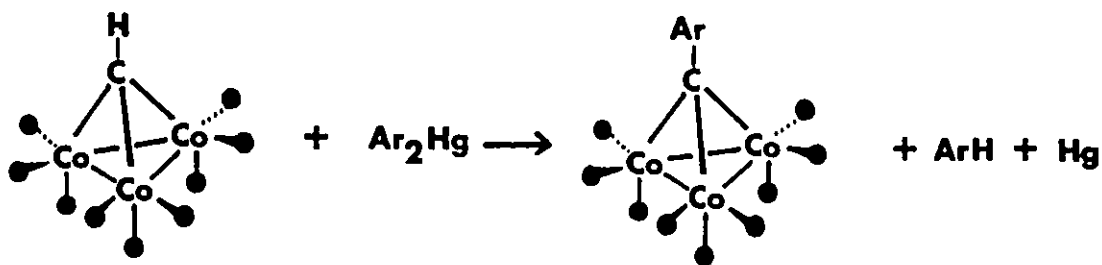
The important factor in these substitutions is that upon replacement of the carbonyl groups, the incoming ligand donates the correct amount of electrons to the cobalt vertex to complete its shell of eighteen electrons. The cobalt atom, as a transition metal, is most stable when its effective atomic number (EAN) includes eighteen electrons in its valence shell; this corresponds to filled s, p and d shells [11].

#### (1.1.2.2) APICAL GROUP MANIPULATION

The apical carbon can be bound to a wide variety of alkyl groups which can undergo "normal" organic reactions, but also the groups can react in some less-common ways, some of which will be discussed here.

It was found that the tricobalt system bearing a CH vertex would react with aryl mercurials (Ar<sub>2</sub>Hg) under heat to replace the H with an arene ring [12].

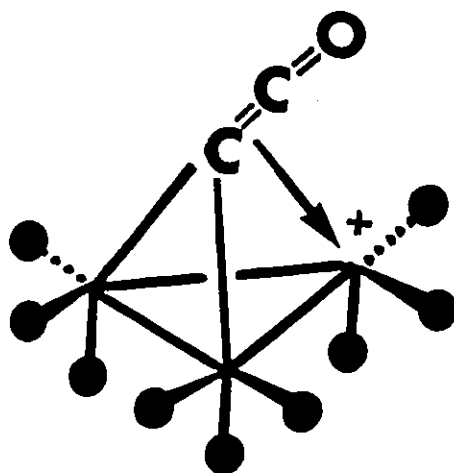
Scheme 2: The Aryl-Mercurial Reaction



The new bond to the aryl ring forms at the point on the ring where the Hg was bound, and consequently the reaction is subject to steric hindrance in the aryl groups. Organomercurials with bulky *ortho* substituents on the aryl rings will not react,

and *para*-substituted rings react in greater yield than those with groups in the *ortho* position. The analogous reaction with aliphatic groups requires much longer reaction times and gives significantly lower yields. As such, the reaction is only applicable for aryl substitution onto the cluster.

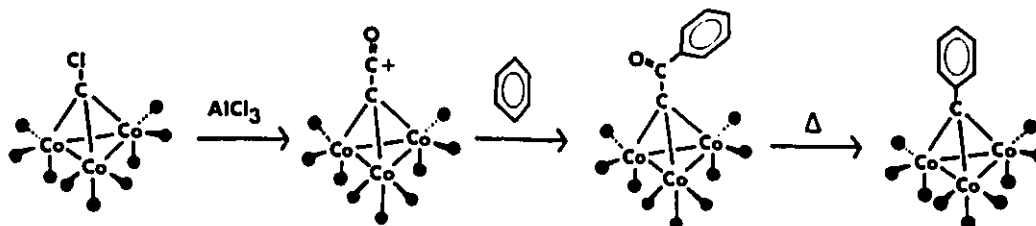
The tricobalt molecules are susceptible to destruction by base: an attempted base hydrolysis of  $\text{Co}_3(\text{CO})_9\text{C-CO}_2\text{CH}_2\text{CH}_3$  by  $\text{Na}_2\text{CO}_3$  results in complete loss of the cluster [13]. The systems are not destroyed by Lewis acids or protonic acids, however, which leads to some very useful reactions. A cluster bearing an ester functionality on the apical carbon atom, when mixed with  $\text{H}_2\text{SO}_4$ , shows attack on the ester carbonyl group, resulting in a yellow-brown cloudy solution. Quenching the reaction with water leaves the cluster with a carboxylic acid group in place of the ester. When the intermediate is allowed to react instead with an alcohol, a new ester is formed. The intermediate formed is proposed to be a tricobalt-monocarbon-deca-carbonyl cation, in which the positive charge is localized on the carbonyl group on the apical carbon, 2. Previously unknown clusters such as  $\text{Co}_3(\text{CO})_9\text{C-CO}_2\text{CH}(\text{CH}_3)_2$  and  $\text{Co}_3(\text{CO})_9\text{C-CO}_2\text{CH}_2\text{CH}_2\text{OH}$  are preparable using this reaction, but the sulphuric acid is too harsh to be used in conjunction with some nucleophiles of interest. Another route was necessary for preparation of the intermediate cationic cluster.



2

Addition of  $\text{AlCl}_3$  to a halogen-capped cluster,  $\text{Co}_3(\text{CO})_9\text{C-X}$ , in  $\text{CH}_2\text{Cl}_2$  solution will also produce a yellow-brown reaction mixture [14]. This solution is stable for days under a nitrogen atmosphere, and will react with aryl rings in a Friedel-Crafts fashion, via electrophilic substitution at the most activated site(s) on the ring [15]. Initially, the complex  $[\text{Co}_3(\text{CO})_9\text{CCO}^+][\text{AlCl}_3\text{X}^-]$  is formed, followed by electrophilic attack on the aromatic ring. The final step is a decarbonylation to lose the group bridging the apical carbon to the aromatic ring (Scheme 3). Because the decarbonylation is facile at elevated temperatures, the reaction intermediate is not isolated [16].

Scheme 3: Preparation of  $\text{Co}_3(\text{CO})_9\text{C-arene}$



Seyferth *et al.* discovered that the cation can also be prepared as a stable salt of  $\text{HPF}_6$  (or analogously with  $\text{HBF}_4$ ), forming shiny black crystals [13]. The salt is made by addition of  $\text{HPF}_6$  in propionic anhydride to any cluster bearing an ester as the apical group. The  $[\text{Co}_3(\text{CO})_9\text{CCO}^+][\text{PF}_6^-]$  crystals can be filtered out of the reaction mixture and stored under nitrogen until further use.

The advantage to cation preparation in this manner is that the mass of the salt can be accurately measured, an impossibility with the  $\text{AlCl}_3$ -generated cation in solution. Thus, further stoichiometrically-correct reactions are possible using this

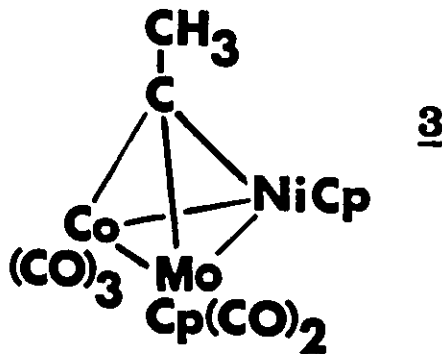
synthesis, and the intermediate may be characterized. The  $[\text{Co}_3(\text{CO})_9\text{CCO}^+]\text{PF}_6^-$  cluster has been used in the preparation of several previously unknown clusters, as shown in Table 2.

Table 2: Clusters Prepared via the  $[\text{PF}_6^-]$  Salts [13]

Nucleophile	Product
$\text{CH}_3\text{CH}_2\text{SH}$	$\text{Co}_3(\text{CO})_9\text{CC}(=\text{O})\text{SCH}_2\text{CH}_3$
$\text{NH}_3$	$\text{Co}_3(\text{CO})_9\text{CC}(=\text{O})\text{NH}_2$
$\text{CH}_3\text{NH}_2$	$\text{Co}_3(\text{CO})_9\text{CC}(=\text{O})\text{NHCH}_3$
$\text{HC}(=\text{O})\text{NH}_2$	$\text{Co}_3(\text{CO})_9\text{CC}(=\text{O})\text{NHC}(=\text{O})\text{H}$
$\text{Cp-Fe-Cp}$	$\text{Co}_3(\text{CO})_9\text{CC}(=\text{O})-\text{C}_5\text{H}_4-\text{Fe-Cp}$

### (1.1.2.3) VERTEX SUBSTITUTION

The  $\text{Co}(\text{CO})_3$  moiety can be replaced by other organometallic vertices resulting in heterometallic clusters, as discovered by Vahrenkamp [17]. For example, a  $\text{Co}(\text{CO})_3$  vertex can be replaced by a  $(\text{C}_5\text{H}_5)\text{Ni}$ ,  $(\text{C}_5\text{H}_5)\text{Mo}(\text{CO})_2$  or  $(\text{C}_5\text{H}_5)\text{FeCO}$  moiety, producing an cluster isoelectronic to the original. These substitutions can be effected by thermal reaction of the tricobalt molecule with the dimer of the desired new vertex, *e.g.*,  $[(\text{C}_5\text{H}_5)\text{Mo}(\text{CO})_2]_2$ . Further substitutions can occur, producing chiral systems such as 3.



The electronic criteria for one vertex to be replaced by another are explained later in the section on isolobality (Section 1.2.1.3). Cluster expansion is a vast topic and, as such, is beyond the scope of this thesis; it involves not merely vertex replacement but addition of new vertices to a system, resulting in molecules of more complex polyhedra than the tetrahedron [18].

## (1.2) STRUCTURAL STUDIES

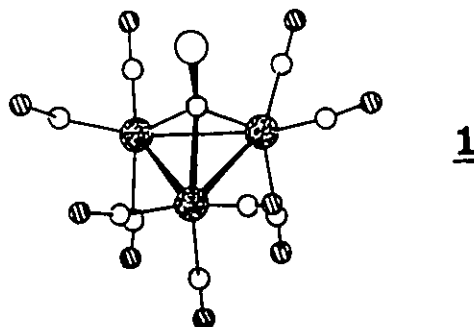
### (1.2.1) STATIC STRUCTURES

Crystallographically determined structures of the cobalt clusters show a common geometry, and theories as to why the molecules assume these structures have been developed. This section will deal with the static structures revealed by solution of the crystal structure, and the proposed reasons for the adopted shapes.

#### (1.2.1.1) X-RAY CRYSTALLOGRAPHY

The crystal structure of the first identified tricobalt-monocarbon cluster,  $\text{Co}_3(\text{CO})_9\text{C-CH}_3$ , 1, is shown in Figure 1 [19], and it has the basic appearance found in all these tricobalt clusters. The carbon vertex is placed symmetrically above all three cobalt atoms, but the tetrahedral shape is slightly distorted. The Co-Co bonds (average  $\sim 2.47 \text{ \AA}$ ) are noticeably longer than the Co-C bonds (average  $\sim 1.90 \text{ \AA}$ ). The carbonyl ligands are of two types: axial (three) and equatorial (six in total).

Figure 1: X-Ray Diffraction Crystal Structure of  $\text{Co}_3(\text{CO})_9\text{C-CH}_3$ , 1

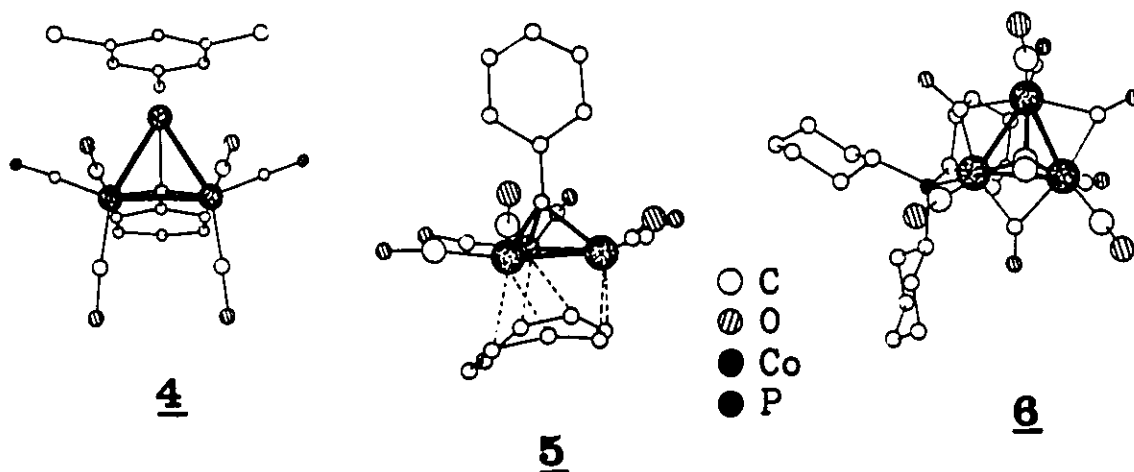


The cluster bearing a phenyl ring in place of the methyl group shows essentially identical skeletal measurements as 1, with an average Co-Co bond distance of 2.466(1) Å and average Co-C bond length of 1.906(6) Å [20]. Replacement of three carbonyl groups with a mesitylene ring  $\eta^6$ -bound to one cobalt vertex gives 4, with each ring carbon equidistant from the cobalt vertex, at a distance of 2.15(3) Å [21]. The bonds joining the mesitylene-bearing cobalt to the other two cobalt vertices are shorter (2.441(2) Å) than the linkage between the two  $\text{Co}(\text{CO})_3$  termini (2.477(3) Å).

Coordination of the polyene  $\text{C}_8\text{H}_8$  to the base of the tricobalt system produces 5, in which one Co-(apical C) bond is significantly shorter (1.85 Å) than the other Co-C bonds in the cluster (1.90 Å av.) [22].

Replacement of a carbonyl ligand by a phosphine does not have a major effect on the skeletal bond lengths. In this example, a carbonyl group of equatorial coordination has been replaced by the phosphine  $\text{P}(\text{C}_6\text{H}_{11})_3$  to produce  $\text{Co}_3(\text{CO})_8$ - (tricyclohexylphosphine)C- $\text{CH}_3$ , 6 [23].

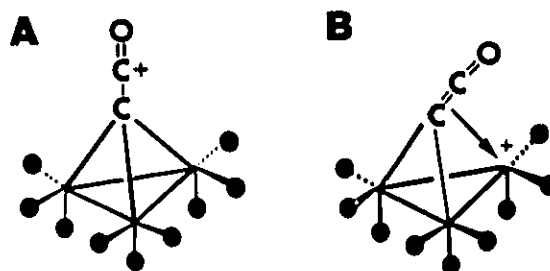
Figure 2: X-Ray Diffraction Crystal Structures of 4, 5 and 6



The basic solid-state structure in all these examples is that of a slightly distorted tetrahedron, or a triangular pyramidal structure, with the shorter bonds being the cobalt-carbon linkages in all cases, as would be expected on the basis of atomic radii.

The structures of the acylium salt  $[\text{Co}_3(\text{CO})_{10}\text{C}^+][\text{PF}_6^-]$  and other analogous salts have been the subject of some speculation, with both the linear structure A and bent geometry B (Figure 3) being proposed. Recent theoretical and experimental data favour the bent structure [24], but despite prolonged efforts, crystallographic data have not yet been obtained.

Figure 3: Proposed Geometries of the Acylium Cation



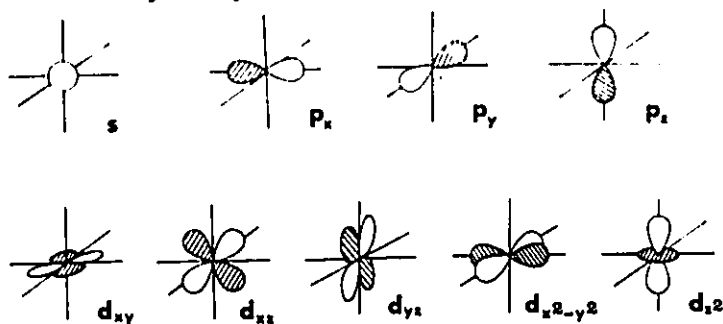
#### (1.2.1.2) MOLECULAR ORBITAL STUDIES

The structure as determined by X-ray diffraction crystallography is essentially the same for all these tricobalt-monocarbon molecules. An explanation for the observed structure can be found in molecular orbital theory, an outline of which is presented here.

Though it is difficult to observe the electronic structure of a system directly, scientists have devised a theory by which atoms may be described. Each atom has atomic orbitals, regions of space in which their electrons are likely to be found. The s electrons are in a spherical orbital centered on the nucleus. The p and d orbitals,

conversely, have a node at the nucleus, which means the **p** and **d** electrons have zero probability of being located at the atomic nucleus. These main areas of electron density are found in lobes around, rather than on, the centre of the atom. The shapes of the atomic orbitals in a transition metal are shown in Figure 4.

Figure 4: Electron Density in s, p, and d Orbitals

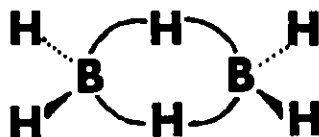


When an atom is a component of a larger molecule, the atomic orbitals can combine to form molecular orbitals [25]. These M.O.'s, as they are called, are a linear combination of the atomic orbitals. For example, two atomic orbitals of similar energy will combine ("interact") to form one molecular orbital of lower energy than either of the original atomic orbitals (an "in-phase" or "bonding" combination), and one M.O. of higher energy (an "out-of-phase" or "anti-bonding" combination). The driving force for these combinations is that upon filling the molecular orbitals with electrons, the molecule's electrons will be at a lower energy level than without the interaction *i.e.*, the electronic energy will be lower if the atoms are in the molecule than if they were isolated atoms. If the molecule has an appropriate number of electrons to allow filling of the bonding M.O.'s while leaving the antibonding orbitals vacant, stabilization of the compound will result. However, if the molecule has too many electrons to place only in the bonding M.O.'s, and if it must fill both the bonding and antibonding M.O.'s, then an effective destabilization of the molecule with respect to its constituent parts occurs, because of electron-electron repulsion.



Before we discuss organometallic complexes, it is best to describe the boranes which form clusters of many different sizes and shapes from very simple building blocks: hydrogen atoms with their s orbitals, and boron with its s and p orbitals. While molecules are often thought to have their electrons localized in bonds along edges of the cluster, with two electrons on each edge, there is another way of looking at the situation. The electrons may actually be delocalized over the entire molecule, shared between all vertices. This idea arose because of the unusual electron count in the borane clusters. Molecules such as  $B_2H_6$  do not have enough electrons to allow for "normal" bonding, *i.e.*, bonding in which a single interaction between two atoms uses two electrons. The molecule instead was proposed to have three-centre two-electron bonds, a concept of delocalized electron distribution [26].

Figure 5:  $B_2H_6$ , Containing Three-Centre Two-Electron Bonds



After studying the borane and carborane series extensively, it became clear to Wade that a pattern for bonding existed [27]. A borane cluster adopts a polyhedron of triangular faces. Each boron atom possesses three valence electrons, some of which are used to form B-H bonds. If the molecule has the formula  $B_nH_m$ , and  $(n + 1)$  electron pairs available for skeletal bonding (those electrons not used in B-H bonds), then the cluster will be closed, *closo*. If there are more electron pairs present, for example  $(n + 2)$ , with  $n$  boron vertices, the structure will be *nido*. A *nido* structure has the appearance of a *closo* structure with one vertex removed. The third common type of polyhedron is referred to as *arachno*, occurring when  $(n + 3)$  skeletal electron pairs are available to bond  $n$  vertices. This cluster has the resultant shape derived by

removing two vertices from a *closo* molecule. The polyhedra formed in the *closo* situation are presented in Table 3 and the *nido* and *arachno* derivatives in Table 4.

Table 3: Polyhedral Shapes: *Closo* Clusters




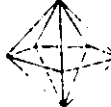
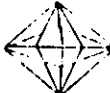













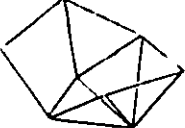
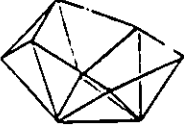




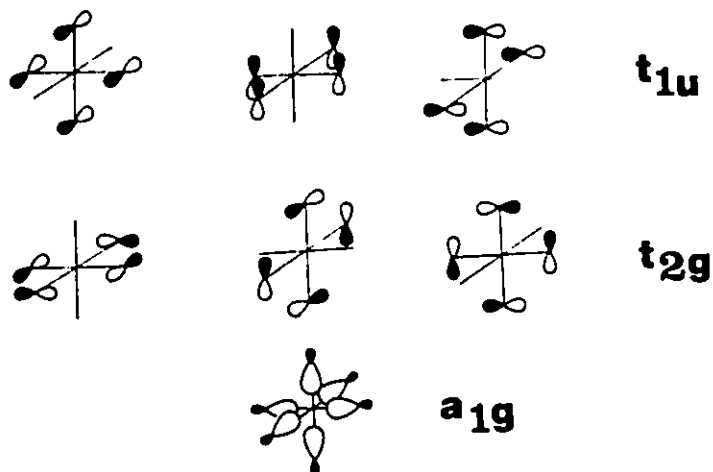
Number of Vertices	Cluster Shape	
4	tetrahedron	
5	trigonal bipyramid	
6	octahedron	
7	pentagonal bipyramid	
8	dodecahedron	
9	tricapped trigonal prism	
10	bicapped Archimedean antiprism	
11	octadecahedron	
12	icosahedron	

Table 4: Polyhedral Shapes: *Nido* and *Arachno* Clusters

Number of Vertices	<i>Nido</i> Cluster	<i>Arachno</i> Cluster
4		
5		
6		
7		
8		
9		
10		
11		

In  $B_6H_6^{2-}$ , for example, there are 12 atoms and 26 electrons, 12 of which are used in BH bonds. Thus 14 electrons (7 electron pairs) are left to hold together six boron vertices. The edge-localized view of electron distribution states that if the vertices form an octahedron, then the number of edges would be 12, requiring 12 electron pairs -- far more than actually are present in the molecule. However, consider the atomic orbitals on the boron atoms: combination of the atomic orbitals into molecular orbitals as shown in Figure 6 leads to a set of filled bonding orbitals while leaving all antibonding orbitals empty. Now the molecule which originally appeared electron-deficient when using the edge-localized model actually has the appropriate number of electrons for stability according to the delocalization theory. The molecular orbitals represent the mode by which the delocalization of electrons can occur, and these electrons can be analyzed in terms of Wade's rules to derive the expected cluster shape.

Figure 6: Bonding Molecular Orbitals of  $B_6H_6^{2-}$



The ideas developed by Wade for polyhedral cluster shapes dependent upon available electron pairs were fully extended by Mingos to transition metal systems, termed the Polyhedral Skeletal Electron Pair Theory, PSEPT [28]. The same method

of electron counting used for the boranes can be used very effectively for transition metal systems.

The relationship between M.O. theory and organotransition metal complexes was comprehensively reviewed by Albright in 1982 [29]. A metal-containing molecule is complicated because of the metal's many valence atomic orbitals (one s, three p and five d). The eighteen-electron rule for metals states that most transition metals, in order to be stable, require eighteen electrons in their valence shell (the effective atomic number, EAN) [11]. This corresponds to two electrons in each of the s, p and d orbitals.

The electron count of an isolated metal atom depends on its position in the periodic table (Figure 7). These values correspond to a metal in oxidation state zero.

Figure 7: d Electrons of the Transition Metals

d <sup>3</sup>	d <sup>4</sup>	d <sup>5</sup>	d <sup>6</sup>	d <sup>7</sup>	d <sup>8</sup>	d <sup>9</sup>	d <sup>10</sup>
Sc	Ti	V	Cr	Mn	Fe	Co	Ni
Y	Zr	Nb	Mo	Tc	Ru	Rh	Pd
La	Hf	Ta	W	Re	Os	Ir	Pt

To construct our organometallic clusters theoretically, we first build the vertices by combining the metal atom with ligands. Each metal atomic orbital has a specific symmetry, and it will only combine with a ligand orbital of matching symmetry. The convention for ligands used here is that a ligand will always donate an even number of electrons to the metal [25]. Thus, a carbonyl will donate two electrons (as neutral C=O), but a hydrogen is considered as H<sup>-</sup>, a two-electron donor. To compensate for the electron gained by the H, the metal bearing the hydride ligand will now be considered to be in oxidation state +1. (This is merely a convention, and it does

not alter the chemistry if we say instead that the hydrogen is neutral and the metal is in the oxidation state of zero.) A list of commonly encountered ligands with their donor counts is presented below.

Table 5: Electronic Donations of Various Ligands

Ligand	Number of Electrons
CO H <sup>-</sup> phosphines arsines X <sup>-</sup> (X = halogen) CNR CR <sub>2</sub> $\eta^2$ -alkenes	2
$\eta^4$ -dienes	4
$\eta^6$ -benzene Cp <sup>-</sup>	6

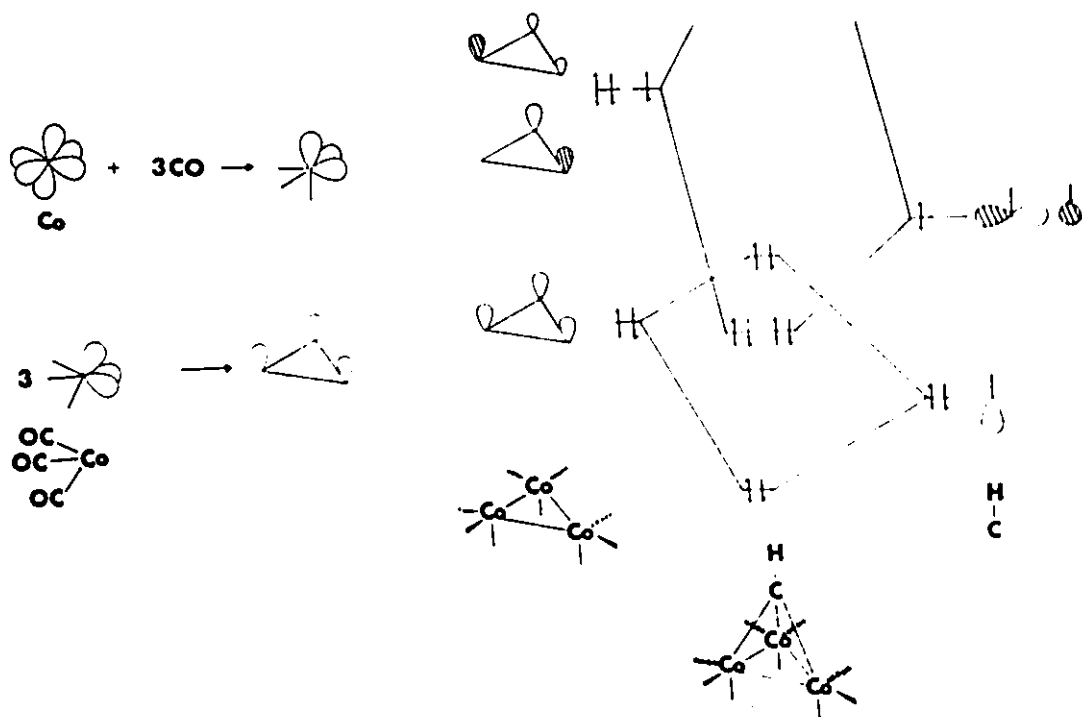
As an organometallic example of the two ways of looking at the electron distribution in these clusters, the molecule  $\text{Co}_3(\text{CO})_9\text{C-H}$  will be examined: edge-localization, wherein the EAN rule for each metal is satisfied, and globally-delocalized electron density, in which the surprising reactivity of the molecule is explained, will both be presented.

The cluster has 27 valence electrons from the cobalt atoms, 90 from the carbonyl groups, and 5 from the CH moiety. Each CO group uses 2 electrons in an oxygen lone pair and 6 electrons in the CO  $\sigma$  and  $\pi$  bonding. The C-H bond uses 2, and the Co-CO linkages use 2 electrons each. Thus the molecule is left with 12 electrons (6

electron pairs) with which to bond four vertices.

For these vertices to form a tetrahedron would require six pairs of electrons using the edge-localized electron pair model, as a tetrahedron has six edges. This fits the electron count perfectly. But why is the cluster so reactive then, undergoing vertex substitutions readily? The answer lies in the delocalized-electron explanation. The electrons are delocalized via molecular orbitals as in the borane clusters, with the difference that the transition metal uses its *d* atomic orbitals as well as the *s* and *p* orbitals. Hybridized  $d^2sp^3$  metal orbitals are considered to be those used in cluster bonding. Three unhybridized metal *d* orbitals are also available. The molecular orbital diagram is shown in Figure 8. The six electron pairs available for cluster bonding correspond to a five-vertex structure (trigonal bipyramid), but as the molecule has only four vertices, the cluster is *nido*. *Nido* clusters are notorious for their tendency to experience fluxionality [30] and their reactivity (*e.g.* vertex substitution). The behaviour of the  $\text{Co}_3(\text{CO})_9\text{C-R}$  molecules is thus rationalized.

Figure 8: Molecular Orbital Diagram of  $\text{Co}_3(\text{CO})_9\text{C-H}$



Molecular Orbital theory was originally developed for simple hydrocarbons in which each "bond" was considered to be made up of only atomic orbitals on the two directly bound atoms [31]. Aromatic molecules were described by Hückel using the approximation of interaction only between neighbouring atoms, which led to the development of the  $(4n + 2)$  rule of aromaticity [32]. It is, however, unrealistic to believe that orbital overlap will not occur between atoms separated by greater than one bond. NMR couplings occur through several bond separations, so clearly there is some orbital interaction over more than one bond. Hoffmann and Lipscomb recognized this additional orbital interaction from non-directly-bonded groups, calling it Extended Hückel Molecular Orbital theory, EHMO, and it formed the basis for global delocalization of electron density throughout the molecule [33]. The contribution by other atomic orbitals to a M.O. made up principally from atomic orbitals of two atoms will, in most cases, be small because of the increased distance and often unfavourable geometry. However, these small contributions may account for the subtle differences in structure and reactivity in the molecules. Because many different overlap integrals must be evaluated, EHMO calculations for any other than the most simple molecules are very complex, and computer programs are necessary to aid in this endeavour.

The EHMO program uses atomic positional values and parameters that are specific for the atom type to produce a set of data, including a table of all the molecular orbitals that will describe the electronic structure in a molecule. A molecular orbital described by EHMO theory may contain some small part of every valence shell atomic orbital in the compound, but usually each M.O. consists of contributions from only a few atomic orbitals on various atoms in the molecule.

The EHMO calculation also assigns a value of energy to each M.O. formed. The lowest energy molecular orbitals (corresponding to the most stable bonds) can invariably be assigned to C-H bonds (*i.e.*, most of the M.O. consists of hydrogen s and



carbon s and p atomic orbitals.) The next lowest energy M.O.'s are attributed to carbon-carbon bonds, with very little involvement from the metals' atomic orbitals.

It is generally believed that the reactivity of a molecule is determined by the highest occupied M.O. (HOMO) and lowest unoccupied M.O. (LUMO) which are comprised almost entirely of cluster-bonding orbitals (*i.e.*, the Co and apical C orbitals). Any reaction that occurs will likely involve changes in the skeletal cluster orbitals, as opposed to a C-H or C-C bond breakage, for example.

Though the numerical values for the energy of a system may not be quantitatively accurate (even Hoffmann admits this), the qualitative results are very good. The program generates a "sum of one-electron energies" for the system under scrutiny, and given a choice of conformations, that conformation with the lowest calculated energy is considered to be the favoured one. Out of a selection of possible conformations of one molecule, the EHMO-calculated favoured orientation often corresponds exactly to the experimentally observed conformation. It can be used, therefore, as a tool to predict orientational behaviour of cluster moieties. This is precisely the application that has been used in this thesis.

### (1.2.1.3) ISOLOBALITY

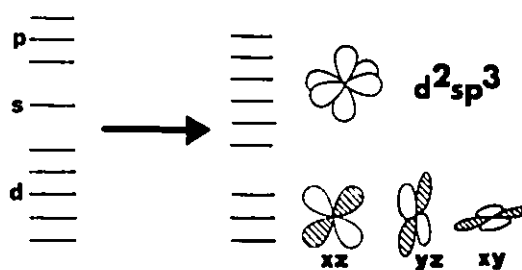
At first glance, the clusters presented in this thesis may appear to have little in common. Is  $\text{Co}_3(\text{CO})_7[(\text{C}_6\text{H}_5)_2\text{As}(\text{CH}_2)_2\text{P}(\text{C}_6\text{H}_5)_2]\text{C}-\text{CO}_2\text{CH}(\text{CH}_3)_2$  electronically similar to  $(\text{C}_5\text{H}_5)\text{Mo}(\text{CO})_2\text{Co}_2(\text{CO})_6\text{C}-\text{CO}_2$ -podocarpic acid? Could it be predicted that  $\text{W}[\text{C}_5(\text{CH}_3)_5](\text{CO})_2$  or  $\text{NiC}_5\text{H}_5$  would replace the vertex  $\text{Co}(\text{CO})_3$  in  $\text{Co}_3(\text{CO})_9\text{CR}$ ? The answers to these questions can be found in the work of Roald Hoffmann and his theory of isolobality [25,34].

Isolobality is a term coined by Hoffmann to denote that quality which accounts for the similar bonding behaviour of moieties which appear to be otherwise

completely different. A summary of the explanation will be presented here.

The valence atomic orbitals on a metal atom in a cluster can be thought of as an octahedron. As previously described, the valence orbitals of the metal, one *s*, three *p* and two of the five *d* orbitals, can be combined to form hybrids as shown in Figure 9.

Figure 9: Hybridized Transition Metal Orbitals



The hybrid  $d^2sp^3$  orbitals each point to a corner of the octahedron. If the metal bears six ligands, each ligand can interact with one of the hybrid orbitals lying along the *x*, *y* and *z* axes. As discussed before, the ligands donate pairs of electrons to the metal during bonding, and form bonding and antibonding M.O.'s in combination with the metal orbitals. The metal's electrons enter the  $t_{2g}$  (leftover *d*) orbitals and any unused  $d^2sp^3$  hybrids.

In a six-ligand complex, all six  $d^2sp^3$  hybrids would interact with incoming ligands. If the compound had only five ligands, or four, the metal would have one or two  $d^2sp^3$  hybrid orbitals left, respectively, as shown in Figure 10. The number of electrons available to fill these unused orbitals is determined by the electron counting rules presented in the section on Molecular Orbital theory, (1.2.1.2). As well, the  $t_{2g}$  set of three unhybridized metal *d* orbitals remains available for interaction with other molecular fragments.

The important point is that, depending on the number of ligands bound to

the  $O_h$  metal, the frontier orbitals can vary. The remaining  $d^2sp^3$  orbitals can hybridize as well (Figure 11).

Figure 10: Frontier Orbitals Remaining on the Transition Metal After Coordination

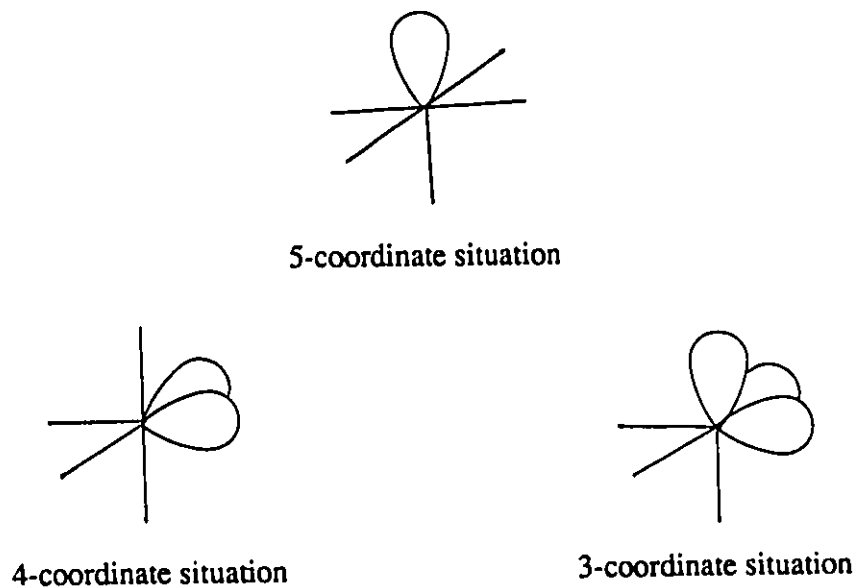
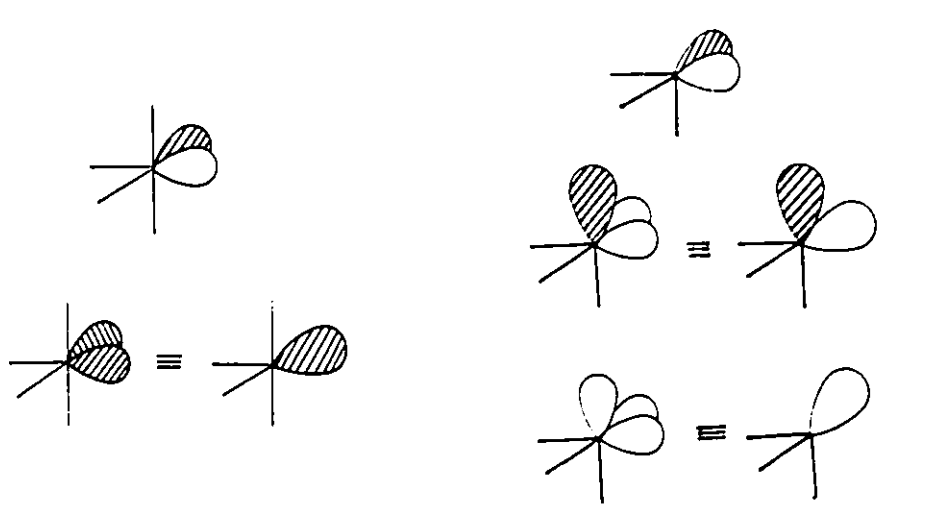
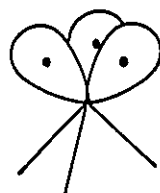


Figure 11: Hybridization of Remaining M.O.'s



As an example,  $\text{Co}(\text{CO})_3$  would use three  $d^2sp^3$  hybrids in bonding to the three carbonyl ligands. Its frontier orbitals are shown in Figure 12.

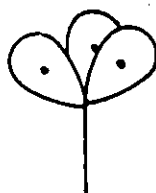
Figure 12: Frontier Orbitals of the  $\text{Co}(\text{CO})_3$  Moiety



Cobalt is  $d^9$ , which would fill the three  $t_{2g}$  orbitals and leave three electrons, one for each of the remaining  $d^2sp^3$  hybrids.

A parallel can be drawn between  $O_h$  metals and  $T_d$  carbon atoms. The  $s$  and three  $p$  orbitals on carbon can form four  $sp^3$  hybrid orbitals. If one  $H^-$  interacts with the carbon (in oxidation state +1), the  $\text{CH}$  fragment is formed, leaving three frontier orbitals on carbon. Three electrons are available on the carbon atom to enter these three  $sp^3$  orbitals, and the orbital picture formed is analogous to that of  $\text{Co}(\text{CO})_3$ .

Figure 13: Frontier Orbitals of the  $\text{CH}$  Fragment



In the case of  $\text{Co}(\text{CO})_3$  and  $\text{CH}$ , the frontier orbitals are similar in (a) symmetry; (b) energy; (c) extent in space; and (d) number.

Fragments that share these properties are said to be isolobal. The symbol denoting isolobality is an two-headed arrow with a lobe in the middle.

The utility of this designation will become clear presently. Isolobal fragments often behave in the same manner. This is not surprising, as the behaviour of fragments and molecules is directly related to their valence molecular orbitals, and isolobal fragments have essentially identical frontier orbitals. An illustration of this principle is given below.

$\text{Co}_4(\text{CO})_{12}$  is a stable molecule. It does not readily break down in air, and can be subjected to X-ray diffraction analysis with little decomposition. As  $\text{Co}(\text{CO})_3$  is isolobal with CH, it might be predicted that  $\text{Co}_3(\text{CO})_9\text{CH}$  would be stable also, and this is indeed true. Further, though the molecular orbital structure of  $\text{Mo}(\text{C}_5\text{H}_5)(\text{CO})_2$  is different from  $\text{Co}(\text{CO})_3$  because of the cyclopentadienyl ring, the frontier lobes are similar enough to define  $\text{Mo}(\text{C}_5\text{H}_5)(\text{CO})_2$  as isolobal with  $\text{Co}(\text{CO})_3$ . It is for this reason that replacement of a  $\text{Co}(\text{CO})_3$  vertex in  $\text{Co}_3(\text{CO})_9\text{C-CO}_2\text{CH}(\text{CH}_3)_2$  yields the stable  $(\text{C}_5\text{H}_5)\text{Mo}(\text{CO})_2\text{Co}_2(\text{CO})_6\text{C-CO}_2\text{CH}(\text{CH}_3)_2$ . Replacement of the capping vertex  $\text{C-CO}_2\text{CH}(\text{CH}_3)_2$  by  $\text{C-Cl}$ ,  $\text{C-CH}(\text{4-Cl-C}_6\text{H}_4)_2$  or  $\text{C-CO}_2$ -podocarpic acid does not alter the frontier orbitals of the carbon atom enough to cause instability in the resulting cluster. Thus, the molecules bearing the above-mentioned groups may look different but actually have a good deal in common -- their many similar chemical features result because their constituent vertices are isolobal.

### (1.2.2) DYNAMIC STRUCTURES

The structures presented above appear to have all parts of the molecule frozen into place, but this does not tell the whole story. Rapid intramolecular motions often occur, resulting in "averaged" structures being predicted from many spectroscopic studies. This section will discuss what these motions are, and how they can be studied.

### (1.2.2.1) FLUXIONALITY

A phenomenon often encountered in organometallic chemistry is fluxionality. This can occur in a system as, for example, carbonyl groups in motion: they appear in the crystal structure to be bound to a single metal, but in solution they move from one metal vertex to another [35]. There can be conformational fluxionality, whereby a ring flips from chair to boat conformations, for example. Fluxionality can also take the form of a skeletal rearrangement, such that a molecule of one absolute configuration becomes its enantiomer [18].

Fluxionality is observable when a molecule possesses more than one minimum energy configuration [36]. These configurations need not be equivalent, either in appearance or in energy -- they could give rise to completely different NMR and IR spectra. Fluxionality may also result in a molecule which is chemically and physically indistinguishable from the original, as in carbonyl exchange between metal vertices.

A molecule will be fluxional if the energy barrier between the energy minima can be overcome under the conditions of observation. There must also be at least one additional structure of the complex which is only slightly less stable than the lowest energy structure, and this will provide a pathway between the stable configurations.

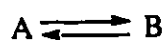
### (1.2.2.2) DETECTION METHODS

Fluxionality is observed using various methods of spectroscopy to elucidate the mechanisms. However, each technique works on a different timescale [37]. For a process which exchanges isomers once every  $10^{-10}$  seconds, the "picture must be taken" (*i.e.*, detection must be completed) in less than  $10^{-10}$  seconds. If the detection time is longer than this, the fluxional process will have occurred in this period, and the

technique will have detected an average picture of the exchanging isomers. Infrared spectroscopy can detect isomers which exchange up to  $10^{13}$  times per second. Even more extreme, X-ray diffraction is one of the fastest techniques commonly utilized in chemistry, with a timescale of  $10^{-18}$  seconds. Molecules that are fluxional in solution are often locked into one conformation by crystal packing forces in the solid state. Thus, IR spectroscopy and X-ray diffraction can be used to elucidate "instantaneous" structures.

Nuclear magnetic resonance can be used to give a good representation of one structure of a molecule only if the structure remains unchanged for more than  $10^{-1}$  to  $10^{-9}$  seconds. Fluxional processes that are faster than this will result in the NMR detector "seeing" an average of structures. Processes that exchange isomers on a timescale very close to that of the NMR machine can be studied by NMR to reveal the energy required for exchange. This is known as the "line-broadening" technique [38].

A fluxional molecule can be considered as an equilibrium with its separate conformations:



The rate of interconversion of conformers is given by equation (1).

$$k = \frac{RT e^{(-\Delta G^\ddagger/RT)}}{Nh} \quad (1)$$

where  $\Delta G^\ddagger$  = free energy of activation ( $\text{kcal mol}^{-1}$ )

R = gas constant =  $1.987 \times 10^{-3} \text{ kcal deg}^{-1} \text{ mol}^{-1}$

N = Avogadro constant =  $6.022 \times 10^{23} \text{ molecules mol}^{-1}$

h = Planck constant =  $1.584 \times 10^{-37} \text{ kcal s}$

This relationship can be applied to an NMR spectrum in which interconversion of isomers is apparent. If the isomer exchange is slow, (and if exchange does not occur during the course of detection), then a separate signal will appear in the spectrum at a specific frequency,  $\nu$ , for each conformer. If, however, exchange is faster than the NMR timescale, the two signals will be coalesced into one, with a chemical shift value equal to the weighted average of the shifts of the two separate peaks (equation (2)).

$$\nu_{\text{average}} = n_A \nu_A + n_B \nu_B \quad (2)$$

The fractions of molecules in conformations A and B are denoted by  $n_A$  and  $n_B$ , and the mole fractions  $n_A$  and  $n_B$  total one. Discrete peaks can, on occasion, be coalesced by increasing the temperature of the system. The temperature rise gives the molecules the needed energy to overcome the energy of activation barrier,  $\Delta G^\ddagger$ .

The lifetime of nuclei in environments A and B at the coalescence point is  $\tau$ , where:

$$\tau = \sqrt{2}/\pi\delta\nu \quad (3)$$

$$\delta\nu = \nu_A - \nu_B \quad (4)$$

$\delta\nu$  is the maximum separation of the signals A and B (Hz). The rate constant for the exchange from environment A to B is  $k = 1/\tau$ .

Combination of these terms into the equation, and rearrangement, gives:

$$\Delta G^\ddagger = RT_c (\ln \sqrt{2R/\pi N h} + \ln T_c / \delta\nu) \quad (5)$$



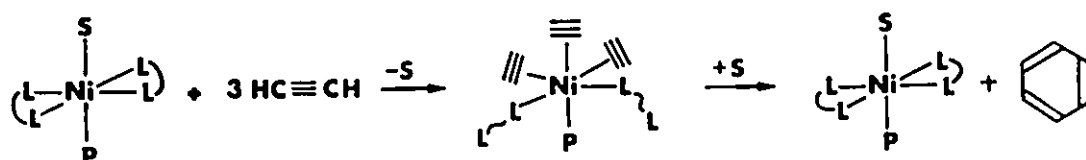
$T_c$  is the temperature of peak coalescence. The first term of the equation is a constant, 22.96. Thus, the chemical shift separation of two peaks and the temperature of coalescence can be used to give a value for the energy barrier between the two isomers represented by the peaks. It must be noted that (3) is valid only when there are equal populations in the two states at equilibrium. If there is a difference in energy between the states, the states will be unequally populated. For this reason, the energy calculation using (5) can only be performed when there is an equal distribution of the molecules between the possible isomers.

Because this technique is based upon observation of broadening of the NMR resonance signals, it is termed the "line-broadening method". It is used in this thesis to calculate the energy barrier to exchange of isopropyl methyl groups between two environments in the tetrahedral clusters of study. It cannot be applied to all our systems for various reasons: some clusters have exchange between more than two environments, which complicates the definition of  $\delta\nu$  (Chapter 2), and some examples involve molecules with unequal populations of their isomeric states (Chapter 5).

### (1.3) CATALYSIS

The interest in these organometallics is based not only in scientific curiosity but in the potential use of these compounds as catalysts in industry. An example of an organometallic complex serving as catalyst is the cyclo-oligomerization of alkynes by a nickel system, to form benzene and regenerate the organometallic molecule (Figure 14) [39].

Figure 14: A Cyclo-Oligomerization Using a Catalyst

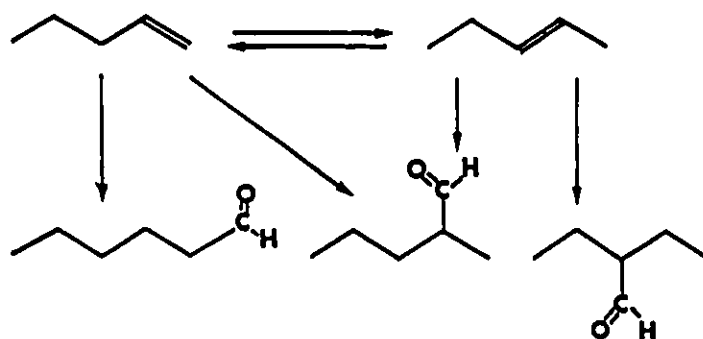


Another widely used organometallic system is the Ziegler-Natta catalyst. This involves a combination of titanium chloride and triethyl aluminum, which together catalyse production of stereoregular polypropylene from propylene monomers [40]. These systems are referred to as "homogeneous" catalysts because the reagents and catalyst are in the same phase.

"Heterogeneous" catalysts, (those in which the reagents are in solution while the catalyst is in the solid state, for example), have been previously popular, but they incur many problems. For example, it is difficult to ensure the entire surface of a catalyst is consistent, and this can lead to impure products [41]. Heterogeneous catalysts are also more susceptible to poisoning, during which a foreign substance becomes involved with the catalyst surface to result in a smaller effective catalytic area [42]. If a catalyst could be made in which the surface remained ideal at all times, and all the metal atoms were accessible to reagents, only then could it be used with complete confidence.

Metal clusters have the potential to be these surfaces. A cluster is defined in this case as two or more metal atoms bound together with various carbon-containing ligands [43]. Each cluster is a microsurface upon which a catalytic process can occur. The clusters in this thesis are trimetallic tetrahedra in which the fourth atom of the tetrahedral skeleton is carbon. These types of clusters have been investigated extensively by Seyferth [44], but while his studies focussed mainly on the synthesis of clusters with various groups bound to the carbynyl carbon, this study involves the synthesis and subsequent mechanistic studies of the fluxional processes that can occur with different ligands bound in different manners to the complex.

Preliminary catalysis studies involving  $\text{Co}_3(\text{CO})_9\text{C-R}$  clusters have been performed. Hydroformylation of 1- and 2-pentene to form aldehydes has been achieved, with yields as high as 99% based on pentene consumption [45].

Scheme 4: A Process Catalyzed by a  $\text{Co}_3(\text{CO})_9\text{C-R}$  Cluster

Studies by Collin, Jossart and Balavoine have shown that  $\text{Co}_3(\text{CO})_9\text{C-CH}_3$  can catalyse hydroformylation of styrene as well [46]. Derivation of these molecules by coordination of phosphines can lead to less catalyst decomposition, and greater yields. Cobalt clusters should, in fact, make good catalysts because the carbonyl ligand is so labile, giving potential sites on the cluster for complexation of a substrate.

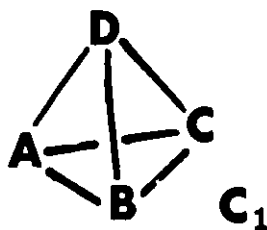
Great interest has developed towards development of chiral clusters in application as catalysts, because many molecules are only active in one of their enantiomeric forms. The importance of this became apparent in the thalidomide tragedy of the 1960's [47]. While one enantiomer of the molecule is safe for human consumption in the prevention of nausea, the other enantiomer was found, too late, to cause birth defects. These two molecules are identical in all ways save for their R or S designation. If one could catalyze the synthesis of enantiomerically pure drugs using organometallic clusters, great potential for helping modern medicine and organic synthesis could be realized.

#### (1.4) DEVELOPMENT OF CHIRALITY

· Various routes can be used to make these clusters chiral and subsequently increase their potential usefulness as chiral catalysts.

(a) If all four vertices of the tetrahedron are different, the molecule is chiral (Figure 15). This type of system was examined in the work of Vahrenkamp and Beurich [17]. Difficulty arises in the synthesis and isolation of one specific enantiomer. Current methods of vertex substitution do not allow for stereospecific vertex replacement in the molecule, and post-production separation of a racemic mixture is not necessarily a simple procedure. Enantiomers have the same physical and chemical characteristics: equivalent melting and boiling points, appearance, and solubility.

Figure 15: Chirality by Virtue of the Skeleton



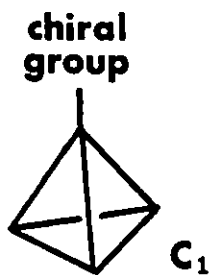
Chiral column chromatography can be difficult to carry out effectively, and expensive [48]. Reaction of the enantiomeric mixture with a known enantiomerically pure compound for diastereomer formation is possible [49]. Diastereomers have different chemical and physical behaviour, and are inequivalent in the NMR experiment. However, regeneration of the original compound after separation of the diastereomers can be problematic. As well, under some circumstances, clusters can subsequently lose their stereochemical integrity by intramolecular vertex fluxionality [50].

(b) Another mode of instilling chirality into an organometallic cluster is to incorporate a chiral group in the form of a ligand, bound to either the metal or the carbon vertex. Natural products, often inexpensive and easily attainable, (*e.g.*,

menthol), would destroy any mirror plane or axial symmetry inherent in a cluster and render it chiral (Figure 16). This route has an advantage in its capacity to prepare an enantiomerically pure product through choice of a single enantiomer as the starting material.

Ideally, it is desirable to have the chiral site as close to the metal as possible, since the catalytic reaction will clearly occur at a metal atom. However, ligands bound to metal atoms are more likely to detach than those on a carbon vertex, and balancing these two factors must be a consideration.

Figure 16: Chirality via Natural Products

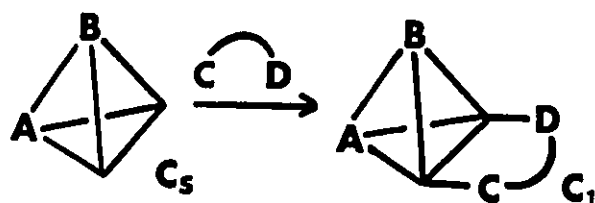


(c) A third method of rendering a cluster chiral is through coordination of an appropriate ligand or ligands. This can involve bonding two separate and different ligands to two of the vertices, thus breaking mirror symmetry within the cluster. A related route to this type of chirality is to attach a bidentate asymmetric ligand to a cluster possessing a mirror plane. This also can result in breakage of the  $\sigma$ -plane, leaving the cluster chiral. It can be achieved by using as simple a ligand as ARPHOS,  $(C_6H_5)_2As(CH_2)_2P(C_6H_5)_2$ .

Much work has been done by Bosnich towards the incorporation of chiral chelating ligands onto clusters. His CHIRAPHOS ligand, for example, is chiral in

itself, and as such, is like a combination of the second and third techniques of instilling chirality in a molecule [51].

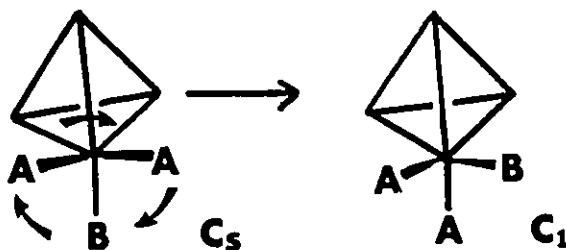
Figure 17: Chirality from a Bidentate Ligand



(d) Another method not previously mentioned can render a molecule chiral. A cluster may have a mirror plane on the NMR timescale because the molecule is racemizing at least once during the NMR detection time. If the conditions are altered so as to slow down the racemization process, then the molecule can appear chiral. That is, if the cluster is undergoing fluxional behaviour, such as a ligand rotating around a vertex, then if the intramolecular motion can be stopped with the ligand in a position that leaves the cluster with no symmetry, the molecule is chiral.

Stopping fluxionality is a relatively easy way of introducing chirality to individual molecules as it may simply require selection of the correct temperature. A drawback of this method is that a racemic mixture is usually created.

Figure 18: Chirality Upon Cessation of Fluxionality



This thesis examines three of these modes of generating chirality in a cluster: the addition of natural products, the chelation of an asymmetric ligand, and the freezing out of fluxional processes in solution and in the solid state. Understanding fluxional processes is important because it provides insight into the racemization of chiral catalysts and the motion of reagents on the catalyst surface.

Since the initial studies outlined here, several groups have focussed attention on these types of clusters: those led by Farrugia, Vahrenkamp, Stone, to name just a few. Our research studied molecules based upon the tricobalt tetrahedron. Through variation of groups bound to the cobalt atoms and of groups attached to the apical carbon, and often via substitution of another metal vertex for a  $\text{Co}(\text{CO})_3$  moiety, several new clusters were synthesized. The study of their properties and mechanistic behaviour is the focus of this thesis.

## CHAPTER TWO

### (2.1) TETRAHEDRAL CLUSTERS BEARING CHELATING LIGANDS

The replacement of carbonyl groups on the metal vertices by other ligands is one potential method for instilling chirality in a cluster. Two types of ligands which may lead towards this goal are the series known as phosphines and arsines.

#### (2.1.1) CHELATING PHOSPHINES AND ARSINES

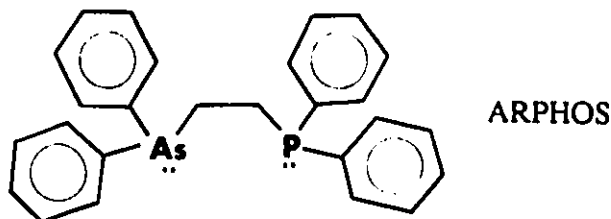
Phosphines and arsines,  $PR_3$  and  $AsR_3$ , have a lone pair of electrons on the Group V atom which can be used to donate two electrons to a metal atom in an organometallic complex [52]. Carbonyl groups are also two-electron donors, and can be replaced by the phosphines and arsines. Indeed, clusters often prefer the electron-rich phosphine ligands to the relatively electronegative carbonyl groups. This is evident from the ease of reaction of phosphines with cobalt clusters [53]. In many cases, the major products were monosubstituted only, thought to be a result of steric restrictions [7].

Arsines do not bind as tightly to cobalt as do phosphines [7], perhaps because of arsenic's position in the periodic table: stronger bonds are often formed between atoms in the same row, because of the similarity of atomic orbitals used in bonding.

Combination of two phosphine (or arsine) groups onto a backbone results in a compound which can act in a chelating manner, forming a ring as both ends of the diphosphine molecule coordinate to metal vertices. These bidentate ligands are the focus of this chapter, which will investigate bonding of 1,2-bis-(diphenylphosphino)-ethane (DIPHOS) and 1-diphenylarsino-2-diphenylphosphino-ethane (ARPHOS) onto



clusters of cobalt, molybdenum, tungsten and carbon.



Before the study of bidentate phosphines and arsines with our compounds is begun, it is of interest to review modes of bonding found in previous research on chelates of this type with similar clusters to those which we will be utilizing.

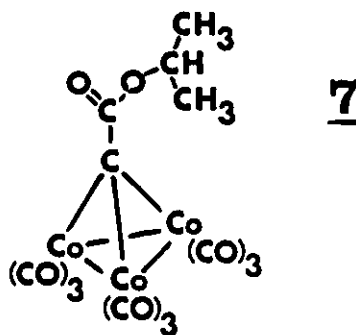
Two products are seen from the reaction of  $\text{Co}_3(\text{CO})_9\text{C-CH}_3$  with bis-diphenylphosphinomethane, (DPPM), characterized as diequatorially- and diaxially-substituted complexes [54]. The  $^{31}\text{P}$  NMR spectrum shows a signal at 36.1 ppm for the equatorial case, and 89.2 ppm in the axial situation; axial ligands such as carbonyls and phosphines tend to appear downfield in the NMR spectrum in comparison with their equatorial partners [55]. Heating of the diequatorial complex,  $\text{Co}_3(\text{CO})_7(\text{DPPM})\text{-C-CH}_3$ , in toluene with more DPPM results in a second substitution. A cluster with two chelates, each equatorially oriented along separate Co-Co bonds, is the product, confirmed by the  $^{31}\text{P}$  and  $^{13}\text{C}$  NMR spectra. In the coordination of the less bulky  $(\text{CH}_3)_2\text{PCH}_2\text{P}(\text{C}_6\text{H}_5)_2$  to  $\text{Co}_3(\text{CO})_9\text{CCH}_3$ , the product was substituted on adjacent metal vertices, with no evidence of frangibility in the Co-P linkages [56]. The reaction of  $\text{Co}_3(\text{CO})_9\text{C-C}_6\text{H}_5$  with DPPE yields a molecule with two cobalt skeletons joined by one bidentate ligand, in which each cluster has the phosphine in an equatorial position [57].

The trend is that diphosphines generally substitute carbonyl ligands in a diequatorial manner, but a contrast is seen in diarsines. The bidentate ligand  $(\text{CH}_3)_2\text{As-CH}(\text{CF}_2)_2\text{CHAs}(\text{CH}_3)_2$ , (FFARS), adopts a diaxial conformation with respect to the basal plane of the three cobalt atoms in  $\text{Co}_3(\text{CO})_7(\text{FFARS})\text{C-CH}_3$ . This structure has

bridging carbonyls, in contrast to the terminal carbonyl groups in the phosphine-substituted clusters above [58]. Unfortunately, little is known about the crystal structures of other arsine complexes, because most of the synthetic work was performed in the 1960's, before single crystal diffraction studies became routine.

### (2.1.2) METHODS OF ANALYSIS

The molecule  $\text{Co}_3(\text{CO})_9\text{C}-\text{CO}_2\text{CH}(\text{CH}_3)_2$ , 7, was chosen as the achiral starting material to be rendered chiral by the incorporation of an asymmetric ligand.



The synthesis of this type of cluster has been developed by Seyferth [44] and by Robinson [59], and the behaviour of these systems is well understood. The cluster is known to be stable in solution under a nitrogen atmosphere for several days, which allows ligand substitution studies to be carried out. As well, the molecule is a good choice for study because there are many built-in NMR probes: both  $^{13}\text{C}$  and  $^1\text{H}$  nuclei are observable by nuclear magnetic resonance spectroscopy. The incorporation of a phosphine ligand into the system will add another NMR probe ( $^{31}\text{P}$ ) to be used in mechanistic and structural studies.

Proton NMR is a vastly useful technique, because of the high sensitivity of the nucleus and because the  $^1\text{H}$  nucleus is 100%-abundant and spin 1/2. Unfortunately, complications can develop in the use of this spectroscopy to observe tricobalt clusters. The proximity of the quadrupolar cobalt nuclei to the protons in the cluster can cause

broadening of the proton signals. This problem becomes heightened as the magnetic field of the spectrometer is increased. For this reason, a  $^1\text{H}$  NMR spectrum of these compounds will often be better-resolved on a spectrometer of low frequency, for example 90 MHz, than on a 500 MHz machine.

Two problems potentially arise in using  $^{13}\text{C}$  NMR: (a) the  $^{13}\text{C}$  nucleus has a much lower natural abundance than  $^1\text{H}$ ; and (b) the nuclear sensitivity of  $^{13}\text{C}$  is a fraction of that of  $^1\text{H}$  (Table 6) [60]. The low natural abundance can be dealt with by using enrichments of the NMR-active nucleus. Incorporation of 25-30% of  $^{13}\text{C}$  in the form of CO ligands was achieved in all molecules of this study by stirring a THF solution of the cluster under an atmosphere of  $^{13}\text{CO}$  gas. The sensitivity can be enhanced by using NMR spectrometers of very high field. Fourier transform NMR, in which repeated scans over the chosen frequency range are taken, gives the improvement of "adding up" information, thus increasing the signal-to-noise ratio. Quadrupolar broadening of the signals is not as much of a problem with  $^{13}\text{C}$  NMR as with  $^1\text{H}$  NMR, because carbon-13 has a much larger spectral width.  $^{13}\text{C}$  signals are generally found between 0 and 300 ppm, while the spectral width of the  $^1\text{H}$  spectrum is approximately 13 ppm [61]. This can result in signal overlap if the  $^1\text{H}$  signals experience broadening, while the  $^{13}\text{C}$  signals are less likely to show this effect.

Table 6: NMR Parameters of Several Nuclei [60]

Isotope	Abundance (%)	NMR Frequency in 10 KGauss	Relative Sensitivity	Spin (I)
$^1\text{H}$	99.9844	42.577	1.0000	1/2
$^{13}\text{C}$	1.108	10.705	0.0159	1/2
$^{31}\text{P}$	100	17.235	0.0664	1/2
$^{59}\text{Co}$	100	10.103	0.281	7/2

The phosphorus-containing ligands under observation are ideal for NMR study, because the  $^{31}\text{P}$  nucleus is 100 % abundant and is spin 1/2. The chemical shift range is great -- more than 200 ppm, so that different bonding modes result in an easily detectable change in the spectrum [61]. The difference between axial and equatorial substitution in tricobalt clusters, for example, can lead to a  $^{31}\text{P}$  chemical shift difference of 25 ppm or more. The methylene backbone of the bidentate chelate contains both  $^{13}\text{C}$  and  $^1\text{H}$  nuclei, which can also aid in structural elucidation.

## (2.2) A SIMPLE SYSTEM: $\text{Co}_3(\text{CO})_9\text{C-CO}_2\text{CH}(\text{CH}_3)_2$

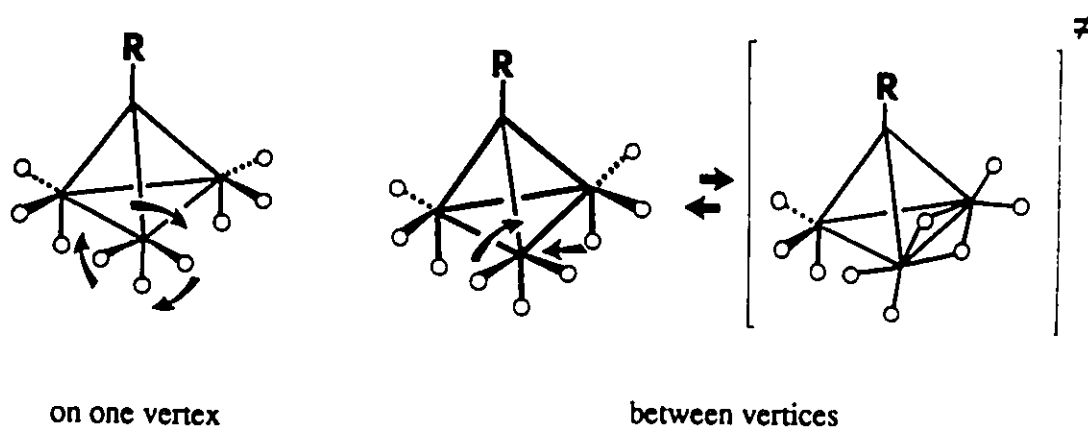
The tricobalt cluster  $\text{Co}_3(\text{CO})_9\text{C-CO}_2\text{CH}(\text{CH}_3)_2$ , 7, is not chiral, as it possesses a mirror plane. However, the isopropyl methyl groups at the apex of the molecule are diastereotopic, which means they will become inequivalent if another part of the cluster is made chiral. As they experience different magnetic environments when the molecule is chiral, they will produce discrete signals in the NMR experiment, both in the  $^{13}\text{C}$  and in the  $^1\text{H}$  spectrum. In this way, the isopropyl group can be used as a probe for chirality.

### (2.2.1) NMR STUDY

The  $^1\text{H}$  NMR spectrum of the starting molecule shows one doublet for the two methyl groups, at 1.2 ppm. The doublet arises from coupling to the isopropyl CH, and the corresponding septet of that proton appears downfield, at 5.2 ppm. The  $^{13}\text{C}$  NMR spectrum shows a broad singlet for all nine carbonyl ligands. This may seem unusual, because crystal structures of similar clusters exhibit two types of carbonyl ligands -- six equatorial and three axial [19]. However, fluxional processes may be occurring in solution which are not occurring in the solid state. Axial-equatorial exchange of all carbonyl groups occurs at each Co vertex, and this type of motion has

never been "stopped" on the NMR timescale. Intermetal exchange of carbonyl ligands may also occur, postulated as a merry-go-round mechanism [62]. However, vertex rotation alone can explain the observed  $^{13}\text{C}$  NMR spectrum, and it is impossible to state unequivocally that in this molecule, intervertex exchange is occurring as well. The rapid exchange of carbonyls between axial and equatorial positions leads to an averaged spectrum being observed.

Figure 19: Possible Intramolecular Carbonyl Motions



The temperature of the sample was lowered to 193 K, and the  $^{13}\text{C}$  NMR spectrum was examined to discern if the fluxionality of the carbonyl ligands was slowing. If exchange stops, one would expect to see separate signals for axial and equatorial carbonyl groups (though cessation of intermetal exchange would be undetectable). No change was evident, as the carbonyl signal remained a sharp single peak at 198.8 ppm. The  $^1\text{H}$  NMR spectrum also remained unchanged.

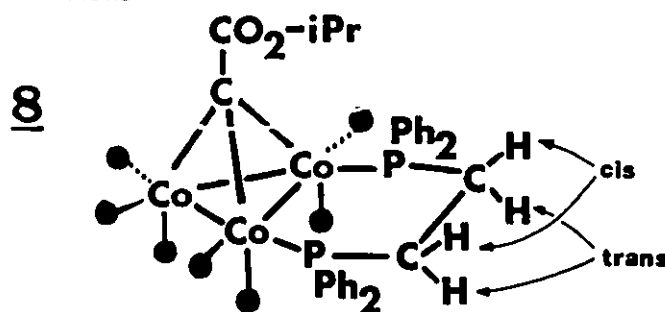
### (2.2.2) DIPHOS REACTIONS

The incorporation of a symmetric bidentate ligand was the next step, in order to discern the behaviour of our cluster in a simple chelated system.

The tricobalt tetrahedron,  $\text{Co}_3(\text{CO})_9\text{C-CO}_2\text{CH}(\text{CH}_3)_2$ , 7, was reacted with the chelating ligand DIPHOS,  $(\text{C}_6\text{H}_5)_2\text{P}(\text{CH}_2)_2\text{P}(\text{C}_6\text{H}_5)_2$ . As described in Section (2.1.1), reaction with DIPHOS can lead to mono- or multi-substitution, inter- or intra-molecular substitution, diaxial or diequatorial substitution. Each possibility is considered in the product analysis.

The reaction of 7 with DIPHOS proceeded easily, giving a single product,  $\text{Co}_3(\text{CO})_7(\text{DIPHOS})\text{C-CO}_2\text{CH}(\text{CH}_3)_2$ , 8. The  $^1\text{H}$  NMR spectrum revealed the cluster was monosubstituted, evidenced by the integrated areas of the signals in the phenyl region as compared to those in the isopropyl region. Two peaks can be seen for the methylene protons on the DIPHOS backbone. This reveals more than may be immediately obvious. The bidentate ligand is symmetric (*i.e.*, both ends of the chain are equivalent). Therefore, the DIPHOS must be fastened tightly to the cobalt vertices. The two signals arise from the protons on the two sides of the  $\text{Co}_2\text{P}_2\text{C}_2$  ring (*e.g.*, two protons "*trans*" and two "*cis*" to the apical carbon (Figure 20). The chelating ligand shows no sign of intramolecular migration between cobalt vertices at ambient temperature.

Figure 20:  $\text{Co}_3(\text{CO})_7(\text{DIPHOS})\text{C-CO}_2\text{CH}(\text{CH}_3)_2$ , Displaying *Cis* and *Trans* Nature of the Chelate Protons

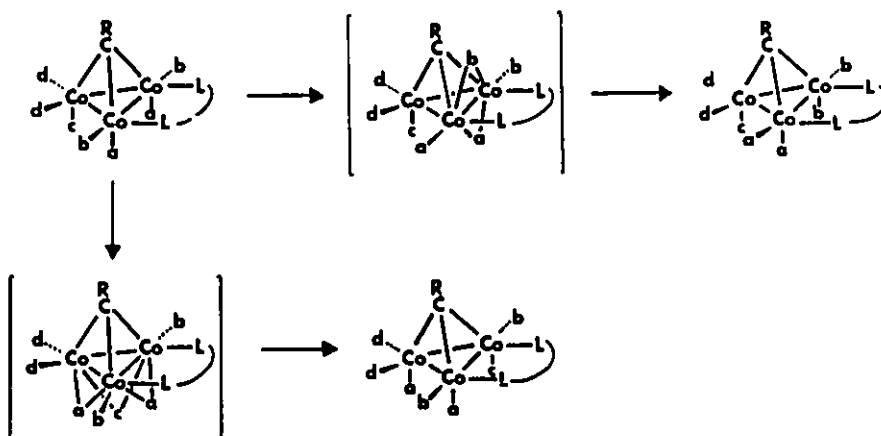


The  $^{31}\text{P}$  NMR spectrum showed one peak only. The single signal at 42 ppm leads to the conclusion that the DIPHOS ligand is substituted in a diequatorial

manner, as illustrated in Figure 20.

The ambient temperature  $^{13}\text{C}$  NMR study exposed motion of the carbonyl ligands even as the DIPHOS ligand remained fixed. At room temperature, all the carbonyl groups were exchanging, resulting in a single broad peak at 205 ppm. One might think that if certain positions on the metal vertices were blocked (by the DIPHOS ligand, for example), fluxionality of the other ligands in the system would be prevented. This is not the case, and the observed behaviour may be explained by drawing a parallel with the proposed mechanism of Cotton and Hanson to explain carbonyl exchange in  $\text{Ru}_3(\text{CO})_{10}[(\text{C}_6\text{H}_5)_2\text{PCH}_2\text{P}(\text{C}_6\text{H}_5)_2]$ . The transition state for this process is proposed to consist of two bridging and four terminal carbonyls [63]. The analogous modes of migration for our  $\text{Co}_3$  clusters are shown in Figure 21. All carbonyls could be exchanged by this mechanism, regardless of the presence of the bulky bidentate ligand.

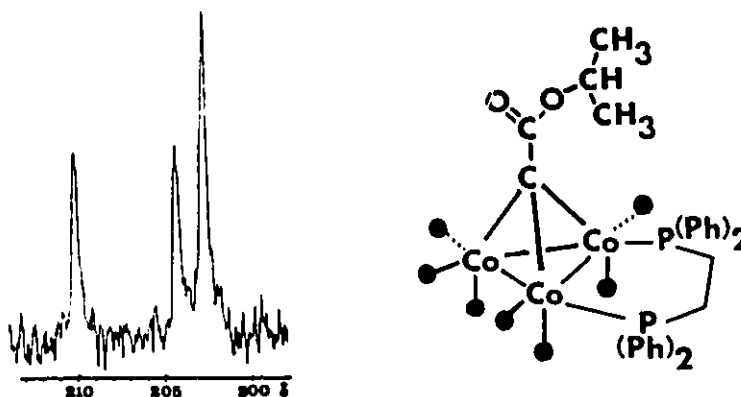
Figure 21: Carbonyl Exchange in the Presence of a Bidentate Ligand



Upon cooling, the carbonyl fluxionality ceases, giving a spectrum with three resonances in the carbonyl region (Figure 22). These signals can be assigned to the axial and equatorial CO's on the DIPHOS-substituted cobalts ( $\delta$  210.2 and 204.3,

respectively), and the three remaining CO's on the unsubstituted cobalt vertex ( $\delta$  202.5). The axial carbonyls are assigned to the most downfield signal based upon the research of Aime, who noted that axial carbonyls experience less shielding than their corresponding equatorial neighbours [54].

Figure 22:  $^{13}\text{C}$  NMR Spectrum of **8**, Carbonyl Region,  $T = 193\text{ K}$ , S.F. = 62.9 MHz



It has thus been demonstrated that a bidentate diphosphine is strongly bound to our tricobalt cluster, and that fluxional processes do not depend upon the ability of the entire metal vertex to rotate.

### (2.2.3) ARPHOS INCORPORATION

Now that the reactivity of the tricobalt system with a chelating diphosphine has been explored and understood, the study of a similar reaction with an asymmetric ligand can be undertaken.

The bidentate ligand ARPHOS,  $(\text{C}_6\text{H}_5)_2\text{As}(\text{CH}_2)_2\text{P}(\text{C}_6\text{H}_5)_2$ , reacted with the  $\text{Co}_3(\text{CO})_9\text{C}-\text{CO}_2\text{CH}(\text{CH}_3)_2$  cluster, to yield the compound  $\text{Co}_3(\text{CO})_7(\text{ARPHOS})-\text{C}-\text{CO}_2\text{CH}(\text{CH}_3)_2$ , **9**. This ligand has an arsine at one end of the chain and a phosphine at the other. As discussed in the introduction, most phosphines will complex diequatorially to tetrahedral trimetal-monocarbon clusters, while diarsines tend to bond in a



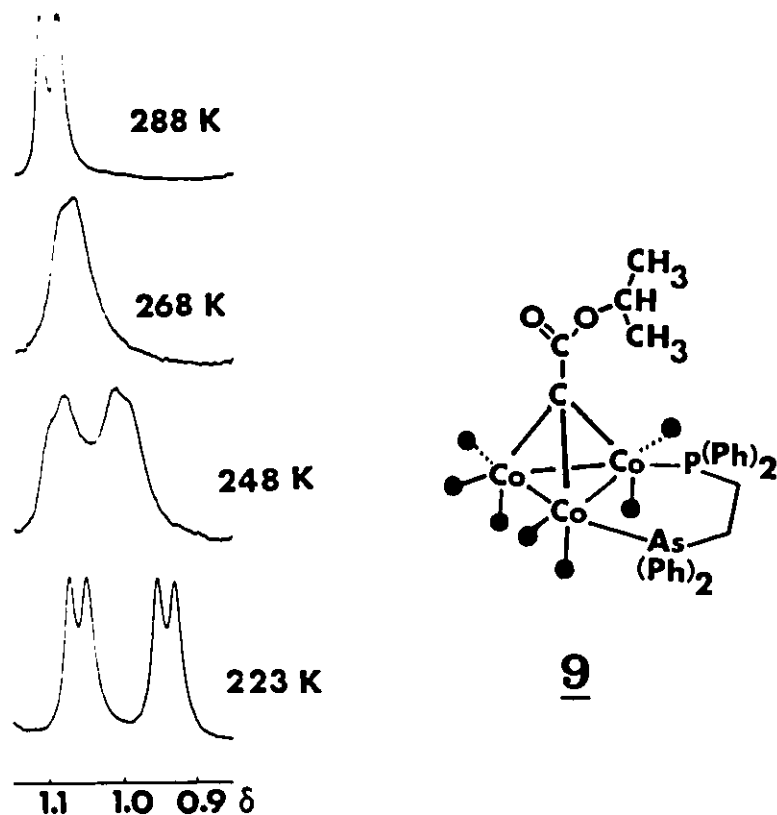
diaxial fashion. It will be of interest to determine which mode results when the chelate possesses a combination of both atoms.

The infrared spectrum shows carbonyl absorbance bands between 2060 and 1955  $\text{cm}^{-1}$ , which indicates that all carbonyl ligands in the complex are bound to cobalt in a terminal fashion. Bridging carbonyl groups have a weaker C-O bond and thus would absorb at lower frequencies.

The  $^{31}\text{P}$  NMR spectrum contained a single peak, found in the region characteristic of equatorially-substituted phosphines, at 47.6 ppm. This is reminiscent of the behaviour of the DIPHOS compounds.

Because of the asymmetric nature of the ARPHOS group, coordination of the ligand should cause loss of the molecular mirror plane: the molecule should be chiral, and the diastereotopic isopropyl methyl groups should now be non-equivalent. Observation of the  $^1\text{H}$  NMR of **9** at 223 K revealed the predicted pattern of two doublets, wherein two inequivalent methyl groups experience coupling to the isopropyl H. Under these conditions, therefore, the cluster is chiral. (It is a racemic mixture of enantiomers, as there would be no preference to form one isomer over the other.) An unanticipated result appeared as the temperature was increased: the two doublets coalesced to one doublet, and the limiting high-temperature spectrum was attained at 288 K. The methyl groups appear to be exchanging environments. Because of their diastereotopic nature, they cannot become equivalent by a rotation of the isopropyl group around the (apical-C)-CH bond. Another explanation of the observed behaviour is that the cluster is losing its chirality on the NMR timescale, lending time-averaged mirror symmetry to the system. Rearrangement of the skeleton, as seen in Vahrenkamp's mixed metal clusters [51], could account for the loss in chirality. However, a strongly-bound chelating ligand should aid in maintenance of the molecule's stereochemical integrity. Other possible modes of chirality loss could be

Figure 23: Variable Temperature  $^1\text{H}$  NMR Spectrum of  $\text{Co}_3(\text{CO})_7(\text{ARPHOS})\text{C}-\text{CO}_2\text{-CH}(\text{CH}_3)_2$ , **9**, S.F. = 250 MHz, Isopropyl Methyl Region



through cleavage of the cobalt-ligand link, or by a pathway of ligand migration from one cobalt to another via a symmetric transition state.

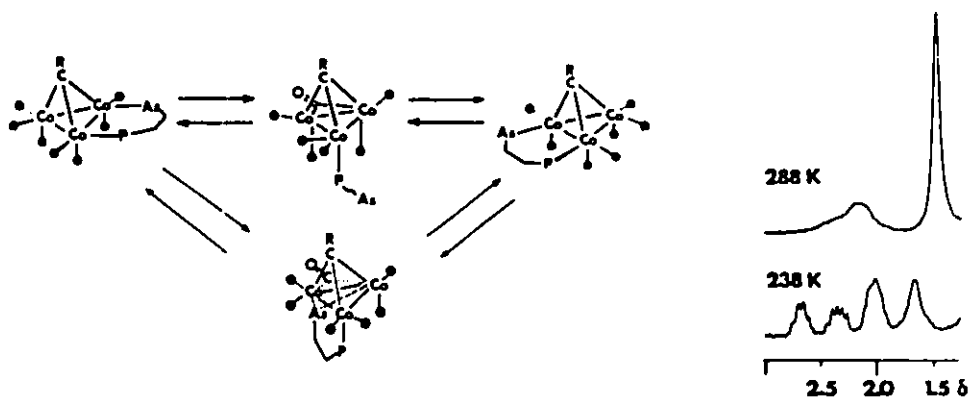
The cobalt-arsenic bond is known to be weaker than the Co-P bond. This was demonstrated in the determination of the solution molecular weight of  $\text{Co}_3(\text{CO})_8\text{-[As}(\text{C}_6\text{H}_5)_3\text{]C-C}_6\text{H}_5$ , in which the measured weight was consistently low, indicating rapid dissociation of the  $\text{As}(\text{C}_6\text{H}_5)_3$  by Co-As bond breakage [7]. This is in contrast to phosphine behaviour as seen in this study. It seems feasible that there is fluxionality based upon the lability of the Co-As bond.

The other NMR probes in the cluster would indicate if the ARPHOS group were dissociating or remaining bound to its vertices. The ethylene bridge between the

P and As atoms will show four separate signals in the  $^1\text{H}$  NMR spectrum if the ligand stays attached to the cluster -- the protons will be proximal to either the P or the As, and they will be *cis* or *trans* (relative to the apical C). The low temperature spectrum shows four signals (Figure 24). The fine structure in two of the peaks results from coupling to the nearby phosphorus nucleus and to the other methylene protons. Quadrupolar broadening can be seen in the signals of the hydrogens  $\alpha$  to the  $^{75}\text{As}$  (spin 3/2) nucleus. This spectrum confirms that the ARPHOS ligand is stationary at low temperature.

The  $^1\text{H}$  NMR spectrum of the methylene region changes as the temperature is raised. The four proton signals coalesce to two signals, one sharp and one broad. There is no longer any differentiation between protons in *cis* and *trans* positions (as had been seen in the DIPHOS complex), as these protons are apparently exchanging surroundings. Co-As bond cleavage combined with subsequent swinging motion of the now-monodentate ligand about the cobalt vertex could move the *cis* protons into a *trans* environment, and vice versa.

Figure 24: Low-Temperature  $^1\text{H}$  NMR Spectrum of **9**, Methylene Bridge Region, S.F. = 250 MHz, with Racemization Mechanisms

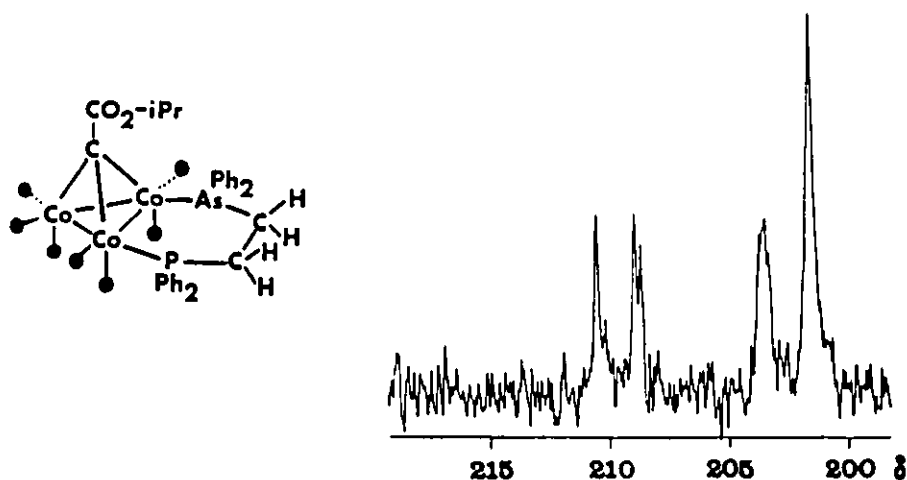


It appears that the As-Co bond is quite intact at reduced temperatures. The barrier to interconversion of the two enantiomeric structures was calculated through use

of the line-broadening technique, equation (5) in Section (1.2.2.2), and gave  $\Delta G^\ddagger = 13.1 \pm 0.5$  kcal/mol.

Clearly, the ARPHOS ligand cannot simply dissociate and associate itself to a cobalt vertex independent of any other ligand motion. There must be a vacant site on the metal in order for the arsenic to be allowed to complex. Carbonyl migration on the metal in order for the arsenic to be allowed to complex. Carbonyl migration from cobalt to cobalt as the As-Co linkage breaks and reforms would result in a vacancy being created. If the only mode for intervertex carbonyl motion at low temperature requires concomitant ARPHOS migration, then the  $^{13}\text{C}$  NMR spectrum should show a freezing out of the intervertex carbonyl exchange at the same temperature. Another possible mechanism involves a transition state in which the arsine terminus and one CO ligand simultaneously bridge two cobalt atoms. This would require that the As atom be temporarily pentacoordinate, but this is not without precedent ( $\text{AsF}_5$ , for example).

Figure 25: Low-Temperature  $^{13}\text{C}$  NMR Spectrum of **9**,  $T = 183$  K, S.F. = 250 MHz



At a different temperature, a typical  $^{13}\text{C}$  NMR spectrum is observed, consisting of one signal in the carbonyl region, indicative of intervertex carbonyl

exchange. As the solution is cooled to 183 K, several peaks are resolved, to give the spectrum shown in Figure 25, a 1:1:1:1:3 pattern. The peak of area three is assigned to the three carbonyls on the unsubstituted cobalt vertex, continually exchanging their axial-equatorial positions. The remaining peaks are due to the four carbonyl groups on the ARPHOS-bound cobalt vertices.

The process of carbonyl migration over the trimetallic base of the tetrahedron must occur as the ARPHOS ligand is undergoing fluxionality, but the carbonyls do not necessarily cease moving once the ARPHOS ligand does. (Carbonyl exchange was observed in the DIPHOS cluster, though it was clear that the DIPHOS ligand was not dissociating.) The energy barrier to the carbonyl motion, calculated from the NMR data using DNMR3 [101], is only 9.4 kcal/mol. This signifies that the carbonyl exchange between the metal vertices is independent of the fluxionality of the bidentate ligand. The carbonyl groups continue to move even as the bidentate ligand is frozen into position. Co-As bond cleavage is the rate-determining step in ARPHOS migration, while the fluxional process of the carbonyl ligands makes ARPHOS motion possible.

#### (2.2.4) X-RAY ANALYSIS OF $\text{Co}_3(\text{CO})_7(\text{ARPHOS})\text{C}-\text{CO}_2\text{CH}(\text{CH}_3)_2$

The X-ray diffraction crystal structure of  $\text{Co}_3(\text{CO})_7(\text{ARPHOS})\text{C}-\text{CO}_2\text{CH}(\text{CH}_3)_2$  has been solved by R. Faggiani and Dr. C.J.L. Lock (Figure 26 A) [100]. The carbonyl groups appear in fully terminal positions, which confirms the analysis made from the infrared spectrum. The chelating ARPHOS ligand is found in the diequatorial position, as predicted from the  $^{31}\text{P}$  solution NMR spectrum. The six-membered ring formed by the two cobalt atoms and the P- $\text{CH}_2\text{CH}_2$ -As chain assumes a distorted half-chair conformation in the solid state.

Figure 26 A: X-Ray Diffraction Crystal Structure of  $\text{Co}_3(\text{CO})_7(\text{ARPHOS})\text{-C-CO}_2\text{CH}(\text{CH}_3)_2$

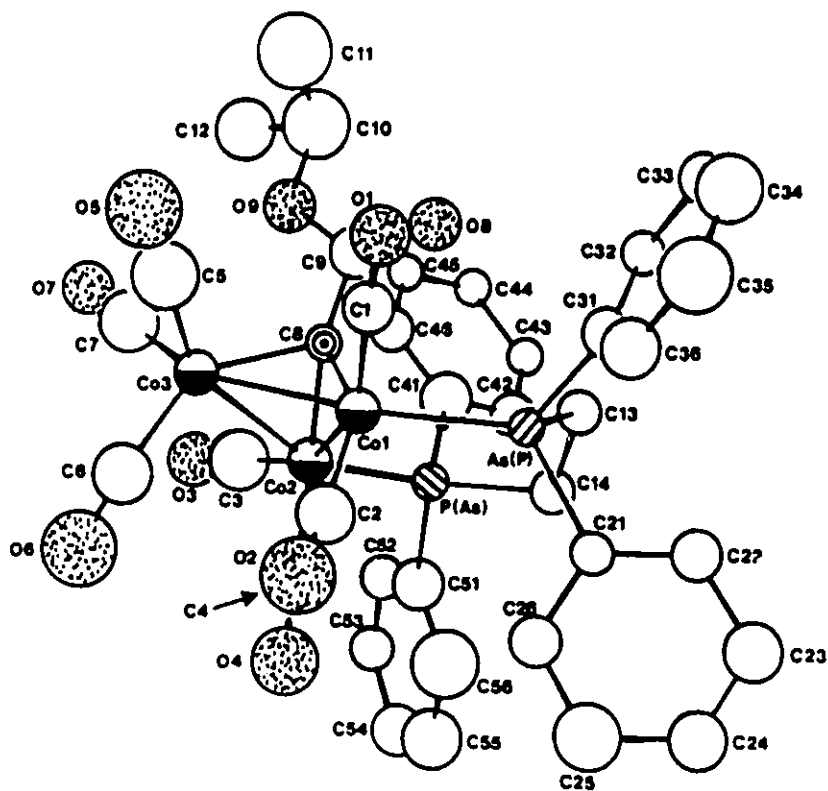
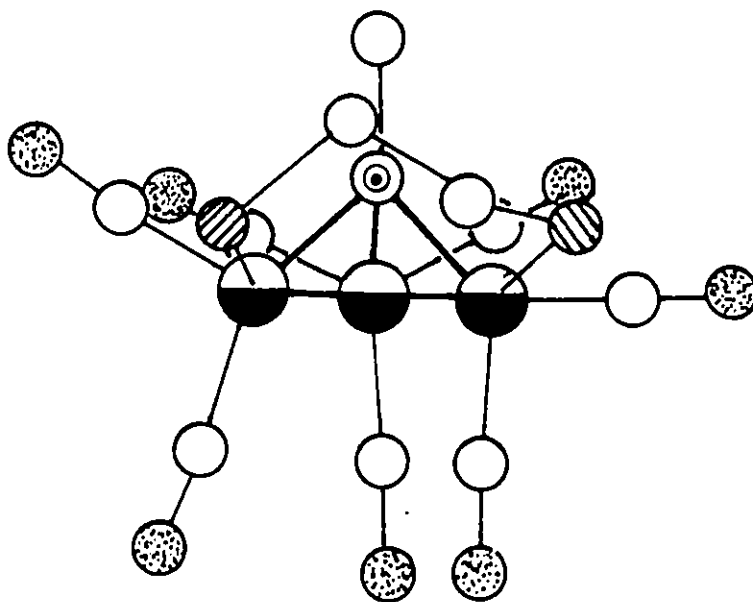


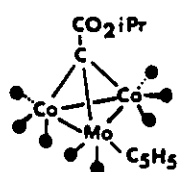
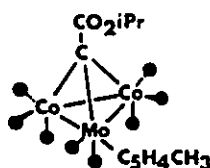
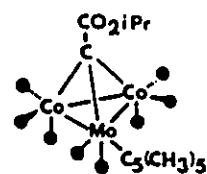
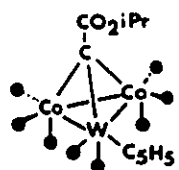
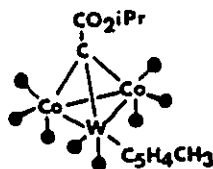
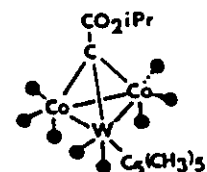
Figure 26 B: X-Ray Diffraction Crystal Structure of  $\text{Co}_3(\text{CO})_7(\text{ARPHOS})\text{-C-CO}_2\text{CH}(\text{CH}_3)_2$ , showing half-chair conformation, (phenyl rings omitted for clarity)



The bond length between the ARPHOS-bridged cobalts is longer than the remaining two Co-Co bonds (2.500(3) Å *c.f.* 2.464(3) and 2.473(3) Å). This feature has been noted in other chelated clusters, such as the example of  $\text{Co}_3(\text{CO})_7(\text{DPPM})\text{C-CH}_3$ , in which the bridged Co-Co bond is 2.49 Å, while the unbridged average 2.47 Å [57]. The greater separation of bridged vertices may be an attempt to avoid steric interactions between the phenyl groups on the phosphorus and arsine atoms. The phosphorus-arsenic positions are disordered, but not completely, as there is not a 50:50 distribution of the two atoms but rather a 79:21 split.

### (2.3) VERTEX REPLACEMENT

A series of more complex molecules was synthesized, to investigate the chelating behaviour of DIPHOS and ARPHOS with mixed metal clusters. The technique developed by Vahrenkamp [17] was used to replace a  $\text{Co}(\text{CO})_3$  vertex by six different vertices:  $\text{M}(\text{CO})_2\text{CP}$ , where  $\text{M} = \text{Mo}, \text{W}$  and  $\text{CP} = (\text{C}_5\text{H}_5), (\text{C}_5\text{H}_4\text{CH}_3),$  and  $[\text{C}_5(\text{CH}_3)_5]$ , producing  $(\text{CP})\text{M}(\text{CO})_2\text{Co}_2(\text{CO})_6\text{C-CO}_2\text{CH}(\text{CH}_3)_2$ , molecules 10-15.

101112131415

### (2.3.1) NMR STUDY OF THE UNCOMPLEXED CLUSTERS (CP)M(CO)<sub>2</sub>Co<sub>2</sub>-(CO)<sub>6</sub>C-CO<sub>2</sub>CH(CH<sub>3</sub>)<sub>2</sub>

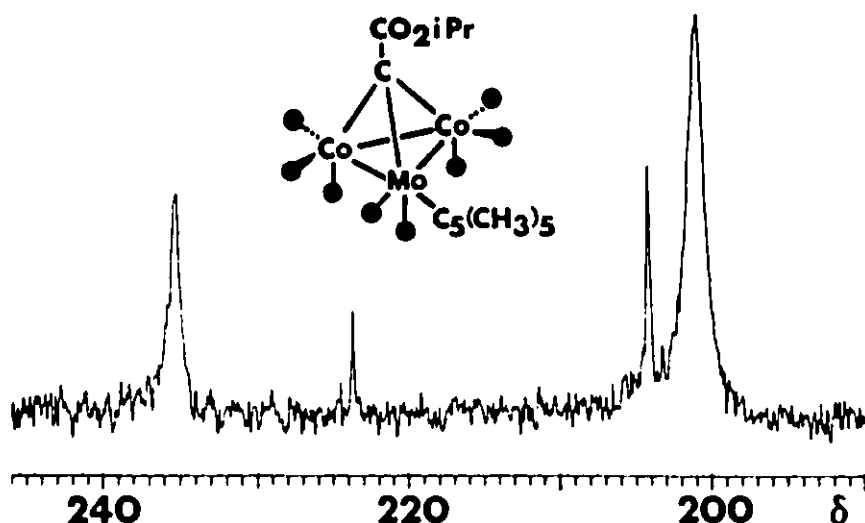
The pentamethylcyclopentadienyl molybdenum cluster, 12, was studied by NMR. The isopropyl region of the proton NMR spectrum showed no significant change from the spectrum of the tricobalt cluster. One signal appears for the five ring methyl groups, because the ring is spinning continually, rendering all the CH<sub>3</sub> groups equivalent. The <sup>13</sup>C NMR spectrum displayed one signal in the carbonyl region, indicative of intervertex carbonyl exchange in addition to axial-equatorial interchange. The chemical shift of the CO signal was the weighted average of the shifts for six Co carbonyls (~ 200 ppm) and two Mo carbonyls (~ 230 ppm), at 209.9 ppm. As well, the carbons in the cyclopentadienyl ring gave rise to a single peak, at 106.1 ppm.

Decreasing the temperature led to both <sup>1</sup>H and <sup>13</sup>C spectra which were more complicated. The <sup>1</sup>H NMR spectrum was quadrupole-broadened and thus uninformative. The <sup>13</sup>C NMR spectrum was very interesting in the carbonyl region (Figure 27). Two types of signals became evident, one in a region typical of carbonyl groups bound to cobalt (190-210 ppm), and the other appearing downfield, with a shift value corresponding to molybdenum-bound carbonyl groups (220-240 ppm) [64]. (The smaller set of peaks are due to a minor isomer, the nature of which will be the subject of Chapter Five.) The resolution of these signals means the exchange of carbonyl ligands between cobalt and molybdenum vertices is stopped on the NMR timescale at reduced temperatures. The integrated areas beneath the peaks are in a ratio of 6:2, matching an assignment of three carbonyls localized on each Co vertex, and two carbonyls on the Mo atom.

The complex spectral pattern of CO signals was seen for molecules 10, 11, 13, 14 and 15 as well, indicating cessation of CO exchange on the NMR timescale at low temperature, leaving systems with all ligands localized on specific metal vertices.



Figure 27: Low-Temperature  $^{13}\text{C}$  NMR Spectrum of 12, Carbonyl Region,  $T = 183\text{ K}$ , S.F. = 69.2 MHz.



### (2.3.2) HETEROMETALLIC CLUSTERS WITH A SYMMETRIC CHELATING LIGAND

This step was accomplished by reaction of the molybdenum-substituted cluster  $[\text{C}_5(\text{CH}_3)_5]\text{Mo}(\text{CO})_2\text{Co}_2(\text{CO})_6\text{C}-\text{CO}_2\text{CH}(\text{CH}_3)_2$ , 12, with DIPHOS.

As with the tricobalt cluster, this reaction was facile at room temperature, giving a single product when the reagents were mixed in stoichiometric amounts. The resulting cluster,  $[\text{C}_5(\text{CH}_3)_5]\text{MoCo}_2(\text{CO})_6(\text{DIPHOS})\text{C}-\text{CO}_2\text{CH}(\text{CH}_3)_2$ , 16, was studied by NMR and IR spectroscopies to determine if the coordination mode was diaxial or diequatorial.

The infrared spectrum showed absorbance peaks between  $2090\text{-}1970\text{ cm}^{-1}$ , typical of terminal metal carbonyl groups. There are also bands at wavenumbers of slightly lower energy. These arise because the pentamethylcyclopentadienyl ring on the molybdenum vertex is an electron-rich ligand. Some of its electron density is donated to the Mo atom, which in turn can backdonate into the  $\pi^*$  orbital of the CO double bond. This weakens the C=O bond of the molybdenum carbonyls, and leads to a lower frequency CO vibration.

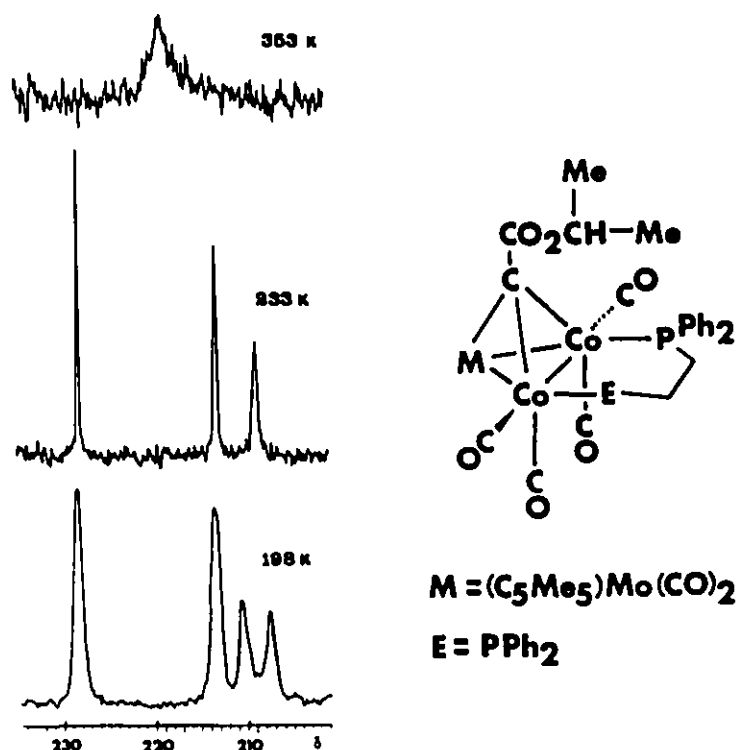
The phosphorus NMR spectrum displayed one signal only, at 37.4 ppm. The ligand must be bound to the cobalt vertices only, because the  $^{31}\text{P}$  chemical shift is comparable to that in the tricobalt-DIPHOS complex, while bonding to molybdenum would cause a significant change in the phosphorus chemical shift -- typical shift values for phosphorus bound to molybdenum are 0 - 20 ppm [65]. It is probable that the molybdenum atom is simply too sterically hindered to react with the chelating phosphine. Again, the chemical shift is indicative of diequatorial bonding of the chelate to the cluster.

The variable temperature  $^{13}\text{C}$  NMR spectra of the carbonyl region are presented in Figure 28. The high-temperature  $^{13}\text{C}$  NMR spectrum of 16 (353 K, S.F. = 20 MHz) revealed intermetal fluxionality of the CO ligands, with a broad signal at 216.6 ppm. This carbonyl migration is a common feature of all clusters discussed in this study, though in this case it is a process with a slightly higher energy barrier ( $\Delta G^\ddagger = 10.4 \pm 0.5$  kcal/mol).

When the system is cooled to 233 K, there is resolution of the carbonyl signals, with 3 types of carbonyl ligands becoming apparent. The cobalt carbonyls are of two types: axial (2) and equatorial (2). The downfield resonances are assigned to the less shielded axial carbonyls on cobalt. The molybdenum carbonyl groups produce one signal only, at  $\delta$  228.5 (2).

Signals in the  $^{13}\text{C}$  spectrum split once more at lower temperature. At 218 K, the line originally at 209.2 ppm (equatorial carbonyls) broadens, and two peaks, at 210.5 and 207.6 ppm, are fully resolved at 198 K. This further splitting of the signals happens only at very low temperatures, and can be assigned to freezing out of the ring "flipping" associated with six-membered rings. The cessation of this motion will render the cluster chiral if the conformation chosen is one lacking a mirror plane, such as a distorted half-chair.

Figure 28: Variable-Temperature  $^{13}\text{C}$  NMR Spectra of 16, S.F. = 62.9 MHz, Carbonyl Region



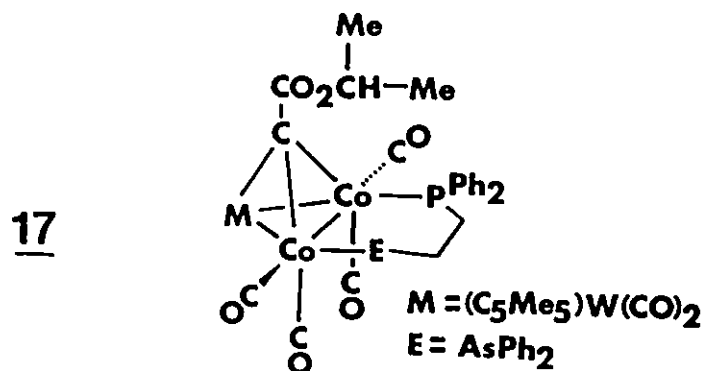
As in the DIPHOS tricobalt complex, the DIPHOS ligand shows no sign of dissociation from the cobalt vertices. This is illustrated by the  $^1\text{H}$  NMR spectrum. At high temperature, there always appear two multiplets for the methylene bridge protons, at 2.4 and 2.9 ppm. This indicates the *cis* and *trans* ring protons do not exchange. The spectrum shows only one doublet for the isopropyl  $\text{CH}_3$  protons at high temperature (303 K), but on cooling of the system, the signal splits into two doublets. This chirality is brought about by cessation of the chelate ring flipping. Thus, the ring conformation can instill chirality into the cluster, but this is a very low-energy process, only ceasing on the NMR timescale at 198 K.  $\Delta G^\ddagger$  calculated for the chelate ring flip is 9.4 kcal/mol.

### (2.3.3) REACTION OF HETEROMETALLIC SYSTEMS WITH ARPHOS

The ARPHOS-substituted tricobalt complex, 9, exhibited fluxionality

whereby the As-Co bond cleaved and reformed at a second cobalt vertex at ambient temperatures. It was also shown in section (2.3.2) that substitution of the DIPHOS ligand into a trimetal cluster of two cobalt atoms and one molybdenum vertex results in substitution only on the cobalt vertices. This was presumed to occur because of steric hindrance preventing reaction at the molybdenum atom. This raises the question, then, that in a heterometallic cluster bearing an ARPHOS group, will the ARPHOS ligand dissociate at the Co-As linkage even when the arsenic atom cannot join to another vertex in the system? An NMR investigation was carried out.

$[\text{C}_5(\text{CH}_3)_5]\text{W}(\text{CO})_2\text{Co}_2(\text{CO})_6\text{C}-\text{CO}_2\text{CH}(\text{CH}_3)_2$ , **15**, was reacted stoichiometrically with  $(\text{C}_6\text{H}_5)_2\text{As}(\text{CH}_2)_2\text{P}(\text{C}_6\text{H}_5)_2$ , giving the product  $[\text{C}_5(\text{CH}_3)_5]\text{WCo}_2(\text{CO})_6-(\text{ARPHOS})\text{C}-\text{CO}_2\text{CH}(\text{CH}_3)_2$ , **17**, in good yield. The  $^{31}\text{P}$  NMR spectrum, a singlet at 41.0 ppm, indicated substitution occurred only on the cobalt atoms, and in an equatorial fashion.



The  $^1\text{H}$  NMR spectrum was very complex. The best-resolved section of the proton spectrum was the isopropyl-methyl region. At reduced temperatures, the spectrum was extremely complicated, with a number of doublets. At ambient temperatures, the spectrum simplified somewhat, but the presence of more than one doublet indicated that chirality still existed in the cluster. Apparently, at low temperatures, even more isomers exist, perhaps relating to both the cyclopentadienyl ring position (Chapter Five) and to the chelate ring conformation.

The crucial difference between this cluster and those previously described is the innate chirality of this molecule. All four tetrahedral vertices are different, and even if the cluster were to form the intermediate structure of a dissociated As terminus (generating a  $16e^-$  vertex) and swing below the tetrahedron, bound only at the P terminus, the cluster would not have a mirror plane. For this reason, only a study of the ARPHOS ligand would reveal if fluxionality involving the bidentate ligand is occurring. Unfortunately, the region of interest in the proton spectrum, that containing signals from the ethylene bridge, was fraught with interferences.

To study the fluxional processes of the carbonyl ligands, a  $^{13}\text{C}$ -enriched sample, prepared as outlined in sections (2.1.2) and (7.2), was observed by variable temperature NMR spectroscopy. At ambient temperature, all carbonyl groups exchange their vertex positions, leading to one signal in the CO region. Upon cooling to 258 K, four signals are resolved initially. One signal appears for each of two tungsten CO's ( $\delta$  228.4, 226.9) and two broad signals are found for the four cobalt carbonyls. Cooling of the sample to still lower temperatures (233 K) resulted in a proliferation of carbonyl signals. Presumably the chelation is complete at this temperature, and the cessation of ring flipping results in a number of conformational isomers which were not detected previously.

It was decided that the study, which had the goal of observing the behaviour of the DIPHOS and ARPHOS ligands in chelation to mixed and non-mixed metal clusters, revealed that given a choice, the bidentate ligands choose to join the less-hindered vertex. The ARPHOS ligand also showed the interesting tendency to cleave at the metal-As linkage, and this was shown to be a higher energy process than simple carbonyl migration between vertices. It was judged unnecessary to react each mixed metal cluster with each bidentate ligand, since little else could be learned about the ligands from such a pursuit.

## (2.4) MASS SPECTROMETRIC ANALYSIS

One property shared by all these clusters is a high molecular weight. Thermal decomposition and pre-analysis fragmentation often occur during conventional study with electron impact mass spectrometry, making characterization using this technique difficult. Fortunately, the past few years have seen the development of Fast Atom Bombardment (FAB) mass spectrometry. This process involves low temperatures, and consequently little undesired decomposition takes place [66,67].

The typical fragmentation pattern of the tricobalt systems invariably reveals several initial cleavages of 28 mass units from the cluster. This is due to the loss of the labile carbon monoxide (28 g/mol) ligands [68]. Parent peaks for each of the molecules discussed in this chapter have been produced by FAB, including a peak at 1016 m/z for the cluster  $[C_5(C^{13})_5]MoCo_2(CO)_6(DIPHOS)C-CO_2CH(CH_3)_2$ , **16**, a truly remarkable accomplishment (Figure 29 B). The combination of  $^{13}C$  enrichment and isotopic distribution of the molybdenum atom produces the peak pattern in the spectrum (Mo has seven major isotopes). An expansion of the parent peak, along with a simulation of the expected peak envelope, (almost identical to the actual spectrum), is presented in Figure 29 A.

Figure 29 A: Parent Peak Region of the FAB Mass Spectrum of  $[C_5(CH_3)_5]MoCo_2(CO)_6(DIPHOS)CCO_2CH(CH_3)_2$ , With Simulated Peak Envelope

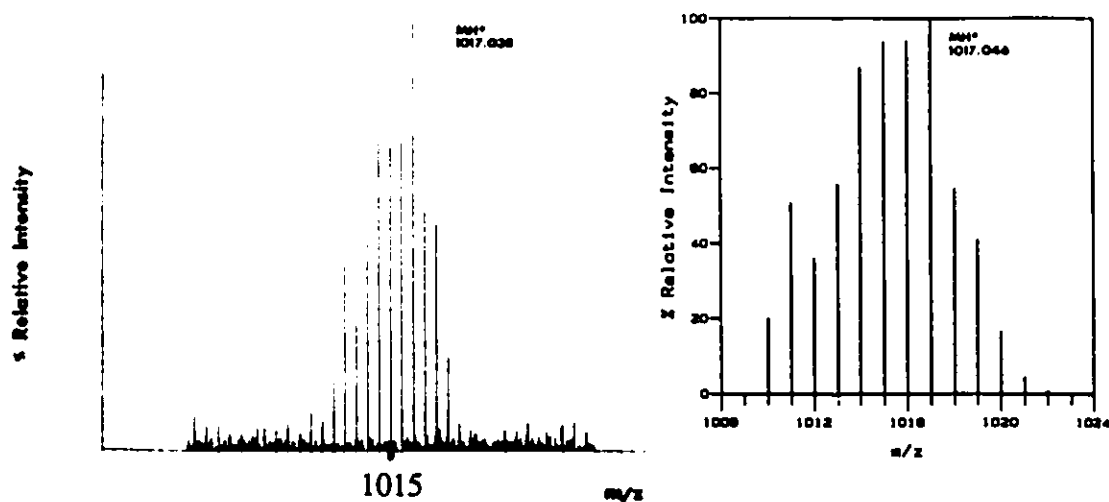
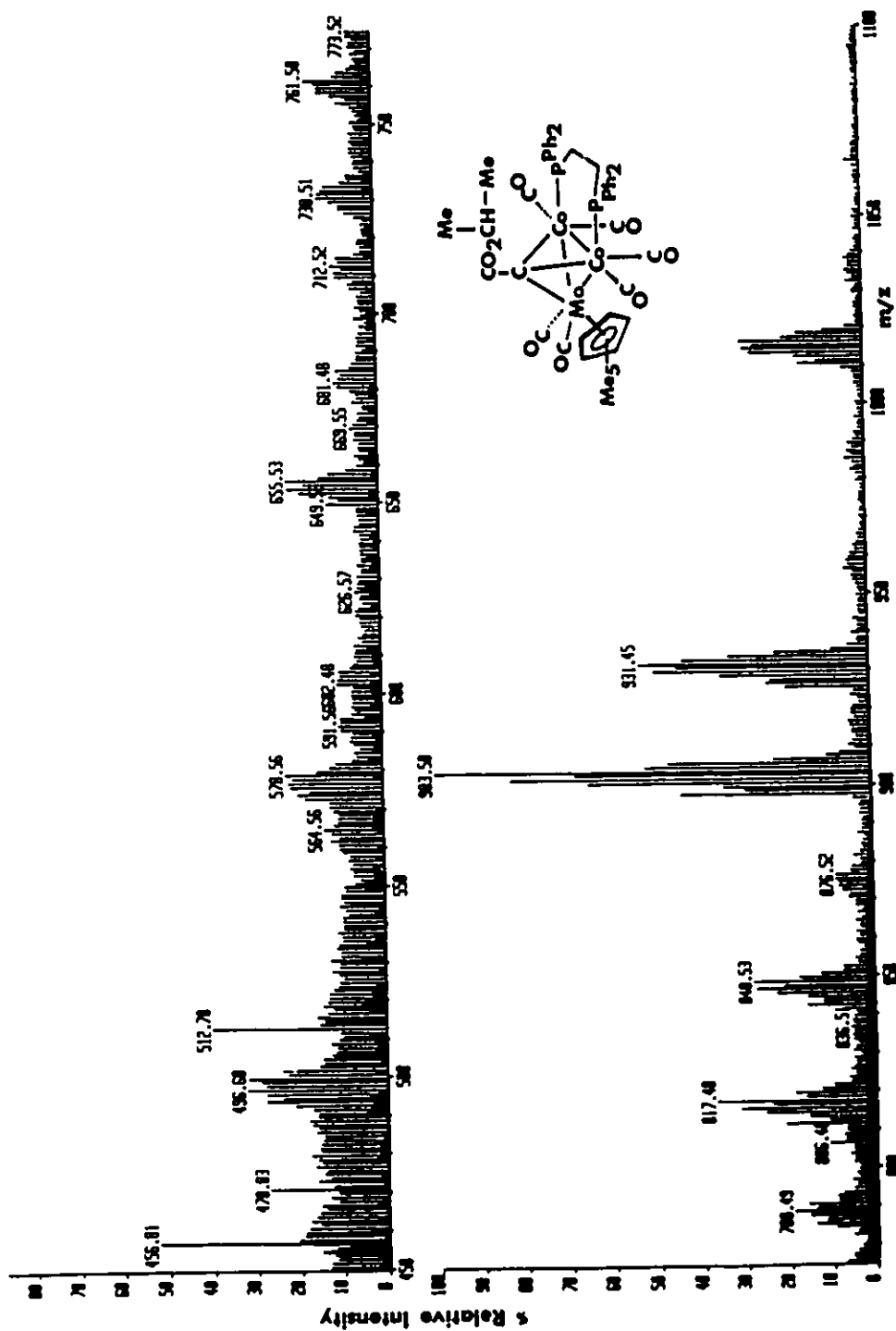


Figure 29 B: FAB Mass Spectrum of  $[\text{C}_5(\text{CH}_3)_5]\text{MoCo}_2(\text{CO})_6(\text{DIPHOS})\text{C-CO}_2\text{CH}(\text{CH}_3)_2$



## (2.5) CONCLUSION

The chelating ligand ARPHOS can render a cluster chiral on the NMR timescale if the conditions are correct -- the temperature of the system is the deciding factor, because at reduced temperature the energy of the system is too low to overcome the barrier to the Co-As bond cleavage. At higher temperatures, this bond-breaking, combined with vertex rotation, results in achirality of the cluster.

This fluxional process is accompanied by carbonyl group migration. At higher temperatures in all complexes studied in this chapter, the carbonyl groups experience intervertex exchange, and are thus rendered equivalent on the NMR timescale. This process, as with the ARPHOS ligand, slows upon decreasing the temperature, and results in all carbonyl groups being localized on specific vertices.

The bidentate ligand DIPHOS, in contrast, shows no evidence of fluxionality other than flipping of the chelate between typical ring conformations, *e.g.*, half-chair converting to twist-boat. The propensity for the diphosphine ligand to remain bound to the cluster does not, however, hinder the carbonyl ligands from moving from one metal vertex to all others. This process, too, slows on the NMR timescale once the temperature is reduced.



## CHAPTER THREE

### (3.1) CLUSTERS WITH THE FOCUS ON THE CAPPING GROUP

In the preceding chapter, various systems were investigated in which fluxionality arose from the ligands bound to the metal vertices of the trimetal tetrahedron. In the ARPHOS/DIPHOS study, the chelating ligand would break its bond to the cobalt vertex at the arsenic link, and the motion could be monitored by observation of the diastereotopic methyl groups on the carbon apex of the tetrahedron. Until now, the apical group has merely been used as a detector for chirality.

Whereas in the previous chapter a bidentate ligand on two metal vertices led to cluster chirality, the focus of this chapter is the attempt to instill chirality in the cluster via the apical group on the tetrahedron. The route used to approach this problem involves a molecule which at room temperature is not chiral because of its fluxionality. We investigate, through nuclear magnetic resonance, infrared spectroscopy and X-ray diffraction crystallography, whether the molecule can be made chiral through cessation of its fluxional process.

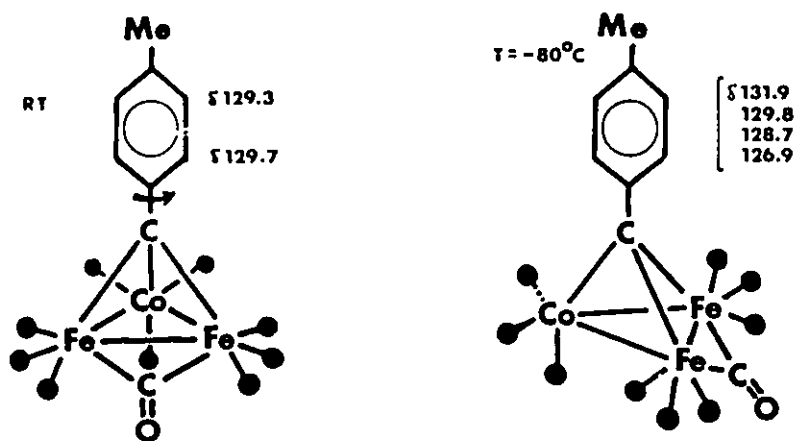
#### (3.1.1) ORIENTATION OF A CAPPING PHENYL RING

It has been proposed that the orientation of the group capping the tricobalt tetrahedral clusters is determined not only by steric effects but also by electronic effects. This was the basis of an discussion presented by Stone [71], and it would not have been so remarkable except that the alleged result of the electronic interaction was to stop a C-C single bond rotation, a very unusual proposition given the type of molecule he was observing.

### (3.1.2) SOLUTION STATE: DYNAMIC OR STATIC?

Stone claimed in 1987 to have stopped rotation of a tolyl ring about a single carbon-carbon bond in the cluster  $\text{Fe}_2\text{Co}(\text{CO})_{10}\text{C}-(4\text{-CH}_3\text{C}_6\text{H}_4)$ , 18 [71]. This conclusion was drawn from the variable temperature  $^{13}\text{C}$  NMR spectra. At room temperature, there were four resonances in the tolyl region -- one each for the *ipso*, *ortho*, *meta* and *para* carbons of the ring. The temperature was decreased to 193 K, and six peaks appeared in the pertinent area of the spectrum. This, according to Stone, indicated that the tolyl ring had stopped rotating about the C-C bond attaching it to the cluster, resulting in inequivalence of all six ring carbons (Figure 30).

Figure 30: Proposed Structure and  $^{13}\text{C}$  NMR Assignments of  $\text{Fe}_2\text{Co}(\text{CO})_{10}\text{C}-(4\text{-CH}_3\text{C}_6\text{H}_4)$ , 18

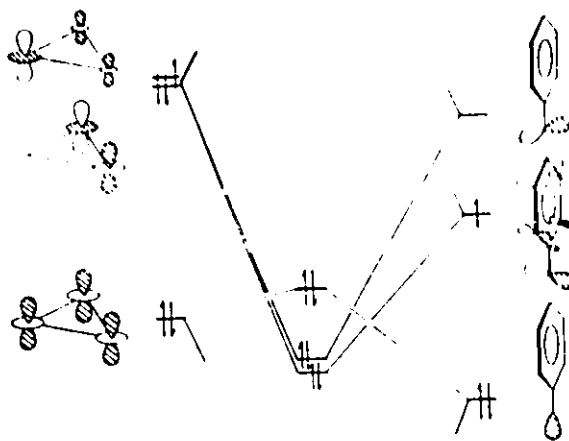


This behaviour would be almost unprecedented, since rotation about a single bond is considered essentially impossible to stop without increasing the bond order to some extent.

How could this be happening? Stone's argument utilizes Molecular Orbital theory to explain the unusual results. The various molecular orbitals which will

describe a system can be predicted by Molecular Orbital theory calculations, and it is presumed that the molecule will be found in the orientation which allows for maximum favourable orbital overlap. A simple structure,  $\text{Co}_3(\text{CO})_9\text{C-C}_6\text{H}_5$ , involving no perturbations to the trimetallic nonacarbonyl system, will be considered as an example. As shown in Figure 31, one frontier orbital on the tolyl-substituted apical carbon fragment points directly at the tri-cobalt triangle, the hybrid  $\text{sp}_z$  orbital. This orbital interacts with the in-phase combination of the  $\text{d}_{z^2}$  orbitals on the cobalt atoms in the trimetal base of the cluster. The remaining p orbitals on the apical carbon,  $\text{p}_x$  and  $\text{p}_y$ , are mutually perpendicular, and can overlap equally well with either of the two degenerate  $2e$  molecular orbitals on the cobalt triangle.

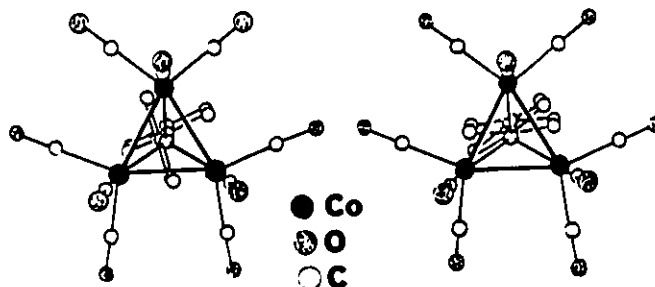
Figure 31: Molecular Orbital Diagram of the Fragments of  $\text{Co}_3(\text{CO})_9\text{C-C}_6\text{H}_5$



Since the capping group's two p orbitals can overlap favourably with either of the e pair of  $\text{d}_{z^2}$  orbital combinations, the resulting structure would be expected to have no preferential orientation of the phenyl ring on the top of the cluster. The crystal structure shows the molecule is disordered with respect to the ring: the unit cell contains four clusters, two per asymmetric unit, each possessing two main orientations

of the ring [20].

Figure 32: Disordered Structures Observed in the X-Ray Diffraction Crystal Structure of  $\text{Co}_3(\text{CO})_9\text{C}-\text{C}_6\text{H}_5$



The crucial change to the system in Stone's cluster is the presence of a bridging carbonyl ligand between the two cobalt atoms. This carbonyl group splits the degeneracy of the  $2e$  set of orbitals on the trimetal base, because the frontier molecular orbitals on the CO group overlap favourably with only one of the two combinations of frontier orbitals on the cobalt atoms (Figure 33). If the overlap is extended throughout the molecule, from the carbonyl  $\pi^*$  orbitals, via the  $d_{z^2}$  orbitals on the cobalts, to the  $\pi$ -orbitals on the phenyl ring, the energy of the entire system would be lowered. This overlap favours one orientation of the phenyl ring, which should have the effect of increasing the barrier to phenyl rotation. The preferred orientation is that which places the orbitals in the appropriate plane for overlapping with the system. Stone claims that this gain in stability for the one rotamer is sufficient to slow the phenyl ring rotation enough to be detectable on the NMR timescale.

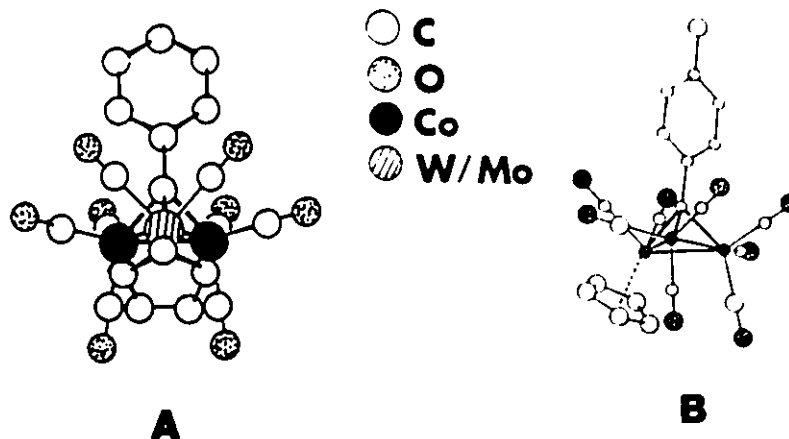
Figure 33: Molecular Orbital Overlap in  $\text{Fe}_2\text{Co}(\text{CO})_{10}\text{C}-(4-\text{CH}_3\text{C}_6\text{H}_4)$



### (3.1.3) SOLID STATE GEOMETRIES

The apical substituents in this study are phenyl, tolyl and xylyl rings. A comparison was made of clusters bearing these rings on their carbon vertex to see if the presence of a bridging carbonyl group affects the orientation of the ring with respect to the trimetallic base in the solid state. Two members of the series  $(C_5H_5)M(CO)_2Co_2(CO)_6C(4-R-C_6H_4)$ , specifically (i)  $M = Mo$ ,  $R = H$  [70], and (ii)  $M = W$ ,  $R = CH_3$  [71], have been characterized by X-ray diffraction crystallography, and the orientation of the ring was found to be, in both cases, parallel to the Co-Co bond (Figure 34). As there is not a bridging C=O present, these clusters should not have any electronic reason to be oriented perpendicular to the cobalt-cobalt vector.

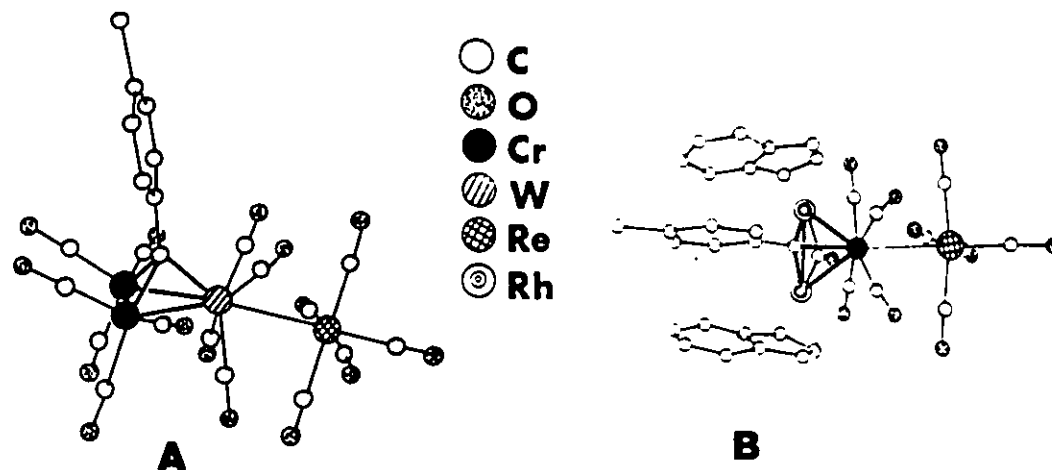
Figure 34: X-Ray Diffraction Crystal Structures of  $(C_5H_5)Mo(CO)_2Co_2(CO)_6C-C_6H_5$ , A, and  $(C_5H_5)W(CO)_2Co_2(CO)_6C-(4-CH_3C_6H_4)$ , B



In a similar cluster,  $W(CO)_4Re(CO)_5Co_2(CO)_6C-(4-CH_3C_6H_4)$  (Figure 35), the tolyl ring also lies parallel to the Co-Co vector, perpendicular to the molecular mirror plane [69]. However, replacement of the  $Co(CO)_3$  vertices in the  $WReCo_2$  cluster by two  $(C_9H_7)Rh$  groups and a bridging carbonyl ligand [72], changes the orientation of the tolyl ring in the solid state, positioning it along the plane of the

bridging carbonyl (Figure 35). The bridging group appears to have an electronic effect strong enough to favour one orientation over all others.

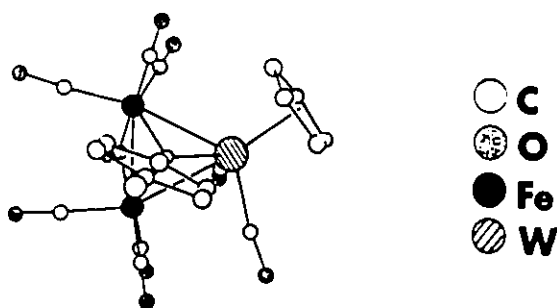
Figure 35: X-Ray Diffraction Crystal Structures of  $W(CO)_4Re(CO)_5Co_2(CO)_6-C-(4-CH_3C_6H_4)$ , A, and  $Cr(CO)_4Re(CO)_5Rh_2(C_9H_7)_2(\mu-CO)C-(4-CH_3C_6H_4)$ , B



Another related cluster with a C=O bridge, the iron-tungsten system

$Fe_2(CO)_6(\mu-CO)W(C_5H_5)(CO)_2C-(4-CH_3C_6H_4)$ , adopts a structure that appears to be a compromise of sorts, as the data reveal the phenyl ring to be rotated approximately  $25^\circ$  from the mirror plane of the cluster [73] (Figure 36). This can be attributed to steric hindrance of the cyclopentadienyl ligand preventing the ring from lying directly in the electronically-favoured plane of the bridging group.

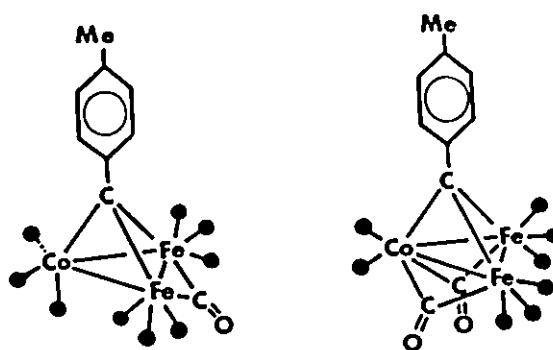
Figure 36: X-Ray Diffraction Crystal Structure of  $Fe_2(CO)_6(\mu-CO)W(C_5H_5)(CO)_2C-(4-CH_3C_6H_4)$



### (3.1.4) A SECOND EXPLANATION

It should be noted that there is another possible explanation for the NMR results seen in the  $\text{Fe}_2\text{Co}(\text{CO})_{10}\text{C}-(4\text{-CH}_3\text{C}_6\text{H}_4)$  cluster. If the phenyl ring were to continue rotating, but the intermetal exchange of the carbonyl groups were to cease, then two isomers of the cluster could be frozen out. In one of them, a single bridging carbonyl is placed between the two cobalt atoms, while the other has two bridging carbonyl groups, one between each cobalt and the iron (Figure 37). Both situations would fulfill the eighteen electron rule for all three metal atoms in the cluster, and the postulate becomes more plausible in light of previous examples of slowed intermetal exchange of iron carbonyl moieties at low temperature [55].

Figure 37: A Second Explanation for the NMR Data -- Two Isomers Related to Carbonyl Distribution



Nevertheless, the idea of preventing rotation about a single  $\sigma$ -bond through no other effect than electronic is an intriguing one. Chirality could be built into a cluster using this method, instead of having to rely on steric bulk to prevent fluxionality and racemization of the system. With this in mind, we decided to investigate a system related to that studied by Stone, one in which the  $\text{Fe}_2(\text{CO})_7$  fragment is replaced by the isolobal  $\text{Co}_2(\text{C}_5\text{H}_5)_2(\text{CO})$  fragment: the  $\text{Co}_3\text{C}$  tetrahedral cluster with two cyclopentadienyl rings,  $\text{Co}_3(\text{C}_5\text{H}_5)_2(\text{CO})_4\text{C}-\text{C}_6\text{H}_5$ , 19.

### (3.2) A MODEL SYSTEM: $\text{Co}_3(\text{C}_5\text{H}_5)_2(\text{CO})_4\text{C}-\text{C}_6\text{H}_5$

#### (3.2.1) SYNTHESIS

This cluster was first synthesized by Dolby and Robinson in 1972 [74]. The procedure entails replacement of five terminal carbonyl ligands from  $\text{Co}_3(\text{CO})_9\text{C}-\text{C}_6\text{H}_5$  by heating the cluster under reflux with excess cyclopentadiene. As the coordinated cyclopentadienyl ligand can be considered to be a five-electron neutral donor, it is necessary to have a one-electron donor on each of the Cp-bearing cobalts to render complete the eighteen-electron outer shell of the cobalt atoms, and the bridging carbonyl fulfills this criterion. (Once again, the cyclopentadienyl ring can be spoken of as a six-electron donor with a charge of -1, requiring the cobalt atom to be in oxidation state +1, a matter of terminology only.)

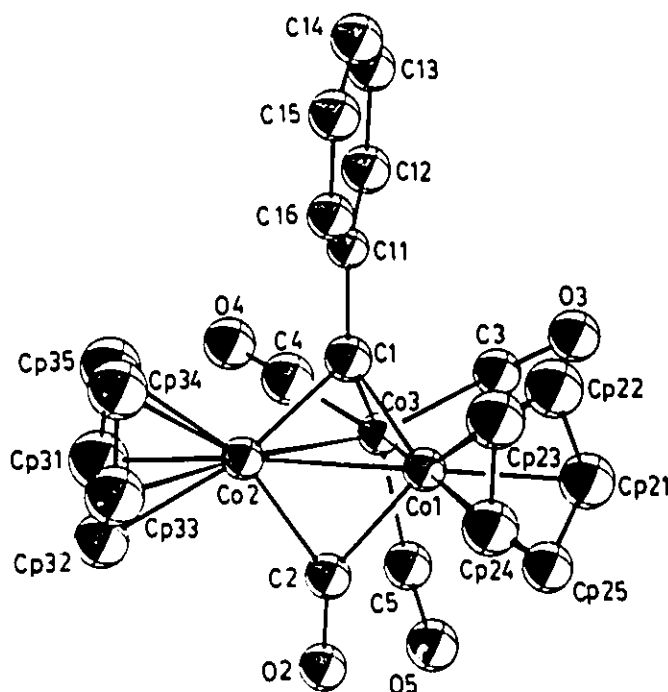
#### (3.2.2) THE STRUCTURE IN THE SOLID STATE: X-RAY DIFFRACTION CRYSTAL STRUCTURE OF $\text{Co}_3(\text{C}_5\text{H}_5)_2(\text{CO})_4\text{C}-\text{C}_6\text{H}_5$

The molecular structure of the compound  $\text{Co}_3(\text{C}_5\text{H}_5)_2(\text{CO})_4\text{C}-\text{C}_6\text{H}_5$ , 19, was determined by using the technique of X-ray diffraction crystallography (Figure 38). The skeleton resembles that of most tricobalt-monocarbon clusters, a slightly distorted tetrahedron. A carbonyl group bridges two cobalt vertices. The average cluster bond lengths are 2.452(1) Å (Co-Co) and 1.884(8) Å (Co-C), though the bridged cobalt-cobalt linkage is shorter (2.397(1) Å) than the unbridged Co-Co bonds. The carbonyl groups on the  $\text{Co}(\text{CO})_3$  moiety are fully terminal, with the axial Co-C bond (1.881(9) Å) slightly longer than the equatorial Co-C bonds (av. 1.79(1) Å). The bond lengths in the cyclopentadienyl and phenyl rings are characteristic of systems displaying aromatic character, with the  $\text{C}_5\text{H}_5$  average bond length of 1.40(2) Å and the average bond length in the phenyl ring of 1.39(1) Å. The angles in the phenyl ring have an average value of 120(1)°, and those in the cyclopentadienyl rings average 108(1)°.



Further information on data collection, positional parameters, bonds and angles can be found in Chapter Seven.

Figure 38: X-Ray Diffraction Crystal Structure of  $\text{Co}_3(\text{C}_5\text{H}_5)_2(\text{CO})_4\text{C}-\text{C}_6\text{H}_5$ , 19



This structure can be compared to the methyl-capped analogue [75], with several interesting points worth noting. In the phenyl cluster, the cyclopentadienyl rings are eclipsed, while in the methyl molecule, they are completely staggered. The angle between the planes of the two rings in the phenyl compound is smaller ( $40^\circ$ ) than the angle in the methyl complex ( $54^\circ$ ), which could indicate the phenyl ring is pushing the rings further apart and back from the bridging carbonyl, thus making them closer to parallel than are the rings in the methyl compound. This is reflected in the ring separation: the centroid-centroid distance is  $5.61 \text{ \AA}$  in the phenyl complex,  $0.21 \text{ \AA}$  greater than that of the methyl analogue. A second factor which could account for the

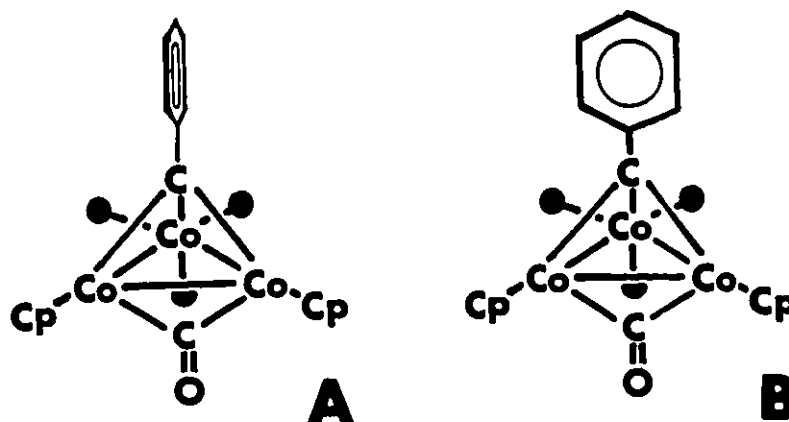
increased separation of the  $C_5H_5$  rings in the phenyl-capped cluster is the position of the bridging  $C=O$ . The bridging carbonyl is bent down at an angle of  $100^\circ$  from the tricobalt plane with the presence of the phenyl ring, while in the methyl-capped compound the angle is  $92.7^\circ$ . The  $C=O$  at  $100^\circ$  is closer to the Cp rings, and would push them apart. (It is tempting to speculate that the position of the bridging carbonyl is that which provides maximum orbital overlap of the type shown in Figure 33.) The centroids of the cyclopentadienyl ligands in both molecules lie essentially coplanar with the cobalt vertices, with a dihedral angle of  $0.6^\circ$  in the phenyl case, and  $2.7^\circ$  in the methyl example. Naturally the most important fact derived from the crystal structure solution is the orientation of the phenyl ring -- it is aligned with the molecular mirror plane, such that molecular orbital overlap is maximized, as predicted by Stone. The question remained: would the electronic effect be strong enough to govern solution state behaviour as well?

### (3.2.3) SOLUTION STATE NMR STUDY

The investigation continued with a variable-temperature  $^{13}C$  NMR study of 19 at high field (S.F. = 125 MHz). At ambient temperature, the data showed four signals in the phenyl region, indicating the phenyl ring was rotating freely about the C-C single bond. Cooling of the sample could lead to two possible results.

If the ring stopped in the plane of the bridging carbonyl group, (Figure 39 A), then the *ortho* and *meta* carbons would be in four different environments, and this should produce four discrete signals in the NMR spectrum. However, if the phenyl ring stopped its rotation in a plane perpendicular to the  $\mu$ -CO (Figure 39 B), the *ortho* carbon on one side of the ring would be equivalent to its partner on the other side of the ring, and the same would hold for the *meta* carbons. If this second scenario reflected the true situation, slowed rotation would remain undetectable in the NMR spectrum.

Figure 39: Two Possible Scenarios for Cessation of Fluxionality Upon Cooling of  $\text{Co}_3(\text{C}_5\text{H}_5)_2(\text{CO})_4\text{C}-\text{C}_6\text{H}_5$



The spectra obtained at room temperature and at 183 K were essentially identical, indicating either the ring has not slowed its rotation, or the ring has stopped in a plane perpendicular to the mirror plane. As the temperature was lowered to 183 K, no change was seen in the spectrum except for a slight broadening of the signals, a common feature of spectra in which the NMR nuclei are bound to quadrupolar nuclei ( $^{59}\text{Co}$ , 100% abundance spin = 7/2). To elucidate what is happening, the ring must be labelled.

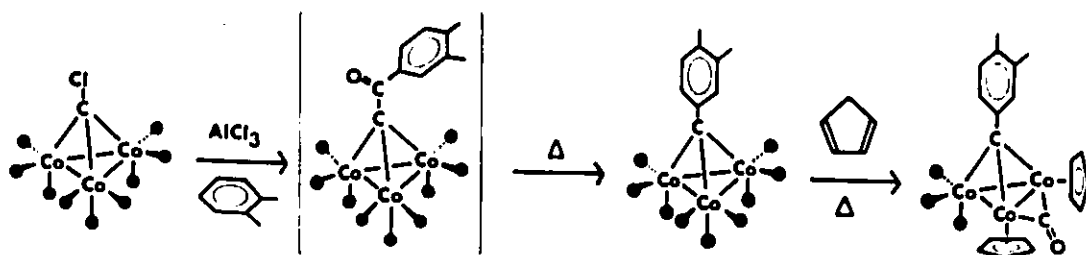
### (3.3) A LABELLED SYSTEM, $\text{Co}_3(\text{CO})_4(\text{C}_5\text{H}_5)_2\text{C}-[3,4-(\text{CH}_3)_2\text{C}_6\text{H}_3]$ , 20

#### (3.3.1) SYNTHESIS

Incorporation of a methyl group in an asymmetric position on the capping phenyl ring was achieved via synthesis of a xylyl cluster using the method of Dolby and Robinson [74].  $[\text{Co}_3(\text{CO})_9\text{CCO}^+][\text{AlCl}_4^-]$ , produced by stirring  $\text{Co}_3(\text{CO})_9\text{C}-\text{Cl}$  with  $\text{AlCl}_3$ , reacts with *ortho*-xylene to form  $\text{Co}_3(\text{CO})_9\text{C}-\text{CO}-[3,4-(\text{CH}_3)_2\text{C}_6\text{H}_3]$ , which in turn decarbonylates rapidly at elevated temperatures in solution [16]. The resulting  $\text{Co}_3(\text{CO})_9\text{C}-[3,4-(\text{CH}_3)_2\text{C}_6\text{H}_3]$  undergoes carbonyl substitution with cyclopentadiene, as before. It should be noted that the sole product of the electrophilic attack on the

xylylene ring is the [3,4-(CH<sub>3</sub>)<sub>2</sub>C<sub>6</sub>H<sub>3</sub>]-capped cluster. No substitution is seen at positions *ortho* to the methyl substituents on the ring, most likely due to the large size of the electrophile.

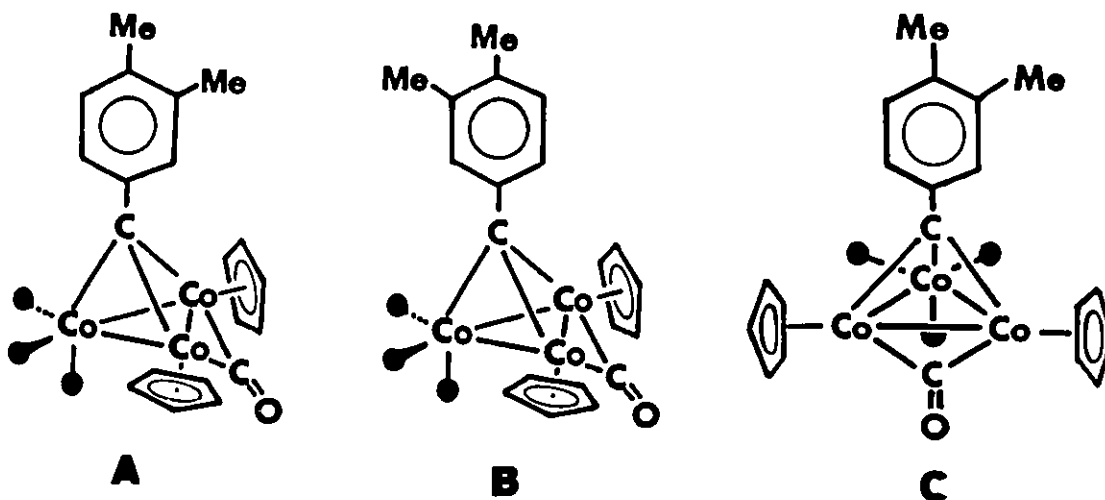
Scheme 5: Preparation of Co<sub>3</sub>(CO)<sub>4</sub>(C<sub>5</sub>H<sub>5</sub>)<sub>2</sub>C-[3,4-(CH<sub>3</sub>)<sub>2</sub>C<sub>6</sub>H<sub>3</sub>]



### (3.3.2) NUCLEAR MAGNETIC RESONANCE STUDY

The NMR spectrum of this new compound, Co<sub>3</sub>(CO)<sub>4</sub>(C<sub>5</sub>H<sub>5</sub>)<sub>2</sub>-C-[3,4-(CH<sub>3</sub>)<sub>2</sub>C<sub>6</sub>H<sub>3</sub>], 20, was recorded under the same conditions as for the phenyl compound. There are three possibilities for behaviour, and each would give a different result in the NMR experiment. (a) If the ring were to stop in a plane parallel to the bridging carbonyl, a fraction of the xylyl methyl groups would point away from the bridging group, while the rest would point towards it. These rotamers would presumably be detectable by NMR (Figures 40 A and B).

Figure 40: Possible Positions of the Xylyl Ring in 20 if Rotation Ceases on the NMR Timescale



(b) Conversely, if the rotation stops and the xylyl group is oriented in a plane perpendicular to the molecular mirror plane, the cyclopentadienyl ligands would become inequivalent, as one Cp ring will be proximal to the methyl group, and one will be further away (Figure 40 C). (c) The ring may continue to rotate, and one set of xylyl signals only would be seen in the NMR spectrum.

The ambient temperature spectrum showed one signal for each methyl group in the xylyl ring, indicating of free rotation of the phenyl ring. As the temperature decreased, there was no sign of any splitting of the signals. Not only was there no change in the methyl or phenyl regions of the spectrum, but the signal from the cyclopentadienyl ligands remained a sharp singlet at all times in the NMR experiment. The addition of the label to the ring did not reveal any previously undetectable cessation of motion by the ring.

### (3.4) CALCULATIONAL RESULTS

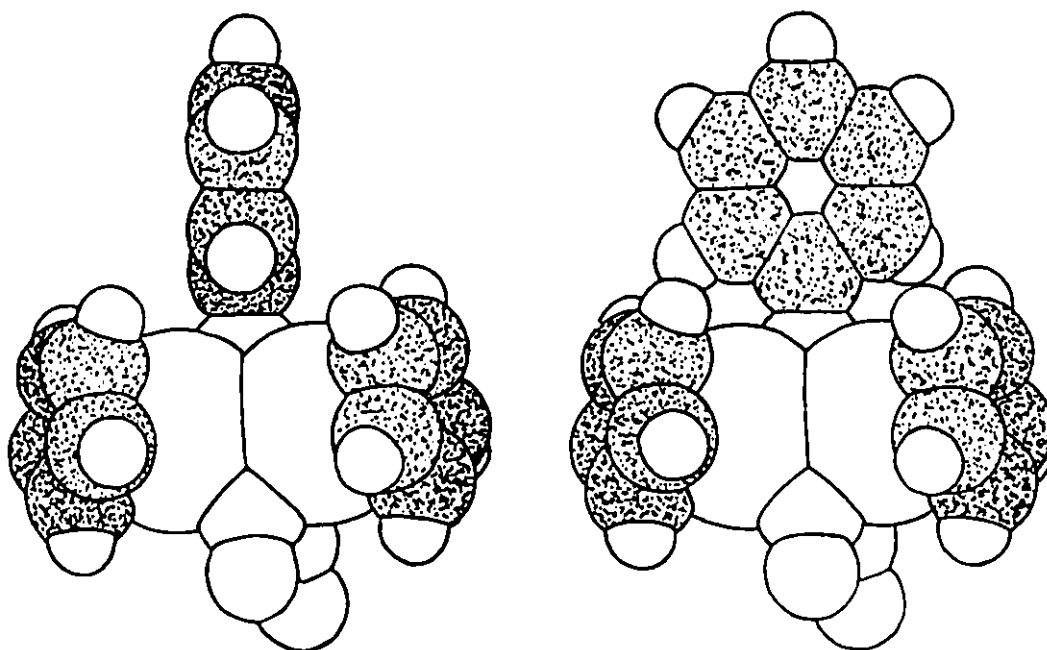
#### (3.4.1) VAN DER WAALS' RADII

The parameters derived from the crystallographic study were entered into the CHEMX program [76], and the data were manipulated to place the phenyl ring in the two orientations of interest, parallel with and perpendicular to the carbonyl bridge. The atoms were then assigned van der Waals' radii, and the cyclopentadienyl rings were rotated so as to maximize through-space overlap. With the greatest possible overlap, the distance of closest approach of the phenyl ring protons to the cyclopentadienyl ring protons is one angstrom, which is certainly not close enough to be a hindrance to rotation of the phenyl ring.

The space-filling diagrams generated using the CHEMX program are a good aid in visualization of this last point (Figure 41). It can be seen that the ring protons never approach each other within interaction distance and thus would not be

expected to be a factor in the cessation of rotation of the apical phenyl ring.

Figure 41: Space-Filling Diagrams of the Two Limiting Orientations of  $\text{Co}_3(\text{CO})_4(\text{C}_5\text{H}_5)_2\text{C}-\text{C}_6\text{H}_5$ , 19



#### (3.4.2) MOLECULAR ORBITAL STUDY

Stone reported the increase in stability of the  $\text{Fe}_2\text{Co}(\text{CO})_{10}\text{C}-(4-\text{CH}_3\text{C}_6\text{H}_4)$  system due to the molecular orbital interaction to be on the order of 58 kJ/mol (13.9 kcal/mol) [71]. Molecular orbital calculations were performed on the  $\text{Co}_3(\text{C}_5\text{H}_5)_2(\text{CO})_4\text{C}-\text{C}_6\text{H}_5$  system, to determine the energy difference between the two conformations -- that with the ring parallel to the molecular mirror plane, and that with the ring orthogonal to it. The energy calculated for the rotamers is presented in Table 7. The barrier to rotation is only 6.6 kcal/mol, which is too low to "freeze out" in the NMR spectrum.

Table 7: Calculated Energies for Rotational Isomers of  $\text{Co}_3(\text{C}_5\text{H}_5)_2(\text{CO})_4\text{C}-\text{C}_6\text{H}_5$ 

Phenyl Ring Orientation Relative to C=O Bridge	Calculated Energy (kcal/mol)
Parallel	-61105.677
Perpendicular	-61099.082

### (3.5) CONCLUSION

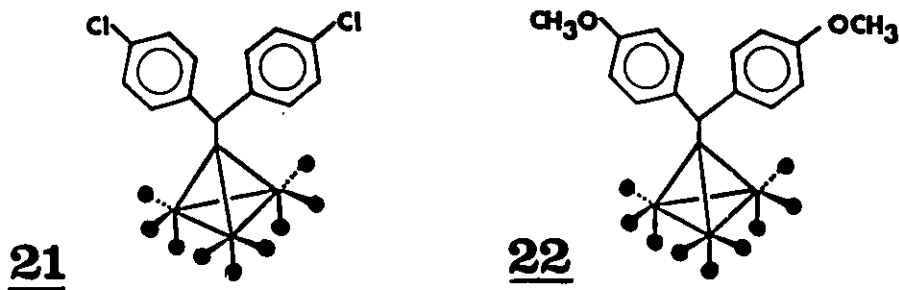
This investigation closes with the conclusion that the phenyl ring bound to the capping carbon of the tricobalt-dicyclopentadienyl-tetrahedron does not stop its rotation on the NMR timescale even with the presence of the bridging carbonyl. The X-ray diffraction crystal structure shows that the phenyl ring is positioned so as to maximize orbital overlap throughout the cluster. It is therefore concluded that the electronic effect, just as predicted by Hoffmann's molecular orbital calculations, is great enough to cause a preferential orientation of the ring in the solid state. This knowledge could potentially be utilized to design a molecule containing even more favourable overlaps with its ligands, with the eventual goal of controlling intramolecular motions (and directing chirality) via purely electronic effects.

## CHAPTER FOUR

### (4.1) EXTREME BULK CAPPING THE CLUSTER

One of the most useful modes of cobalt cluster synthesis is the reaction of a trichlorinated compound with dicobalt octacarbonyl, resulting in replacement of all three chlorine groups to produce a tricobalt monocarbon tetrahedral skeleton bearing various organic ligands on the apex of the molecule.

A specific example, that of DDT with  $\text{Co}_2(\text{CO})_8$ , yields  $\text{Co}_3(\text{CO})_9\text{C}-\text{CH}-(4-\text{ClC}_6\text{H}_4)_2$ , **21** [77]. The analogue  $\text{Co}_3(\text{CO})_9\text{C}-\text{CH}-(4-\text{OCH}_3\text{C}_6\text{H}_4)_2$ , **22**, is produced upon reaction of dicobalt octacarbonyl with METHOXYCHLOR,  $\text{Cl}_3\text{C}-\text{CH}-(4-\text{OCH}_3\text{C}_6\text{H}_4)_2$ . Both molecules display very distinctive behaviour in the nuclear magnetic resonance spectrum [77,78].



The molecules show one signal in the carbonyl region of the  $^{13}\text{C}$  spectrum, indicating axial-equatorial exchange of the carbonyl groups on the NMR timescale. These spectral data, also seen in other molecules in this thesis, do not necessarily imply intervertex exchange of carbonyl ligands. However, in heterometallic clusters such as  $(\text{C}_5\text{H}_5)\text{Mo}(\text{CO})_2\text{Co}_2(\text{CO})_6\text{C}-\text{CO}_2\text{CH}(\text{CH}_3)_2$ , a single  $^{13}\text{C}=\text{O}$  peak is seen at room temperature, showing that intermetal carbonyl migration must occur. It is only at the lower temperature of 183 K that the Mo-CO peak (235.0 ppm) and the Co-CO resonance (200.9 ppm) are observed. Since the exchange process is so facile in

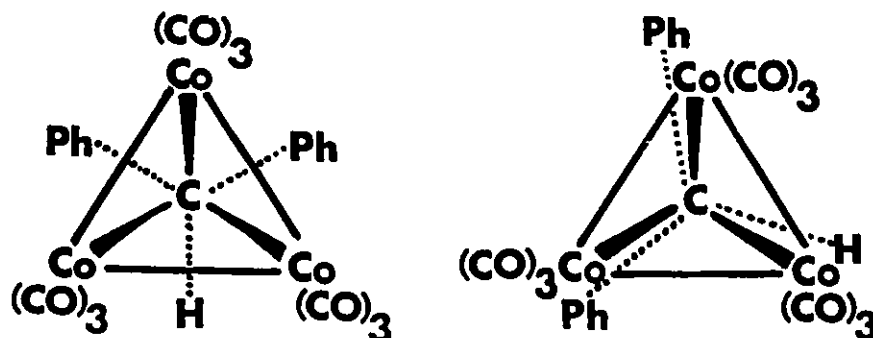


heterometallic clusters, there is little reason to believe that it is not occurring under homometallic circumstances as well.

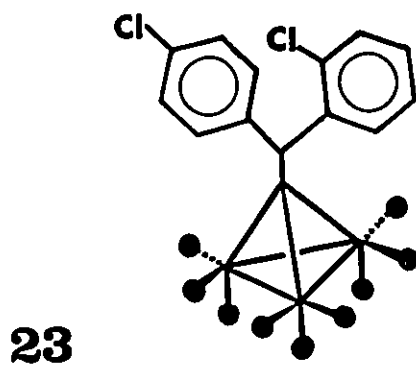
The remarkable behaviour of 21 and 22 appeared in the spectrum upon cooling of the sample to very low temperatures. At 180 K, the single resonance had split into two signals in a 2:1 (6:3) ratio. This is open to two interpretations: (a) If the apical group is still rotating with respect to the cluster, the only scenario that could give rise to a 6:3 pattern of CO signals is cessation of axial-equatorial CO interchange in one of two ways. Either three carbonyls would be axial and six would be equatorial, or three CO's could be bridging below the trimetal plane (in an axial sense) and the remaining six would be equivalent equatorial CO's. However, though Fe carbonyl ligands on an  $\text{Fe}(\text{CO})_3$  moiety have been frozen into axial and equatorial environments [55], cobalt carbonyls have never been unequivocally observed this way. In fact, cobalt carbonyl ligands are notorious for their propensity to continue axial-equatorial exchange at reduced temperatures [55]; (b) The second possible explanation involves cessation of the apical group rotation with respect to the trimetal base of the cluster. Using steric arguments, one could presume the phenyl rings would be staggered from the cobalt vertices to avoid carbonyl interaction (Figure 42 A). A second possible positioning finds the capping groups eclipsing the cobalt tricarbonyl vertices (Figure 42 B). In either case, two cobalt vertices would be in one environment, with the third  $\text{Co}(\text{CO})_3$  in another.

If the carbonyl ligands are not undergoing intermetal exchange, (which is possible, because at this temperature, cessation of intervertex exchange is observed in molecules in which it can be detected, *e.g.*,  $\text{Mo}(\text{CO})_2(\text{C}_5\text{H}_5)\text{Co}_2(\text{CO})_6\text{C}-\text{CO}_2-\text{CH}(\text{CH}_3)_2$ ), then the CO's can still be rotating around their specific vertices while giving rise to two discrete signals -- one for the six carbonyl groups on the equivalent cobalt atoms, and one for the remaining three CO ligands.

Figure 42: Two Possible Orientations of the Capping Group With Respect to the Tetrahedron



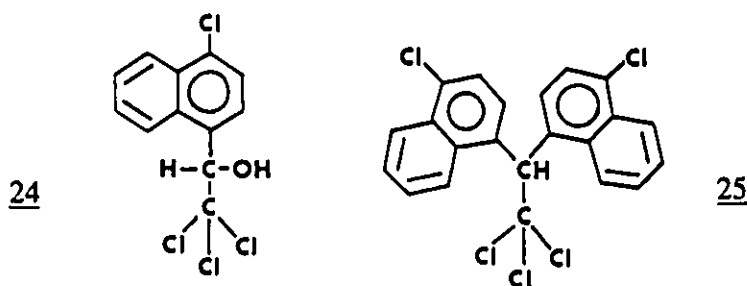
Relevant to these considerations is the recent work of D'Agostino [78], who has noted that in the system 23, derived from *o,p'*-DDT, the 2:1 splitting pattern is again observed in the carbonyl region of the spectrum. If apical rotation had ceased in the manner shown above, it might have been anticipated that a 1:1:1 pattern would appear, since in this chiral molecule, all three  $\text{Co}(\text{CO})_3$  vertices would be rendered inequivalent. One could thus tentatively conclude that it is axial-equatorial exchange that has been slowed on the NMR timescale.



In order to enhance the possible steric effects in this system so as to raise the activation energies to any of these proposed fluxional processes, we chose to incorporate an even bulkier apical group. To this end, a synthesis of the analogous chloronaphthyl cluster was developed.

(4.2) SYNTHESIS AND NMR OF THE STARTING MATERIAL  $\text{Cl}_3\text{C-CH(4-ClC}_{10}\text{H}_6)$ , 25

The preparation of  $\text{Cl}_3\text{C-CH(4-ClC}_{10}\text{H}_6)_2$  was developed by Stephenson and Waters in 1946 [79], with an improved synthesis published the following year by Haskelberg and Lavie [80]. The condensation of chloral,  $\text{Cl}_3\text{CCHO}$ , with  $\alpha$ -chloronaphthalene in the presence of  $\text{H}_2\text{SO}_4$ , results in an intermediate product of the mono-substituted 24. Further attack by  $\text{H}^+$  and loss of  $\text{H}_2\text{O}$  allows reaction with another molecule of chloronaphthalene, to yield 1,1,1-trichloro-2,2-di-(4'-chloronaphthyl)-1'-ethane, 25.



Molecule 25 had not been fully characterized by nuclear magnetic resonance previously, because of the early year of synthesis. Development of two-dimensional NMR techniques [81] allowed for extensive characterization of the compound. The  $^1\text{H}$  NMR 2-D spectrum is presented in Figure 43, with the signal assignments in Table 8.

(4.3) THE NEW CLUSTER:  $\text{Co}_3(\text{CO})_9\text{C-CH-(4-ClC}_{10}\text{H}_6)_2$

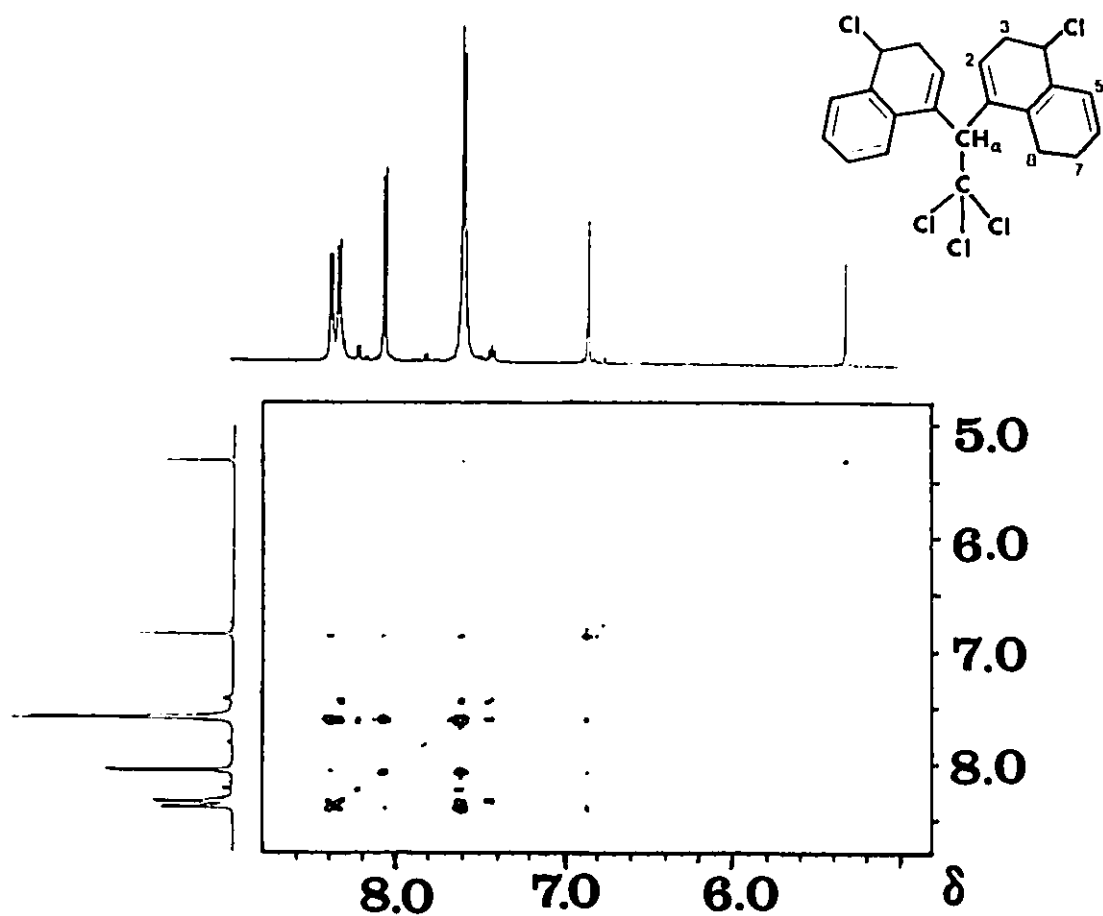
(4.3.1) SYNTHESIS AND NMR

The reaction of 25 with dicobalt octacarbonyl would be predicted to yield a tetrahedral cluster of three  $\text{Co}(\text{CO})_3$  vertices and one carbon vertex bearing the large naphthyl groups. This molecule would be a good example of a system of extreme bulk on the capping group, and should enhance any effects of restricted rotation.

Table 8:  $^1\text{H}$  NMR Data for 1,1,1-trichloro-2,2-di-(4'-chloronaphthyl-1')-ethane, 25

Proton	Chemical Shift ( $\delta$ )	Other Proton Interactions	Coupling Pattern
H <sub>2</sub>	7.6	H <sub>3</sub>	m
H <sub>3</sub>	8.08	H <sub>2</sub>	d
H <sub>5</sub>	8.35	H <sub>6</sub> , H <sub>7</sub> , (H <sub>8</sub> )	dd
H <sub>6</sub>	7.6	H <sub>5</sub> , H <sub>7</sub> , H <sub>8</sub>	m
H <sub>7</sub>	7.6	H <sub>5</sub> , H <sub>6</sub> , H <sub>8</sub>	m
H <sub>8</sub>	8.39	H <sub>7</sub> , H <sub>6</sub> , (H <sub>5</sub> )	dd
H <sub><math>\alpha</math></sub>	6.56	(H <sub>2</sub> , H <sub>8</sub> )	s

Protons in brackets are weakly coupled.

Figure 43: Two-Dimensional Proton-Proton Correlated NMR Spectrum of 25

Reaction of  $\text{Co}_2(\text{CO})_8$  with 25 proceeded in a sluggish fashion. Heating of the reaction mixture above 328 K led to decomposition of any cluster present, while the reaction did not occur at all at room temperature (295 K). Careful heating to 318 K for approximately three hours gave a mixture of products. The sample predominantly consisted of brown-black crystals of  $\text{Co}_4(\text{CO})_{12}$ . This is not surprising, as the reaction conditions are ideal for conversion of  $\text{Co}_2(\text{CO})_8$  into  $\text{Co}_4(\text{CO})_{12}$  [82]. The minor component of the mixture, eluted second from the purification column was the desired cluster,  $\text{Co}_3(\text{CO})_9\text{C-CH-(4-ClC}_{10}\text{H}_6)_2$ , 26.

The NMR spectrum of 26 was investigated. Though clear  $^1\text{H}$  NMR spectra were obtained for the trichlorinated starting material, once the group was incorporated into the cluster, the proximity of the quadrupolar  $^{59}\text{Co}$  nuclei broadened the proton spectrum. Consequently,  $^{13}\text{C}$  nuclear magnetic resonance spectroscopy was the technique used to determine the structure and behaviour of the system.

At ambient temperature, there appeared only one signal in the carbonyl region, at 200.3 ppm, indicating equivalence of all carbonyl ligands. To fulfill this requirement, axial-equatorial exchange of the ligands must be faster than the NMR timescale. The naphthyl region displayed several peaks, but the naphthyl rings were equivalent, as ten signals were found, not twenty. The apical carbon signal of the cluster skeleton appeared at 303 ppm.

The temperature of the sample was lowered to discern if any resolution of the carbonyl ligands signals would occur (as observed with the DDT and METHOXY-CHLOR derivatives 21 and 22). At the limiting temperature of 183 K, there remained a single resonance for the carbonyl groups. The naphthyl rings also maintained their equivalence at low temperature.

### (4.3.2) INFRARED ANALYSIS

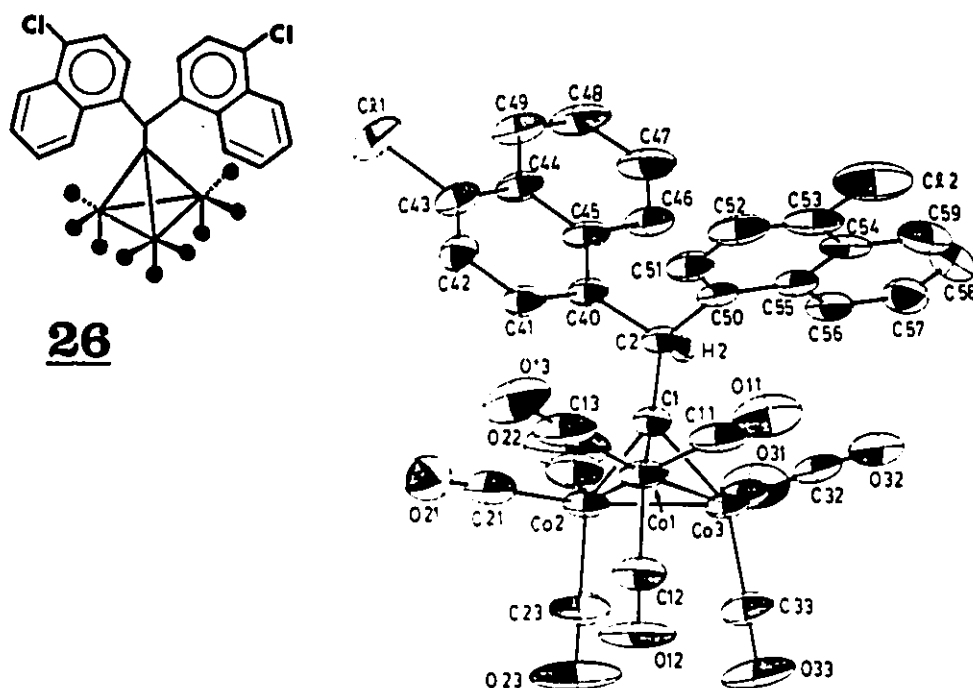
The infrared spectrum correlated perfectly with the NMR conclusions. The carbonyl stretches appeared at 2092, 2038, 2027 and 2010  $\text{cm}^{-1}$ , all in a region of fully terminal metal carbonyl groups (terminal carbonyl ligands on metals absorb infrared energy between 2200 and 1900  $\text{cm}^{-1}$ , while bridging carbonyls show infrared absorbance of lower energy, between 1900 and 1700  $\text{cm}^{-1}$ [83]). The small number of bands (four absorbances from nine CO's) attests to the high symmetry of the molecule: the mirror plane evident in the low-temperature solution NMR spectrum (from the equivalence of the naphthalene rings) appeared present even on the timescale of infrared spectroscopy.

### (4.3.3) X-RAY DIFFRACTION CRYSTAL STRUCTURE OF $\text{Co}_3(\text{CO})_9\text{C-CH-}(4\text{-ClC}_{10}\text{H}_6)_2$

To discover if the molecule has the same geometry as would be predicted from the solution spectroscopic behaviour, the solid state structure of 26 was determined. The dark purple compound formed shiny crystals using rapid crystallization techniques from ether/hexane solution. The speed was necessary because the dinaphthyl cluster tended to decompose in solution to  $\text{Co}_4(\text{CO})_{12}$  and insoluble cobalt salts.

The solid state structure displayed only one isomer of the cluster (Figure 44). The tetrahedral skeleton is typical of all tricobalt clusters, with slightly shorter Co-C bonds (av. 1.922(5) Å) than Co-Co bonds (av. 2.462(1) Å). The carbonyl ligands occupy terminal positions on the cobalt vertices. The axial carbonyl ligands display longer linkages to the cobalt atoms (av. 1.841(7) Å) than do the equatorial CO groups (av. 1.784(7) Å). The bond lengths of the naphthyl rings are characteristic of aromatic ring C-C bonds, with an average value of 1.394(10) Å.

Figure 44: X-Ray Diffraction Crystal Structure of  $\text{Co}_3(\text{CO})_9\text{C}(4\text{-ClC}_{10}\text{H}_6)_2$ , 26



This structure can be compared to the crystal structure determined for the analogous DDT-derivative,  $\text{Co}_3(\text{CO})_9\text{C-CH-(4-ClC}_6\text{H}_4)_2$ , 21 (Figure 45 A) [77]. In both systems, the aromatic rings are twisted relative to the tricobalt plane. This can be seen clearly in Figure 45 B, and the angle of twist can be quantitated using the dihedral angles relative to the (apical C)-CH bond in both molecules. In the DDT-derivative, the dihedral angles C(1)-C(2)-C(41)-C(42) and C(1)-C(2)-C(51)-C(56) are  $+83^\circ$  and  $-58^\circ$ , respectively. In the naphthyl system, those angles are  $+78^\circ$  and  $-34^\circ$ . Clearly, the rings are closer to being related by a mirror plane in the case of the DDT cluster. Though the carbonyl ligands are fully terminal in both systems, they are tilted slightly about one cobalt vertex in the naphthyl molecule, likely an artifact of the proximity of the large naphthyl rings.

National Library  
of Canada

Canadian Theses Service

Bibliothèque nationale  
du Canada

Service des thèses canadiennes

NOTICE

THE QUALITY OF THIS MICROFICHE  
IS HEAVILY DEPENDENT UPON THE  
QUALITY OF THE THESIS SUBMITTED  
FOR MICROFILMING.

UNFORTUNATELY THE COLOURED  
ILLUSTRATIONS OF THIS THESIS  
CAN ONLY YIELD DIFFERENT TONES  
OF GREY.

AVIS

LA QUALITE DE CETTE MICROFICHE  
DEPEND GRANDEMENT DE LA QUALITE DE LA  
THESE SOUMISE AU MICROFILMAGE.

MALHEUREUSEMENT, LES DIFFERENTES  
ILLUSTRATIONS EN COULEURS DE CETTE  
THESE NE PEUVENT DONNER QUE DES  
TEINTES DE GRIS.



Figure 44 A: X-Ray Diffraction Crystal Structure of  $\text{Co}_3(\text{CO})_9\text{C}-(4\text{-ClC}_{10}\text{H}_6)_2$ , 26, Showing Van Der Waals' Radii

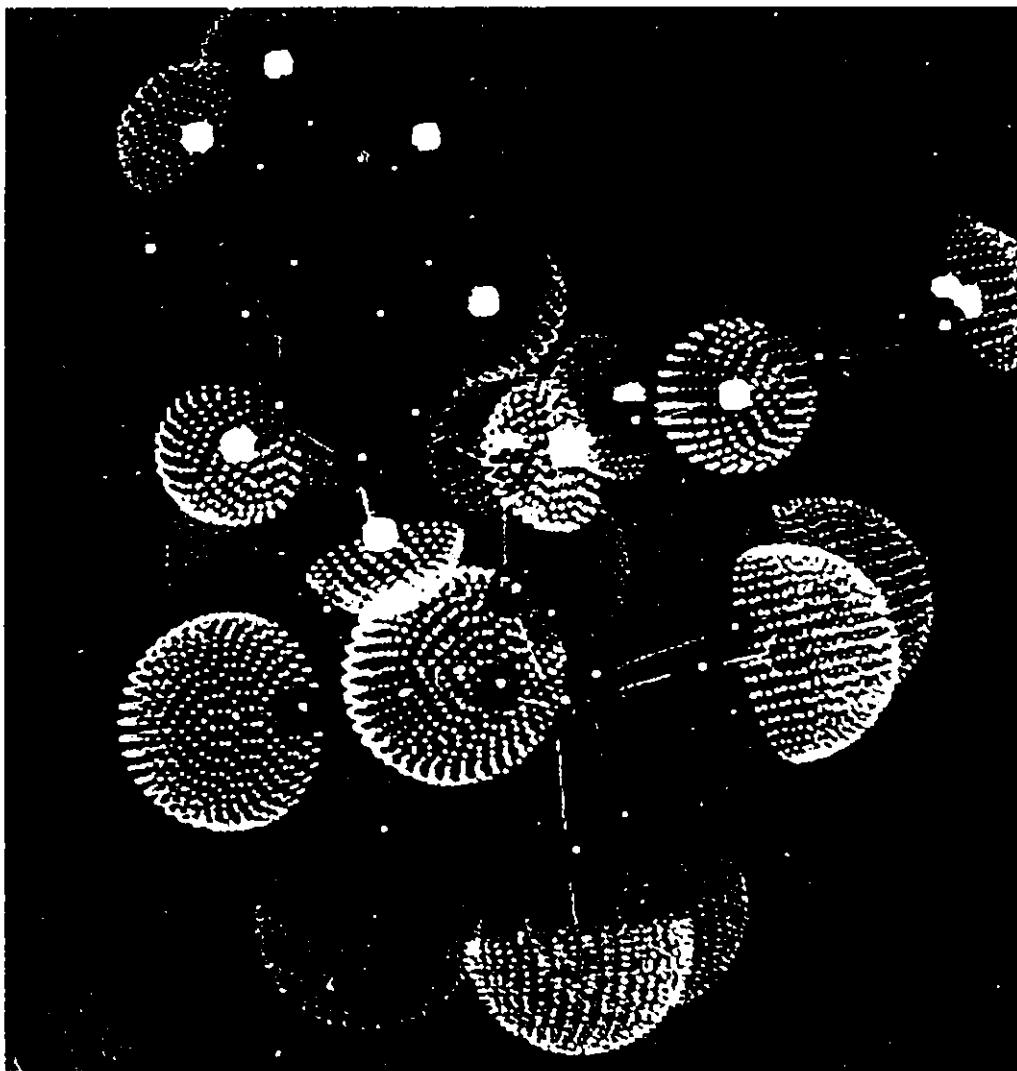


Figure 44 B: X-Ray Diffraction Crystal Structure of  
 $\text{Co}_3(\text{CO})_9\text{C}-(4\text{-ClC}_{10}\text{H}_6)_2$ , 26, Space-filling Model

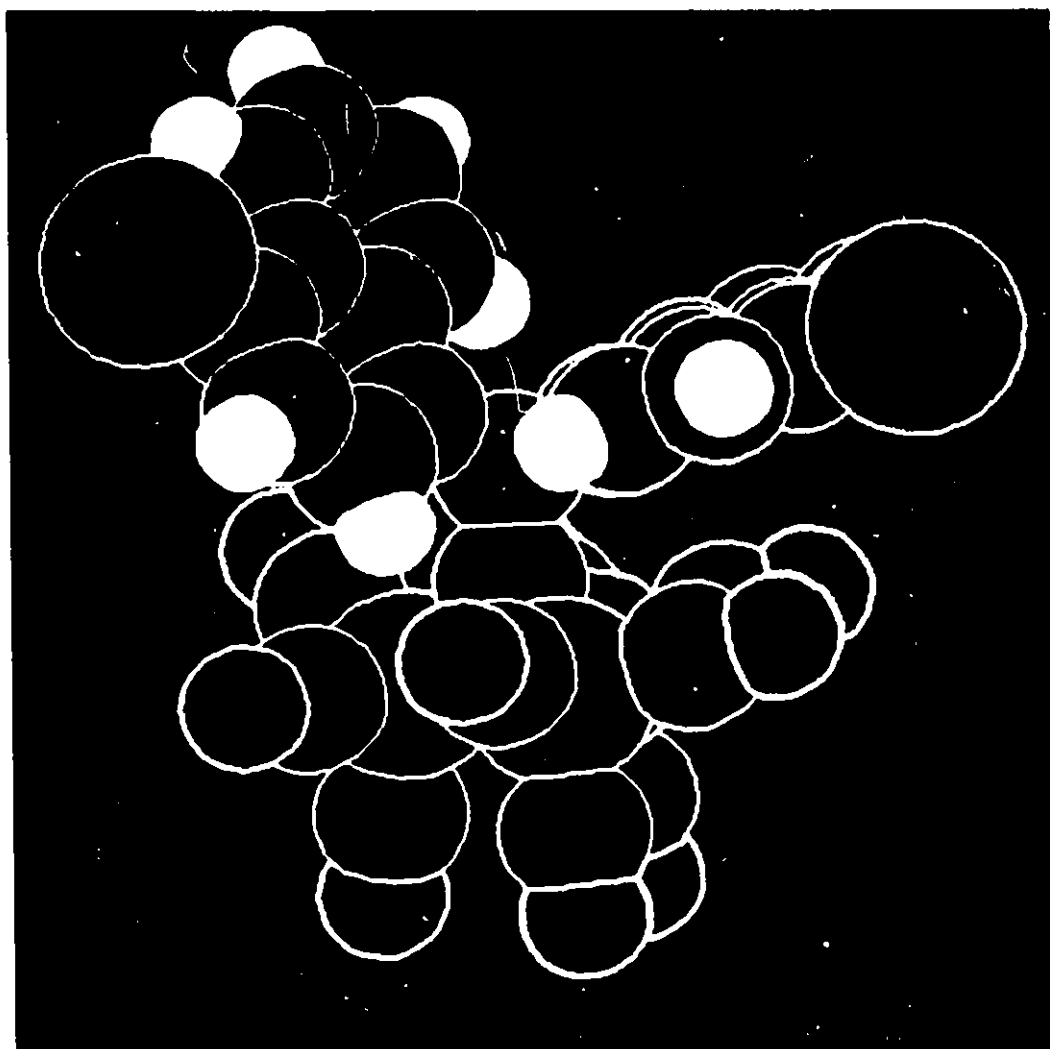


Figure 45 A: X-Ray Diffraction Crystal Structure of the Chlorophenyl Analogue to 26,  $\text{Co}_3(\text{CO})_9\text{C-CH-(4-ClC}_6\text{H}_4)_2$ , 21

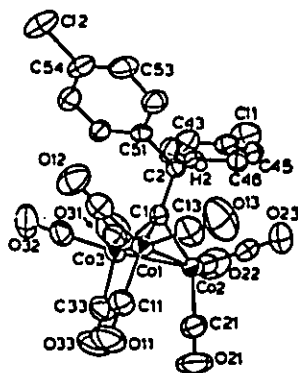
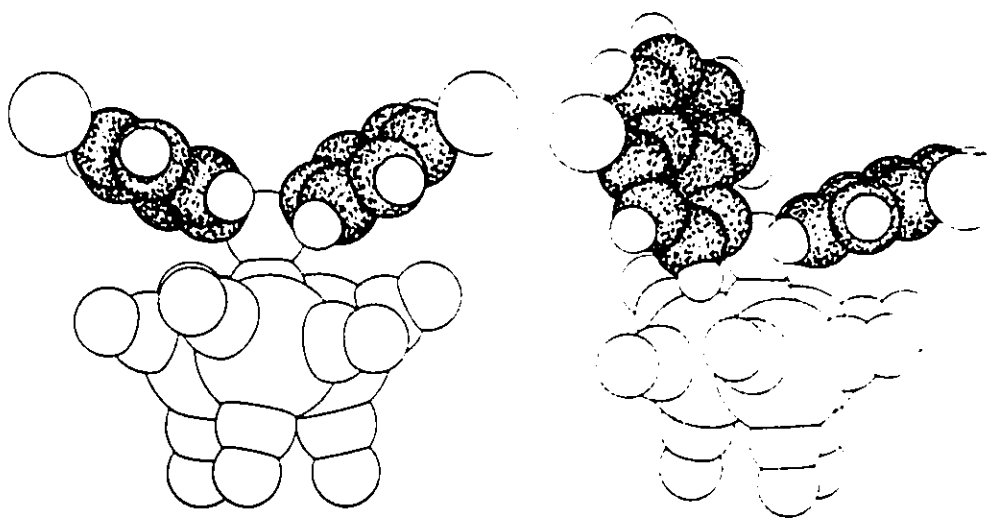


Figure 45 B : Space-filling Models of  $\text{Co}_3(\text{CO})_9\text{C-CH-(4-ClC}_6\text{H}_4)_2$ , 21, and  $\text{Co}_3(\text{CO})_9\text{C-CH-(4-ClC}_{10}\text{H}_6)_2$ , 26

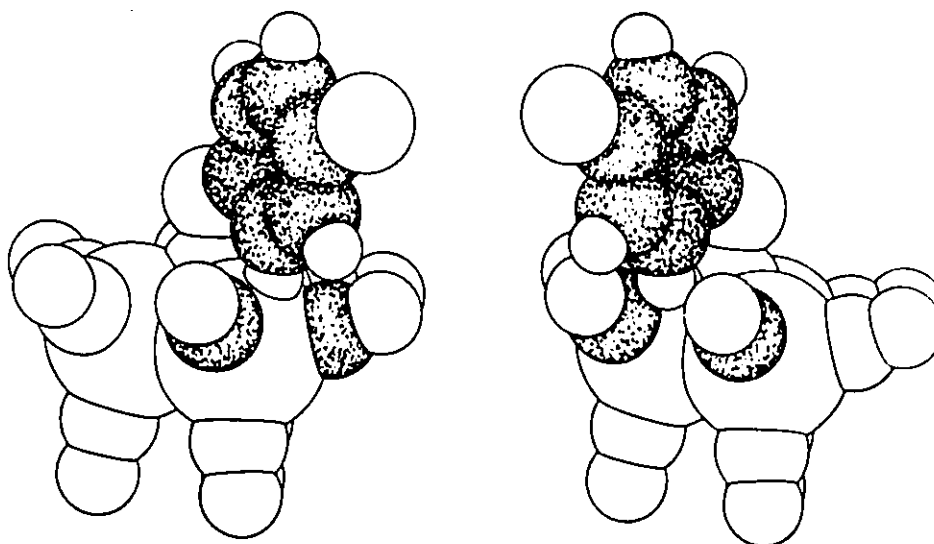


How can the results of this study be explained in light of the observations with the METHOXYCHLOR and DDT clusters? There is a 6:3 splitting of the carbonyl signals in the clusters bearing the small aromatic rings on the apex. This has been interpreted as possibly arising from a cessation of axial-equatorial exchange, leaving six carbonyl ligands different from the other three. It is possible (though unlikely) that the carbonyl ligands are still experiencing vertex interchange while not

exchanging axial-equatorial environments.

Why, then, in the naphthyl cluster, would exchange not stop in the same manner? The key is in the extra ring present in the naphthalene system. Steric hindrance from one naphthyl ring prevents the second naphthalene from orienting itself perpendicular to the tricobalt plane. In contrast, the smaller phenyl ring would almost certainly be rotating about the CH-(*ipso*-C) bond. If the ring can rotate freely, its effective size is greater than if it is static -- a cylinder as compared to a plane. The space-filling model (Figure 46) shows that with an orientation of the phenyl ring perpendicular to the basal plane, the distance of closest approach of the ring to the carbonyl ligands is within their van der Waals' radii, which would account for the cessation of carbonyl exchange seen at reduced temperatures.

Figure 46: Space-Filling Model of Cluster 21: Two Conformations Generated by Rotation of the Phenyl Ring from its Crystallographic Position



Thus, it appears that by introducing two naphthyl rings, rotation about the C-naphthyl bonds has been hindered. This reduces the effective steric bulk of the capping group and it is not able to approach the the CO ligands as closely as does the

phenyl analogue. The result is that the the entire capping group is free to rotate about the  $\mu_3$ -C-CH bond. Consequently, all three cobalt atoms remain equivalent at low temperature, and the carbonyl groups, though perhaps not undergoing intervertex exchange, are equivalent in the limiting situation.

#### (4.4) CONCLUSION

The chloronaphthyl derivative of DDT in combination with  $\text{Co}_2(\text{CO})_8$  produces a cluster which displays very different behaviour from that seen in the DDT and METHOXYCHLOR analogues. It is a very difficult cluster to make, due likely to its extreme bulk which would cause unfavourable steric strain at the apex of the molecule. However, this bulk seems to be the deciding factor as well in allowing carbonyl exchange to continue between cobalt vertices at reduced temperatures in solution: the group on the carbon vertex appears to require a certain amount of rotational flexibility in order to interfere with CO migration, and the naphthyl complex simply does not have the freedom to allow aryl ring rotation and subsequent interaction with the cobalt carbonyl groups.

## CHAPTER FIVE

### (5.1) INTRODUCTION

In Chapter Two, the  $^{13}\text{C}$  NMR spectra of the carbonyl and cyclopentadienyl regions of  $\text{M}(\text{CP})(\text{CO})_2\text{Co}_2(\text{CO})_6\text{C}-\text{CO}_2\text{CH}(\text{CH}_3)_2$  clusters ( $\text{M} = \text{Mo}, \text{W}$ ;  $\text{CP} = (\text{C}_5\text{H}_5)$ ,  $(\text{C}_5\text{H}_4\text{CH}_3)$ ,  $[\text{C}_5(\text{CH}_3)_5]$ ) became more complex at reduced temperatures. Part of this increased splitting of signals was assigned to the cessation of intervertex carbonyl exchange. The remainder of the splitting could not be assigned to stopping of CO motion between vertices, nor could it be accounted for by any explanation involving capping group fluxionality. The proposed reason for the increased amount of NMR signals at low temperature, the cessation of rotation of the CP ring-bearing vertex, is the subject of this chapter.

#### (5.1.1) POSITIONS OF CYCLOPENTADIENYL LIGANDS IN TETRAHEDRAL CLUSTERS

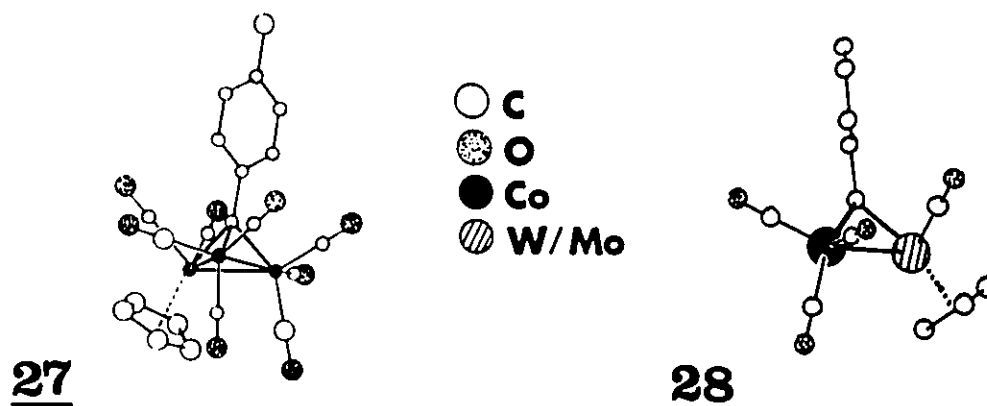
Stone and Vahrenkamp independently solved the crystal structures of similar clusters bearing  $\text{C}_5\text{H}_5$  rings. In Stone's structure of  $(\text{C}_5\text{H}_5)\text{WCo}_2(\text{CO})_8\text{C}-$  $(4-\text{CH}_3\text{C}_6\text{H}_4)$ , 27, the cyclopentadienyl ring is found in an axial position, with the two tungsten carbonyl ligands occupying terminal equatorial positions [71]. The Cp ring does not lie parallel to the trimetal plane, no doubt because of the proximity of the axial carbonyl groups on the cobalt vertices (Figure 47). This deviation from perpendicularity of the (ring centroid)-(metal vertex) vector to the trimetal plane can also be seen in axial carbonyl ligands, and is presumably caused by the direction of the  $\text{d}^2\text{sp}^3$  hybrid bonding the carbonyl/CP ring to the skeleton.

Vahrenkamp elucidated the structure of the cluster  $(\text{C}_5\text{H}_5)\text{MoCo}_2-$  $(\text{CO})_8\text{C}-\text{C}_6\text{H}_5$ , 28 [70]. The cyclopentadienyl ring was found to be in an axial position,

with the carbonyl ligands both equatorial, in the manner of the Stone cluster 27. This structure will be discussed in further detail later in the chapter.

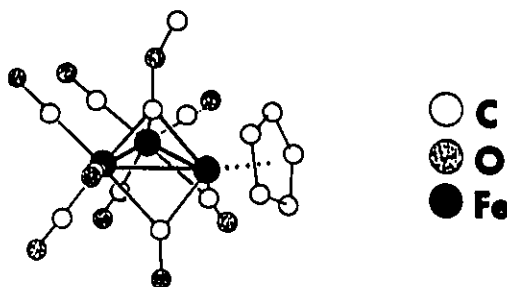
As presented in Chapter Three, the cyclopentadienyl ring in the cluster  $\text{Fe}_2(\text{CO})_6(\mu\text{-CO})\text{W}(\text{C}_5\text{H}_5)(\text{CO})_2\text{C}(4\text{-CH}_3\text{C}_6\text{H}_4)$  assumes an equatorial position on the tungsten atom, leaving the two carbonyl groups on the same moiety in axial and equatorial positions, respectively [73] (Figure 32).

Figure 47: X-Ray Diffraction Crystal Structures of  $(\text{C}_5\text{H}_5)\text{WCo}_2(\text{CO})_8\text{C}(4\text{-CH}_3\text{C}_6\text{H}_4)$ , 27, and  $(\text{C}_5\text{H}_5)\text{MoCo}_2(\text{CO})_8\text{C-C}_6\text{H}_5$ , 28



Farrugia *et al* published a study of a tri-iron complex,  $\text{Fe}_3(\text{CO})_6(\mu\text{-CO})_2(\eta\text{-C}_5\text{H}_5)\text{C-OCH}_3$  [84]. The bridging carbonyl ligands are below the plane of the three iron vertices, pointed away from the capping ether group. The angle to the ring centroid from the  $\text{Fe}_3$  plane is  $21.1^\circ$ , and the Fe-centroid "bond" eclipses the Fe-apical carbon bond. The result of this odd orientation is that the cluster possesses mirror symmetry with respect to the  $\text{Fe}_3\text{C}$  skeleton, the carbonyl groups, and the Cp ring. This means the ring is placed in what shall be described as an "up" position, in neither a conventional axial nor an equatorial environment (Figure 48). Thus, a cyclopentadienyl ligand can adopt a variety of positions with respect to the tetrahedron.

Figure 48: X-Ray Diffraction Crystal Structure of  $\text{Fe}_3(\text{CO})_6(\mu\text{-CO})_2(\eta^5\text{-C}_5\text{H}_5)\text{C-OCH}_3$



### (5.1.2) POSSIBILITIES FOR PREFERENTIAL RING POSITIONING

The variety of positions found for the cyclopentadienyl ring in the solid state clusters leads one to speculate on the nature of the forces promoting a certain molecular geometry. There is presumably a large steric effect, such that the  $\text{CP}(\text{CO})_2\text{M}$  vertex ( $\text{CP} = \text{C}_5\text{H}_5, \text{C}_5\text{H}_4\text{CH}_3$ ) will be oriented at the angle resulting in minimum steric interaction. The entire cluster must be studied to determine which part of the molecule is most bulky and consequently most important to avoid. Though the cyclopentadienyl ring could be thought of as avoiding the capping group when in an axial ("down") position (Figure 47), this placement would incur unfavourable interactions with the CO groups on the other vertices instead. Placing the CP ring in an "up" position (Figure 48) leaves the CP ring in the best area to avoid contact with other parts of the molecule, but then the CO groups (still terminal, not bridging) are much closer to the two other metal moieties in the tetrahedron.

The electronic effect to be considered is the status of the metal vertex bearing the cyclopentadienyl ring. If the metal is electron rich, a potential mode of dealing with the excess electron density is to transfer it to adjacent atoms via bridging carbonyl ligands. This redistribution of electron density would be likely to occur if the metal bears a cyclopentadienyl ligand of great electron-donating character (*e.g.*  $[\text{C}_5(\text{CH}_3)_5]$ ) as compared to an unsubstituted ( $\text{C}_5\text{H}_5$ ) group. The mode of redistribution



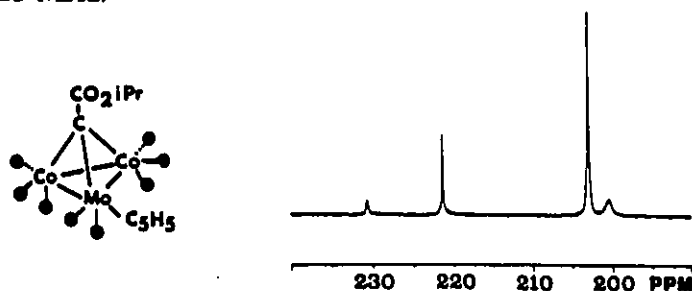
of electron density requires placement of the CP ring in an "up" position, thus allowing the carbonyl groups to semi-bridge to the neighbouring metal centres. (As the 18-electron rule is satisfied for the other vertices, actual bridging of the CO ligand will not occur. A molecule is described as semi-bridged if it has a terminal carbonyl group at one vertex placed close enough to overlap electron density onto a second vertex, accompanied by a distortion in the linearity of the CO group.)

### (5.1.3) STATEMENT OF THE PROBLEM

The study of the intermetal carbonyl exchange in heterometallic tetrahedra revealed that a second fluxional process occurred concomitantly. The clusters of study are 10-15,  $M(\text{CP})(\text{CO})_2\text{Co}_2(\text{CO})_6\text{C-CO}_2\text{CH}(\text{CH}_3)_2$ ;  $M = \text{Mo}, \text{W}$ ;  $\text{CP} = \text{C}_5\text{H}_5$ ,  $\text{C}_5\text{H}_4\text{CH}_3$ ,  $\text{C}_5(\text{CH}_3)_5$ . The cluster  $(\text{C}_5\text{H}_5)\text{Mo}(\text{CO})_2\text{Co}_2(\text{CO})_6\text{C-CO}_2\text{CH}(\text{CH}_3)_2$ , 10, for example, showed a single peak in the  $^{13}\text{C}$  NMR spectrum for all carbonyl ligands at ambient temperatures, indicating exchange of all CO groups between all three metal vertices. At reduced temperatures, the carbonyl ligands were found to be localized -- intermetal exchange had ceased. The cobalt carbonyls produced a signal in the region of 200 ppm, and those carbonyls bound to W or Mo gave a signal between 240 and 220 ppm. The striking part about the  $^{13}\text{C}$  NMR low-temperature carbonyl spectrum was that the presence of two isomers of the cluster became apparent.

The  $^{13}\text{C}$  NMR limiting spectrum of the carbonyl region of  $(\text{C}_5\text{H}_5)\text{-Mo}(\text{CO})_2\text{Co}_2(\text{CO})_6\text{C-CO}_2\text{CH}(\text{CH}_3)_2$ , 10, is presented in Figure 51. A large set of peaks of integrated area 3:1 appear at 221.2 and 202.7 ppm. A smaller set of signals is also present, with the same intensity ratio. One member of each set of peaks appears in the cobalt carbonyl region, while the second signal can be found downfield, with a chemical shift characteristic of a carbonyl group bound to Mo or W. These two sets of peaks apparently arise from two isomers of the cluster.

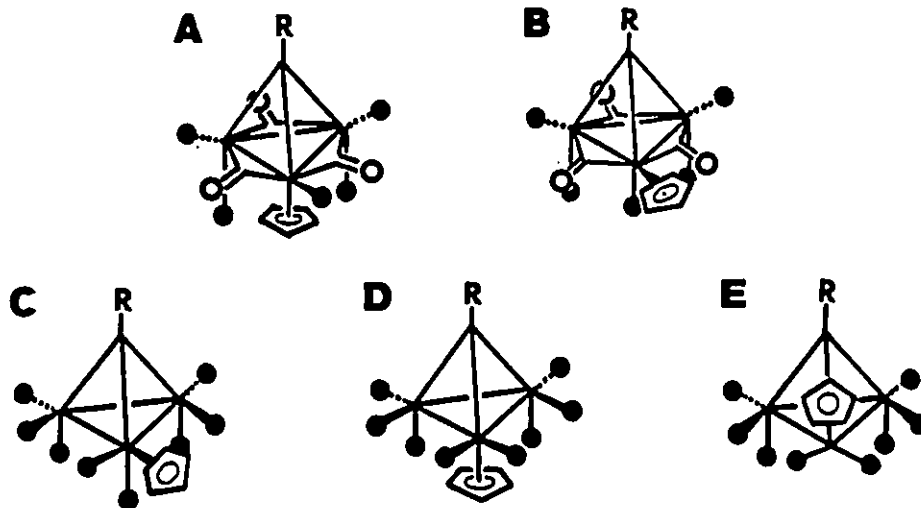
Figure 49: Low Temperature  $^{13}\text{C}$  NMR Spectrum of 10, Carbonyl Region,  $T = 190$  K, S.F. = 125 MHz.



As the high temperature spectrum of the carbonyl region displays one peak only, the isomers must be interconvertible. What process is occurring here, and what is the energy barrier?

The first study undertaken involved clarification of the conformations of the isomers. Different isomers could result from various distributions of the carbonyl ligands about the trimetal base, as illustrated in Figure 50. Each possibility will be considered.

Figure 50: Possible Distributions of Carbonyl Ligands about the Clusters



Situation (A), in which carbonyl groups are bridging, axial and radial, should produce five carbonyl signals in the  $^{13}\text{C}$  NMR spectrum in the ratios 1:1:2:2:2.

This is clearly not the case, because merely two distinct types of signals are seen, not five.

Five carbonyl signals in the ratios 1:1:2:2:2 would also be expected in the limiting spectrum of conformation (B), and consequently this distribution is also ruled out.

Structure (C) would give rise to a 1:1:3:3 pattern, and is therefore not a possible structure, as it does not match the  $^{13}\text{C}$  NMR data.

Structures (D) and (E) are plausible in light of our results, as there exist six cobalt carbonyl groups (probably experiencing continuous axial-equatorial interchange, and perhaps even intermetal exchange), and two symmetry-equivalent molybdenum carbonyls. These structures correspond with the integrated areas of 3:1 (6:2) of both sets of carbonyl NMR peaks. Thus, the isomers are not a consequence of varying carbonyl arrangements about the entire trimetal base of the cluster, but instead the different orientations of the ligands specifically on the Mo (or W) vertex. Structures (D) and (E) are also made plausible in light of the crystal structures shown in Figures 47 and 48.

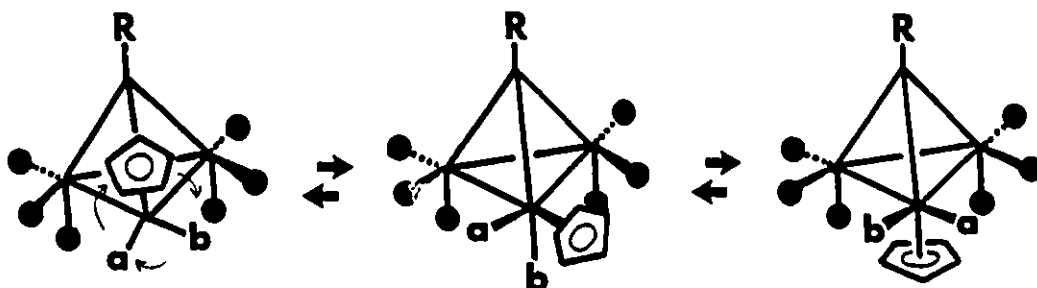
If the isomer interconversion mechanism involves more than one local minimum on the energy pathway, then it may be possible to slow the process on the NMR timescale to result in isolation of more than one isomer.

Precedents, as presented in the introduction to this chapter, have been discovered in which cyclopentadienyl ligands adopt a variety of positions with respect to a three-metal triangle in a tetrahedral cluster. It certainly seems probable that the isomerism could be a result of differing orientations of the cyclopentadienyl ring with respect to the tetrahedron.

The process of interconversion of the isomers could go via a rotation of the  $(\text{CP})\text{M}(\text{CO})_2$  vertex (Figure 51). This would involve passage of the ligands through

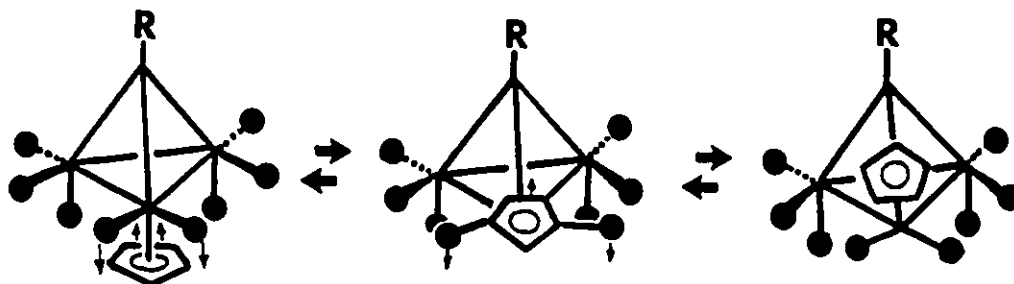
regions of increased interaction with the remainder of the molecule, requiring the overcoming of an energy barrier.

Figure 51: Mechanism of Isomer Interconversion



Another mechanism of interconversion could be that in which the cyclopentadienyl ring passes between the two carbonyl ligands to a position on the opposite side of the trimetal plane, while the CO ligands move simultaneously in the other direction (Figure 52). This second proposed mode of isomerization is improbable because of the extremely high transition state energy when the carbonyl ligands lie in the same plane as the trimetal triangle and the cyclopentadienyl ring.

Figure 52: A Second Possible Mechanism of Isomer Interconversion



#### (5.1.4) MODES OF STRUCTURE ELUCIDATION

There are two probes of chirality built into the clusters which can aid in clarification of the structure:

(a) The isopropyl group -- if the molecule were to become chiral, the isopropyl methyl groups would become inequivalent, and the proton signal would split from a doublet (coupling to the isopropyl H) to a pair of doublets. The  $^{13}\text{C}$  NMR spectrum should also change from a single peak (for the two methyl groups) to a two singlets (each methyl group would give rise to a peak).

(b) The carbonyl groups -- the signals are resolved into Mo and Co carbonyls, each with a major and a minor isomer. If the cyclopentadienyl ring on the Mo were to adopt an equatorial position, (leaving the cluster chiral), the Mo carbonyl ligands would necessarily be in two different environments, axial and equatorial, and should give rise to two signals of equal intensity.

Infrared spectroscopy is also a useful method of product elucidation during synthesis of these clusters [83]. The stretching frequency of metal carbonyl ligands is between  $2200$  and  $1700\text{ cm}^{-1}$ , so they absorb IR energy in these regions, and as will be seen, distinct alterations in a spectrum can accompany small changes in a molecule. Terminal carbonyl groups on an  $\text{M}(\text{CO})_3$  cluster moiety absorb infrared light at the high frequency end of the region,  $2200$ - $1900\text{ cm}^{-1}$ . In a  $\text{CP}(\text{CO})_2\text{M}$  vertex, carbonyl groups experience electron donation from the cyclopentadienyl ligand into the carbonyl  $\pi^*$  orbital. This weakens the CO bond and results in IR absorbances in a slightly lower energy range, between  $2100$  and  $1900\text{ cm}^{-1}$ . Carbonyl groups symmetrically bridging two metal vertices absorb infrared energy at even lower frequency ( $1900$ - $1700\text{ cm}^{-1}$ ). Semi-bridging carbonyl groups, described as terminally bound to one metal vertex but positioned near another, produce IR bands in an intermediate region between those of terminal and bridging CO ligands, around  $1975$ - $1775\text{ cm}^{-1}$ .

## (5.2) STUDY OF CYCLOPENTADIENYL CLUSTERS

### (5.2.1) SYNTHESIS OF $(CP)M(CO)_2Co_2(CO)_6C-CO_2-CH(CH_3)_2$ , $M = Mo, W$ ; $CP = C_5H_5, C_5H_4CH_3$ and $C_5(CH_3)_5$ , 10-15

The compounds 10-15,  $M(CP)(CO)_2Co_2(CO)_6C-CO_2CH(CH_3)_2$ , ( $M = Mo, W$ ;  $CP = C_5H_5, C_5H_4CH_3, C_5(CH_3)_5$ ), were prepared as described in Chapter Two, starting from the tricobalt analogue and effecting the  $M(CP)(CO)_2$  substitution by heating the corresponding metal dimer  $[M(CP)(CO)_3]_2$  with the cobalt cluster, using the technique developed by the Vahrenkamp group [17].

### (5.2.2) NMR OF THE $(C_5H_5)$ - and $(C_5H_4CH_3)$ -LIGATED CLUSTERS

The variable-temperature  $^{13}C$  NMR spectra of the isopropyl methyl carbons were observed, and the resonance remains one singlet throughout the study, showing no change from high to low temperature. This indicates that of the two isomers frozen out, neither is a chiral molecule.

This conclusion can also be drawn from the carbonyl region of the  $^{13}C$  NMR spectrum. There is no further splitting of the molybdenum/tungsten carbonyl signals as the temperature is decreased, which means the carbonyls on Mo or W in each isomer are magnetically equivalent; *i.e.*, one is not axial while the other is equatorial, because in that case, they would display two signals of equal area and different chemical shifts: equatorial CO upfield and axial CO downfield [55]. Thus, the asymmetric isomer (C), in which the cyclopentadienyl ring is situated in an equatorial manner, is ruled out as a possible structure.

The lack of chirality in the products means the clusters likely have at least a mirror plane. The two other potential structures place the Cp ring below the plane, (D), and above the plane, (E), and both possess  $C_s$  symmetry.

If the Cp ring adopts the axial position (D), the carbonyl groups will occupy

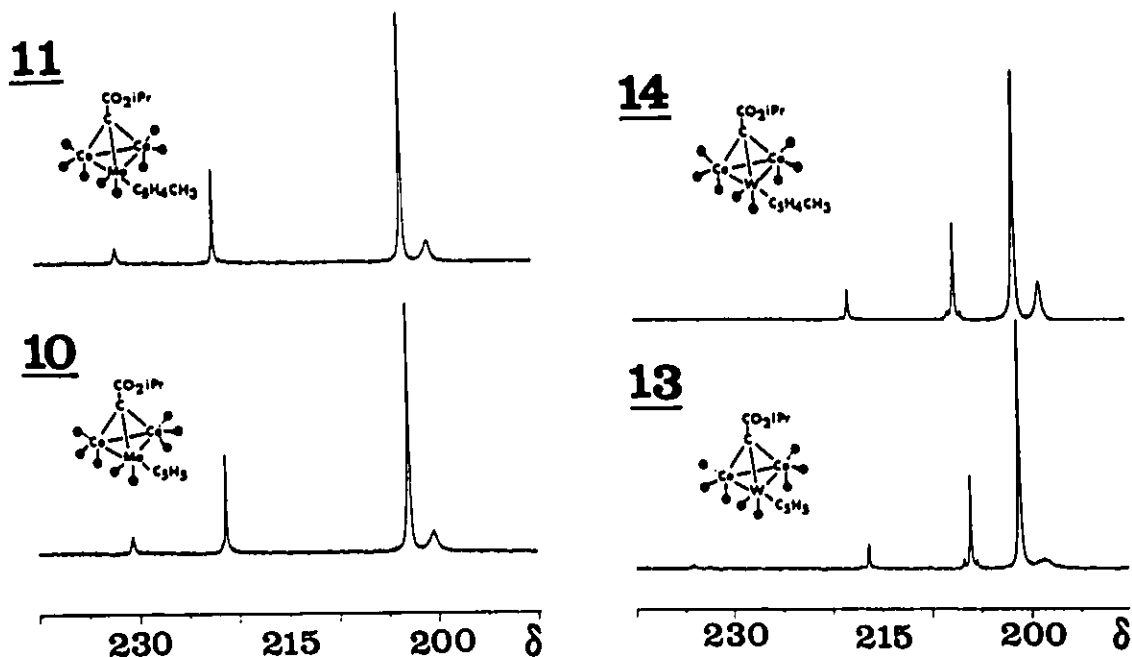
conventional equatorial positions. The  $^{13}\text{C}$  NMR spectrum will show two signals with chemical shifts typical of terminal carbonyl groups on Mo (W) and Co. The infrared absorbance regions could be expected to be at approximately  $2100\text{-}1950\text{ cm}^{-1}$ . This is at slightly lower frequency than typical terminally-bound metal carbonyls ( $2200\text{-}2000\text{ cm}^{-1}$ ), because of the presence of the electron-rich Cp ring, as described earlier.

Placement of the cyclopentadienyl ligand above the trimetal plane, as pictured in (E), would leave the carbonyl ligands somewhere between an axial and an equatorial position, in what could be construed as a "semi-bridging" environment. The trend in  $^{13}\text{C}$  NMR chemical shifts is that bridging carbonyl groups are found at higher frequency than terminal carbonyls [85], often on the order of 50 ppm. Therefore, it is expected that semi-bridging carbonyls will appear downfield of terminal carbonyls, to an extent less than 50 ppm. (Indeed, in the cluster  $\text{FeMo}_2(\mu_3\text{-C}_2(4\text{-CH}_3\text{C}_6\text{H}_4)_2\text{-}(\text{CO})_6(\eta\text{-C}_5\text{H}_5)_2$ , the semi-bridging carbonyl group between two molybdenum atoms gives a signal at 249.9 ppm in the low temperature  $^{13}\text{C}$  NMR spectrum, as compared to shifts around 231 ppm for the terminal carbonyl groups [86].)

A structure with semi-bridging carbonyls would show a shift in the carbonyl infrared absorbance towards lower frequency, to the range of  $1975\text{-}1775\text{ cm}^{-1}$ . (In the molecule  $\text{FeMo}_2[\mu_3\text{-C}_2(4\text{-CH}_3\text{C}_6\text{H}_4)_2](\text{CO})_6(\eta\text{-C}_5\text{H}_5)_2$ , the IR absorbance of the semi-bridging carbonyl is assigned to a band at  $1792\text{ cm}^{-1}$  [86].)

The  $^{13}\text{C}$  NMR spectra of clusters 10, 11, 13, and 14 have the distinct four-signal pattern in the carbonyl region (Figure 53). The carbonyl signals from the CO groups on cobalt show little chemical shift difference between the two isomers. The signals for the heterometal's carbonyl ligands, conversely, display a significant difference in chemical shift from one isomer to the other, consistent with isomerism resulting from orientation of this vertex (approximately 9-11 ppm).

Figure 53: Low Temperature  $^{13}\text{C}$  NMR Spectra, Carbonyl Region, of Molecules 10, 11, 13, and 14.



The major isomer in these four clusters has its Mo/W CO signal upfield of the minor isomer's signal. This leads to the conclusion that the major isomer in solution is that with the cyclopentadienyl ring in the axial position, with the Mo/W carbonyl ligands equatorial. The minor isomer places the Cp/MeCp ring above the trimetal base, with the carbonyls in semi-bridging positions. This accounts for the dramatic shift to higher frequency of their  $^{13}\text{C}=\text{O}$  signals.

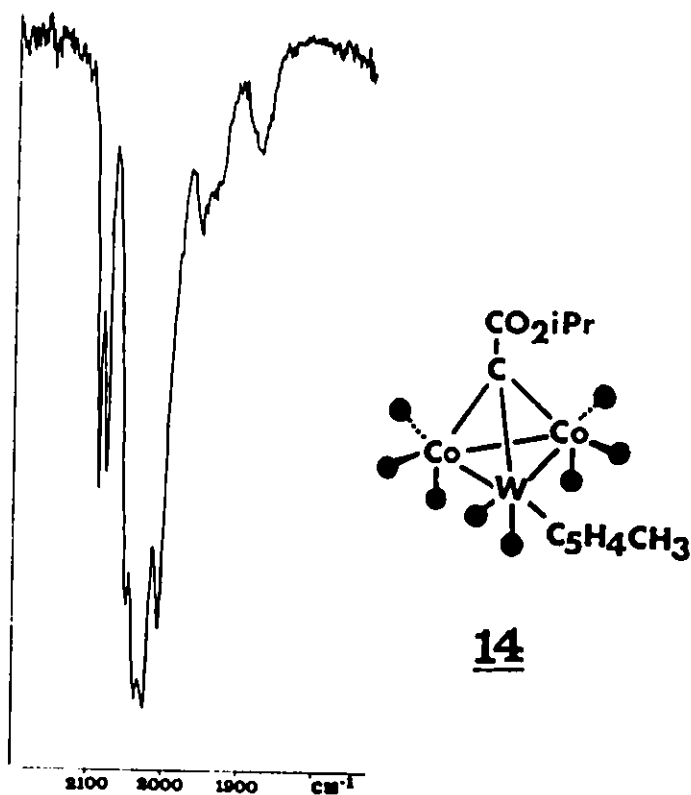
### (5.2.3) INFRARED ANALYSIS

The solution infrared spectra of the clusters are very complex. Stone found that in similar clusters, there were too many IR absorbances to be assigned to a single structure [73]. The maximum number of infrared absorbances possible in the CO region of an eight-carbonyl cluster is eight, and this would only occur in the



absence of any symmetry. Since our spectrum showed several infrared absorbances, in the same manner as Stone's clusters, we agree that more than one structure is present in solution. Of course, this corresponds with the conclusion made from the low-temperature NMR study. The difference between NMR and IR, as explained in Section (1.2.2.2), is that the infrared timescale is many orders of magnitude shorter than the NMR timescale [37], so that fluxional processes which exchange isomers too quickly (*e.g.*,  $10^{10}$  times/sec) to be resolved by nuclear magnetic resonance except at reduced temperatures, can be seen detected by infrared spectroscopy at room temperature.

Figure 54: Infrared Spectrum of  $(C_5H_4CH_3)W(CO)_2Co_2(CO)_6C-CO_2CH(CH_3)_2$ , 14, Carbonyl Region,  $(CH_2Cl_2)$



A typical solution infrared spectrum of one of these clusters,  $(C_5H_4CH_3)W(CO)_2Co_2(CO)_6C-CO_2CH(CH_3)_2$ , 13, is shown in Figure 54. There is a minimum of eight absorbances, some appearing as shoulder peaks under the signals at 2024 and 2005  $cm^{-1}$ . Several strong absorbance bands appear between 2086 and 2005  $cm^{-1}$ , indicating the presence of terminal carbonyl ligands in the cluster. Two very broad and somewhat less intense signals can be seen in the range between 2000 and 1850  $cm^{-1}$ . These may be due to the postulated semi-bridged carbonyl groups in the isomer with the  $C_5H_4CH_3$  ring above the trimetal plane. The infrared spectrum thus strengthens the theory of two isomers, and the proposed structures as well.

### (5.3) COMPARISON WITH A KNOWN COMPOUND

To confirm the theories made about the conformations, a known compound was observed next. The crystal structure of  $(C_5H_5)Mo(CO)_2Co_2(CO)_6C-C_6H_5$ , 28, finds the cyclopentadienyl ring situated below the metal base of the tetrahedron, distal with respect to the apical carbon [70]. This cluster was synthesized with the goal of comparing its spectroscopic behaviour with those of our clusters.

#### (5.3.1) SYNTHESIS OF $(C_5H_5)Mo(CO)_2Co_2(CO)_6C-C_6H_5$ , 28

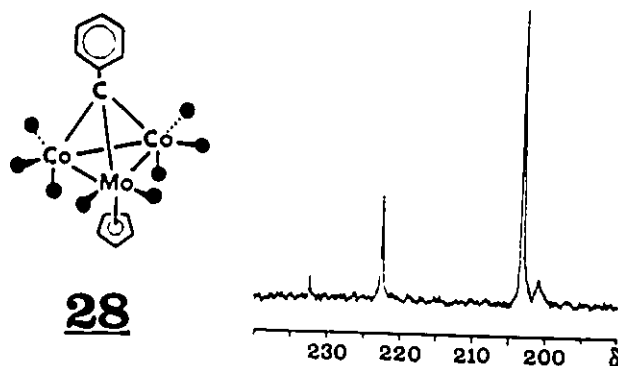
The preparation of  $(C_5H_5)Mo(CO)_2Co_2(CO)_6C-C_6H_5$  is similar to the synthesis of the entire series of clusters in this chapter. The tetrahedral skeleton is formed in the reaction of  $\alpha,\alpha,\alpha$ -trichlorotoluene with dicobalt octacarbonyl via replacement of each of the three chlorine atoms by a  $Co(CO)_3$  group. One cobalt tricarbonyl vertex is subsequently replaced by  $Mo(C_5H_5)(CO)_2$  in the reaction of the tricobalt cluster with the  $[Mo(C_5H_5)(CO)_3]_2$  dimer in tetrahydrofuran under reflux conditions. The resulting green crystals were studied by using NMR and IR spectroscopies.

### (5.3.2) SOLUTION STATE NMR STUDY

The  $^{13}\text{C}$  NMR spectrum of 28 at ambient temperature displays one broad signal at  $\delta$  207.8 ( $\text{CH}_2\text{Cl}_2$ , S.F. = 62.9 MHz), indicating fast intermetal exchange of all carbonyls. One signal appears in the cyclopentadienyl region (92.6 ppm), because at this temperature the molybdenum vertex (with its ligands) is spinning rapidly, and the cyclopentadienyl ring "sees" an average of all its possible environments.

The CO region of the low temperature limiting spectrum is very similar to those of our clusters possessing a  $\text{C}_5\text{H}_5$  or  $\text{C}_5\text{H}_4\text{CH}_3$  ring attached to the Mo/W vertex. There are two sets of peaks, each with an area ratio of 6:2, and the two larger peaks appear between the two smaller peaks (Figure 55). The major isomer gives rise to the molybdenum carbonyl signals assignable to equatorially-positioned carbonyl groups, while the signal for the minor isomer corresponds to carbonyl ligands in semi-bridged positions. The major isomer once again appears to be that with the cyclopentadienyl ring "down", while the minor isomer has the Cp ring "up". The NMR spectroscopic behaviour follows the pattern of the isopropyl ester capped clusters with  $\text{C}_5\text{H}_5$  and  $\text{C}_5\text{H}_4\text{CH}_3$  ligands.

Figure 55: Low Temperature  $^{13}\text{C}$  NMR Spectrum of the Model Compound 28, Carbonyl Region, T = 190 K



### (5.3.3) SOLUTION STATE INFRARED ANALYSIS

The infrared data for this cluster was subsequently investigated. The solution state IR shows the same type of absorbance pattern as the series of clusters 10-14. Six strong absorbances appear in the area between 2082 and 2003  $\text{cm}^{-1}$ , and weaker, broader signals are found in the region between 1960 and 1875  $\text{cm}^{-1}$ . Once again, there are two species present, and both are detected simultaneously by the infrared radiation.

### (5.3.4) THE SOLID STATE STRUCTURE

The crystal structure of the cluster, however, shows the presence of only one rotamer in the solid state, that with the cyclopentadienyl ring below the trimetal base, distal from the capping group of the tetrahedron. (Figures 34 and 47)[70]. One might presume that the solid state structure would prevail as the major isomer once the cluster is in solution, but this has been shown to be not necessarily the case in other systems [87]. Clearly, it was desirable to perform solid state spectroscopy to reveal if the solid state spectra corresponds with the major isomer in the solution spectra.

As there is only one isomer present in the solid state, the  $^{13}\text{C}$  NMR spectrum should show one set of peaks in the carbonyl region. They should have similar chemical shift values to either the larger or smaller set of signals in the solution spectrum, and the solution state isomers will thus be assignable to either the "up" or "down" isomer.

### (5.3.5) SOLID STATE NMR STUDY

The solid state NMR experiment was problematic. It is not a simple matter to attain a solid state  $^{13}\text{C}$  NMR of a cobalt cluster, because the lines are significantly broadened as compared to the solution state [88]. Increasing the abundance of  $^{13}\text{C}$

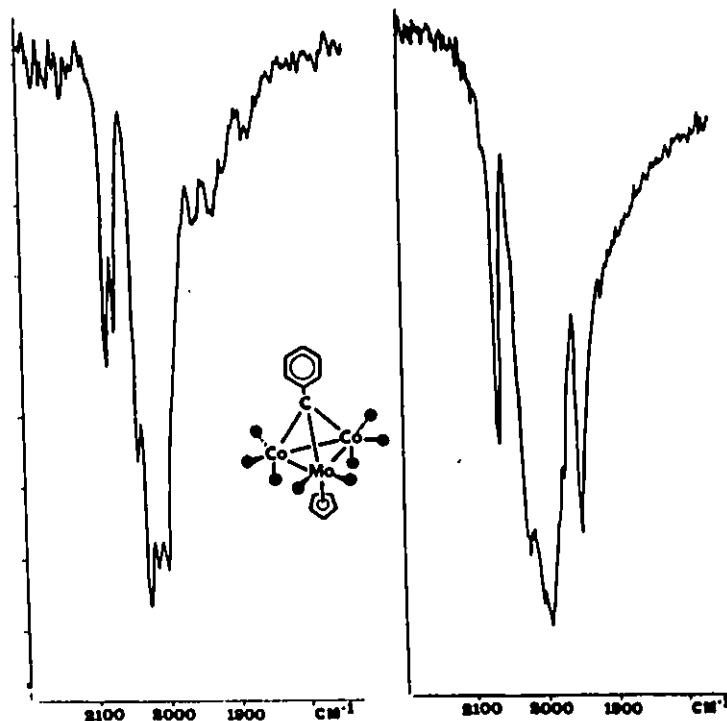
nuclei does not necessarily aid in collection of the spectrum. This is because the CPMAS technique is effective only for dilute nuclei which do not have spin-active neighbours. The resulting spectrum shows two broad signals -- one for the cyclopentadienyl ring carbons and one for the phenyl ring carbons. Unfortunately, the signals corresponding to the metal carbonyls could not be observed, even with repeated attempts.

#### (5.3.6) SOLID STATE INFRARED ANALYSIS

However, solid state infrared spectroscopy is not plagued with these problems, and this technique thus became the method of elucidation. The solid state infrared spectrum was collected by crushing a sample of the cluster together with KBr, (transparent in the carbonyl region), and forming a pellet. The IR spectrum of the cluster in the solid state was greatly simplified as compared to the solution spectrum (Figure 56).

Instead of two absorbances at 2082 and 2070  $\text{cm}^{-1}$  as seen in the solution state, only one signal appears in the solid state spectrum, at 2065  $\text{cm}^{-1}$ . Whereas in the solution spectrum, several semi-bridging absorbances appear (around and below 1900  $\text{cm}^{-1}$ ), they are not present in the solid state spectrum. Instead, there are a number of peaks in the region of absorbance characteristic of terminal carbonyls, as would be expected from the crystal structure. The bands in the solid state spectrum can be assigned to the isomer seen in in the crystal structure, while the remaining signals seen in the solution state IR spectrum are due to the minor solution-state isomer, that with the Cp above the trimetal plane (accounting for the semi-bridging absorbances). The infrared spectral data indicate that the major isomer in solution has the cyclopentadienyl ring "down" in the cluster.

Figure 56: Solution ( $\text{CH}_2\text{Cl}_2$ ) and Solid State (KBr) Infrared Spectra of 28, Carbonyl Region

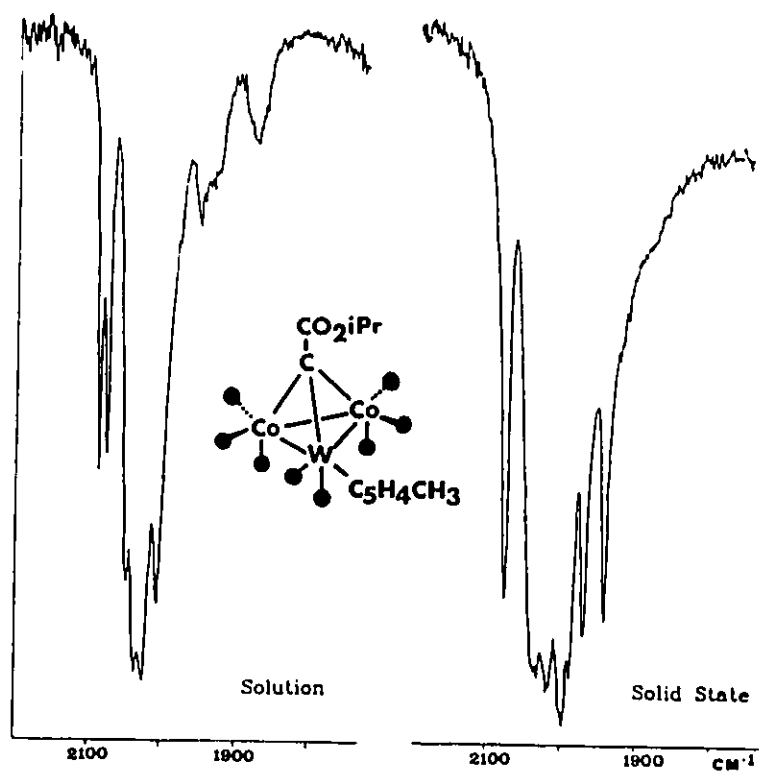


There is a marked difference between the solution and solid state IR spectra of this cluster. Can this behaviour be seen in our clusters as well?

#### (5.4) A SECOND LOOK AT THE $(\text{C}_5\text{H}_5)$ AND $(\text{C}_5\text{H}_4\text{CH}_3)$ CLUSTERS: THE SOLID STATE

Each of the clusters in the series was formed into a KBr pellet for solid state analysis by infrared spectroscopy. The results are just as for the model cluster. In each of the four clusters ( $M = \text{Mo}, \text{W}$ ;  $\text{CP} = \text{C}_5\text{H}_5, \text{C}_5\text{H}_4\text{CH}_3$ ), the set of lower frequency absorbances disappear upon changing to the solid state. A typical spectrum is shown in Figure 57. It indicates that while two isomers are present in solution, the only isomer in the crystalline state must be that with the cyclopentadienyl ring below the plane of the three metals, distal from the apical  $\text{C}-\text{CO}_2\text{CH}(\text{CH}_3)_2$  group, leaving all carbonyls terminal. An easily observable change occurs in the area of  $2075 \text{ cm}^{-1}$ .

Figure 57: Infrared Spectra of 14, Solution ( $\text{CH}_2\text{Cl}_2$ ) and Solid State (KBr), Carbonyl Region



Just as with the model compound, while in solution there are very weak signals which could correspond to semi-bridging carbonyl groups, these peaks disappear upon changing to the solid state. Because these signals are so weak, it is probable that they arise from the minor isomer. (The relative intensities of infrared absorptions cannot be related directly to the number of molecular fragments that are vibrating. Terminal CO stretches are inherently more intense than are those of bridging CO's, and thus isomer ratios cannot simply be obtained by comparing the intensities of such peaks. NMR is a better quantitative tool for this determination.)

Thus far, it can be concluded that all four clusters under scrutiny (plus the model compound 28) exhibit rotation of the Mo/W vertices and their ligands at ambient temperature, on the NMR timescale. Each complex has, as its solid state structure, the cyclopentadienyl ring sitting below the basal plane. Because the NMR spectral pattern

of the carbonyl region is essentially the same in all four molecules (and the same as the model compound), it can be proposed that the major orientation of the vertex in solution is identical for all four small ring compounds, and for the model compound as well.

### (5.5) $\Delta G$ VALUES BETWEEN ISOMERS

At low temperature, there appears to be cessation of a fluxional process in the system, postulated to leave the CP ring in one of two positions. Because both "up" and "down" isomers of the clusters exist in solution once rotation has ceased, and because the rotamers interconvert at room temperature, the energy barrier between the two conformations must be small, in the range of 8-15 kcal/mol. As well, because both isomers are observed at low temperature, they must differ in energy by only a small amount. An estimate of this energy difference can be obtained from the amounts of each isomer present at the limiting temperature. By measuring the areas underneath the NMR peaks, the ratio of isomers can be calculated.

$$\begin{array}{l} \text{The ratio of populations:} \\ \text{(area beneath the peak)} \end{array} \quad \frac{[a]}{[b]} = K \quad (6)$$

$$\text{and} \quad \Delta G_0 = -RT \ln K \quad (7)$$

The difference in energy between the up and down isomers was calculated using equations (6) and (7), and the results are presented in Table 9. It can be seen that a small difference in energy between the two conformations causes a significant population distribution towards the lower energy isomer, which in each of these cases is the "down" isomer.



Table 9: Calculated  $\Delta G$  Values for the "Up" and "Down" Isomers of  $(CP)M(CO)_2Co_2(CO)_6C-CO_2-CH(CH_3)_2$ ,  $M = Mo, W$ ;  $CP = C_5H_5, C_5H_4CH_3$

M	CP	$\Delta G$ (kcal/mol)
Mo	$C_5H_5$	0.4
Mo	$C_5H_4CH_3$	0.4
W	$C_5H_5$	0.5
W	$C_5H_4CH_3$	0.4

#### (5.6) EFFECT OF INCREASED BULK IN THE RING

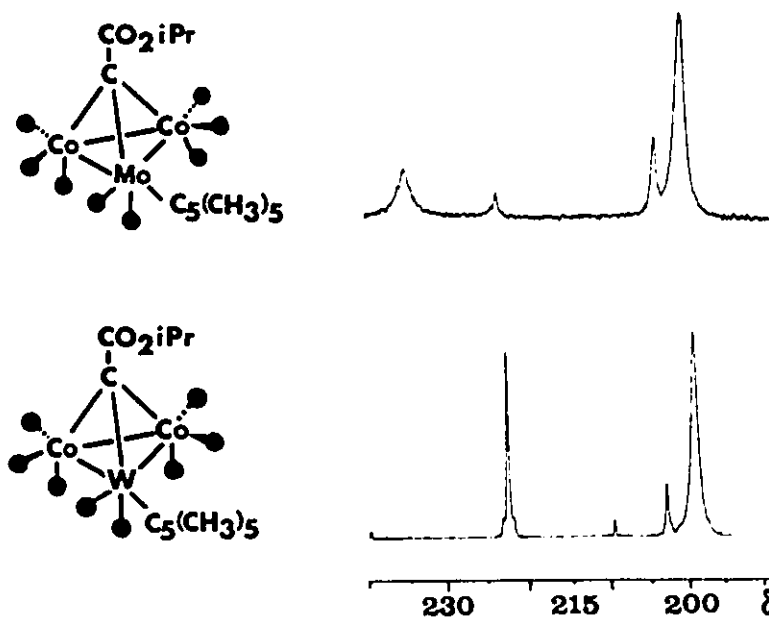
If a change is made to the ligand, it may be possible to alter the predominance of one isomer, and instead favour the other. If the bulk of the ligands on the Mo/W vertex were increased, perhaps the behaviour of the moiety would change. Free rotation about the metal atom by the cyclopentadienyl ring and carbonyl groups is seen in the clusters substituted with less sterically-demanding ligands, but would rotation be restricted because of an increase in size of the ring? Interactions with ligands on other vertices may develop, and ligand rotation may be completely disallowed. If so, which CP position will be chosen?

To investigate these ideas, two clusters were built in which the cyclic ligand bonded to Mo/W was the large  $[C_5(CH_3)_5]$  group, specifically  $[C_5(CH_3)_5]Mo-(CO)_2Co_2(CO)_6C-CO_2CH(CH_3)_2$  and  $[C_5(CH_3)_5]W(CO)_2Co_2(CO)_6C-CO_2CH(CH_3)_2$ , molecules 12 and 15.

### (5.6.1) NMR OF THE $[C_5(CH_3)_5]$ CLUSTERS

The  $^{13}C$  NMR spectra of the  $Mo[C_5(CH_3)_5](CO)_2$  and  $W[C_5(CH_3)_5](CO)_2$  complexes were observed as before, at room temperature, and at a descending series of temperatures with the lowest at 190 K. The limiting spectra are presented in Figure 58. The ambient temperature spectrum included one peak for the methyl groups on the cyclopentadienyl ring, one signal for the ring carbons, and a broad peak for all eight carbonyl ligands. Thus, room-temperature fluxionality of the carbonyls and the  $C_5(CH_3)_5$  ring occurs here in the same manner as in the  $C_5H_5$  and  $C_5H_4CH_3$  compounds.

Figure 58: Limiting Low Temperature  $^{13}C$  NMR Spectra of 12 and 15, Carbonyl Region,  $T = 190$  K, S.F. = 125 MHz

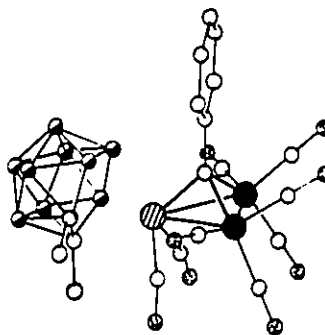


As the temperature is decreased, the single peak in the carbonyl region is resolved into two sets of peaks, but this time the predominant isomer gives rise to the outer set of two peaks, not the inner two as had been seen with the small-ring clusters. That is, the major isomer of this large-ring cluster appears to be that with the semi-

bridging carbonyls. The  $\Delta G$  between the two states is calculated from equations (6) and (7) as 0.6 kcal/mol in the Mo cluster, and 1.0 kcal/mol in the W system. The preferred solution state isomer is apparently that with the cyclopentadienyl group above the basal plane.

This behaviour is not unprecedented. Though a crystal structure of a similar tetrahedral cluster bearing a pentamethylcyclopentadienyl ligand has not been published to our knowledge, there exists a published structure of a cluster bearing a very bulky group in an  $\eta^5$  manner. The compound  $[(\eta^5\text{-C}_2\text{B}_9\text{H}_9(\text{CH}_3)_2)\text{W}(\text{CO})_2\text{-Co}_2(\text{CO})_6\text{C-C}_6\text{H}_5][\text{P}(\text{C}_6\text{H}_5)_4^+]$  displays the carborane ligand in an "up" position relative to the carbonyl ligands on the same vertex (Figure 59) [89]. This is analogous to the structure we propose for our pentamethylcyclopentadienyl clusters, and for the minor isomer of the  $\text{C}_5\text{H}_5$  and  $\text{C}_5\text{H}_4\text{CH}_3$  clusters earlier in the chapter.

Figure 59: X-Ray Diffraction Crystal Structure of  $[(\eta^5\text{-C}_2\text{B}_9\text{H}_9(\text{CH}_3)_2)\text{W}(\text{CO})_2\text{-Co}_2(\text{CO})_6\text{C-C}_6\text{H}_5][\text{P}(\text{C}_6\text{H}_5)_4^+]$

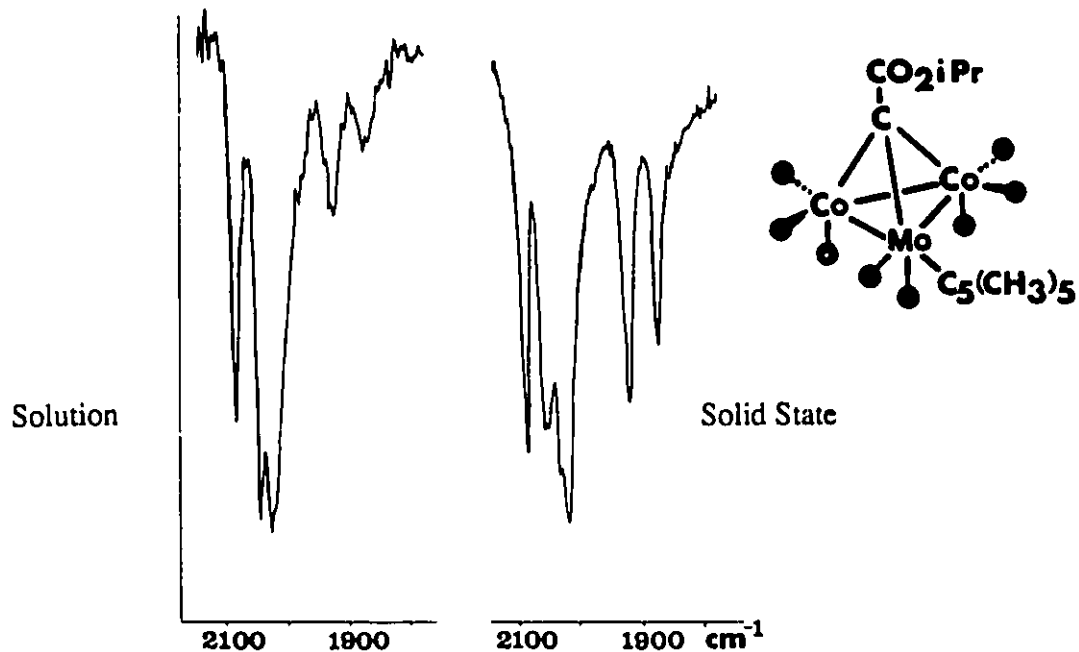


#### (5.6.2) INFRARED INVESTIGATION OF THE $[\text{C}_5(\text{CH}_3)_5]\text{Mo}(\text{CO})_2\text{-Co}_2(\text{CO})_6\text{C-CO}_2\text{CH}(\text{CH}_3)_2$ CLUSTER

The solution infrared spectrum of the pentamethylcyclopentadienyl complex is significantly different from those of compounds with  $\text{C}_5\text{H}_5/\text{C}_5\text{H}_4\text{CH}_3$  rings (Figure 60 A). There are two medium absorbance bands in the area characteristic of

semi-bridging carbonyl groups. In the region around  $2050\text{ cm}^{-1}$ , only one strong absorbance appears. The minor isomer is not readily detectable in the IR spectrum because the major isomer overlaps and obscures the bands from the minor isomer. It appears that the major isomer is the origin of the semi-bridging absorbances in this case, as the corresponding bands are so much more prominent in these spectra than in the Cp and MeCp examples.

Figure 60: Solution ( $\text{CH}_2\text{Cl}_2$ ) and Solid State (KBr) Infrared Spectra of 12, Carbonyl Region



Upon changing from solution to solid state, there is not a significant decrease in the number of signals in the IR spectrum (Figure 60 B). Instead, the change is an increase in the intensity of the Mo carbonyl absorbances relative to the signals in the  $2000\text{--}2100\text{ cm}^{-1}$  range. It appears that the only rotamer present in the crystalline

state is one which has carbonyl ligands in a semi-bridged position. This means that the ring is positioned above the plane of the three metals.

### (5.6.3) X-RAY DIFFRACTION CRYSTAL STRUCTURE OF $[\text{C}_5(\text{CH}_3)_5]\text{Mo}(\text{CO})_2\text{Co}_2(\text{CO})_6\text{C}-\text{CO}_2\text{CH}(\text{CH}_3)_2$

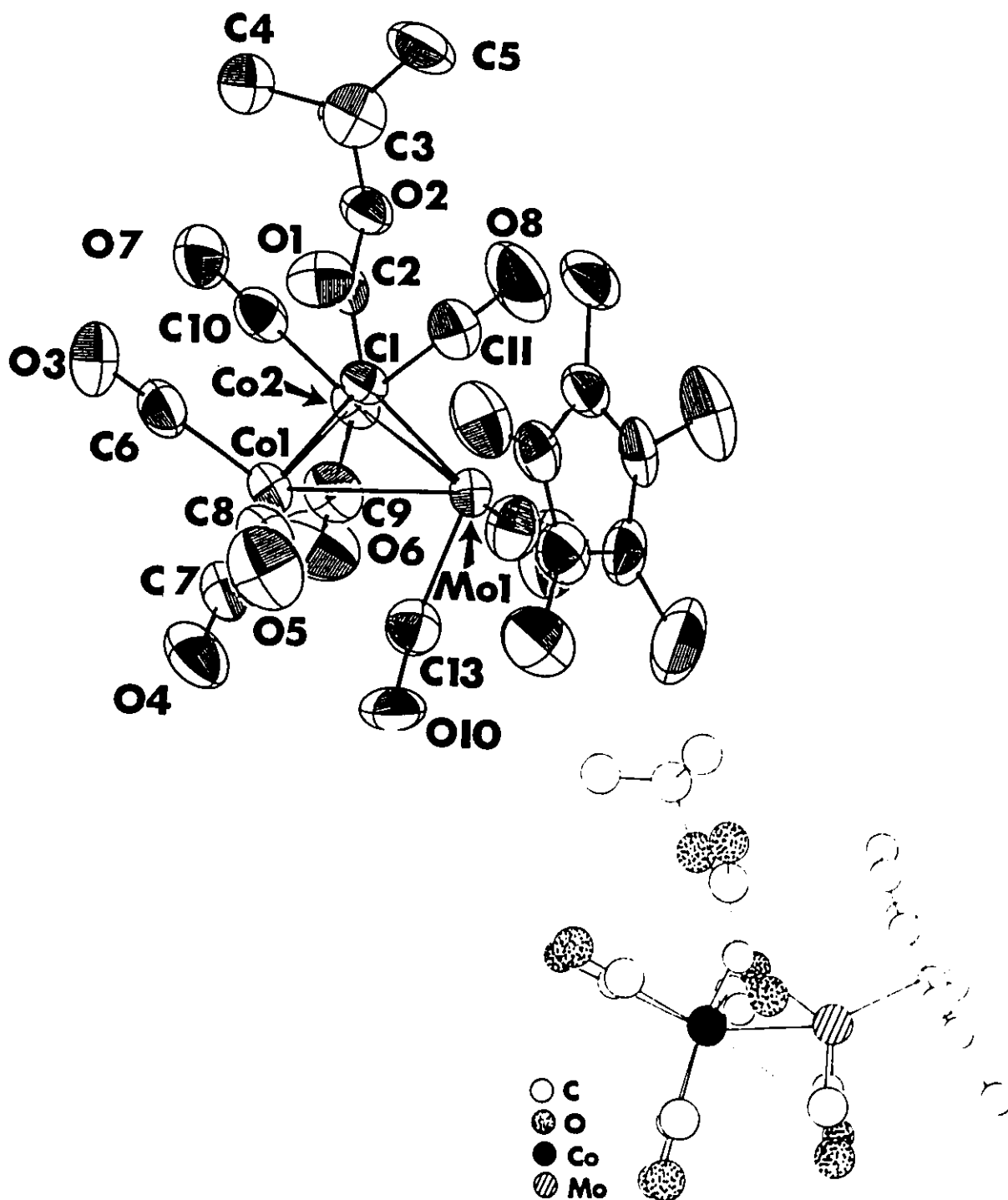
The final piece of evidence necessary to prove this postulate was the crystal structure of a cluster bearing a pentamethylcyclopentadienyl ring. Accordingly, deep purple crystals of  $[\text{C}_5(\text{CH}_3)_5]\text{Mo}(\text{CO})_2\text{Co}_2(\text{CO})_6\text{C}-\text{CO}_2\text{CH}(\text{CH}_3)_2$ , 12, were grown for analysis by single-crystal X-ray diffraction. It must be remembered that the solid state structure as determined by X-ray crystallography will not necessarily be an accurate picture of the system in the solution state, and thus caution must be exercised in using crystal structures to explain behaviour in solution.

The results were exactly as the spectroscopic information had led us to believe: the only structure present in the solid state had the centroid of the bulky  $[\text{C}_5(\text{CH}_3)_5]$  ring placed above the trimetal plane (Figure 61). The molybdenum carbonyl ligands are in a semi-bridged position, with Mo-C-O angles of  $169.3^\circ$  and  $170.5^\circ$ , instead of the typical angle of approximately  $180^\circ$  seen in conventional terminal carbonyl ligands (Section (1.2.1.1).) These angles can be compared to those of the fully bridging carbonyl group in  $\text{Co}_3(\text{C}_5\text{H}_5)_2(\text{CO})_4\text{C}-\text{C}_6\text{H}_5$ , 19, with Co-C-O angles of  $140.6(7)^\circ$  and  $139.6(7)^\circ$ , (Chapter Seven, Table 10E). The centroid of the pentamethylcyclopentadienyl ring sits  $24.1^\circ$  up from the trimetal plane. All cluster skeleton bond lengths are as expected, with Mo-Co distances of  $2.737(1)$  and  $2.732(1)$  Å, and Co-Co separation of  $2.515(1)$  Å. The tetrahedron is slightly distorted, as the Co-C and Mo-C bond lengths are  $1.934(\text{av.})$  and  $2.073(6)$  Å, respectively. The isopropyl group sits directly above one cobalt vertex.

The cyclopentadienyl ring has C-C bond lengths ranging from  $1.404(11)$  to  $1.436(11)$  Å. The axial carbonyl groups are slightly more distant from the cobalt

vertices than are their equatorial partners: axial Co-CO bond lengths average 1.82 Å, while equatorial Co-CO's average 1.78 Å.

Figure 61: X-Ray Diffraction Crystal Structure of 12



The bulk of the ring apparently has a major effect on the ring's final position: the pentamethylcyclopentadienyl group sits "up" from the Mo terminus in the solid state, as if a 180° rotation of the  $[\text{C}_5(\text{CH}_3)_5](\text{CO})_2\text{M}$  vertex from the crystallographically determined structure of  $(\text{C}_5\text{H}_5)\text{Mo}(\text{CO})_2\text{Co}_2(\text{CO})_6\text{C}-\text{C}_6\text{H}_5$  [70] was performed around an axis through the Mo vertex and passing through the Co-Co-C triangle centroid. This occurs with a concomitant motion of the carbonyl ligands to a semi-bridged environment, thus accounting for the strong IR absorbances between 1850-1950  $\text{cm}^{-1}$ .

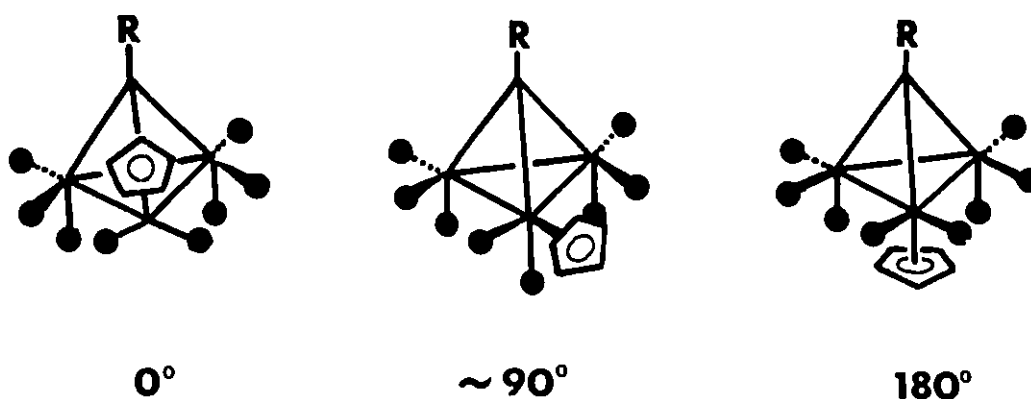
The geometry of the cluster must be rethought. Though one might think the preferred placement of the ring would be below the trimetal base, avoiding steric interactions with the capping group of the tetrahedron, the "up" placement of the ring is actually the less sterically straining conformation, because the ring is pointing essentially directly away from the bulk of the tetrahedron. The axial ("down") orientation would involve much more unfavourable interactions of the  $[\text{C}_5(\text{CH}_3)_5]$  group with the carbonyl ligands on neighbouring Co vertices. The strain imposed on the Mo carbonyls by the proximity of the other CO groups is evident in their bent conformation -- terminal carbonyls are generally linear, while the Mo carbonyls in this complex are at angles of 169.3° and 170.5°.

#### (5.7) MOLECULAR ORBITAL STUDIES

It would be interesting to perform EHMO calculations on these  $(\text{CP})\text{M}(\text{CO})_2\text{Co}_2(\text{CO})_6\text{C}-\text{CO}_2\text{CH}(\text{CH}_3)_2$  systems, to see if the program can accurately predict the observed behaviour. The initial calculation will follow the cluster through a full rotation from "up" to "down" positions, and the second will compare energies of the system at the two limiting positions. If the results are correct, it may help towards understanding the factors affecting ligand positioning.

Using the EHMO approach of Hoffmann [33] via the computer program ICON8 [90], energy calculations for a progression of orientations of the (CP)M(CO)<sub>2</sub> vertex in the cluster were performed. The original atomic positional parameters utilized were from the crystal structure of the tolyl cluster (C<sub>5</sub>H<sub>5</sub>)W-(CO)<sub>2</sub>Co<sub>2</sub>(CO)<sub>6</sub>C-(4-CH<sub>3</sub>C<sub>6</sub>H<sub>4</sub>), 27 [69].

Figure 62: Generation of Atomic Coordinates Through Rotation of the Vertex About an Axis



An axis was constructed from the centroid of the Co<sub>2</sub>C face through the W vertex. Rotations in 10° increments around this axis were effected using the CHEMX program [76], as pictured in Figure 62. New positional coordinates of the cyclopentadienyl ring and the two carbonyl ligands were thus generated, and used in the EHMO program to calculate the energy of the cluster in each orientation. Due to the limitations of the EHMO program, the apical group chosen for the model was CH. This may affect the calculated energies, probably making the "up" isomer more favoured than it should be, because the apical group will have a smaller effective size.

The results were not as we had hoped. Though a plot of derived energies of the system followed a smooth curve during the 180° rotation, the energy difference between the "up" and "down" positions and the transition states (where the CO's passed the trimetal plane, for example) was on the order of 3 eV/molecule, which converts to



values upwards of 60 kcal/mol. Obviously, these barriers would not be easy to overcome, and rapid isomer interconversion would not be expected at room temperature.

A second disappointment came in the calculated differences between the energies of the "up" and "down" limiting conformations. In the case of the  $C_5H_5$  rotation, the energy difference was calculated to be 5.1 kcal/mol, significantly higher than the values in Table 9, and the incorrect structure was chosen as the favoured (lower energy) system.

The calculations were carried out again, using the atomic positional parameters from the crystal structure of the molecule 12,  $[C_5(CH_3)_5]Mo(CO)_2-Co_2(CO)_6C-CO_2CH(CH_3)_2$ , containing the pentamethylcyclopentadienyl ligand. Once again the group on top of the cluster was simplified to a CH group, because of the limitations of the calculational program. The energy of the cluster was calculated initially using the original atomic positions, and then a manipulation of the cyclopentadienyl ring and carbonyl ligands was performed, rotating them around an axis which passed through the Mo atom and the centroid of the  $Co_2$ -(apical C) face. The newly generated atomic positions were put into the EHMO program, and a second energy of the cluster was calculated. The results reinforced what was concluded from the crystal structure, NMR and IR data: the energy of the system is lower when the pentamethylcyclopentadienyl ligand is in the "up" position. However, the "sum of one-electron energies" calculated are -2985.86 eV for the "up" structure, and -2984.77 eV in the case of the cyclopentadienyl ring "down" system, which is equivalent to an energy difference of approximately 25 kcal/mol between the two states. This is obviously incorrect, and emphasizes the sensitivity of the program to changes in molecular structure:

The EHMO program must not, therefore, be considered as the definitive

answer to an M.O. problem. In a case such as ours, EHMO theory should be used only as a tool for prediction, and not as the source of an experimental result.

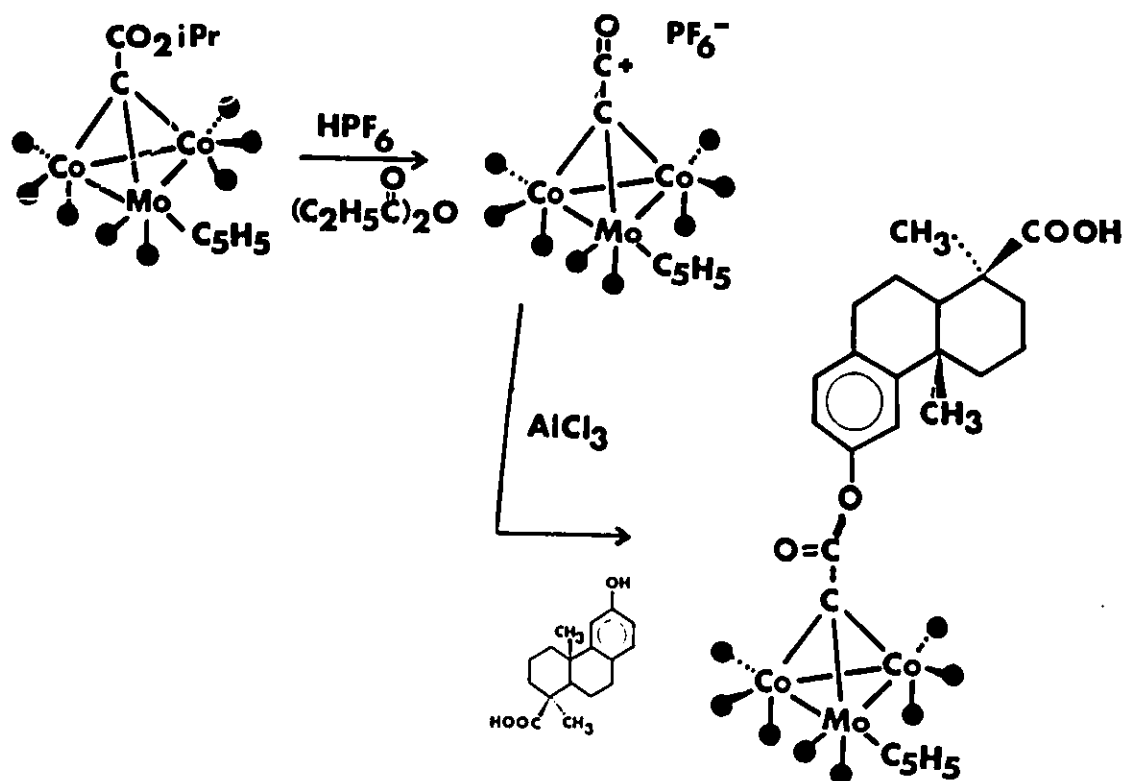
### (5.8) CYCLOPENTADIENYL RING POSITIONS IN CHIRAL CLUSTERS

In the previous study, an achiral molecule containing a vertex with a cyclopentadienyl ring ligand was observed to have two isomers in solution. The addition of a chiral group to the molecule might reveal previously unseen behaviour. The cobalt carbonyl groups in the achiral molecule may have stopped exchanging between vertices on the NMR timescale, but this could not be known unequivocally because of the magnetic equivalence of the cobalt moieties. A chiral group in the cluster would leave the two cobalt vertices diastereotopic, and thus localization of the CO ligands should be observable.

To render the cluster chiral, the route chosen was the incorporation of an inherently chiral natural product. The system was observed in an effort to study previously undetectable fluxional behaviour.

#### (5.8.1) SYNTHESIS OF $(C_5H_5)Mo(CO)_2Co_2(CO)_6C-CO_2-C_{17}O_3H_{22}$

The chiral group decided upon for this study was the natural product podocarpic acid. The synthetic pathway developed was to initially replace one  $Co(CO)_3$  vertex in  $Co_3(CO)_9C-CO_2CH(CH_3)_2$  by an  $(C_5H_5)Mo(CO)_2$  moiety [17], followed by conversion into the  $[PF_6^-]$  salt via the method developed by Seyferth [13]. The resulting salt,  $[(C_5H_5)Mo(CO)_2Co_2(CO)_6C-CO^+][PF_6^-]$ , upon reaction with podocarpic acid, afforded the desired ester,  $(C_5H_5)Mo(CO)_2Co_2(CO)_6C-CO_2-C_{17}O_3H_{22}$ , 30 (Scheme 6).

Scheme 6: Preparation of  $(C_5H_5)Mo(CO)_2Co_2(CO)_6C-CO_2-C_{17}O_3H_{22}$ , **30**

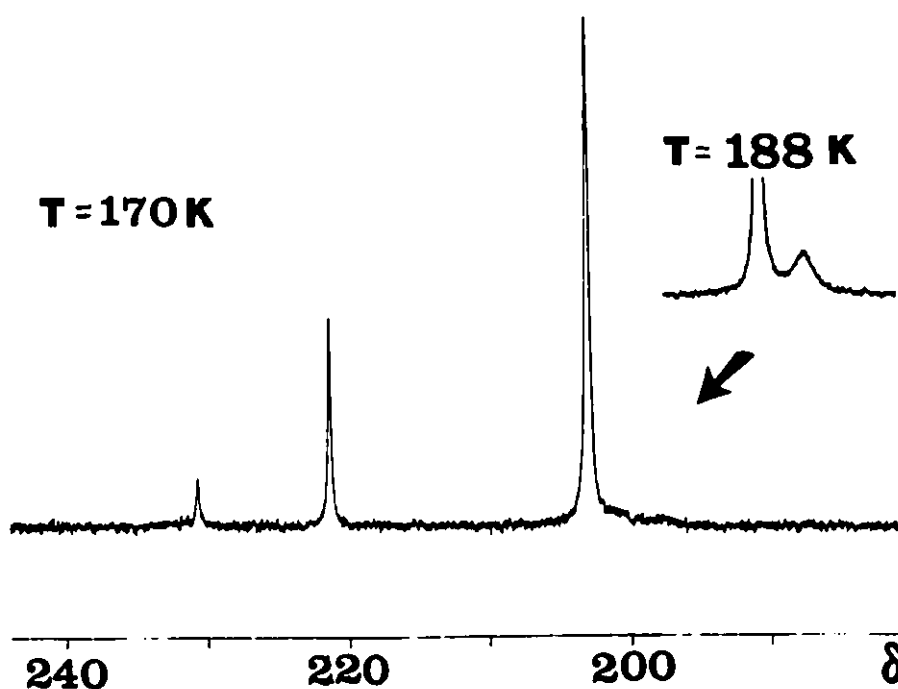
### (5.8.2) NMR STUDY

The variable temperature  $^{13}C$  NMR spectrum of **30** was collected at 62.9 MHz, and interpreted using our previously developed criteria for carbonyl exchange. The ambient temperature spectrum indicated motion on the NMR timescale of all carbonyl ligands between the three metals, producing a broad peak at 208.4 ppm. The sample was cooled to 188 K, whereupon the signature pattern of four signals appeared in the region between 200 and 230 ppm, characteristic of the two-isomer situation. The inner two resonances arise from the major isomer (Co carbonyl signal: 201.7 ppm; Mo carbonyl signal: 220.1 ppm). This can be assigned as the isomer with the cyclopentadienyl ring below the plane of the metals, distal from the chiral group. This is accompanied by the Mo carbonyl ligands in fully terminal positions. The minor

isomer, with its molybdenum carbonyl signal significantly downfield (229.4 ppm), is that with the ring up, proximal to the apical group of the molecule. The carbonyl ligands assume a semi-bridging orientation, resulting in  $^{13}\text{C}$  carbonyl resonance signals downfield of those from the fully terminal structure.

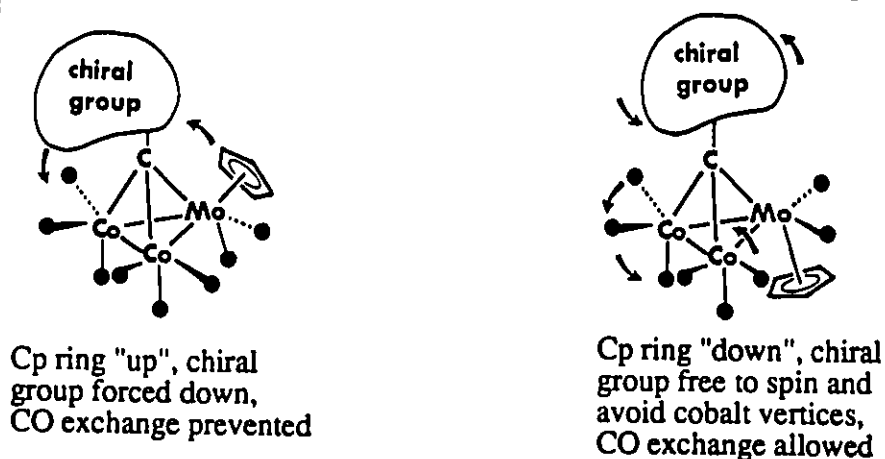
Upon repeating the experiment at higher field, (S.F. = 125 MHz), a new feature appeared in the spectrum. The signal for the cobalt carbonyl ligands of the less abundant isomer appeared broadened, suggesting a decoalescence was occurring. The temperature was decreased to 175 K, at which point the signal had disappeared into the baseline. The limiting spectrum, at 170 K, showed signs of resolution of two peaks, at 198 ppm and at 201 ppm, but sharply resolved spectra were unobtainable due to mechanical temperature restrictions. All three other carbonyl peaks were unchanged with temperature.

Figure 62: Low Temperature  $^{13}\text{C}$  NMR Spectrum of 30, Carbonyl Region, S.F. = 125 MHz



This behaviour occurs in the minor isomer only. What possible mechanism would only affect the cobalt carbonyl ligands of the minor isomer, yet leave the molybdenum carbonyls unaffected, and why would this mechanism not occur in the more abundant isomer? A potential explanation for the inequivalence of the cobalt carbonyls at low temperature is represented in Figure 63.

Figure 63: Carbonyl Group Exchange Under Varying Cyclopentadienyl Ring Positions



When the carbonyls stop their exchange between Mo and Co, it is possible (but not necessary) that they have ceased intercobalt exchange as well. At very low temperatures, the intercobalt exchange could cease in the minor isomer because with the cyclopentadienyl ring up, the capping group is forced to sit closer to the cobalt carbonyls -- so close that exchange of carbonyls between cobalts would be prevented by steric constraints. Three carbonyl ligands are localized on each cobalt vertex, and they still experience axial-equatorial rotation, but cannot move between cobalt termini. When the cyclopentadienyl ring is up (proximal to the capping alkyl group), as is the case in the minor isomer, there is more steric hindrance to rotation for the apical chiral group. In fact, the large podocarpic acid group is probably pushed towards the two cobalt vertices to avoid contact with the Cp ring. The cobalt atoms are, of course,

diastereotopic, and the proximity of the chiral group enhances this effect, resulting in separate resonances (of equal intensity) for the cobalt carbonyl groups. The diastereotopic molybdenum carbonyl groups are simply too distant from the chiral capping group to display this effect, or their shift differences are minimal and thus their signals overlap. The reason the splitting is not seen in the case of the more abundant isomer is that the chiral group is not forced to sit close to the Co vertices because the potentially hindering Cp ring is far away, (below the MoCo<sub>2</sub> plane), and thus the carbonyl ligands on the cobalt atoms can interchange positions.

This postulate was intriguing -- perhaps with a large chiral group held closer to the cluster skeleton, the steric repulsion from the cyclopentadienyl ligand would be larger, causing the same signal splitting seen in molecule 30, but on a more detectable scale. Accordingly, another chiral group was chosen, with the goal of bringing its bulk and chirality closer to the cluster.

### (5.8.3) AN EFFECTIVELY LARGER LIGAND: THE MENTHYL CLUSTER

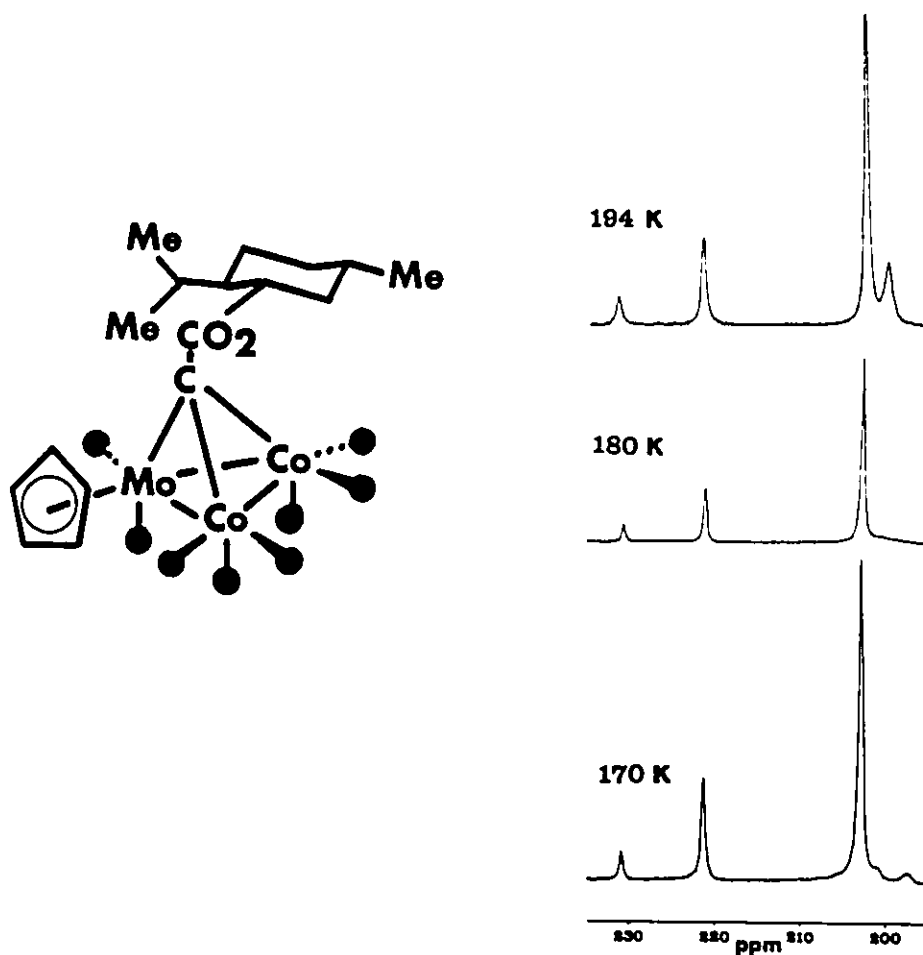
The menthyl analogue to 30, (C<sub>5</sub>H<sub>5</sub>)Mo(CO)<sub>2</sub>Co<sub>2</sub>(CO)<sub>6</sub>C-CO<sub>2</sub>-C<sub>10</sub>H<sub>17</sub>, 31, was synthesized, resulting in a potentially bulkier alkyl group than podocarpic acid positioned close to the skeleton. Any hindering behaviour to carbonyl exchange should be evident in this molecule.

The typical two-isomer pattern appeared in the carbonyl region of the low-temperature <sup>13</sup>C NMR spectrum of 31. The minor isomer was, as with the podocarpic acid derivative, that with the cyclopentadienyl ring up and the Mo carbonyls semi-bridging the Mo-Co bonds. Broadening of the cobalt carbonyl signals was first seen at 190 K at a spectral frequency of 125 MHz. Again, the spectrum only altered in the peak corresponding to the cobalt carbonyl ligands of the minor isomer. The best resolved spectrum was obtained at 170 K. While all three other CO signals remained

sharp, the fourth resonance was resolved into two peaks of equal intensity, at 201.0 and 197.6 ppm (Figure 65). This confirms the suspected behaviour observed in the podocarpic acid cluster 30.

Though the spectrum is not well resolved, a crude barrier to exchange of CO groups between Co vertices in the minor isomer can be calculated. The limiting peak separation of 3.4 ppm (422.5 Hz) and coalescence temperature of 180 K on a 500 MHz spectrometer leads to a  $\Delta G^\ddagger$  value of 8.5 kcal/mol. This is plausible considering the low temperature and high spectrometer field required to freeze out the process. It could be postulated that this barrier would be even lower in most other systems, as this complex is particularly hindered in the area of the  $\text{Co}_2(\text{CO})_6$  fragment.

Figure 65: Variable Temperature  $^{13}\text{C}$  NMR of 31, Carbonyl Region, S.F. = 125 MHz



#### (5.8.4) CONCLUSION

At high temperatures, the carbonyl groups exchange between all three metal vertices. This involves a high energy rotation of the molybdenum vertex (and the Cp and CO ligands) in order to place the carbonyl ligands in a favourable position to move between metal atoms. As the temperature of the system is lowered, the molecule lacks the energy to overcome the vertex rotation barrier, and CO exchange between the Co and Mo vertices slows on the NMR timescale. Two isomers are frozen out in the NMR spectrum -- Cp "up" and Cp "down". However, intercobalt carbonyl exchange is not slow enough to define the CO's as vertex-localized at this temperature. This fluxionality continues between cobalt vertices until around 190 K, at which temperature this process ceases on the NMR timescale in the less abundant isomer. Cessation of exchange is only seen in the molecule with the cyclopentadienyl ring "up" because the large chiral menthyl group is forced to sit close to the two cobalt vertices, thus hindering CO exchange between Co atoms. Because the carbonyl ligands in the major isomer do not experience steric hindrance from the capping group, they have a lower barrier to exchange between cobalt atoms, and thus produce a single peak in the NMR spectrum. It is important to note that the cobalt vertices are diastereotopic at all times, regardless of the rotational status of the chiral group, and as such, if the carbonyl ligands in the major isomer were localized they would surely exhibit separate chemical shifts.

It has been shown that a cyclopentadienyl ligand on a vertex in our clusters can adopt different positions, dependent upon the temperature, physical state (solution versus solid), and size of the groups under examination. This knowledge can potentially be used to plan clusters in which alteration of conditions will promote specific conformations and subsequent usefulness of the cluster.



## CHAPTER SIX

### (6) Future Work

Studies of these clusters has been extensive, evidenced by the numerous reviews and other articles about tetrahedra based upon three cobalt vertices and one carbon terminus. However, in answering one set of questions, a number of new questions have arisen, suggesting directions in which research is warranted.

#### (6.1) Further Work in Chelation

The first study in this thesis, in which ARPHOS coordination to a tricobalt cluster, revealed that the cluster was fluxional via migration of the arsenic end of the chelating ligand. This process was under temperature control. No cleavage of the Co-P linkages was seen. It would be of interest to study similar clusters with bidentate diarsine ligands, such as  $(\text{CH}_3)_2\text{AsCH}(\text{CF}_2)_2\text{CHAs}(\text{CH}_3)_2$ , (FFARS), to discern if the ligand migration occurs in the same fashion as with the ARPHOS group. Molecules of this type have been synthesized by other researchers, but to our knowledge there has been no study of fluxionality in these systems. The lack of protons in the backbone of the ligand would not cause difficulty in monitoring any ligand motion, because the  $^{19}\text{F}$  atoms are 100% abundant and spin 1/2, making ideal probes for chelate behaviour. This study would lead to increased information regarding the strength of the Co-As link, which is important as there is a scarcity of information on this topic. X-ray diffraction crystallography studies of chelated arsine systems need further investigation also, to determine the manner in which coordination occurs: if the molecules are to be used as catalysts, for example, the surface of the systems must be fully characterized.

Another aspect of chelation which was studied during the course of this thesis

involved coordination of a very bulky diphosphine. The results of this investigation were not conclusive, and thus were not presented in the main body of the thesis. The goal of this research was to see how bulk would affect the bonding of the bidentate ligand onto the cluster, as all our other diphosphine complexes exhibited strong linkages to the clusters. The fluxionality seen with the ARPHOS group was intriguing, and it was wondered whether fluxionality of the type seen with ARPHOS could be induced by making bonding conditions less favourable via steric hindrance. The bulky ligand chosen was a derivative of a carborane,  $B_{10}C_2H_{12}^{-2}$ , converted to a diphosphine by lithiation, followed by replacement of the Li groups by diphenylphosphino groups. Preliminary tests indicated some coordination of the ligand to a tricobalt nonacarbonyl cluster was occurring. However, possibly because the phosphine was so bulky, full ligand dissociation took place during purification of the products, leaving only starting materials. It would be valuable, therefore, to repeat the experiment using a less-hindered (but still bulky) carborane, such as dimethyl-diphosphino-carborane, or the diethyl derivative. It would be expected that the products of these reactions would be less likely to undergo complete cleavage of the ligand, and thus may display fluxional behaviour of the type in which we are interested.

## (6.2) Phenyl Rotation

An attempt was made to coordinate indene to two vertices of the cluster in the same manner as the two cyclopentadienyl rings had been bound, leaving the cluster with a bridging carbonyl group. The goal of the project was to observe if the electronic effect of the  $\mu$ -CO was strong enough to influence the orientation of the aryl ring on the cluster apex. Thus far, the bridging group has been given credit for causing the preferred solid state position of the phenyl/tolyl ring, but the rotation of the ring in the solution state has not been stopped. The indene rings appeared to react with the molecule, but the product was so unstable that it could not be characterized before reversion to the tricobalt nonacarbonyl

starting material occurred. As with all reactions involving transition metals in this thesis, preparations were performed under a nitrogen atmosphere, in the absence of air. If the products are kept in strict anaerobic conditions after purification, the replacement of the ligating rings by CO may be prevented, and the possibility of further characterization and study of the products may be achieved.

### (6.3) The Two-Isomer Cyclopentadienyl Clusters

The vertex  $M(\text{CP})(\text{CO})_2$  in the clusters  $(\text{CP})M(\text{CO})_2\text{Co}_2(\text{CO})_6\text{C}-\text{CO}_2\text{CH}(\text{CH}_3)_2$  was found to rotate with respect to the cluster on the NMR timescale, and the cyclopentadienyl ligand would spend the greatest amount of time in one of two positions, either "up" or "down". The chosen major conformation depends on the size of cyclopentadienyl ring: a larger ring will sit "up", towards the apex of the cluster, while the smaller rings can fit below the trimetal plane, in the axial position. It was concluded that the deciding factor at work here was the steric requirement -- the cyclopentadienyl ring could fit best in the "up" position. A second aspect of this situation which was not investigated in this thesis was the effect of electron-donating capability of the cyclopentadienyl ring on its favoured position. It has been proposed that another reason the  $\text{C}_5(\text{CH}_3)_5$  ring sits "up" is to allow the carbonyl ligands to semi-bridge to the two cobalt vertices, leading to distribution of excess electron density from the electron-rich pentamethylcyclopentadienyl ring into the rest of the molecule. If the ring was substituted with groups of decreased electron-donor capability, such as halogens or cyano groups, and if steric considerations were not the guiding force, it would be expected that the ring may shift to a preferred position below the cluster. The accompanying carbonyl groups would be fully terminal as the carbonyl ligands would not be required to distribute excess electron density about the cluster. Parallel to that research, small electron-rich rings could be incorporated into the clusters to study their chosen positions with respect to the trimetal basal plane. Would they sit "up" so that the carbonyl

groups on that vertex could semi-bridge to the remaining vertices? With this knowledge, it would be possible to compare the determining factors in Cp ring positioning, both electronic and steric effects.

#### (6.4) Conclusion

Though the field of organometallic chemistry is new, it has proven to be interesting in all its facets, and very useful in its applications. It will only be through further research that clusters will be fully understood and that fulfillment of their potential will be realized.

## CHAPTER SEVEN

### EXPERIMENTAL

Unless noted otherwise, all syntheses were performed under a nitrogen atmosphere. All solvents were dried according to published techniques [91]. Infrared spectra were obtained on a Nicolet 7199 FTIR using NaCl solution cells or KBr pellets. NMR spectra were recorded on Bruker AM-500, WM-400, WM-250 and Varian EM-390 spectrometers. The chemical shifts of  $^1\text{H}$  and  $^{13}\text{C}$  are reported relative to tetramethylsilane. Chemical shifts of  $^{31}\text{P}$  are quoted relative to 85%  $\text{H}_3\text{PO}_4$ . NMR spectra were recorded at ambient temperature unless otherwise noted. Microanalyses were performed by Guelph Chemical Laboratories in Guelph, Ontario. Fast Atom Bombardment (FAB) mass spectra were obtained on a VG Analytical ZAB-E mass spectrometer, with an accelerating potential of 8kV and a resolving power of 10,000. 3-Nitro benzyl alcohol or thioglycerol was used as the sample matrix with Xe as the bombarding gas.

#### (7.1) MELTING POINT TECHNIQUE

Melting points of the clusters could not be obtained in the conventional manner of slow heating until melting was observed, either in a sealed tube in an oil bath or in the atmosphere on a hot stage melting apparatus. Gradual heating of the samples led to decomposition. Instead, the samples were introduced onto a hot stage melting point machine at various temperatures, at which time they either did or did not melt. The melting point could, in this way, be narrowed down to one degree at which melting would occur, below which the sample would remain crystalline.

## (7.2) CARBONYL ENRICHMENTS

In a typical experiment,  $\text{Co}_3(\text{CO})_7(\text{DIPHOS})\text{C}-\text{CO}_2\text{CH}(\text{CH}_3)_2$ , 8, (0.1 g, 0.11 mmol) in 35 mL tetrahydrofuran (THF) was stirred under an atmosphere of  $^{13}\text{C}$ O for 48 hours. The solvent was removed in vacuo, and the product analysed using mass spectrometry; enrichment was on the order of 25-30%. This enabled collection of an acceptable  $^{13}\text{C}$  NMR spectrum in 100 scans.

## (7.3) SYNTHESSES AND SPECTRAL DATA

### $\text{Co}_3(\text{CO})_9\text{C}-\text{CO}_2\text{CH}(\text{CH}_3)_2$ , 7

Following the procedure of Seyferth [5],  $\text{Co}_2(\text{CO})_8$  (7.26 g, 21.2 mmol) and  $\text{Cl}_3\text{C}-\text{CO}_2\text{CH}(\text{CH}_3)_2$  (2.42 g, 11.8 mmol) were heated under reflux in tetrahydrofuran (75 mL) for 3.5 hours. After the mixture was cooled to room temperature and filtered to remove the cobalt salts, the filtrate was evaporated to dryness and the crude product was recrystallized from hexane to give 7 (4.17 g, 7.89 mmol, 66%); melting point 337 K (lit. 336-337 K) [92]; IR ( $\text{C}_6\text{H}_{12}$ )  $\nu_{\text{CO}}$  2100 (w), 2055 (s), 2035 (s), 1687 (ester)  $\text{cm}^{-1}$ ;  $^1\text{H}$  NMR (WM-250;  $\text{C}_6\text{D}_6$ )  $\delta$  5.22 (septet,  $J_{\text{HH}} = 6.2$  Hz, iPr H), 1.23 (doublet, iPr  $\text{CH}_3$ 's);  $^{13}\text{C}$  NMR (WM-400;  $\text{CD}_2\text{Cl}_2$ )  $\delta$  198.8 (all CO's), 69.7 (CH), 21.7 ( $\text{CH}_3$ 's).

### $\text{Co}_3(\text{CO})_7[(\text{C}_6\text{H}_5)_2\text{P}(\text{CH}_2)_2\text{P}(\text{C}_6\text{H}_5)_2]\text{C}-\text{CO}_2\text{CH}(\text{CH}_3)_2$ , 8

A solution of 7 (0.34 g, 0.66 mmol) and  $(\text{C}_6\text{H}_5)_2\text{P}(\text{CH}_2)_2\text{P}(\text{C}_6\text{H}_5)_2$  (0.26 g, 0.66 mmol) in THF (35 mL) was stirred at ambient temperature for 45 minutes. The progress of the reaction was monitored by thin layer chromatography (TLC) on Kieselgel (eluent ether/petroleum ether, 15/85) which revealed the formation of 8 ( $R_F = 0.14$ ) as a green spot. Chromatography on silica gel (eluent ether/hexane, 10/90) gave dark green crystals of 8 (0.19 g, 0.22 mmol, 33%); melting point 396 K; IR ( $\text{C}_6\text{H}_{12}$ )  $\nu_{\text{CO}}$  2085 (m), 2075 (s), 2050 (m), 2030(s), 2020 (s), 1980 (m), 1650 (ester)  $\text{cm}^{-1}$ ;  $^1\text{H}$

NMR (WM-250; CD<sub>2</sub>Cl<sub>2</sub>) δ 7.7-7.3 (multiplet, phenyl H's), 4.63 (septet, J<sub>HH</sub> = 6.4 Hz, iPr H), 2.47 (multiplet, 2 DIPHOS H's), 2.06 (multiplet, 2 DIPHOS H's), 1.14 (doublet, iPr CH<sub>3</sub>'s); <sup>13</sup>C NMR (WM-400; CD<sub>2</sub>Cl<sub>2</sub>; 223 K) δ 210.2 (2 CO's), 204.3 (2 CO's), 202.5 (3 CO's), 181.7 (ester CO), 136.2, 131.8, 130.3, 128.6 (Ph), 68.2 (CH), 24.1 (doublet, J<sub>CP</sub> = 24 Hz, CH<sub>2</sub>P), 21.6 (CH<sub>3</sub>'s); <sup>31</sup>P NMR (C<sub>6</sub>D<sub>6</sub>) 42.0 ppm. FAB mass spectrum: m/z (%) 870 (28) C<sub>38</sub>H<sub>31</sub>Co<sub>3</sub>O<sub>9</sub>P<sub>2</sub> (M<sup>+</sup>); 842 (22) (M-CO)<sup>+</sup>; 786 (69) (M-3CO)<sup>+</sup>; 758 (35) (M-4CO)<sup>+</sup>; 730 (23) (M-5CO)<sup>+</sup>; 702 (54) (M-6CO)<sup>+</sup>; 674 (52) (M-7CO)<sup>+</sup>; 616 (80) C<sub>28</sub>H<sub>25</sub>Co<sub>3</sub>OP<sub>2</sub>; 588 (90) C<sub>27</sub>H<sub>25</sub>Co<sub>3</sub>P<sub>2</sub>; 431 (100) C<sub>16</sub>H<sub>15</sub>Co<sub>3</sub>P. Anal. calc. for C<sub>38</sub>H<sub>31</sub>Co<sub>3</sub>O<sub>9</sub>P<sub>2</sub>: C, 52.44; H, 3.59. Found: C, 52.69; H, 3.71.

Co<sub>3</sub>(CO)<sub>7</sub>[(C<sub>6</sub>H<sub>5</sub>)<sub>2</sub>As(CH<sub>2</sub>)<sub>2</sub>P(C<sub>6</sub>H<sub>5</sub>)<sub>2</sub>]C-CO<sub>2</sub>CH(CH<sub>3</sub>)<sub>2</sub>, 9

A solution of 7 (0.26 g, 0.50 mmol) and (C<sub>6</sub>H<sub>5</sub>)<sub>2</sub>As(CH<sub>2</sub>)<sub>2</sub>P(C<sub>6</sub>H<sub>5</sub>)<sub>2</sub> (0.22 g, 0.50 mmol) in THF (50 mL) was heated under reflux for 1.5 hours. Column chromatography on silica gel (eluent ether/hexane, 10/90) gave dark purple crystals of 9 (0.25 g, 0.27 mmol, 54%); melting point: 449 K; IR (C<sub>6</sub>H<sub>12</sub>) ν<sub>CO</sub> 2060 (s), 2015 (s), 2005 (s), 1980 (s), 1955 (m, br), 1650 (ester) cm<sup>-1</sup>; <sup>1</sup>H NMR (WM-250; CD<sub>2</sub>Cl<sub>2</sub>; 223 K) δ 7.7-7.3 (multiplet, phenyl H's), 4.58 (septet, J<sub>HH</sub> = 6.3 Hz, iPr H), 2.65 (multiplet, 1 ARPHOS H), 2.34 (multiplet, 1 ARPHOS H), 2.01 (multiplet, 1 ARPHOS H), 1.98 (multiplet, 1 ARPHOS H), 1.10 (doublet, iPr CH<sub>3</sub>), 0.99 (doublet, iPr CH<sub>3</sub>); <sup>13</sup>C NMR (WM-400; CD<sub>2</sub>Cl<sub>2</sub>; 183 K) δ 243.1 (apical C), 210.5 (1 CO), 208.8 (1 CO), 203.5 (2 CO's), 201.6 (3 CO's), 182.2 (ester CO), 137.7, 132.1, 130.5, 130.2, 129.2, 129.0 (Ph), 68.5 (CH), 25.4 (d, J<sub>CP</sub> = 23 Hz, CH<sub>2</sub>P), 23.1 (CH<sub>2</sub>As), 22.0 (CH<sub>3</sub>); <sup>31</sup>P NMR (C<sub>6</sub>D<sub>6</sub>) 47.6 ppm. FAB mass spectrum: m/z (%) 914 (28) C<sub>38</sub>H<sub>31</sub>Co<sub>3</sub>O<sub>9</sub>AsP (M<sup>+</sup>); 886 (4) (M-CO)<sup>+</sup>; 858 (4) (M-2CO)<sup>+</sup>; 830 (10) (M-3CO)<sup>+</sup>; 802 (4) (M-4CO)<sup>+</sup>; 774 (8) (M-5CO)<sup>+</sup>; 746 (4) (M-6CO)<sup>+</sup>; 718 (9) (M-7CO)<sup>+</sup>; 660 (14) C<sub>28</sub>H<sub>25</sub>Co<sub>3</sub>OAsP; 632 (17) C<sub>27</sub>H<sub>25</sub>Co<sub>3</sub>AsP; 59 (100) Co. Anal. calc. for C<sub>38</sub>H<sub>31</sub>AsCo<sub>3</sub>O<sub>9</sub>P: C, 49.92; H, 3.36.

Found: C, 49.88; H, 3.52.

$(C_5H_5)MoCo_2(CO)_8C-CO_2CH(CH_3)_2$ , 10

$[(C_5H_5)Mo(CO)_3]_2$  (0.82 g, 1.89 mmol) and 7 (1.00 g, 1.89 mmol) were heated under reflux in tetrahydrofuran (35 mL) for six hours, monitored by TLC on Kieselgel (eluent ether/petroleum ether 1/3) which displayed a green spot at  $R_F = 0.16$ . Column chromatography on silica gel (100-200 mesh) with the same solvent system resulted in 200 mg of green crystals of 10 (0.33 mmol, 18% yield). Melting point 364 K. IR ( $CH_2Cl_2$ )  $\nu_{CO}$  2085 (w), 2077 (m), 2050 (m), 2028 (s), 2006 (s), 1964 (w), 1942 (w), 1886 (w), 1664 (ester)  $cm^{-1}$ ; IR (KBr)  $\nu_{CO}$  2076 (m), 2021 (s), 1999 (s), 1971 (m), 1955 (m), 1663 (ester)  $cm^{-1}$ .  $^{13}C$  NMR (AM-500;  $CD_2Cl_2$ )  $\delta$  207.9 (all CO's); 177.7 (ester CO); 92.3 (Cp ring); 69.3 (iPr CH); 22.1 (iPr  $CH_3$ 's). Low temperature  $^{13}C$  NMR (AM-500;  $CD_2Cl_2$ ; 193 K)  $\delta$  230.5 (Mo CO's, minor isomer); 221.2 (Mo CO's, major isomer); 202.8 (Co CO's, major isomer); 200.2 (Co CO's, minor isomer); 94.0, 90.1 (Cp rings, minor and major isomer, respectively).

$(C_5H_4CH_3)MoCo_2(CO)_8C-CO_2CH(CH_3)_2$ , 11

$[(C_5H_4CH_3)Mo(CO)_3]_2$  (0.15 g, 0.29 mmol) was heated under reflux in 20 mL THF with 0.30 g (0.57 mmol) 7. Reaction progress was observed by using TLC on Kieselgel (eluent ether/petroleum ether 15/85); the desired product 11 gave a green spot at  $R_F = 0.47$ . After eight hours, the solution was evaporated and the solids purified by column chromatography on silica gel (100/200 mesh), yielding dark green crystals, 80 mg, 23% from  $Co_3$  cluster as limiting reagent. Melting point 365 K. IR ( $CH_2Cl_2$ )  $\nu_{CO}$  2087(m), 2076 (m), 2050 (s), 2028 (s), 2006 (s), 1961 (w), 1938 (m), 1885 (m), 1666 (ester)  $cm^{-1}$ ; IR (KBr)  $\nu_{CO}$  2074 (m), 2018 (s), 2001 (s), 1974 (m), 1952 (m), 1920 (m), 1661 (ester)  $cm^{-1}$ .  $^{13}C$  NMR (AM-500;  $CD_2Cl_2$ )  $\delta$  247.2 (apical C, observed in



D<sub>8</sub>-toluene); 208.3 (all CO's); 184.5 (ester CO); 95.0 (substituted Cp ring C); 91.3, 89.5 (unsubstituted ring C's); 69.4 (iPr CH); 22.1 (iPr CH<sub>3</sub>'s); 14.1 (Cp CH<sub>3</sub>). Low temperature <sup>13</sup>C NMR (AM-500; CD<sub>2</sub>Cl<sub>2</sub>; 193 K) δ 231.8 (Mo CO's, minor isomer), 222.2 (Mo CO's, major isomer), 203.1 (Co CO's, major isomer), 200.6 (Co CO's, minor isomer). Anal. Calc. for Co<sub>2</sub>MoC<sub>19</sub>O<sub>10</sub>H<sub>14</sub>: C, 37.04; H, 2.29. Found: C, 37.07; H, 2.04.

[C<sub>5</sub>(CH<sub>3</sub>)<sub>5</sub>]MoCo<sub>2</sub>(CO)<sub>8</sub>C-CO<sub>2</sub>CH(CH<sub>3</sub>)<sub>2</sub>, 12

[(C<sub>5</sub>(CH<sub>3</sub>)<sub>5</sub>)Mo(CO)<sub>3</sub>]<sub>2</sub> (0.21 g, 0.33 mmol) and 7 (0.34 g, 0.66 mmol) were heated under reflux in tetrahydrofuran (50 mL) for 18 hours. Progress of the reaction was followed by TLC on Kieselgel (eluent, ether/petroleum ether, 15/85) showing a purple-brown spot, 7, (R<sub>F</sub> = 0.76), and a green spot, 12 (R<sub>F</sub> = 0.37). After filtration and removal of the solvent, chromatography on silica gel (100-200 mesh) using ether/petroleum ether (15/85) yielded green crystals of 13, (0.067 g, 0.1 mmol, 15% based on 7 as limiting reagent); melting point 408 K. Crystals of crystallographic quality were grown from a cooled solution of ether/hexane (15:85). IR (CH<sub>2</sub>Cl<sub>2</sub>) ν<sub>CO</sub> 2080 (s), 2043 (s), 2025 (s), 1916 (m), 1869 (m), 1654 (ester) cm<sup>-1</sup>; IR (KB.) ν<sub>CO</sub> 2076 (s), 2047 (m), 2043 (m), 2025 (s), 2012 (s), 1913 (m), 1863 (m), 1662 (ester) cm<sup>-1</sup>. <sup>1</sup>H NMR (WM-250; C<sub>6</sub>D<sub>6</sub>) δ 5.2 (septet, J<sub>HH</sub> = 6.2 Hz, iPr H), 1.79 (singlet, Cp CH<sub>3</sub>'s, 15 H), 1.33 (doublet, iPr CH<sub>3</sub>'s); <sup>13</sup>C NMR (AM-500; CD<sub>2</sub>Cl<sub>2</sub>) δ 248.3 (apical C); 209.9 (all CO's); 178.5 (ester CO); 106.1 (Cp C's); 69.0 (iPr CH); 22.1 (iPr CH<sub>3</sub>'s); 10.2 (Cp CH<sub>3</sub>'s). Low temperature <sup>13</sup>C NMR (AM-500; CD<sub>2</sub>Cl<sub>2</sub>; 183 K) δ 235.0 (Mo CO's, major isomer); 223.5 (Mo CO's, minor isomer, 8:1 ratio); 204.1 (Co CO's, minor isomer); 200.9 (Co CO's, major isomer, 1:8 ratio); 105.3, 104.8 (Cp C's, major and minor isomers); 12.0, 10.2 (Cp CH<sub>3</sub>'s, minor and major isomers). FAB mass spectrum: m/z (%) 674 (8) C<sub>23</sub>H<sub>22</sub>Co<sub>2</sub>MoO<sub>10</sub> (M<sup>+</sup>); 646 (2) (M-CO)<sup>+</sup>; 618 (10) (M-2CO)<sup>+</sup>; 590

(9) (M-3CO)<sup>+</sup>; 562 (7) (M-4CO)<sup>+</sup>; 534 (7) (M-5CO)<sup>+</sup>; 506 (10) (M-6CO)<sup>+</sup>; 478 (6) (M-7CO)<sup>+</sup>; 450 (15) (M-8CO)<sup>+</sup>; 135 (100) C<sub>10</sub>H<sub>15</sub><sup>+</sup>. Molybdenum-containing peak masses are calculated only on the basis of <sup>98</sup>Mo, but all such ions give peak patterns showing the correct isotopic distribution. Anal. calc. for C<sub>23</sub>H<sub>22</sub>Co<sub>2</sub>MoO<sub>10</sub>: C, 41.09; H, 3.30. Found: C, 41.19; H, 3.37. Recrystallization from hexane/ether 85/15 afforded a dark purple air-stable crystal (0.30 × 0.25 × 0.20 mm<sup>3</sup>) suitable for structure solution by X-ray diffraction crystallography. Precession photographs revealed the crystal was monoclinic, and accurate cell parameters were determined from a least-squares fit of  $\chi$ ,  $\phi$ , and  $2\Theta$  for 15 reflections in the range  $21.5^\circ < 2\Theta < 29.6^\circ$ . Measurements were made on a Nicolet P3 diffractometer with use of graphite-monochromated Mo K $\alpha$  radiation. Data collection over  $h,k,\pm l$  resulted in 3454 unique reflections and 2267 observed reflections with  $I > 3\sigma(I)$ . Data were corrected for Lorentz-polarization effects, and for absorption using a  $\phi$ -scan [99] ( $\mu(\text{Mo K}\alpha) = 18.02 \text{ cm}^{-1}$ ). Considering only observed data, heavy-atom positions were found by direct methods (SHELXS [97]). Subsequent Fourier difference maps revealed the positions of all remaining atoms (excluding the hydrogens, which were placed at calculated positions) (SHELX [94]). Anisotropic refinements of all non-hydrogen atoms by full matrix least-squares methods resulted in final  $R_1$  and  $R_2$  values of 0.0355 and 0.0389. Scattering curves from [95] were applied during refinement of the structure, and anomalous dispersion corrections for Co and Mo were applied from [96]. Atomic positional parameters, temperature factors, and selected bond lengths and angles appear in Tables 12A-12E.

(C<sub>5</sub>H<sub>5</sub>)WCo<sub>2</sub>(CO)<sub>8</sub>C-CO<sub>2</sub>CH(CH<sub>3</sub>)<sub>2</sub>, 13

As with the molybdenum substitutions into the tricobalt clusters, tungsten dimers were heated with the starting material 7, to produce monosubstituted products. [(C<sub>5</sub>H<sub>5</sub>)W(CO)<sub>3</sub>]<sub>2</sub> (2.02 g, 3.04 mmol) was reacted with 7 (1.60 g, 3.04 mmol) in THF

(100 mL) under reflux for 43 hours. The resulting mixture showed a brown spot on Kieselgel TLC plates with eluent ether/petroleum ether 15:85 ( $R_F = 0.37$ ). The reaction mixture was dried under vacuum and purified by column chromatography, yielding a brown compound, 13, with melting point 372 K. Yield 55 mg, 0.08 mmol, 3%. IR ( $\text{CH}_2\text{Cl}_2$ )  $\nu_{\text{CO}}$  2087 (m), 2077 (m), 2040 (s), 2025 (s), 2006 (s), 1956 (w), 1933 (w), 1879 (w), 1668 (ester)  $\text{cm}^{-1}$ ; IR (KBr)  $\nu_{\text{CO}}$  2076 (m), 2019 (s), 1998 (s), 1970 (m), 1947 (m), 1921 (w), 1661 (m).  $^{13}\text{C}$  NMR (AM-500;  $\text{CH}_2\text{Cl}_2$ )  $\delta$  202.6 (all CO's); 90.5 (Cp C's); 69.3 (iPr CH); 22.1 (iPr  $\text{CH}_3$ ). Low temperature  $^{13}\text{C}$  NMR (AM-500;  $\text{CD}_2\text{Cl}_2$ ; 193 K)  $\delta$  216.3 (W CO's, minor isomer), 206.0 (W CO's, major isomer,  $^{183}\text{W}$  satellites at 206.6 and 205.3,  $J_{\text{C-W}} = 165$  Hz, 14%), 201.0 (Co CO's, major isomer), 198.6 (Co CO's, minor isomer). Anal. Calc. for  $\text{Co}_2\text{WC}_{18}\text{O}_{10}\text{H}_{12}$ : C, 31.33; H, 1.75. Found: C 31.42, H, 1.93.

$(\text{C}_5\text{H}_4\text{CH}_3)\text{WCo}_2(\text{CO})_8\text{C-CO}_2\text{CH}(\text{CH}_3)_2$ , 14

$[(\text{C}_5\text{H}_4\text{CH}_3)\text{W}(\text{CO})_3]_2$  (1.3 g, 1.89 mmol) was heated in 150 mL THF under reflux for 24 hours with 1.0 g of 7 (1.89 mmol), and the reaction progress was monitored by TLC on Kieselgel. The product, 14, gave a gray spot on the TLC plate at  $R_F = 0.17$  in eluent ether/petroleum ether 15:85. The reaction vessel was evacuated of liquid, and the residue was purified by column chromatography as before, producing 101 mg of the desired compound (0.14 mmol, 8%). IR ( $\text{CH}_2\text{Cl}_2$ )  $\nu_{\text{CO}}$  2086 (m), 2076 (m), 2048 (s), 2024 (s), 2005 (s), 1953 (m), 1931 (m), 1875 (w), 1662 (ester)  $\text{cm}^{-1}$ ; IR (KBr)  $\nu_{\text{CO}}$  2076 (m), 2031 (s), 1997 (s), 1970 (m), 1941 (m), 1661 (ester)  $\text{cm}^{-1}$ .  $^1\text{H}$  NMR (WM-250;  $\text{D}_6$ -acetone)  $\delta$  5.80 - 5.70 (multiplet, Cp H's); 5.17 (septet,  $J_{\text{HH}} = 6.2$  Hz, iPr H); 2.46 (singlet, Cp  $\text{CH}_3$ ); 1.41 (doublet,  $J_{\text{HH}} = 6.2$  Hz, iPr  $\text{CH}_3$ 's).  $^{13}\text{C}$  NMR (AM-500;  $\text{CD}_2\text{Cl}_2$ )  $\delta$  202.9 (all CO's); 185.0 (ester CO); 106.5 (substituted Cp C); 91.6, 90.1 (unsubstituted Cp C's); 69.2 (iPr CH); 22.1 (iPr  $\text{CH}_3$ 's); 13.8 (Cp  $\text{CH}_3$ ).

Low temperature  $^{13}\text{C}$  NMR (AM-500;  $\text{CD}_2\text{Cl}_2$ ; 183 K)  $\delta$  218.1 (W CO's, minor isomer); 207.3 (major isomer, W satellites at 208.0 and 206.9 ppm,  $J_{\text{W,C}} = 164$  Hz); 201.2 (Co CO's, major isomer); 198.7 (Co CO's, minor isomer). Splitting of the methylcyclopentadienyl carbon signals was also observed, with the minor isomer appearing slightly downfield of the major one. Anal. Calc. for  $\text{Co}_2\text{WC}_{19}\text{O}_{10}\text{H}_{14}$ : C, 32.41; H, 2.00. Found: C, 32.36; H, 2.23.

$[\text{C}_5(\text{CH}_3)_5]\text{WCo}_2(\text{CO})_8\text{C-CO}_2\text{CH}(\text{CH}_3)_2$ , 15

$[(\text{C}_5(\text{CH}_3)_5)\text{W}(\text{CO})_3]_2$  (0.83 g, 1.1 mmol) and 7 (1.17 g, 2.2 mmol) were heated together in 35 mL THF under reflux conditions. When the reaction was complete as indicated by TLC (Keisegel, eluent ether/petroleum ether 15:85, green-brown spot at  $R_F = 0.28$ ), the solvent was removed under vacuum, and the solids were subsequently purified by column chromatography on silica gel (100-200 mesh) using the solvent composition used in the TLC procedure. The resulting 55 mg (0.07 mmol, 3% based on 7 as limiting reagent) of green crystals had a melting point of 446 K. IR ( $\text{CH}_2\text{Cl}_2$ )  $\nu_{\text{CO}}$  2081 (s), 2044 (s), 2023 (s), 1915 (m), 1856 (w), 1656 (ester)  $\text{cm}^{-1}$ ; IR (KBr)  $\nu_{\text{CO}}$  2080 (s), 2042 (s), 2009 (s), 1905 (m), 1858 (m), 1665 (ester)  $\text{cm}^{-1}$ .  $^{13}\text{C}$  NMR (AM-500;  $\text{CH}_2\text{Cl}_2$ )  $\delta$  239.7 (apical C); 205.4 (all CO's); 182.2 (ester CO); 104.1 (Cp ring); 69.0 (iPr CH); 22.0 (iPr  $\text{CH}_3$ 's); 10.1 (Cp  $\text{CH}_3$ 's). Low temperature  $^{13}\text{C}$  NMR (AM-500;  $\text{CD}_2\text{Cl}_2$ ; 183 K)  $\delta$  222.3 (W CO's, major isomer); 209.3 (W CO's, minor isomer); 202.7 (Co CO's, minor isomer); 199.2 (Co CO's, major isomer).

$[\text{C}_5(\text{CH}_3)_5]\text{MoCo}_2(\text{CO})_6[(\text{C}_6\text{H}_5)_2\text{P}(\text{CH}_2)_2\text{P}(\text{C}_6\text{H}_5)_2]\text{C-CO}_2\text{CH}(\text{CH}_3)_2$ , 16

As with the synthesis of the tricobalt complex 8, DIPHOS (148 mg, 0.37 mmol) and 12 (250 mg, 0.37 mmol) in 50 mL THF under reflux conditions for two hours produced 16 (210 mg, 0.21 mmol, 56% yield). Melting point 390 K; IR ( $\text{C}_6\text{H}_{12}$ )

$\nu_{\text{CO}}$  2090 (w), 2050 (m), 2040 (m), 2010 (m), 1990 (s), 1970 (s), 1945 (s), 1920 (w), 1910 (w), 1660 (ester)  $\text{cm}^{-1}$ ;  $^1\text{H}$  NMR (WM-250;  $\text{CD}_2\text{Cl}_2$ )  $\delta$  7.6-7.3 (multiplet, phenyl H's), 4.2 (septet,  $J_{\text{HH}} = 6.0$  Hz, iPr H), 2.80 (multiplet, 2 DIPHOS H's), 2.45 (multiplet, 2 DIPHOS H's), 2.04 (singlet, Cp  $\text{CH}_3$ 's), 1.06 (doublet, iPr  $\text{CH}_3$ 's);  $^{13}\text{C}$  NMR (WM-400;  $\text{CD}_2\text{Cl}_2$ ; 198 K)  $\delta$  228.0 (2 CO, on Mo), 213.2 (2 CO, on Co), 210.5 (1 CO, on Co), 207.6 (1 CO, on Co), 133.5, 129.5, 127.9 (Ph), 102.0 (Cp ring), 68.2 (CH), 24.1 (d,  $J_{\text{CP}} = 24$  Hz,  $\text{CH}_2\text{P}$ ), 24.1 ( $\text{CH}_3$ ), 11.2 (Cp- $\text{CH}_3$ 's);  $^{31}\text{P}$  NMR ( $\text{C}_6\text{D}_6$ ) 37.4 ppm. FAB mass spectrum:  $m/z$  (%) 1016 (28)  $\text{C}_{47}\text{H}_{46}\text{Co}_2\text{MoO}_8\text{P}_2$  ( $\text{M}^+$ ); 988 (4) ( $\text{M}-\text{CO}$ ) $^+$ ; 960 (5) ( $\text{M}-2\text{CO}$ ) $^+$ ; 932 (53) ( $\text{M}-3\text{CO}$ ) $^+$ ; 904 (100) ( $\text{M}-4\text{CO}$ ) $^+$ ; 876 (8) ( $\text{M}-5\text{CO}$ ) $^+$ ; 848 (28) ( $\text{M}-6\text{CO}$ ) $^+$ ; 713 (10) ( $\text{M}-6\text{CO}-\text{C}_5\text{Me}_5$ ) $^+$ . Anal. calc. for  $\text{C}_{47}\text{H}_{46}\text{Co}_2\text{MoO}_8\text{P}_2$ : C, 55.64; H, 4.57. Found: C, 55.32; H, 4.81.

$[\text{C}_5(\text{CH}_3)_5]\text{WCo}_2(\text{CO})_6[(\text{C}_6\text{H}_5)_2\text{As}(\text{CH}_2)_2\text{P}(\text{C}_6\text{H}_5)_2]\text{C}-\text{CO}_2\text{CH}(\text{CH}_3)_2$ , 17

$[\text{C}_5(\text{CH}_3)_5]\text{WCo}_2(\text{CO})_6[(\text{C}_6\text{H}_5)_2\text{As}(\text{CH}_2)_2\text{P}(\text{C}_6\text{H}_5)_2]\text{C}-\text{CO}_2\text{CH}(\text{CH}_3)_2$  was prepared analogously to 9:  $(\text{C}_6\text{H}_5)_2\text{As}(\text{CH}_2)_2\text{P}(\text{C}_6\text{H}_5)_2$  (26 mg, 0.06 mmol) in THF (35 mL) with  $[\text{C}_5(\text{CH}_3)_5]\text{WCo}_2(\text{CO})_6\text{C}-\text{CO}_2\text{CH}(\text{CH}_3)_2$  (42 mg, 0.06 mmol) gave 17 in a yield of 76% (52 mg, 0.045 mmol); melting point 378 K; IR ( $\text{C}_6\text{H}_{12}$ )  $\nu_{\text{CO}}$  2065 (s), 2020 (s), 2015 (s), 1655 (ester)  $\text{cm}^{-1}$ ;  $^1\text{H}$  NMR (WM-250;  $\text{CD}_2\text{Cl}_2$ )  $\delta$  7.7-7.2 (multiplet, phenyl H's), 4.1 (septet,  $J_{\text{HH}} = 6.2$  Hz, iPr H), 3.02 (multiplet, one ARPHOS H), 2.65 (multiplet, one ARPHOS H), 2.44 (multiplet, one ARPHOS H), 2.10 (multiplet, one ARPHOS H), 2.05 (singlet, Cp  $\text{CH}_3$ 's), 1.10 (doublet, iPr  $\text{CH}_3$ 's);  $^{13}\text{C}$  NMR (WM-400;  $\text{CD}_2\text{Cl}_2$ ; 213 K)  $\delta$  228.4 (Mo CO), 226.9 (Mo CO), 213.1 (2 Co CO's), 208.6 (Co CO), 208.0 (Co CO), 132.5, 130.2, 128.3, 127.8 (Ph), 101.7 (Cp ring), 67.4 (CH), 25.3 (d,  $J_{\text{CP}} = 24$  Hz,  $\text{CH}_2-\text{P}$ ), 21.2 ( $\text{CH}_2-\text{As}$ ), 20.9 ( $\text{CH}_3$ ), 11.0 (Cp- $\text{CH}_3$ 's); at 183 K, extra CO resonances appear at  $\delta$  235.5, 231.5, 209.2, 204.3, 201.0;  $^{31}\text{P}$  NMR ( $\text{C}_6\text{D}_6$ ) 41.0 ppm. Anal. calc. for  $\text{C}_{47}\text{H}_{46}\text{AsCo}_2\text{MoO}_8\text{P}$ : C, 53.33; H, 4.38. Found: C, 53.40; H, 3.99.

$\text{Co}_3(\text{C}_5\text{H}_5)_2(\text{CO})_4\text{C-C}_6\text{H}_5$ , 19

$\text{Co}_3(\text{CO})_9\text{C-C}_6\text{H}_5$  (1.04 g, 2.0 mmol), prepared via the reaction of  $\alpha,\alpha,\alpha$ -trichlorotoluene with dicobalt octacarbonyl, was heated under reflux with 2.5 mL (2 g, 30 mmol) of freshly cracked cyclopentadiene in 35 ml THF. The reaction was monitored by TLC, which showed a green-brown spot at  $R_F = 0.45$  (eluent ether/petroleum ether 15:85) for the desired product. After 21 hours, the solvent was removed and the mixture was purified by column chromatography on silica gel (100-200 mesh, eluent as above) to give 445 mg of crystals (0.87 mmol, 44% yield). IR ( $\text{CH}_2\text{Cl}_2$ )  $\nu_{\text{CO}}$  2044 (s), 1995 (s), 1987 (s)  $\text{cm}^{-1}$ .  $^1\text{H}$  NMR (EM-390,  $\text{D}_6$ -acetone)  $\delta$  7.3 - 6.6 (phenyl ring H's), 4.08 (singlet,  $\text{C}_5\text{H}_5$  ring H's);  $^{13}\text{C}$  NMR (WM-500;  $\text{CH}_2\text{Cl}_2$ )  $\delta$  198.98 (terminal CO's), 164.5 (*ipso* phenyl C), 128.6, 127.6 (*meta* and *ortho* phenyl C's), 127.0 (*para* phenyl C), 88.8 ( $\text{C}_5\text{H}_5$ ). Anal. calc. for  $\text{Co}_3\text{C}_{21}\text{H}_{15}\text{O}_4$ : C, 49.539; H, 3.167. Found: C, 49.73; H, 3.02.

Recrystallization from ether/hexane gave cube-shaped crystals suitable for solution by X-ray diffraction crystallography. Precession photographs revealed the crystal was orthorhombic. Crystal density was measured by flotation in a  $\text{ZnCl}_2/\text{H}_2\text{O}$  solution. Data collection over  $h, k, \pm l$  resulted in 2854 reflections, which after averaging equivalent reflections, reduced to 2460 unique reflections, and 2392 reflections with  $I > 3\sigma(I)$ . Two standard reflections were measured every 48 reflections and negligible decay was observed during data collection. Corrections were made for Lorentz-polarization effects, and for absorption. An empirical absorption correction was applied from  $\phi$ -scan data on the basis of 20 reflections in the  $2\Theta$  range of  $5.8$ - $40.9^\circ$ , leading to a range in relative transmission factors of 0.328-1.000. The heavy atoms were located by direct methods (MULTAN [93]), and subsequent Fourier difference maps revealed the positions of all atoms, including the hydrogens (SHELX

[94]). Temperature factors of all non-hydrogen atoms were made anisotropic, and refinement of all non-hydrogen atoms by full matrix least-squares methods resulted in final  $R_1$  and  $R_2$  values of 0.053 and 0.068. Scattering curves from [95] were applied during refinement of the structure, and anomalous dispersion corrections for Co were applied from [96]. Atomic positional parameters, temperature factors, and selected bond lengths and angles appear in Tables 10A-10E.

#### $\text{Co}_3(\text{CO})_9\text{C}-[3,4-(\text{CH}_3)_2\text{C}_6\text{H}_3]$

To a mixture of  $\text{Co}_3(\text{CO})_9\text{C}-\text{Cl}$  (1.1 g, 2.3 mmol) and 5 mL *ortho*-xylene (4.5 g, 42 mmol) in 25 mL  $\text{CH}_2\text{Cl}_2$  was added 0.5 g (3.7 mmol) anhydrous  $\text{AlCl}_3$ . The reaction was heated under reflux conditions for 3 hours, at which time the solution was orange-brown, but not cloudy. The mixture was shaken with 50 mL 10% HCl to consume excess  $\text{AlCl}_3$ , and the organic layer was dried over  $\text{Ca}(\text{CO}_3)$ . Removal of the solvent and purification of the product by column chromatography on silica gel (100-200 mesh, eluent ether/petroleum ether 15:85) gave 650 mg of  $\text{Co}_3(\text{CO})_9\text{C}-[3,4-(\text{CH}_3)_2\text{C}_6\text{H}_3]$ , 52% yield. IR (xylene)  $\nu_{\text{CO}}$  2099 (m), 2050 (s), 2034 (s), 2017 (w)  $\text{cm}^{-1}$ .  $^1\text{H}$  NMR ( $\text{D}_6$ -acetone)  $\delta$  7.46 (singlet, 1 phenyl H), 7.34 (doublet,  $J_{\text{HH}} = 7.4$  Hz, 1 phenyl H), 7.11 (doublet, 1 phenyl H), 2.22, 2.04 (singlets, phenyl  $\text{CH}_3$ 's).  $^{13}\text{C}$  NMR (WM-250,  $\text{CH}_2\text{Cl}_2$ )  $\delta$  200.4 (all CO's), 156.0, 137.2, 136.6, 129.8 (area 2), 126.3 (phenyl C's), 19.64, 19.46 ( $\text{CH}_3$ 's).

#### $\text{Co}_3(\text{C}_5\text{H}_5)_2(\text{CO})_4\text{C}-[3,4-(\text{CH}_3)_2\text{C}_6\text{H}_3]$ , 20

$\text{Co}_3(\text{CO})_9\text{C}-[3,4-(\text{CH}_3)_2\text{C}_6\text{H}_3]$  (0.75 g, 1.4 mmol) was heated under reflux with freshly cracked cyclopentadiene (2.0 g, 30 mmol) in tetrahydrofuran (35 mL) for 20 hours. After evaporation of the solvent, column chromatography on neutral alumina (80-200 mesh) with hexane eluent produced a dark green-brown band which, upon

drying, yielded dark crystals of  $\text{Co}_3(\text{C}_5\text{H}_5)_2(\text{CO})_4\text{C}-(3,4-(\text{CH}_3)_2\text{C}_6\text{H}_3)$ , 20, (0.20 g, 0.37 mmol, 27%). IR ( $\text{CH}_2\text{Cl}_2$ )  $\nu_{\text{CO}}$  2039 (s), 1992 (s,br), 1785 (m,br)  $\text{cm}^{-1}$ ;  $^1\text{H}$  NMR (EM-390,  $\text{D}_6$ -acetone)  $\delta$  7.1 (singlet, phenyl H), 7.0 (doublet,  $J_{\text{HH}} = 7.5$  Hz, phenyl H), 6.65 (doublet, phenyl H), 4.15 (singlet, Cp H's), 1.80, 1.75 (singlets, phenyl  $\text{CH}_3$ 's);  $^{13}\text{C}$  NMR (WM-500;  $\text{CH}_2\text{Cl}_2$ )  $\delta$  200.0 (terminal CO's), 162.7 (*ipso* xylyl C), 135.9, 135.5 (subst. xylyl C's), 129.7, 128.7, 126.3 (unsubst. xylyl C's), 88.8 ( $\text{C}_5\text{H}_5$ ), 19.7, 19.4 ( $\text{CH}_3$ 's). FAB mass spectrum  $m/z$  (%): 536 (11) ( $\text{M}^+$ ); 508 (8) ( $\text{M}-\text{CO}^+$ ); 480 (100) ( $\text{M}-2\text{CO}^+$ ); 452 (78) ( $\text{M}-3\text{CO}^+$ ); 424 (68) ( $\text{M}-4\text{CO}^+$ ); 365 (24) ( $\text{M}-4\text{CO}-\text{C}-\text{xylyl}^+$ ); 248 (22) ( $\text{M}-4\text{CO}-\text{C}-\text{xylyl}-\text{Co}^+$ ). Anal. calc. for  $\text{Co}_3\text{C}_{23}\text{O}_4\text{H}_{19}$ : C, 51.52; H, 3.57. Found: C, 51.38; H, 3.72.

$\text{Co}_3(\text{CO})_9\text{C}-\text{CH}(4-\text{ClC}_{10}\text{H}_6)_2$ , 26

The starting material  $\text{Cl}_3\text{C}-\text{CH}(4-\text{ClC}_{10}\text{H}_6)_2$ , 25, was prepared following the general method of Haskelberg and Lavie [80]. This product (3.66 g, 8.0 mmol) and dicobalt octacarbonyl (4.95 g, 14.5 mmol) were heated under reflux in tetrahydrofuran (75 mL) in a nitrogen atmosphere for 3 hours. The solvent was removed by evaporation, and column chromatography on neutral alumina with hexane eluent gave two products. The first band from the column was  $\text{Co}_4(\text{CO})_{12}$ , the major product. The second band evaporated to dark purple crystals of  $\text{Co}_3(\text{CO})_9\text{C}-\text{CH}(4-\text{ClC}_{10}\text{H}_6)_2$  (0.17 g, 0.21 mmol, 2.65%). IR ( $\text{CH}_2\text{Cl}_2$ )  $\nu_{\text{CO}}$  2092(m), 2038(s), 2027(s), 2010(m)  $\text{cm}^{-1}$ ;  $^{13}\text{C}$  NMR (AM-500;  $\text{CH}_2\text{Cl}_2$ )  $\delta$  303.7 (apical C), 199.8 (CO's), 141.4 (C-Cl), 131.8-122.5 (ring C's), 61.7 (C-H). Mass spec.  $m/z$  (%): 748 (8) ( $\text{M}-\text{CO}^+$ ); 720 (17) ( $\text{M}-2\text{CO}^+$ ); 692 (88) ( $\text{M}-3\text{CO}^+$ ); 664 (100) ( $\text{M}-4\text{CO}^+$ ); 636 (77) ( $\text{M}-5\text{CO}^+$ ); 608 (32) ( $\text{M}-6\text{CO}^+$ ); 580 (32) ( $\text{M}-7\text{CO}^+$ ); 552 (17) ( $\text{M}-8\text{CO}^+$ ); 524 (70) ( $\text{M}-9\text{CO}^+$ ). Anal. calc. for  $\text{C}_{31}\text{H}_{13}\text{Cl}_2\text{Co}_3\text{O}_9$ : C, 47.91; Cl, 9.12; H, 1.69. Found: C, 48.02; Cl, 9.31; H, 1.81.

Rapid recrystallization from hexane/ether 85/15 afforded a black, air-stable



crystal ( $0.16 \times 0.32 \times 0.35 \text{ mm}^3$ ) suitable for structure solution by X-ray diffraction crystallography. Precession photographs revealed the crystal was triclinic, and accurate cell parameters were determined from a least-squares fit of  $\chi$ ,  $\phi$ , and  $2\Theta$  for 15 reflections in the range  $21.5^\circ < 2\Theta < 29.6^\circ$ . Measurements were made on a Nicolet P3 diffractometer with use of graphite-monochromated Mo  $K\alpha$  radiation. Data collection over  $h, \pm k, \pm l$  resulted in 3620 unique reflections and 2784 observed reflections with  $I > 3\sigma(I)$ . Data were corrected for Lorentz-polarization effects, but not for absorption ( $\mu(\text{Mo } K\alpha) = 19.22 \text{ cm}^{-1}$ ). Considering only observed data, heavy-atom positions were found by direct methods (SHELXS [97]). Subsequent Fourier difference maps revealed the positions of all remaining atoms, including the hydrogens (SHELX [94]). Anisotropic refinements of all non-hydrogen atoms by full matrix least-squares methods resulted in final  $R_1$  and  $R_2$  values of 0.048 and 0.053. Scattering curves from [95] were applied during refinement of the structure, and anomalous dispersion corrections for Co and Cl were applied from [96]. Atomic positional parameters, temperature factors, and selected bond lengths and angles appear in Tables 11A-11D. Geometry calculations were performed by using MOLGEOM [98].

$(\text{C}_5\text{H}_5)\text{Mo}(\text{CO})_2\text{Co}_2(\text{CO})_6\text{C-CO}_2\text{C}_{17}\text{O}_3\text{H}_{21}$ , 30

Cluster 10,  $(\text{C}_5\text{H}_5)\text{Mo}(\text{CO})_2\text{Co}_2(\text{CO})_6\text{C-CO}_2\text{CH}(\text{CH}_3)_2$ , (545 mg, 1.15 mmol) was stirred with 8.6 mL propionic anhydride in a two-necked 100 mL flask. To this flask was added 0.21 mL (0.345 g) of a 65% aqueous solution of  $\text{HPF}_6$ . After five minutes, the resulting black crystals were filtered under  $\text{N}_2$  and rinsed twice with 2.5 mL aliquots of  $\text{CH}_2\text{Cl}_2$  (yield of  $[\text{Mo}(\text{C}_5\text{H}_5)(\text{CO})_2\text{Co}_2(\text{CO})_6\text{C-CO}^+][\text{PF}_6^-]$ : 436 mg, 0.715 mmol, 62%). The crystals of the salt were placed in a flask with 197 mg podocarpic acid ( $\text{C}_{17}\text{O}_3\text{H}_{22}$ , 0.72 mmol) in 10 mL  $\text{CH}_2\text{Cl}_2$ . This slurry was then solubilized by the addition of 3 mL ether. Immediately the reagents dissolved and the

flask contents turned dark green. Column chromatography on silica gel (100-200 mesh) did not separate the remaining podocarpic acid from the desired cluster, but as the metal carbonyl groups were to be the only groups observed in the  $^{13}\text{C}$  NMR spectrum, there would be no interferences in the region of interest in the spectrum.  $^{13}\text{C}$  NMR (AM-500;  $\text{CH}_2\text{Cl}_2$ ; carbonyl region)  $\delta$  208.6 (all CO's). Low temperature  $^{13}\text{C}$  NMR (AM-500;  $\text{CH}_2\text{Cl}_2$ ; 183 K; carbonyl region)  $\delta$  229.5 (Mo CO's, minor isomer); 220.1 (Mo CO's, major isomer); 201.8 (Co CO's, major isomer); 199.5 (Co CO's, minor isomer). Further splitting of the carbonyl signal at 199.5 appeared to occur at reduced temperatures, but resolution could not be achieved.



The menthyl analogue to cluster 30, was generously supplied by D.T. Clark.  $^{13}\text{C}$  NMR (AM-500;  $\text{CD}_2\text{Cl}_2$ ; 194 K; carbonyl region)  $\delta$  230.8 (Mo CO's, minor isomer); 221.3 (Mo CO's, major isomer); 202.8 (Co CO's, major isomer); 200.2 (Co CO's, minor isomer). At 190 K, the signal at 200.2 ppm had split into two signals of equal intensity, at 201.0 and 197.6 ppm.

#### CRYSTALLOGRAPHY NOTE:

Tables of supplementary data (observed and calculated structure factors) may be found on microfiche in the pocket inside the back cover of the thesis.

Table 10A:

Crystal and Data Collection Parameters for  
 $\text{Co}_3(\text{C}_5\text{H}_5)_2(\text{CO})_4\text{C}-\text{C}_6\text{H}_5$

Molecular formula	$\text{C}_{21}\text{H}_{15}\text{Co}_3\text{O}_4$
Formula weight (amu)	509.2
Crystal system	orthorhombic
Space group	$\text{P}2_12_12_1$ (No. 19)
a (Å)	7.880 (3)
b (Å)	15.447 (5)
c (Å)	15.688 (4)
Volume (Å <sup>3</sup> )	1909.6 (10)
Z	4
$\rho_{\text{calcd}}$ (g cm <sup>-3</sup> )	1.772
$\rho_{\text{obsd}}$ (g cm <sup>-3</sup> )	1.74 (3) (flotation)
F(000)	974.957
Diffractometer	Nicolet P2 <sub>1</sub>
Temperature (°C)	22
Radiation	Mo K $\alpha$ ( $\lambda = 0.71069$ Å)
$\mu$ (Mo K $\alpha$ ), (cm <sup>-1</sup> )	27.00
Standard reflections	3,4,-5 2,5,-5
Data collected	h, k, $\pm$ l
2 $\theta$ range, (°)	0 (min), 45 (max)
No. of total data	2854
No. of unique data	2460
No. of obsd data ( $I > 3\sigma(I)$ )	2392
Final shift/error, max (ave)	0.017 (0.002)
No. of variables	314
Final $R_1, R_2^a$	0.0534, 0.0680
Weighting scheme	$w = [\sigma^2(F) + 0.004F^2]^{-1}$
Highest peak, (eÅ <sup>-3</sup> )	0.968
Lowest valley, (eÅ <sup>-3</sup> )	-0.841

$$^a R_1 = (\sum ||F_o| - |F_c|| / \sum |F_o|); R_2 = [\sum w(|F_o| - |F_c|)^2 / \sum w|F_o|^2]^{1/2}$$

Table 10B:

Atomic Positional Parameters and Temperature Factors ( $\text{\AA}^2$ ) for  
 $(\text{C}_5\text{H}_5)_2\text{Co}_3(\text{CO})_4\text{C}-\text{C}_6\text{H}_5$

Atom	x ( $\times 10^4$ )	y ( $\times 10^4$ )	z ( $\times 10^4$ )	$U_{\text{eq}}$ ( $\times 10^3$ )
Co(1)	-2747(1)	-404.8(6)	-7092.2(6)	28.9
Co(2)	-2771(1)	881.3(6)	-6237.0(6)	27.2
Co(3)	-4877(1)	-284.3(7)	-5943.9(6)	30.1
C(1)	-4463(10)	412(5)	-6934(5)	30
C(2)	-1362(11)	-88(5)	-6167(6)	38
O(2)	-173(7)	-335(5)	-5804(5)	54
C(3)	-6387(12)	-1023(6)	-6374(6)	43
O(3)	-7320(10)	-1512(5)	-6647(6)	75
C(4)	-6202(12)	395(7)	-5292(7)	49
O(4)	-7042(11)	830(6)	-4884(6)	83
C(5)	-3824(11)	-1014(6)	-5191(6)	36
O(5)	-3208(10)	-1503(5)	-4764(5)	65
C(11)	-5569(10)	826(5)	-7574(5)	32
C(12)	-7338(13)	816(6)	-7510(7)	44
C(13)	-8354(14)	1164(7)	-8139(7)	53
C(14)	-7633(13)	1545(7)	-8843(6)	54
C(15)	-5850(14)	1598(7)	-8919(6)	48
C(16)	-4878(14)	1238(7)	-8284(6)	42
C(21)	-3152(12)	-1644(6)	-7577(7)	48
C(22)	-3680(14)	-1009(6)	-8170(6)	46
C(23)	-2233(20)	-525(7)	-8382(6)	64
C(24)	-854(16)	-833(7)	-7923(8)	56
C(25)	-1401(13)	-1535(6)	-7423(7)	47
C(31)	-3080(13)	1784(6)	-5256(6)	45
C(32)	-1358(15)	1637(7)	-5387(7)	46
C(33)	-949(16)	1865(7)	-6241(8)	58
C(34)	-2406(19)	2167(6)	-6620(7)	61
C(35)	-3735(16)	2099(7)	-6021(7)	51

Table 10C:

Hydrogen Positional Parameters for  $(C_5H_5)_2Co_3(CO)_4C-C_6H_5$ 

Atom	x ( $\times 10^4$ )	y ( $\times 10^4$ )	z ( $\times 10^4$ )	$U_{eq}$ ( $\times 10^2$ )
H(12)	-755(14)	67(7)	-708(7)	6
H(13)	-956(11)	114(5)	-814(5)	3
H(14)	-837(9)	168(4)	-930(4)	1
H(15)	-547(11)	187(6)	-938(6)	5
H(16)	-379(13)	134(6)	-830(6)	4
H(21)	-379(9)	-209(5)	-723(4)	2
H(22)	-482(19)	-84(10)	-842(9)	11
H(23)	-204(13)	-4(6)	-877(6)	6
H(24)	16(10)	-65(5)	-787(5)	2
H(25)	-63(10)	-167(5)	-704(5)	2
H(31)	-375(9)	165(4)	-474(5)	2
H(32)	-62(10)	148(5)	-513(5)	1
H(33)	6(11)	187(5)	-653(5)	3
H(34)	-277(11)	228(5)	-715(6)	4
H(35)	-472(13)	220(7)	-606(6)	5

$$U_{eq} = \frac{1}{3}(U_{11} + U_{22} + U_{33})$$

Table 10D:

Anisotropic Temperature Factors ( $\text{\AA}^2, \times 10^3$ ) for  $(\text{C}_5\text{H}_5)_2\text{Co}_3(\text{CO})_4\text{C}-\text{C}_6\text{H}_5$ 

Atom	$U_{11}$	$U_{22}$	$U_{33}$	$U_{12}$	$U_{13}$	$U_{23}$
Co(1)	31.7(6)	25.4(6)	29.7(6)	-4.8(4)	4.2(5)	0.1(5)
Co(2)	30.6(6)	23.9(5)	27.1(6)	-2.4(4)	-2.0(5)	-2.3(5)
Co(3)	30.0(6)	31.6(7)	28.8(6)	-1.1(5)	2.8(5)	-2.9(5)
C(1)	37(4)	32(4)	21(4)	-5(3)	6(3)	-8(4)
C(2)	35(5)	29(5)	49(5)	-6(4)	5(4)	-8(4)
O(2)	37(4)	53(4)	72(4)	4(3)	-16(4)	11(4)
C(3)	38(5)	42(5)	50(6)	-5(5)	2(5)	7(5)
O(3)	45(4)	58(4)	121(7)	-35(5)	0.0(4)	-10(4)
C(4)	45(6)	46(6)	55(6)	-6(5)	-9(5)	1(5)
O(4)	70(5)	87(6)	90(6)	-33(5)	29(5)	17(5)
C(5)	39(5)	40(5)	30(5)	2(4)	2(4)	-9(4)
O(5)	70(5)	68(5)	56(5)	23(4)	-18(4)	-6(4)
C(11)	29(4)	32(4)	35(5)	-8(4)	-16(4)	-1(4)
C(12)	46(6)	41(5)	45(6)	3(5)	-1(5)	-3(5)
C(13)	40(6)	57(6)	61(7)	3(5)	-24(5)	1(5)
C(14)	62(7)	59(6)	42(6)	-1(5)	-25(6)	11(6)
C(15)	69(7)	47(6)	30(5)	6(5)	-1(5)	9(5)
C(16)	37(6)	54(6)	34(5)	2(4)	-3(4)	5(5)
C(21)	52(6)	40(5)	52(6)	-19(5)	6(5)	-3(5)
C(22)	58(6)	41(6)	38(6)	-18(5)	-3(5)	6(5)
C(23)	122(11)	42(5)	27(5)	-12(4)	21(7)	-14(7)
C(24)	53(6)	44(6)	70(8)	-13(6)	28(6)	-11(6)
C(25)	43(6)	34(5)	63(7)	-13(5)	-5(5)	8(5)
C(31)	60(7)	37(5)	39(6)	-15(4)	6(5)	-7(5)
C(32)	50(6)	36(6)	53(7)	-7(5)	-20(6)	-7(5)
C(33)	61(7)	57(7)	58(7)	-15(6)	14(7)	-23(6)
C(34)	109(11)	32(5)	43(6)	10(4)	-9(8)	-12(7)
C(35)	62(7)	38(6)	54(7)	-1(5)	-7(6)	12(5)

Table 10E:

Selected Bond Distances and Angles for  $\text{Co}_3(\text{C}_5\text{H}_5)_2(\text{CO})_4\text{C}-\text{C}_6\text{H}_5$ 

## (a) Cobalt-cobalt and cobalt-carbon distances (Å)

Co(1)-Co(2)	2.397(1)	Co(1)-Co(3)	2.469(1)
Co(2)-Co(3)	2.491(1)	Co(1)-C(1)	1.865(8)
Co(2)-C(1)	1.870(8)	Co(3)-C(1)	1.917(8)
Co(1)-C(2)	1.881(9)	Co(2)-C(2)	1.868(8)
Co(3)-C(3)	1.782(10)	Co(3)-C(4)	1.799(10)
Co(3)-C(5)	1.832(9)	Co(1)-C(21)	2.084(10)
Co(1)-C(22)	2.066(10)	Co(1)-C(23)	2.072(9)
Co(1)-C(24)	2.089(12)	Co(1)-C(25)	2.108(10)
Co(2)-C(31)	2.091(9)	Co(2)-C(32)	2.093(11)
Co(2)-C(33)	2.091(12)	Co(2)-C(34)	2.095(10)
Co(2)-C(35)	2.056(11)		

## (b) Carbon-oxygen distances (Å)

C(2)-O(2)	1.161(11)	C(3)-O(3)	1.138(12)
C(4)-O(4)	1.140(13)	C(5)-O(5)	1.120(12)

## (c) Carbon-carbon distances (Å)

C(11)-C(12)	1.398(13)	C(12)-C(13)	1.380(15)
C(13)-C(14)	1.374(15)	C(14)-C(15)	1.412(15)
C(15)-C(16)	1.373(14)	C(16)-C(11)	1.394(12)
C(1)-C(11)	1.475(11)	C(21)-C(22)	1.415(14)
C(22)-C(23)	1.403(17)	C(23)-C(24)	1.388(18)
C(24)-C(25)	1.406(15)	C(25)-C(21)	1.411(14)
C(31)-C(32)	1.392(16)	C(32)-C(33)	1.422(17)
C(33)-C(34)	1.375(19)	C(34)-C(35)	1.411(18)
C(35)-C(31)	1.394(15)		

## (d) Angles involving cobalt (°)

Co(1)-Co(2)-Co(3)	60.63(4)	Co(2)-Co(3)-Co(1)	57.81(4)
Co(3)-Co(1)-Co(2)	61.56(4)	Co(1)-Co(2)-C(1)	50.0(2)
Co(2)-Co(3)-C(1)	48.1(2)	Co(3)-Co(1)-C(1)	50.2(2)
Co(1)-Co(3)-C(1)	48.3(2)	Co(2)-Co(1)-C(1)	50.2(2)
Co(3)-Co(2)-C(1)	49.7(2)	Co(1)-C(1)-Co(2)	79.9(3)
Co(2)-C(1)-Co(3)	82.2(3)	Co(3)-C(1)-Co(1)	81.5(3)
C(11)-C(1)-Co(1)	129.2(6)	C(11)-C(1)-Co(2)	130.6(6)
C(11)-C(1)-Co(3)	133.9(6)	Co(1)-C(2)-O(2)	139.6(7)
Co(2)-C(2)-O(2)	140.6(7)	Co(1)-C(2)-Co(2)	79.5(4)
Co(2)-Co(1)-C(2)	50.0(3)	Co(1)-Co(2)-C(2)	50.5(3)
C(3)-Co(3)-C(4)	101.6(4)	C(4)-Co(3)-C(5)	104.8(4)
C(3)-Co(3)-C(5)	98.8(4)	Co(3)-C(3)-O(3)	178.2(9)
Co(3)-C(4)-O(4)	179.5(9)	Co(3)-C(5)-O(5)	175.5(8)

## (e) Angles in phenyl and cyclopentadienyl rings (°)

C(11)-C(12)-C(13)	121.5(9)	C(12)-C(13)-C(14)	120.1(9)
C(13)-C(14)-C(15)	120.2(9)	C(14)-C(15)-C(16)	118.1(9)
C(15)-C(16)-C(11)	123.1(10)	C(16)-C(11)-C(12)	116.9(8)
C(21)-C(22)-C(23)	106.6(10)	C(22)-C(23)-C(24)	109.3(9)
C(23)-C(24)-C(25)	108.3(10)	C(24)-C(25)-C(21)	107.2(9)
C(25)-C(21)-C(22)	108.5(9)	C(31)-C(32)-C(33)	108.6(9)
C(32)-C(33)-C(34)	107.6(11)	C(33)-C(34)-C(35)	107.8(9)
C(34)-C(35)-C(31)	109.0(11)	C(35)-C(31)-C(32)	106.9(9)



Table 11A:

Crystal and Data Collection Parameters for  $\text{Co}_3(\text{CO})_9\text{C-CH(4-ClC}_{10}\text{H}_6)_2$ 

Molecular formula	$\text{C}_{31}\text{H}_{13}\text{O}_9\text{Cl}_2\text{Co}_3$
Formula weight (amu)	777.15
Crystal system	triclinic
Space group	$P\bar{1}$ , no. 2
a (Å)	8.839 (3)
b (Å)	12.156 (4)
c (Å)	16.513 (5)
$\alpha$ (°)	105.97 (3)
$\beta$ (°)	92.28 (3)
$\gamma$ (°)	115.51 (2)
Volume (Å <sup>3</sup> )	1513.57 (84)
Z	2
$\rho_{\text{calcd}}$ (g cm <sup>-3</sup> )	1.705
F(000)	748.62
Diffractometer	Nicolet P <sub>3</sub>
Temperature (°C)	22 (295K)
Radiation	Mo K $\alpha$ ( $\lambda = 0.71069$ Å)
$\mu$ (Mo K $\alpha$ ), (cm <sup>-1</sup> )	19.22
Standard reflections	1,-4,-5 1,3,-8
Data collected	+h, $\pm$ k, $\pm$ l
2 $\theta$ range (°)	0 (min), 45 (max)
No. of total data	4477
No. of unique data	3620
No. of obsd data ( $I > 3\sigma(I)$ )	2784
Final shift/error, max (ave)	0.065 (0.017)
No. of variables	190
Final $R_1, R_2^a$	0.054, 0.048
Weighting scheme	$w = (\sigma^2(F) + 0.001181F^2)^{-1}$
Error in obsvn of unit wt <sup>b</sup>	1.0835
Highest peak (eÅ <sup>-3</sup> )	0.484
Lowest valley (eÅ <sup>-3</sup> )	-0.693

$$^a R_1 = \frac{\sum |F_o| - |F_c|}{\sum |F_o|}; \quad R_2 = \left( \frac{\sum w(|F_o| - |F_c|)^2}{\sum w|F_o|^2} \right)^{\frac{1}{2}}$$

$$^b S = \left( \frac{\sum w(|F_o| - |F_c|)^2}{(m-n)} \right)^{\frac{1}{2}}; \quad m = \text{no. of reflections}, \quad n = \text{no. of variables}$$

Table 11B:

Atomic Positional Parameters and Temperature Factors ( $\text{\AA}^2$ ) for  
 $\text{Co}_3(\text{CO})_9\text{C-CH}(4\text{-ClC}_{10}\text{H}_6)_2$

Atom	x ( $\times 10^4$ )	y ( $\times 10^4$ )	z ( $\times 10^4$ )	$U_{\text{eq}}$ ( $\times 10^3$ )
Co(1)	955.1(8)	2409.4(6)	8417.0(4)	31.8
Co(2)	1593.3(8)	1141.6(5)	7150.7(4)	33.3
Co(3)	3894.8(7)	3114.2(6)	8176.1(3)	29.8
C(11)	1376(7)	3891(5)	9217(3)	43
C(12)	1065(6)	1493(5)	9124(3)	43
C(13)	-1295(8)	1815(6)	8151(3)	50
C(21)	-573(8)	4(5)	6740(3)	51
C(22)	2313(7)	1134(5)	6150(4)	49
C(23)	2186(7)	78(5)	7524(3)	50
C(31)	5296(6)	3287(5)	7426(3)	41
C(32)	4886(6)	4757(5)	8864(3)	38
C(33)	4693(6)	2457(5)	8883(3)	42
O(11)	1656(6)	4822(4)	9743(2)	65
O(12)	1158(5)	942(4)	9549(3)	65
O(13)	-2727(6)	1456(5)	7995(3)	76
O(21)	-1963(6)	-755(4)	6455(3)	83
O(22)	2724(7)	1167(4)	5514(3)	82
O(23)	2529(7)	-588(4)	7770(3)	86
O(31)	6185(5)	3423(4)	6940(3)	68
O(32)	5561(5)	5785(4)	9317(2)	57
O(33)	5158(5)	2044(4)	9312(2)	63
Cl(1)	-3989(2)	1532(2)	3980.2(9)	63
Cl(2)	2028(3)	8467(2)	9443(1)	76
C(1)	1899(5)	2865(4)	7462(2)	29
C(2)	1904(6)	3713(4)	6932(3)	27
C(40)	470(5)	3109(4)	6153(2)	28
C(41)	-1136(6)	2208(5)	6159(3)	37
C(42)	-2501(6)	1728(5)	5480(3)	40

C(43)	-2241(6)	2118(5)	4794(3)	38
C(44)	-623(6)	3018(4)	4721(3)	34
C(45)	767(6)	3524(4)	5418(3)	30
C(46)	2372(6)	4443(5)	5352(3)	38
C(47)	2611(8)	4846(6)	4645(3)	50
C(48)	1263(8)	4311(6)	3969(4)	52
C(49)	-316(7)	3442(5)	3995(3)	43
C(50)	2015(6)	4987(4)	7510(2)	29
C(51)	554(7)	4977(5)	7778(3)	37
C(52)	575(8)	6065(6)	8357(3)	44
C(53)	2036(8)	7162(5)	8670(3)	45
C(54)	3571(7)	7271(4)	8407(3)	43
C(55)	3568(6)	6161(4)	7798(3)	35
C(56)	5123(7)	6297(5)	7532(3)	42
C(57)	6582(8)	7431(7)	7842(5)	59
C(58)	6584(10)	8489(6)	8429(5)	72
C(59)	5143(10)	8431(5)	8716(4)	62

Table 11C:

Hydrogen Atom Positional Parameters and Temperature Factors ( $\text{\AA}^2$ ) for  
 $\text{Co}_3(\text{CO})_9\text{CCH}(4\text{-ClC}_{10}\text{H}_6)_2$

Atom	x ( $\times 10^3$ )	y ( $\times 10^3$ )	z ( $\times 10^3$ )	$U_{\text{eq}}$ ( $\times 10^2$ )
H(2)	290(5)	384(3)	671(2)	2
H(41)	-130(6)	188(5)	662(3)	6
H(42)	-361(7)	110(5)	551(3)	6
H(46)	342(6)	479(5)	585(3)	7
H(47)	378(6)	558(5)	466(3)	6
H(48)	143(7)	458(6)	354(4)	8
H(49)	-136(6)	301(4)	353(3)	6
H(51)	-54(7)	415(5)	753(3)	7
H(52)	-42(8)	603(6)	847(4)	8
H(56)	506(6)	549(5)	709(3)	5
H(57)	749(7)	744(5)	772(3)	5
H(58)	763(7)	923(6)	873(3)	7
H(59)	526(5)	922(4)	920(3)	5

Table 11D:

Selected Bond Distances and Angles for  $\text{Co}_3(\text{CO})_9\text{C-CH}(4\text{-ClC}_{10}\text{H}_6)_2$ 

## (a) Co-Co and Co-C(methyldyne) distances (Å)

Co(1)-Co(2)	2.477(1)	Co(1)-C(1)	1.918(4)
Co(1)-Co(3)	2.449(1)	Co(2)-C(1)	1.906(5)
Co(2)-Co(3)	2.459(1)	Co(3)-C(1)	1.942(5)

## (b) Co-CO and C-O distances (Å)

Co(1)-C(11)	1.789(6)	C(11)-O(11)	1.139(7)
Co(1)-C(12)	1.848(7)	C(12)-O(12)	1.117(9)
Co(1)-C(13)	1.785(7)	C(13)-O(13)	1.138(8)
Co(2)-C(21)	1.771(5)	C(21)-O(21)	1.149(6)
Co(2)-C(22)	1.794(6)	C(22)-O(22)	1.129(8)
Co(2)-C(23)	1.823(7)	C(23)-O(23)	1.138(10)
Co(3)-C(31)	1.775(5)	C(31)-O(31)	1.141(7)
Co(3)-C(32)	1.792(5)	C(32)-O(32)	1.133(6)
Co(3)-C(33)	1.853(7)	C(33)-O(33)	1.129(9)

(c) Distances involving the  $\mu_3\text{-C-CH-(C)}_2$  system (Å)

C(1)-C(2)	1.524(7)	C(2)-C(40)	1.533(6)
C(2)-C(50)	1.539(6)		

(d) Distances within the  $\text{C}_{10}\text{H}_6\text{Cl}$  systems (Å)

C(40)-C(41)	1.372(6)	C(50)-C(51)	1.378(8)
C(41)-C(42)	1.406(7)	C(51)-C(52)	1.395(8)
C(42)-C(43)	1.336(8)	C(52)-C(53)	1.341(7)
C(43)-C(44)	1.413(6)	C(53)-C(54)	1.404(10)
C(44)-C(45)	1.436(6)	C(54)-C(55)	1.443(7)
C(45)-C(46)	1.409(6)	C(55)-C(56)	1.415(8)

C(46)-C(47)	1.375(9)	C(56)-C(57)	1.362(7)
C(47)-C(48)	1.384(8)	C(57)-C(58)	1.380(11)
C(48)-C(49)	1.351(8)	C(58)-C(59)	1.357(13)
C(40)-C(45)	1.429(7)	C(50)-C(55)	1.426(5)
C(44)-C(49)	1.422(8)	C(54)-C(59)	1.428(7)
C(43)-Cl(1)	1.749(5)	C(53)-Cl(2)	1.744(6)

(e) Angles within the  $\text{Co}_3(\mu_3\text{-C})$  core ( $^\circ$ )

Co(1)-Co(2)-Co(3)	59.49(2)	Co(1)-C(1)-Co(2)	80.74(18)
Co(3)-Co(1)-Co(2)	59.88(2)	Co(1)-C(1)-Co(3)	78.74(18)
Co(2)-Co(3)-Co(1)	60.63(2)	Co(2)-C(1)-Co(3)	79.41(21)
Co(1)-Co(2)-C(1)	49.84(13)	Co(3)-Co(2)-C(1)	50.94(13)
Co(1)-Co(3)-C(1)	50.19(13)	Co(2)-Co(1)-C(1)	49.42(14)
Co(2)-Co(3)-C(1)	49.65(13)	Co(3)-Co(1)-C(1)	51.06(14)

(f) Co-Co-CO angles ( $^\circ$ )

Co(2)-Co(1)-C(11)	152.2(2)	Co(3)-Co(1)-C(11)	95.4(2)
Co(2)-Co(1)-C(12)	96.2(2)	Co(3)-Co(1)-C(12)	96.0(2)
Co(2)-Co(1)-C(13)	103.0(2)	Co(3)-Co(1)-C(13)	157.2(2)
Co(1)-Co(2)-C(21)	94.0(2)	Co(3)-Co(2)-C(21)	153.4(2)
Co(1)-Co(2)-C(22)	145.0(2)	Co(3)-Co(2)-C(22)	103.0(1)
Co(1)-Co(2)-C(23)	105.5(2)	Co(3)-Co(2)-C(23)	93.7(1)
Co(1)-Co(3)-C(31)	147.4(2)	Co(2)-Co(3)-C(31)	92.6(1)
Co(1)-Co(3)-C(32)	100.8(2)	Co(2)-Co(3)-C(32)	155.5(2)
Co(1)-Co(3)-C(33)	100.8(2)	Co(2)-Co(3)-C(33)	101.8(1)

(g) Co-C-O angles ( $^\circ$ )

Co(1)-C(11)-O(11)	178.1(6)	Co(2)-C(21)-O(21)	177.9(6)
Co(1)-C(12)-O(12)	178.9(5)	Co(2)-C(22)-O(22)	176.3(7)
Co(1)-C(13)-O(13)	178.6(5)	Co(2)-C(23)-O(23)	178.3(6)
Co(3)-C(31)-O(31)	178.1(6)	Co(3)-C(32)-O(32)	177.1(6)

Co(3)-C(33)-O(33) 179.1(4)

(h) Angles involving the  $\mu_3$ -C-CH-(C)<sub>2</sub> systems (Å)

Co(1)-C(1)-C(2)	138.6(4)	C(1)-C(2)-C(40)	117.3(3)
Co(2)-C(1)-C(2)	132.3(3)	C(1)-C(2)-C(50)	110.5(4)
Co(3)-C(1)-C(2)	125.0(3)	C(1)-C(2)-H(2)	100.5(30)
C(2)-C(40)-C(41)	121.1(4)	C(40)-C(2)-C(50)	110.3(5)
C(2)-C(40)-C(45)	120.2(3)	C(40)-C(2)-H(2)	106.0(21)
C(2)-C(50)-C(51)	118.2(4)	C(50)-C(2)-H(2)	111.7(20)
C(2)-C(50)-C(55)	122.9(5)		

(i) Angles within the C<sub>10</sub>H<sub>6</sub>Cl groups (Å)

C(45)-C(40)-C(41)	118.7(4)	C(55)-C(50)-C(51)	118.9(4)
C(40)-C(41)-C(42)	121.8(5)	C(50)-C(51)-C(52)	121.7(4)
C(41)-C(42)-C(43)	120.0(4)	C(51)-C(52)-C(53)	120.5(7)
C(42)-C(43)-C(44)	122.2(4)	C(52)-C(53)-C(54)	121.6(6)
C(43)-C(44)-C(45)	117.8(4)	C(53)-C(54)-C(55)	118.7(4)
C(44)-C(45)-C(46)	117.8(5)	C(54)-C(55)-C(56)	117.8(4)
C(45)-C(46)-C(47)	121.5(5)	C(55)-C(56)-C(57)	121.5(6)
C(46)-C(47)-C(48)	119.6(5)	C(56)-C(57)-C(58)	120.6(7)
C(47)-C(48)-C(49)	122.0(6)	C(57)-C(58)-C(59)	121.3(6)
C(48)-C(49)-C(44)	120.1(5)	C(58)-C(59)-C(54)	120.6(6)
C(49)-C(44)-C(45)	119.0(4)	C(59)-C(54)-C(55)	118.3(6)
C(40)-C(44)-C(45)	119.4(4)	C(50)-C(54)-C(55)	118.5(5)
C(42)-C(43)-Cl(1)	118.4(4)	C(52)-C(53)-Cl(2)	118.9(6)
C(44)-C(43)-Cl(1)	119.3(4)	C(54)-C(53)-Cl(2)	119.5(3)



Table 12A:

Crystal and Data Collection Parameters for  
 $[\text{C}_5(\text{CH}_3)_5]\text{Mo}(\text{CO})_2\text{Co}_2(\text{CO})_6\text{C-CO}_2\text{CH}(\text{CH}_3)_2$

Molecular formula	$\text{C}_{23}\text{H}_{22}\text{O}_{10}\text{Co}_2\text{Mo}$
Formula weight (amu)	672.22
Crystal system	monoclinic
Space group	$\text{P2}_1/\text{n}$ , no. 14
a (Å)	9.781 (2)
b (Å)	10.217 (2)
c (Å)	27.225 (9)
$\alpha$ (°)	90.00 (2)
$\beta$ (°)	103.80 (2)
$\gamma$ (°)	90.00 (2)
Volume (Å <sup>3</sup> )	2642.12
Z	4
$\rho_{\text{calcd}}$ (g cm <sup>-3</sup> )	1.689
F(000)	1281.64
Diffractometer	Nicolet P2 <sub>1</sub>
Temperature (°C)	22 (295K)
Radiation	Mo K $\alpha$ ( $\lambda = 0.71069$ Å)
$\mu$ (Mo K $\alpha$ ), (cm <sup>-1</sup> )	18.02
Standard reflections	2,0,0 0,0,-4
Data collected	h, k, $\pm$ l
2 $\Theta$ range (°)	0, 45
No. of total data	4110
No. of unique data	3454
$R_{\text{int}}^{\text{a}}$	0.0068
No. of observed data ( $I > 3\sigma(I)$ )	2267
Final shift/error, max (ave)	0.009 (0.002)
No. of variables	326
Final $R_1, R_2^{\text{b}}$	3.55, 3.89
Error in obsv'n of unit wt <sup>c</sup>	0.8696
Secondary extinction, $x^{\text{d}}$	0.00028

Weighting scheme	$w = (\sigma^2(F) + 0.001753F^2)^{-1}$
Highest peak ( $e\text{\AA}^{-3}$ )	0.32
Lowest valley ( $e\text{\AA}^{-3}$ )	-0.33

$$^a R_{\text{int}} = (\Sigma(N\Sigma(w\langle F \rangle - F)^2)) / \Sigma(N - 1)\Sigma wF_o^2)^{\frac{1}{2}}$$

$$^b R_1 = \Sigma||F_o| - |F_c|| / \Sigma|F_o|; R_2 = (\Sigma w(|F_o| - |F_c|)^2 / \Sigma wF_o^2)^{\frac{1}{2}}$$

$$^c S = (\Sigma w(|F_o| - |F_c|)^2 / (m-n))^{\frac{1}{2}}; m = \text{no. of reflections}, n = \text{no. of variables}$$

$$^d F^* = F(1 - 0.0001xF^2 / \sin\theta)$$

Table 12B:

Atomic Positional Parameters and Temperature Factors ( $\text{\AA}^2$ ) for  
 $[\text{C}_5(\text{CH}_3)_5]\text{Mo}(\text{CO})_2\text{Co}_2(\text{CO})_6\text{C}-\text{CO}_2\text{CH}(\text{CH}_3)_2$ 

Atom	x ( $\times 10^4$ )	y ( $\times 10^4$ )	z ( $\times 10^4$ )	$U_{\text{eq}}$ ( $\times 10^3$ )
Mo(1)	4544.2(6)	2029.3(6)	652.6(2)	40
Co(1)	4176.6(10)	4071.9(9)	984.6(4)	43
Co(2)	5779.6(i0)	2246.9(9)	857.3(4)	44
C(1)	3820(6)	2222(6)	880(2)	41
C(2)	2715(6)	1630(6)	485(2)	41
C(3)	435(8)	2011(8)	-98(3)	58
C(4)	749(10)	2509(11)	-575(3)	86
C(5)	-856(9)	2570(13)	2(4)	121
O(1)	2752(6)	552(5)	301(2)	70
O(2)	1592(5)	2435(5)	326(2)	54
C(6)	3653(8)	4512(6)	333(3)	54
O(3)	3300(6)	4798(6)	-84(2)	73
C(7)	5457(9)	5351(8)	1235(3)	61
O(4)	6250(6)	6144(6)	1384(3)	98
C(8)	2597(9)	4594(8)	1145(3)	61
O(5)	1580(6)	4905(8)	1247(3)	106
C(9)	7396(9)	3180(8)	1054(3)	54
O(6)	8393(6)	3768(6)	1178(2)	83
C(10)	5456(8)	2273(8)	174(3)	58
O(7)	5253(6)	2294(6)	-254(2)	84
C(11)	6386(9)	603(9)	933(3)	66
O(8)	6785(8)	-436(6)	1002(3)	99
C(12)	6619(9)	1899(6)	1869(3)	58
O(9)	7789(6)	1741(6)	2053(2)	75
C(13)	4747(9)	3743(8)	1995(3)	64
O(10)	4856(8)	4631(6)	2261(2)	95
C(14)	3568(8)	-107(6)	1694(3)	51
C(15)	4698(9)	118(8)	2134(3)	63
C(16)	4312(10)	1167(9)	2411(3)	65
C(17)	2956(9)	1597(8)	2151(3)	61
C(18)	2497(6)	828(6)	1713(3)	50

C(19)	3504(10)	-1217(8)	1331(4)	76
C(20)	5967(10)	-761(9)	2300(4)	92
C(21)	5108(13)	1638(12)	2936(4)	116
C(22)	2028(12)	2576(11)	2335(4)	101
C(23)	1044(8)	850(9)	1368(3)	74

$$U_{eq} = \frac{1}{2}(U_{11} + U_{22} + U_{33} + 2\cos\beta U_{13})$$

Table 12C:

Hydrogen Positional Parameters ( $\times 10^3$ ) for  
 $[\text{C}_5(\text{CH}_3)_5]\text{Mo}(\text{CO})_2\text{Co}_2(\text{CO})_6\text{C}-\text{CO}_2\text{CH}(\text{CH}_3)_2$

Atom	x	y	z
H(3)	34	110	-11
H(41)	78	356	-53
H(42)	-10	226	-90
H(43)	173	217	-65
H(51)	-79	364	6
H(52)	-110	212	32
H(53)	-168	238	-34
H(191)	274	-93	99
H(192)	314	-208	149
H(193)	449	-145	123
H(201)	618	-120	196
H(202)	582	-154	255
H(203)	681	-14	248
H(211)	616	139	292
H(212)	492	122	329
H(213)	498	268	295
H(221)	277	313	262
H(222)	132	206	252
H(223)	145	323	205
H(231)	105	24	105
H(232)	64	181	125
H(233)	37	41	159

Note: Hydrogen atoms do not have reported errors because they were not refined.

Table 12D:

Anisotropic temperature factors ( $\text{\AA}^2, \times 10^3$ ) for  
 $[\text{C}_5(\text{CH}_3)_5]\text{Mo}(\text{CO})_2\text{Co}_2(\text{CO})_6\text{C}-\text{CO}_2\text{CH}(\text{CH}_3)_2$   
 with standard errors in parentheses.

Atom	$U_{11}$	$U_{22}$	$U_{33}$	$U_{23}$	$U_{13}$	$U_{12}$
Mo(1)	41.1(4)	45.8(4)	36.1(4)	0.3(3)	5.1(3)	0.3(3)
Co(1)	39.0(5)	41.4(6)	52.7(6)	2.0(5)	6.4(5)	0.6(4)
Co(2)	38.3(6)	49.4(6)	48.8(6)	-2.0(5)	11.1(5)	0.8(5)
C(1)	32(4)	44(4)	48(4)	3(3)	2(3)	-2(3)
C(2)	41(4)	48(4)	40(4)	1(3)	11(3)	-4(4)
C(3)	44(4)	67(5)	56(5)	-9(4)	-16(4)	-2(4)
C(4)	69(6)	130(9)	61(6)	-10(6)	5(5)	4(6)
C(5)	39(5)	232(14)	93(8)	-59(9)	2(5)	15(7)
O(1)	70(4)	55(4)	79(4)	-14(3)	-15(3)	-1(3)
O(2)	38(3)	66(3)	58(3)	-15(3)	2(2)	-6(3)
C(6)	47(5)	50(5)	71(6)	16(4)	12(4)	-1(4)
O(3)	70(4)	86(4)	70(4)	24(4)	13(3)	-5(3)
C(7)	61(6)	48(5)	77(6)	0(4)	6(5)	6(4)
O(4)	80(5)	68(4)	142(6)	-19(4)	-6(4)	-25(4)
C(8)	60(5)	65(5)	63(5)	-2(4)	11(4)	3(4)
O(5)	84(5)	132(6)	126(6)	9(5)	50(4)	42(5)
C(9)	54(5)	60(5)	57(5)	-4(4)	17(4)	-7(4)
O(6)	59(4)	98(5)	101(5)	-13(4)	18(4)	-26(4)
C(10)	49(5)	74(6)	59(5)	-12(4)	15(4)	-3(4)
O(7)	96(5)	113(5)	53(4)	-8(4)	24(4)	3(4)
C(11)	55(5)	71(6)	78(6)	-14(5)	14(4)	-1(5)
O(8)	112(6)	61(4)	136(6)	-8(4)	27(5)	27(4)
C(12)	60(6)	54(5)	60(5)	-1(4)	1(4)	-6(4)
O(9)	45(4)	93(4)	77(4)	7(3)	-20(3)	-10(3)
C(13)	83(6)	56(5)	57(5)	-4(4)	7(5)	3(5)
O(10)	142(6)	75(4)	79(4)	-35(4)	25(4)	-2(4)
C(14)	56(5)	47(4)	59(5)	15(4)	19(4)	-11(4)
C(15)	62(5)	64(5)	68(6)	27(5)	11(5)	7(4)
C(16)	79(6)	79(6)	45(5)	15(4)	14(4)	-16(5)

C(17)	68(6)	77(6)	54(5)	-2(4)	35(4)	5(5)
C(18)	42(4)	58(5)	56(5)	10(4)	11(4)	-4(1)
C(19)	86(7)	57(5)	99(7)	-13(50)	31(6)	-14(5)
C(20)	78(7)	80(7)	123(9)	45(6)	10(6)	13(6)
C(21)	150(11)	155(11)	50(6)	11(6)	12(6)	-16(9)
C(22)	117(9)	107(8)	112(9)	-6(7)	68(8)	6(7)
C(23)	47(5)	91(7)	91(7)	25(5)	15(5)	-11(5)

Anisotropic temperature factors are of the form:

$$\exp[-2\pi^2(h^2a^2U_{11}+k^2b^2U_{22}+l^2c^2U_{33}+2hka*b*U_{12}+2hla*c*U_{13}+2klb*c*U_{23})]$$

Table 12E:

Selected Bond Distances and Angles for  
 $[\text{C}_5(\text{CH}_3)_5]\text{Mo}(\text{CO})_2\text{Co}_2(\text{CO})_6\text{C}-\text{CO}_2\text{CH}(\text{CH}_3)_2$

## (a) Distances involving the dicobalt-molybdenum-carbon tetrahedron (Å)

Co(1)-Co(2)	2.515(1)	Co(1)-Mo(1)	2.737(1)
Co(2)-Mo(1)	2.732(1)	Co(1)-C(1)	1.940(7)
Co(2)-C(1)	1.927(7)	Mo(1)-C(1)	2.073(6)
Co(1)-C(6)	1.787(9)	Co(1)-C(7)	1.824(9)
Co(1)-C(8)	1.796(9)	Co(2)-C(9)	1.815(9)
Co(2)-C(10)	1.804(9)	Co(2)-C(11)	1.77(1)
Mo(1)-C(12)	1.979(9)	Mo(1)-C(13)	1.969(9)
Mo(1)-C(14)	2.387(7)	Mo(1)-C(15)	2.343(8)
Mo(1)-C(16)	2.306(8)	Mo(1)-C(17)	2.344(8)
Mo(1)-C(18)	2.384(7)		

## (b) Carbon-oxygen distances (Å)

C(2)-O(1)	1.207(8)	C(2)-O(2)	1.360(8)
O(2)-C(3)	1.463(8)	C(6)-O(3)	1.140(9)
C(7)-O(4)	1.131(9)	C(8)-O(5)	1.125(9)
C(9)-O(6)	1.127(9)	C(10)-O(7)	1.138(9)
C(11)-O(8)	1.138(9)	C(12)-O(9)	1.147(9)
C(13)-O(10)	1.160(9)		

## (c) Carbon-carbon distances (Å)

C(1)-C(2)	1.459(9)	C(3)-C(4)	1.494(12)
C(3)-C(5)	1.464(12)	C(14)-C(15)	1.436(11)
C(15)-C(16)	1.413(12)	C(16)-C(17)	1.411(12)
C(17)-C(18)	1.404(11)	C(18)-C(14)	1.433(10)
C(14)-C(19)	1.501(11)	C(15)-C(20)	1.512(12)
C(16)-C(21)	1.523(13)	C(17)-C(22)	1.507(12)



C(18)-C(23) 1.521(11)

(d) Angles in the tetrahedral skeleton (°)

Co(1)-Co(2)-Mo(1)	62.7(0)	Co(2)-Mo(1)-Co(1)	54.8(0)
Mo(1)-Co(1)-Co(2)	62.5(0)	Co(1)-Co(2)-C(1)	49.6(2)
Co(2)-Mo(1)-C(1)	44.7(2)	Mo(1)-Co(1)-C(1)	49.1(2)
Co(1)-Mo(1)-C(1)	45.0(2)	Co(2)-Co(1)-C(1)	49.2(2)
Mo(1)-Co(2)-C(1)	49.2(2)	Co(1)-C(1)-Co(2)	81.1(3)
Co(2)-C(1)-Mo(1)	86.1(3)	Mo(1)-C(1)-Co(1)	85.9(3)

(e) Angles external to the tetrahedral skeleton (°)

C(2)-C(1)-Co(1)	126.2(5)	C(2)-C(1)-Co(2)	124.0(5)
C(2)-C(1)-Mo(1)	136.0(5)	Co(1)-C(6)-O(3)	178.7(8)
Co(1)-C(7)-O(4)	178.9(9)	Co(1)-C(8)-O(5)	178.6(8)
Co(2)-C(9)-O(6)	178.7(8)	Co(2)-C(10)-O(7)	179.3(8)
Co(2)-C(11)-O(8)	178.5(9)	Mo(1)-C(12)-O(9)	170.1(7)
Mo(1)-C(13)-O(10)	169.1(8)		

(f) Angles in the cyclopentadienyl ring (°)

C(14)-C(15)-C(16)	121.5(9)	C(15)-C(16)-C(17)	120.1(9)
C(16)-C(17)-C(18)	120.2(9)	C(17)-C(18)-C(14)	118.1(9)
C(18)-C(14)-C(15)	123.1(10)		

## List of References

1. Markby, R., Wender, I. Friedel, R.A., Cotton, F.A., Sternberg, H.W., *J. Am. Chem. Soc.*, 80 (1958) 6529.
2. Dent, W.T., Duncanson, L.A., Guy, R.G., Reed, H.W.B., Shaw, B.L., *Proc. Chem. Soc.* 169 (1961).
3. Ercoli, R., Santambrogio, E., Tettamanti-Casagrande, G., *Chim. Ind. (Milano)* 44 (1962) 1344.
4. Bor, G., Markó, L., Markó, B., *Acta Chim. Acad. Sci. Hung.* 27 (1961) 395.
5. Seyferth, D., Hallgren, J.E., Hung, P.L.K., *J. Organomet. Chem.* 50 (1973) 265.
6. Robinson, B.H., Tham, W.S., *J. Organomet. Chem.* 16 (1969) 45.
7. Matheson, T.W., Robinson, B.H., Tham, W.S., *J. Chem. Soc., A* (1971) 1457.
8. Robinson, B.H., Spencer, J.L. Hodges, R., *Chem. Commun.* (1968) 1480.
9. Robinson, B.H., Spencer, J.L., *J. Organomet. Chem.* 33 (1971) 97.
10. Robinson, B.H., Spencer, J.L., *J. Chem. Soc., A* (1971) 2045.
11. Huheey, J.E., "Inorganic Chemistry, Principles of Structure and Reactivity, Second Edition" Harper and Row, New York (1978) 336.
12. Seyferth, D., Hallgren, J.E., Spohn, R.J., Williams, G.H., Nestle, M.O., Hung, P.L.K., *J. Organomet. Chem.* 50 (1974) 99.
13. Seyferth, D., Hallgren, J.E., Esbach, C.S., *J. Am. Chem. Soc.* 96 (1974) 1730.
14. Seyferth, D. Williams, G.H., *J. Organomet. Chem.* 38 (1972) C11.
15. Dolby, R., Robinson, B.H., *Chem. Commun.* (1970) 1058.
16. Gates, R.A., D'Agostino, M.F., Perrier, R.E., Sayer, B.G., McGlinchey, M.J., *Organometal.* 6 (1987) 1181.
17. Beurich, H., Vahrenkamp, H., *Angew. Chem., Int. Ed. Engl.* 20 (1981) 98.
18. Vahrenkamp, H., *Adv. Organomet. Chem.* 22 169 (1983).

19. Sutton, P.W., Dahl, L.F., *J. Am. Chem. Soc.* 89 (1967) 261.
20. Ahlgrén, M., Pakkanen, T.T., Tahvanianen, I., *J. Organomet. Chem.* 323 (1987) 97.
21. Dellaca, R.J., Penfold, B.R., *Inorg. Chem.* 11 (1972) 1855.
22. Brice, M.D., Dellaca, R.J., Spencer, J.L., *Chem. Commun.* (1971) 72.
23. Penfold, B.R., Robinson, B.H., *Accts. Chem. Res.* 6 (1973) 73.
24. D'Agostino, M.F., Mlekuz, M., Kolis, J., Sayer, B.G., Rodger, C.A., Halet, J.F., Saillard, J.-Y., McGlinchey, M.J., *Organometal.* 5 (1986) 2345.
25. Hoffmann, R., *Science* 211 (1981) 995.
26. Wade, K., "Electron Deficient Compounds" Nelson, Great Britain (1971).
27. Wade, K., *Chem. Commun.* 792 (1971).
28. Mingos, D.M.P., *Nature, Physical Science* 236 (1972) 99.
29. Albright, T.A., *Tetrahedron* 38 (1982) 1339.
30. McGlinchey, M.J., Mlekuz, M., Bougeard, P., Sayer, B.G., Marinetti, A., Saillard, J.-Y., Jaouen, G., *Can J. Chem.* 61 (1983) 1319.
31. Hoffmann, R., *Accts. Chem Res.* 4 (1971) 1.
32. Streitwieser, A., Jr., "Molecular Orbital Theory for Organic Chemists" John Wiley and Sons, New York (1961) 256.
33. Hoffmann, R., *J. Chem. Phys.* 39 (1963) 1397.
34. Hoffmann, R., *Angew. Chem., Intl. Ed. Engl.* 21 (1982) 711.
35. Cotton, F.A., *Accts. Chem. Res.* 1 (1968) 257.
36. Adams, R.D., Cotton, F.A., "Dynamic Nuclear Magnetic Resonance Spectroscopy" Jackman and Cotton, Eds., Academic Press, New York (1975) 489.
37. Muetterties, E.L., *Inorg. Chem.* 4 (1965) 769.
38. Abraham, R.J., Loftus, P., "Proton and Carbon-13 NMR Spectroscopy" Heyden and Son, Ltd., Great Britain (1979) 165.
39. Purcell, K.F., Kotz, J.C., "Inorganic Chemistry" W.B. Saunders Company,

- Toronto (1977) 976.
40. Natta, G., *Scientific American* 205 (Aug.1961) 33.
  41. Thomas, J.M., Thomas, W.J., "Introduction to the Principles of Heterogeneous Catalysis" Academic Press, New York, (1967) 180.
  42. Rideal, E.K., "Concepts in Catalysis" Academic Press, New York (1968) 38.
  43. Cotton, F.A., Wilkinson, G., "Advanced Inorganic Chemistry" John Wiley and Sons, New York (1980) 1081.
  44. Seyferth, D., *Adv. Inorg. Chem.*, 14 (1976) 97.
  45. Ryan, R.C., Pittman, C.U., Jr., O'Connor, J.P., *J. Am. Chem. Soc.* 99 (1977) 1986.
  46. Collin, J., Jossart, C., Balavoine, G., *Organometal.* 5 (1986) 203.
  47. Heimbach, P., Bartik, T., Drescher, U., Gerdes, I., Knott, W., Rienäcker, R., Schulte, H.-G., Tani, K., *Kontakte (Darmstadt)* 3 (1988) 19.
  48. Zief, M., Crane, L.J., Eds., "Chromatographic Chiral Separations" Marcel Dekker, Inc. (1988).
  49. Poole, C.F., Schuette, S.A., "Contemporary Practice of Chromatography" Elsevier Science Publishing Company, Inc., New York, (1984) 544.
  50. Jaouen, G., Marinetti, A., Saillard, J.-Y., Sayer, B.G., McGlinchey, M.J., *Organometal.* 1 (1982) 225.
  51. Fryzuk, M.D., Bosnich, B., *J. Am. Chem. Soc.* 99 (1977) 6262.
  52. Powell, P., "Principles of Organometallic Chemistry, Second Edition" Chapman and Hall, Great Britain, (1988) 159.
  53. Aime, S., Botta, M., Gobetto, R., Osella, D. Milone, L., *Gazz. Chim. Ital.* 117 (1987) 773.
  54. Aime, S., Botta, M., Gobetto, R., Osella, D., *J. Organomet. Chem.* 320 (1987) 229.
  55. Aime, S., Milone, L. Rossetti, R. Stanghellini, P.L., *Inorg. Chim. Acta* 25 (1977) 103.
  56. Balavoine, G., Collin, J., Bonnet, J.J., Lavigne G., *J. Organomet. Chem.*

- 280 (1985) 429.
57. Downard, A.J., Robinson, B.H., Simpson, J., *Organometal.* 5 (1986) 1122.
58. Einstein, F.W.B., Jones, R.D.G., *Inorg. Chem.* 11 (1972) 395.
59. Penfold, B.R., Robinson, B.H., *Acct. Chem. Res.* 6 (1973) 73.
60. Drago, R.S., "Physical Methods in Chemistry" W.B. Saunders Company, Toronto, (1977).
61. Harris, R.K., Mann, B.E., "NMR and the Periodic Table" Academic Press, New York, (1978) 88, 93, 101.
62. Matheson, T.W., Robinson, B.H., *J. Organomet. Chem.* 88 (1975) 367.
63. Cotton, F.A., Hanson, B.E., *Inorg. Chem.* 16 (1977) 3369.
64. Harris, R.K., Mann, B.E., "NMR and the Periodic Table" Academic Press, New York, (1978) 156, 178.
65. Santure, D.J., Sattleberger, A.P., *Inorg. Chem.* 24 (1985) 3477.
66. Miller, J.M., *J. Organomet. Chem.*, 249 (1983) 299.
67. Blumenthal, T., Bruce, M.I., Shawkataly, O.B., Green, B.N., Lewis, I., *J. Organomet. Chem.*, 269 (1984) C10.
68. Robinson, B.H., Tham, W.S., *J. Chem. Soc (A)* (1968) 1784.
69. Evans, D.G., Howard, J.A.K., Jeffery, J.C., Lewis, D.B., Lewis, G.E., Grosse-Ophoff, M.J., Parrott, M.J., Stone F.G.A., *J. Chem. Soc., Dalton Trans.*, (1986) 1723.
70. Beurich, H. Vahrenkamp, H., *Chem. Ber.* 115 (1982) 2385.
71. Chetcuti, M.J., Chetcuti, P.A.M., Jeffery, J.C., Mills, R.M., Mitprachachon, P., Pickering, S.J., Stone, F.G.A., *J. Chem. Soc., Dalton Trans.* (1982) 699.
72. Abad, J.A., Delgado, E., Grosse-Ophoff, M.J., Hart, I.J., Jeffery, J.C., Simmons, M.S., Stone, F.G.A., *J. Chem. Soc., Dalton Trans.*, (1987) 41.
73. Busetto, L., Jeffery, J.C. Mills, R.M., Stone, F.G.A., Went, M.J., Woodward, P., *J. Chem. Soc., Dalton Trans.* (1983) 101.

74. Dolby, R., Robinson, B.H., *J. Chem. Soc., Dalton Trans.*, (1972) 2046.
75. McCallum, R.S., Penfold, B.R., *Acta Cryst.* B34 (1978) 1688.
76. CHEMX, Chemical Design Ltd., Oxford, England (1986).
77. Gates, R.A., D'Agostino, M.F., Sutin, K.A., McGlinchey, M.J., Janik, T.S., Churchill, M.R., *Organometal.*, 9 (1990) 20.
78. D'Agostino, M.F., personal communication.
79. Stephenson, O., Waters, W.A., *J. Chem. Soc.* (1946) 339.
80. Haskelberg, L., Lavie, D., *J. Am. Chem. Soc.* (1947) 2267.
81. Derome, A.D. "Modern NMR Techniques for Chemistry Research" Pergamon Press, Toronto, (1987) 183.
82. "Comprehensive Organometallic Chemistry", Wilkinson, G., Ed., Pergamon Press, Toronto, 5, (1982) 7.
83. "Comprehensive Organometallic Chemistry", Wilkinson, G., Ed., Pergamon Press, Toronto, 6, (1982) 794.
84. Aitchison, A.A., Farrugia, L.J., *Organometal.* 6 (1987) 819.
85. Mann, B.E., Taylor, B.F. "<sup>13</sup>C NMR Data for Organometallic Compounds", Academic Press, New York, (1981).
86. Garcia, M.E., Jeffery, J.C., Sherwood, P., Stone, F.G.A., *J. Chem. Soc., Dalton Trans.* (1987) 1209.
87. Cotton, F.A. *Inorg. Chem.* 5 (1966) 1083.
88. Mason, J., Ed. "Multinuclear NMR" Plenum Press, New York.
89. Baumann, F.-E., Howard, J.A.K., Musgrove, R.J., Sherwood, P., Stone, F.G.A., *J. Chem. Soc., Dalton Trans.* (1988) 1891.
90. Ammeter, J.H., Burgi, H.-B., Thibeault, J.C., Hoffmann, R., *J. Am. Chem. Soc.* 100, (1978) 3686.
91. Perrin, D.D., Perrin, D.R. "Purification of Laboratory Chemicals" Pergamon

- Press, New York (1980).
92. Jaouen, G., Marinetti, A., Saillard, J.-Y., Sayer, B.G., McGlinchey, M.J.,  
*Organometal.* 1 (1982) 225.
  93. Germain, G., Main, P., Woolfson, M.M., *Acta. Crystallogr., Sect. A.* A27 (1971) 368.
  94. Sheldrick, G.M., Cambridge University, Cambridge, England (1976).
  95. Cromer, D.T., Waber, J.T., "International Tables for X-Ray Crystallography",  
Ibers, J.A., Hamilton, W.C., Eds., Kynoch Press, Birmingham, England, (1974)  
Vol. IV, Table 2.2.B, pp 99-101.
  96. Cromer, D.T., Waber, J.T., "International Tables for X-Ray Crystallography",  
Ibers, J.A., Hamilton, W.C., Eds., Kynoch Press, Birmingham, England, (1974)  
Vol. IV, Table 2.3.1, pp 149-150.
  97. Sheldrick, G.M., SHELXS86, Program for Crystal Structure Determination,  
University of Göttingen, Göttingen, Federal Republic of Germany, (1986).
  98. Stephens, J., MOLGEOM adapted from CUDLS: McMaster University, Hamilton,  
Ontario, Canada (1973).
  99. Calabrese, J.C., Burnett, R.M., TAPER, locally modified by Z. Tun with the  
permission of Nicolet XRD Corporation, (1980).
  100. Sutin, K.A., Kolis, J.W., Mlekuz, M., Bougeard, P., Sayer, B.G., Quilliam, M.A.,  
Faggioli, R., Lock, C.J.L., McGlinchey, M.J., Jaouen, G., *Organometal.*, 6,  
(1987), 439.
  101. Kleier, D.A., Binsch, G., Quantum Chemistry Program Exchange, No. 165,  
Indiana University, (1969).